Dissertation

Mathematical models of mineral and bone metabolism in patients with end stage renal disease treated with hemodialysis

submitted by

Mag.rer.nat Dr.rer.nat

Gudrun SCHAPPACHER-TILP

for the Academic Degree of

Doctor of Medical Science

(Dr. scient. med)

at the

Medical University of Graz

Institute of Human Genetics

under the Supervision of

Prof. Mag. DDr. Erwin Petek

2020

Declaration

I hereby declare that this thesis is my own original work and that I have fully acknowledged by name all of those individuals and organisations that have contributed to the research for this thesis. Due acknowledgement has been made in the text to all other material used. Throughout this thesis and in all related publications I followed the ”Guidelines of the Medical University of Graz on Good Scientific Practice”.

August 2020

DISCLOSURES

Parts of this thesis have been published:

Published articles:

A multi-compartment model capturing the pharmacokinetics of the calcimimetic cinacalcet. Schappacher-Tilp G, Fuertinger DH, Kotanko P. Cell Physiol Biochem. 2019;53(2):429-438.

A mathematical model of parathyroid gland biology. Schappacher-Tilp G, Cherif A, Fuertinger DH, Bushinsky D, Kotanko P. Physiol Rep. 2019 Apr;7(7):e14045.

Patents:

Techniques for modeling parathyroid gland functionality and calcimimetic drug activity. Filed Oct. 17 2019. Inventors: Schappacher-Tilp G, Fuertinger DH, Kotanko P.

Conference proceedings:

Thrice Weekly vs. Daily Cinacalcet: Virtual clinical trial and its subsequent clinical validation in a large US hemodialysis population. Schappacher-Tip G, Hymes J, Fuertinger DH, Stennett A, Kotanko P. ASN Kidney Week 2019 Washington, USA. Abstract: FR-PO130

CKD progression and bone metabolism: novel insights from a multi-scale physiology-based model. Schappacher-Tilp G, Cherif A, Fuertinger DH, et al. Nephrology Dialysis Transplantation 2019; 34 Supp: 1 Meeting Abstract: FP470

Virtual clinical trial of cinacalcet in hemodialysis patients shows profound impact of patient adherence on parathyroid hormone levels. Schappacher-Tilp G, Fuertinger DH, Hymes J et al. Nephrology Dialysis Transplantation 2018; 33 Supp: 1 Pages: 168-168 Meeting Abstract: FP398

A mathematical model of parathyroid gland biology in uremic patients. Schappacher-Tilp G, Perciado P, Maheshwari V et al. ASN Kidney Week 2017 New Orleans, USA. Abstract: R-PO283

An in silico method to predict net calcium transfer during hemodialysis. Maheshwari V, Cherif A, Fuertinger D, Schappacher-Tilp G, et al. Conf Proc IEEE Eng Med Biol Soc. 2017: 2740-2743

All co-authors have agreed to the inclusion of their published data in the dissertation. Permission to reproduce illustrations and figures from own or third-party publications has been granted. These permissions together with the source are mentioned in the appropriate figure legends.

The funding for this research was provided by the Renal Research Institute, a wholly owned subsidiary of Fresenius Medical Care.

ACKNOWLEDGEMENT

This work has been done in the Doctoral School for Lifestyle-Related Diseases.

It is a great pleasure to acknowledge my deepest thanks to my first supervisor, ao.Univ.Prof. DDr. Erwin Petek for his support in the development and execution of this work.

The warmest thanks are given to the other two supervisors and members of the dissertation committee, Dr. Peter Kotanko and em.Univ.Prof. Dr. Franz Kappel. It was a great privilege to work with Dr. Kotanko, who always provided great inspiration and contagious enthusiasm regarding mathematical models and their possible clinical applications. Without his vast expertise in the field of nephrology, this work would not have been possible. Prof. Kappel, former Dean of the University of Graz and Chair of the Department for Mathematics and Scientific Computing, was a brilliant mathematician and an inspiring advocate for applying rigorous science and mathematics to medical questions. Tragically, he succumbed to COVID-19 in March 2020. He is missed greatly.

I would like to thank my father, Univ.Prof.i.R. Dr. Wilhelm Schappacher, for showing me the value of a critical mind and his inspiration, support, and encouragement throughout my whole academic career. Moreover, I thank Christa Schappacher for making my life and daily juggling work and family so much easier.

And finally, I would like to thank my husband, Univ.Prof. Dr. Markus Tilp, for being my intellectual sparring partner and for his constant encouragement and support for the last decades.

This work is dedicated to my beautiful daughters Marlene and Clara, who never cease to amaze me.

Contents

Abbreviations and Definitions

ATP	Adenosine triphosphate
BCL-2	B-cell lymphoma 2
Ca^{2+}	Plasma ionized calcium concentration
CaSR	Calcium sensing receptor
CKD	Chronic kidney disease
CI	Confidence interval
FDA	Food and drug administration
MBD	Mineral and bone disorder
Ca^{2+}	Ionized plasma calcium concentration
CREB	cAMP response element-binding protein (transcription factor)
ECF	Extracellular fluid
ECC	Extracellular compartment
FGF-23	Fibroblast growth factor 23
GFR	Glomuerular filtration rate, amount of filtrate produced by both kidneys in an hour
HD	Hemodialysis
HBS	Hungry bone syndrome
IC	Intracellular
OPG	Osteoprotegerin
PTH	Parathyroid hormone
PHP	Primary hyperparathyroidism
PTG	Parathyroid gland
RANK	Receptor activator of NF-κB

RANKL	Receptor activator of NF-κB ligand
Runx2	Runt-related transcription factor 2
SD	Standard deviation
SHPT	Secondary hyperparathyroidism
TGF-β	Transforming growth factor beta
VDR	Vitamin D receptor

DEFINITIONS

Parameter		Description	Formula
Dose	D	Amount of drug administered	
Plasma concentration	C	(Time dependent) plasma concentration of a drug	
C_{max}	C_{max}	Peak plasma concentration of a drug after administration	
t_{max}	t_{max}	Time to reach C_{max}	
Terminal half-life	$t_{1/2}$	Half-life of elimination phase	
Distribution half-life	$t_{1/2}^{D}$	Half-life of distribution phase	
Area under the curve	AUC_{τ}	Integral over the plasma concentration	$\int_0^{\tau} C(t)dt$
Total exposure	AUC_{∞}	Total amount of drug in the plasma	$\int_0^{\infty} C(t)dt$
Bioavailability	BIO	The systemically available fraction of a drug. It is estimated by the ratio of the AUC of an orally administered drug and the AUC of an intravenously (iv) administered drug. In our formula we assume the same dose for oral and iv administration	$Bio = \frac{\int_0^{\infty} C_{oral}(t)dt}{\int_0^{\infty} C_{iv}(t)dt}$
Apparent oral clearance	CL/F	Apparent clearance of the drug from plasma after oral administration	$CL/F = \frac{D}{AUC_{\infty}}$
Apparent volume of distribution at steady state	V_D	Apparent volume in which a drug is distributed at steady state	$V_D = D\frac{\int_0^{\infty} t \cdot C(t)dt}{\left(\int_0^{\infty} C(t)dt\right)^2}$

List of Figures

List of Tables

1 Zusammenfassung

Im gesunden Körper wird Kalzium- und Phosphathomöostase durch ein komplexes regulatorisches System gewährleistet. Das System umfasst etliche Ionen und Hormone sowie deren Auswirkung auf Niere, Knochen und Darm. Gerät das Gleichgewicht durch den Verlust der Nierenfunktion ins Wanken, kommt es bei der großen Mehrheit von PatientInnen mit Nierenerkrankung im Endstadium zu einer Störung des Mineral- und Knochenhaushaltes. Klinisch manifestiert sich diese systemische Störung unter anderem durch sekundären Hyperparathyreoidismus, renale Osteodystrophie sowie vaskuläre Kalzifizierung.

Jene Mechanismen, die letztendlich zur Störung des Mineral- und Knochenhaushaltes führen, sind hoch komplex und multidimensional. Mathematische Modelle können helfen, im komplexen regulatorischen System der Kalzium- und Phosphathomöostase die zentralen Mechanismen zu identifizieren und analysieren und dadurch Rückschlüsse auf das System sowie mögliche Behandlungen zu ziehen.

Ziel dieser Arbeit war es, die physiologischen Schlüsseleigenschaften der Hauptregulatoren des Mineral- und Knochenhaushalts in mathematische Modelle zu übersetzen. Der Fokus lag dabei auf HämodialysepatientInnen. Die Vorhersagekraft der Modelle wurden mit Hilfe klinischer und experimenteller Daten getestet. Das integrierte Mineral- und Knochenhaushaltsmodell kann etwa Hypokalzämia als Folge einer Phosphatinfusion sowie Hyperkalzämie und Hyperkalziurie in PatientInnen mit primären Hyperparathyreoidismus erklären. In PatientInnen mit chronischer Nierenerkrankung sagt das Modell sekundären Hyperparathyreoidismus sowie erhöhten Knochenumsatz und Knochenschwund voraus. Aufgrund der Divergenz zwischen den auf einem Basismodell vorhergesagten Phosphatverläufen und jenen aus klinischen Studien mit dem Kalzimimetik Cinacalcet, stellten wir eine Hypothese betreffend der Bildung von Kalzium-Phosphatkomplexen auf.

Alle Modelle und ihre Parameter basieren auf physiologischen Prinzipien und Daten. Daher können sowohl die Modelle als auch die Parameter problemlos an unterschiedliche Rahmenbedingungen angepasst werden. Beispiel hierfür wären Mutationen des kalziumsensitiven Rezeptors oder langfristige Änderungen des Lebensstils wie etwa eine Diätumstellung.

2 Abstract

Chronic kidney disease - bone mineral disorder (CKD-MBD) is a complex disorder affecting the vast majority of chronic kidney disease patients. A hallmark of CKD-MBD is altered parathyroid gland biology resulting in secondary hyperparathyroidism, renal osteodystrophy, and vascular calcification.

CKD-MBD evolves due to an imbalance in the highly complex and multi-dimensional regulatory system ensuring calcium and phosphate homeostasis. This regulatory system involves many ions and hormones and their actions on the kidney, bone, intestine, and parathyroid gland. Due to the disorder's complexity, mathematical models help gain new insight into the disorders' development. Moreover, they could prove useful in finding the optimal strategy regarding the combination of standard treatments such as calcimimetics, even under the aspect of genetic variances of the calcium-sensing receptor (CaSR), calcitriol therapy, or lifestyle changes including phosphate diet or the administration of phosphate binders.

The aim of this thesis was to translate critical physiological properties of the primary regulators of calcium and phosphate homeostasis into mathematical models and integrate these models into a comprehensive model of calcium and phosphate homeostasis. The main focus lies on patients suffering from end-stage renal disease. We test the integrated model against various clinical manifestations during acute and chronic disturbances of homeostasis. For example, the model can explain hypocalcemia as a response to phosphate infusion or hypophosphatemia and hypercalcemia in primary hyperparathyroidism patients. In patients with chronic kidney disease (CKD) and hemodialysis (HD) patients, the model predicts secondary hyperparathyroidism and high bone turnover and bone loss. The divergence between model predictions and clinical observations regarding cinacalcet treatment suggests the existent of a point of no return regarding calcium-phosphate precipitation resulting in vascular calcification.

All models and their parameters are physiologically meaningful such that adaptations of the models to different conditions are straightforward. Such adaptations would be mutations of the calcium-sensing receptor or changes such as low or high phosphate diet.

3 Introduction

Chronic kidney disease (CKD) is a general term for abnormal kidney structure or function present for more than three months, irrespective of cause (135). CKD is divided into 5 stages (135):

G1 - Glomerular filtration rate (GFR) is normal ($\geq$ 90 ml/min/1.73 m^2), but other kidney damage signs such as proteinuria or hematuria are present

G2 - GFR is between 60-89 ml/min/1.73 m^2

G3a - GFR is between 45-59 ml/min/1.73 m^2

G3b - GFR is between 30-44 ml/min/1.73 m^2

G4 - GFR is between 15-29 ml/min/1.73 m^2

G5 - Kidney failure or end-stage renal disease: GFR is below 15 ml/min/1.73 m^2 or treatment by hemodialysis

Reduced GFR is associated with a higher risk of hospitalization, death, and cardiovascular events (79, 218). Cardiovascular disease is the leading cause of death in CKD patients of all stages (44, 79, 179, 190). As the global prevalence for all five CKD stages is around 13.5% (100), CKD provides a significant global public health problem. In 2017, about 750,000 adults in the USA needed hemodialysis or a kidney transplant to survive (72).

The two main causes of CKD are diabetes and high blood pressure (109). Development and progression of CKD is also closely related to unhealthy lifestyles such as obesity, lack of exercise, or smoking (88, 97, 106, 153, 159). Furthermore, unhealthy diets such as high sodium, soft drinks, or animal protein and fat intake may result in CKD (88, 137, 138).

The vast majority of CKD patients suffers from a systemic disorder called chronic kidney disease - mineral and bone disorder (CKD-MBD) (155, 171). Its hallmarks are one or a combination of the following (109, 171, 226):

(1) abnormalities of calcium, phosphate, parathyroid hormone (PTH) or vitamin D metabolites

(2) abnormalities in bone turnover and mineralization

(3) extra-skeletal calcification

CKD-MBD is associated with high morbidity and mortality in hemodialysis patients (155, 171, 190). The declining kidney function in CKD patients results in an imbalance in the exquisite and multi-factorial regulatory system, ensuring calcium and phosphate homeostasis. This mineral imbalance results in various abnormalities of mineral and bone metabolism.

3.1 CALCIUM AND PHOSPHATE HOMEOSTASIS

Calcium is the most abundant mineral in the human body (173). About 99% of the roughly 30 mol of calcium an adult body contains is stored in the bone (46, 173), only 1% is present in the body fluids. Non-bone calcium exists in three forms: complexed with other ions such as phosphate (5-10%), bound to proteins, most prominently to albumin (40%), or in an ionized form (50-55%) (162, 173).

Ionized plasma calcium concentration (Ca^{2+}) has to be maintained within a narrow physiologic range. In each individual, $Ca^{2+}$is kept within $\pm$ 1-2% (35). Since $Ca^{2+}$is essential for many physiological processes, such as nerve transmission and nerve conduction, cardiac contractility and muscle contraction, bone formation, or blood coagulation, acute or chronic deviations from homeostasis generally result in metabolic disorder and pathologic conditions such as tetany, seizures, or ectopic calcification of soft tissue, e.g., (16, 49). Calcium homeostasis is coupled with phosphate homeostasis (17, 183), although phosphate is not as tightly regulated as calcium (12, 201).

Phosphate accounts for approximately 1% of body weight in an adult (147). About 85% of phosphate is stored in the bone; the remaining 15% is stored in the extracellular fluid and the soft tissue (147). In the plasma, 15% of inorganic phosphate is protein-bound (147, 213).

An exquisite system of feedback regulators ensures $Ca^{2+}$and phosphate homeostasis (17, 183). These regulators involve the major organs that transport or store calcium and phosphate (i.e., the intestine, the kidney, and bone) and endocrine organs. The key endocrine organ for the regulation of calcium is the parathyroid gland (PTG), which produces, stores, and eventually releases the parathyroid hormone (PTH) (27).

In the next sections, we discuss the physiology of the critical regulators of calcium and phosphate homeostasis relevant for CKD patients and CKD-MBD development in more detail.

3.2 PARATHYROID GLAND

PTH is the key endocrine regulator for calcium homeostasis. It directly stimulates

- renal calcium reabsorption (17, 142)
- renal phosphate excretion (119, 125)
- renal-hydroxylase to convert 25-hydrocycholecalciferol to its bioactive form 1,25-Dihydroxycholecalciferol (calcitriol) (172)
- bone resorption resulting in a net flux of calcium and phosphate from the bone to the extracellular fluid (ECF) (126)
- Fibroblast growth factor 23 (FGF-23) synthesis in the bone (116, 201)

In indirectly stimulates intestinal calcium and phosphate absorption via calcitriol, which enhances active transport of calcium and phosphate in the small intestines.

PTH is synthesized by the PTG where is either degraded, stored, or released. Glandular cells cycle through a secretory active and a secretory quiet state (70, 217). Only secretory quiescent cells can undergo proliferation or apoptosis (217). The life-span of PTG cells is in the order of years. PTG cells are replicating discontinuously and conditionally. The replication rate is evaluated by analyzing the Ki-67 cell marker, a nuclear protein associated with cellular proliferation (1). The geometric mean PTG cell-birth rate of 5.24% per year (CI: 0.81 - 33.8% per year) is neither influenced by age, sex, nor race (224). Moreover, the cell-birth rate is the same between central and peripheral regions (224), indicating that there might be no need for a spatial cell proliferation model in healthy subjects.

Two mechanisms are ensuring high levels of PTH release:

(A) increase of PTH release of each secretory active cell by
  - the increased release of stored PTH
  - decreased intracellular degradation
  - increased biosynthesis of PTH

(B) the rise in the number of contribution cells by enhanced cellular proliferation.

The different adaptive responses manifest on significantly different time scales, reacting within seconds to weeks. In acute hypocalcemia, the body responds by quickly releasing

stored PTH within seconds to minutes. If the issue is not resolved, the intracellular PTH degradation rate declines within 20 minutes (197). If normocalcemia is still not achieved, the PTH production rate increases within hours (89). Subsequently, the PTG will increase its cellular proliferation rate within two days (217). If untreated, the chronic scenario eventually leads to hyperplasia whereby the PTG mass can increase 10-100 fold or more (75) (Figure 3.1).

The mathematical model's two main challenges are: (1) the time scales for the adaptation mechanisms are significantly different, ranging from seconds to months, and (2) the history dependence of the system's state. It is not sufficient to know the current calcium, phosphate, and calcitriol concentrations to determine the system's state. We instead need to know the condition's whole history to assess whether or not different adaptation mechanisms are already in place.

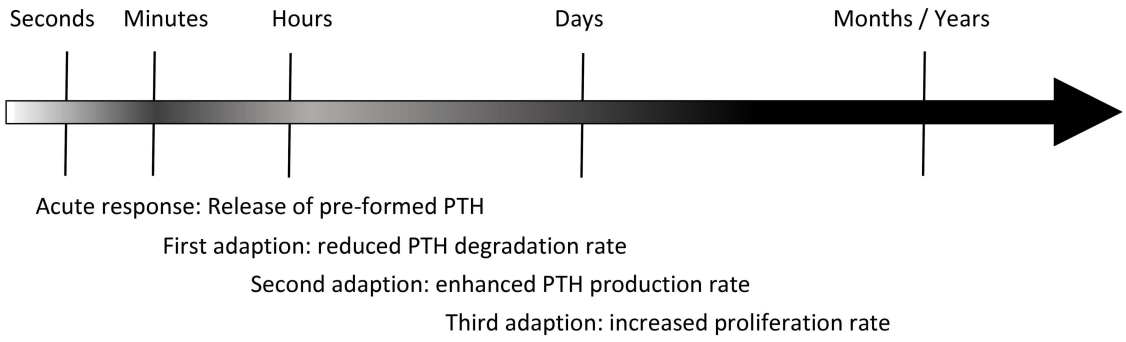

Figure 3.1 Graph from Schappacher-Tilp et al. (192) by CC-BY. Timeline for PTH secretory rate summarizing results presented in (34, 83, 89, 160, 197, 217). Darker color corresponds to a higher PTH secretory rate. The various mechanisms working of different timelines ensure elevated PTH secretion over a long period.

3.2.1 CaSR

The CaSR regulates PTG biology. It is a G-protein coupled receptor (39, 42, 47, 96). Its signaling cascade, triggered by the binding of Ca^{2+}, inhibits the release of PTH, cellular proliferation, and PTH synthesis (42, 47, 96). The response of PTH to small changes of serum $Ca^{2+}$is dramatic and most likely due to positive cooperativity (176). There is a positive feedback loop between the CaSR and the vitamin D receptor (37, 217). It has been shown that calcimimetics increase vitamin D receptor expression in rat PTG (187). On the other hand, calcitriol proved to be effective in lowering PTH serum levels in most patients (Fig. 3.2). While in some studies, oral pulse therapy of calcitriol was even effective in reducing hyperplastic PTG volume (76), other studies could not find the same effect (76). The main difference between these studies was the baseline

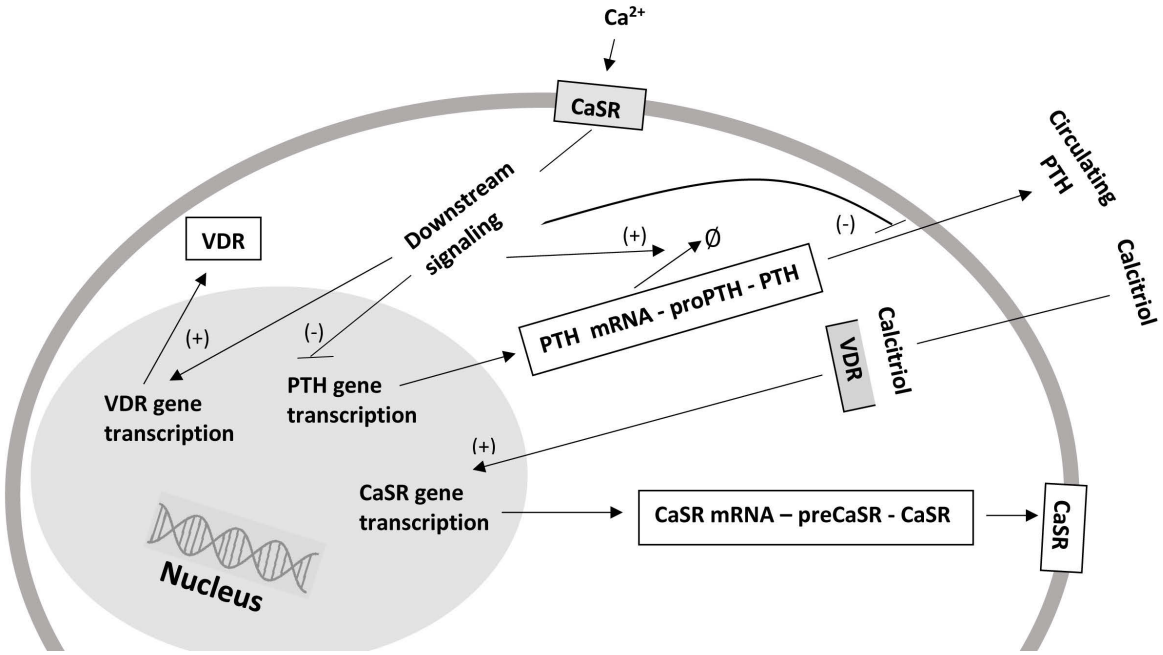

Figure 3.2 Sketch of a secretory active PTG cell. The activated CaSR inhibits PTH synthesis rate, increases PTH intracellular degradation rate, and inhibits PTH release. There is a positive feedback loop between the CaSR and the VDR. For the sake of clarity, we did not include the effect of phosphate on CaSR and VDR expression. Phosphate decreases CaSR and VDR expression and diminishes the positive feedback loop between CaSR and VDR.

phosphate levels, which were significantly higher in the second study (5.8 vs. 6.4-7.33 mg/dl). Moreover, glandular volume was 2-fold higher in the second study. In (217), the authors could provide evidence that the likelihood of a positive effect of calcitriol of PTG proliferation decreases with increasing PTG volume.

Another primary regulator of the CaSR is phosphate. Various studies in uremic rats showed that a high phosphate diet enhances PTG proliferation within a few days (55, 160, 208). While low calcium intake leads to similar results, the time is significantly longer. Notably, the presence of high phosphate levels effectively diminishes the positive feedback loop between CaSR and VDR (37). Recently, researchers showed that phosphate acts directly on the CaSR via non-competitive antagonism (38). Pathophysiologic phosphate concentrations frequently observed in CKD patients quickly increase PTH secretion from isolated PTG cells. This effect is reversible. Phosphate reduced diet at the onset of CKD can help to control PTH levels (188).

In patients suffering from end-stage renal disease, the loss of the regulatory kidney function triggers a cascade of pathologies, eventually leading to secondary hyper-

parathyroidism (SHPT). One hallmark of chronic kidney disease is the impaired synthesis of calcitriol and the significantly impaired renal clearance of phosphate and PTH (136). Due to the positive feedback between phosphate and PTH, the retention of phosphate increases PTH levels further. PTH increases bone resorption over bone formation, resulting in a net release of $Ca^{2+}$and phosphate from the bone (84). As a consequence, PTH and phosphate levels increase further. Expression of CaSR and VDR is reduced and, therefore, also the sensitivity of the PTG to $Ca^{2+}$and calcitriol (24, 80). If not treated, PTG will develop hyperplasia (83, 217).

3.2.2 Cinacalcet

Cinacalcet is a calcimimetic that effectively lowers PTH release by allosteric activation of the CaSR (19, 22, 58). It is commonly used in hemodialysis patients to treat secondary hyperparathyroidism (19, 58). A single oral dose leads to an inverse relationship between PTH and cinacalcet. PTH concentration is greatest when cinacalcet concentration is lowest (90) while the lowest PTH concentration point is reached at t_{max} of cinacalcet (90). The effect - concentration profile can be approximated by an inhibitory maximal effective concentration E_{max} model:

$$E = \frac{E_{max} \cdot \mathrm{Conc}}{C_{50} + \mathrm{Conc}}$$

E is the effect and C_{50} the concentration of cinacalcet, where 50% of the maximal effect is reached. From effect-concentration curves, we can deduce that C_{50} is 6.2ng/ml and E_{max} is around 99% (90). In another study, the authors investigated PTH - time curves after a single dose of cinacalcet at a pharmacokinetic steady state, i.e., each patient was treated with cinacalcet for at least six days (57). The study showed that cinacalcet lowers PTH significantly. However, a substantial decrease in PTH is accompanied by elevated PTH concentrations after around 12 hours.

Cinacalcet is highly protein-bound (67). Therefore, hemodialysis does not influence the plasma-drug curve. Pharmacokinetics of cinacalcet is the same in HD patients and healthy subjects (168). Cinacalcet treatment lowers maximum PTH levels over months (19, 20, 168). A long-term study showed that even the volume of hemodialysis patients' hyperplastic parathyroid glands is reduced by cinacalcet treatment (151). Depending on the PTG baseline volume, the reduction was between 68% and 54%. The decrease in PTG volume was accompanied by a significant decrease in PTH concentrations (1196 $\pm$ 381 pg/ml vs. 256 $\pm$ 160 pg/ml).

Another main observation of clinical studies was that plasma Ca^{2+}declines signif-

icantly during the administration of cinacalcet, reaching a minimum after around 8-10 weeks after the start of cinacalcet administration (19, 21). The majority of studies also reported a mean decrease in phosphate plasma concentration (21, 58, 66, 154). Notably, the reduction of calcium during cinacalcet therapy resembles the so-called hungry bone syndrome (HBS). HBS is prolonged hypocalcemia with hypophosphatemia in patients undergoing parathyroidectomy and is associated with intensive bone turnover (26, 81). However, cinacalcet induced hypocalcemia recovers in most patients spontaneously as the PTG can still react to falling calcium levels (19, 21, 43, 154).

3.3 INTESTINAL CALCIUM AND PHOSPHATE ABSORPTION

We distinguish between net absorption and true absorption. Net absorption is defined as the intake minus the loss in feces in a normalized amount of time. However, there is also a flux of endogenous calcium and phosphate to the intestine due to their presence in digestive juices. A fraction of the secreted calcium and phosphate will be reabsorbed. Therefore, the true amount of absorbed calcium and phosphate is higher than the net absorption. Fractional true absorption declines with intake, while fractional net calcium absorption rises from a negative value to a maximum before it falls towards the diffusion fraction (29). The difference between net absorption and true absorption is most prominent at low calcium diets where net absorption might be negative, while true absorption is always positive. The amount of calcium re-entering the intestines and, therefore, true absorption can be quantified by dual-isotope methods, e.g., (61, 228).

Several approaches are trying to predict the amount of endogenous calcium re-entering the intestines. While it seems that the fraction is independent of plasma ionized calcium concentration, it correlates with phosphate intake, i.e., endogenous calcium rises by 0.037 mmol for every mmol of phosphorus ingested in healthy subjects (54). Furthermore, body size plays a role, i.e., the surface area defined as $0.20247 \cdot \mathrm{Height}^{0.725} \cdot \mathrm{Weight}^{0.425}$, where height is measured in m and weight is measured in kg, correlates significantly with endogenous calcium (r=0.655, $p<0.01$). Interestingly, also height correlates with endogenous calcium (r=0.862, $p<0.01$). Both results are presented in the same paper (54), suggesting that surface area does not capture the effect of the body size. However, it is expected that endogenous calcium varies with ingested intake and, therefore, body size since the mucosal mass increases linearly with body size (56). Another parameter to describe body size is lean body mass. In (94), the authors reported that the mean total concentration of endogenous calcium increased by 1.6 mg/day on average for every kg lean mass. Lean body mass is defined as lean mass = body weight - body fat. Lean mass can be approximated by $0.32810 \cdot \mathrm{Weight} + 0.33929 \cdot \mathrm{Height} - 29.5336$ in men and $0.2957 \cdot \mathrm{Weight} + 0.4181 \cdot \mathrm{Height} - 43.2933$ in women, where weight is measured in kg, height is measured in cm.

3.3.1 Physiology

Intestinal calcium and phosphate absorption occur in the small intestines. Both cross the intestinal barrier via two pathways (71, 91, 92, 158, 180, 222):

(a) transcellular pathway

(b) paracellular pathway

Paracellular transport is passive and takes place across all of the small intestines.

Transcellular or active transport is saturable and takes mainly place in the duodenum and upper jejunum (30, 71, 91, 92). Active transport involves three steps: (1) entry across the brush border, (2) intracellular diffusion, and (3) extrusion (Fig. 3.3). For calcium, step 1 is mediated by calcium-selective ion channels (CaT1) and step 3 by CaATPase (CaBP) (30, 71, 158). Biosynthesis of CaT1 is roughly 90% calcitriol dependent, CaBP synthesis if fully calcitriol dependent (71, 199). Since calcitriol synthesis is down-regulated by calcium, active transport is saturable. In high calcium diets, passive transport accounts for the major part of absorbed calcium (71, 199). In hemodialysis patients, the synthesis of calcitriol is impaired, which results in significantly less calcium absorption. In (199), the authors reported mean net absorption of calcium in healthy subjects, HD patients, and HD patients with calcitriol therapy. Mean calcitriol plasma concentrations ($\pm$ standard error of the mean) were 48 pg/ml ($\pm$ 4) in healthy subjects, 9 pg/ml ($\pm$ 1) in HD patients, and 84 pg/ml ($\pm$ 13) in HD patients with calcitriol therapy. Net calcium absorption of a meal containing approximately 300 mg calcium was only 43 mg ($\pm$ 31) in HD patients compared to 119 mg ($\pm$ 21) in healthy control subjects (199). With calcitriol therapy, the mean net absorption in HD patients was 175 mg ($\pm$ 40). This effect is emphasized when the calcium content of the meal is small, i.e., 120 mg. Mean net absorption in healthy subjects, HD patients, and HD patients receiving calcitriol therapy was approximately 44 ($\pm$ 22), -26 ($\pm$ 4), and 88 ($\pm$ 15), respectively.

For phosphate, transcellular transport is mainly based on sodium-dependent phosphate co-transporter NaPi-IIb (91, 92, 149, 156, 158, 222), which regulates approximately 90% of active absorption (189). Again, calcitriol up-regulates the synthesis of NaPi-IIb (149). In (180), the authors reported net phosphate absorption in healthy subjects (mean calcitriol plasma concentration 48 pg/ml ($\pm$ 4)), HD patients (mean calcitriol plasma concentration 7 pg/ml ($\pm$ 2)) and HD patients with calcitriol therapy (mean calcitriol plasma concentration 94 pg/ml ($\pm$ 14)). A mean intake ($\pm$ standard error of the mean) of 303 mg ($\pm$ 4) phosphorus led to net absorption of 242 mg ($\pm$ 30 mg) in healthy subjects, while a mean intake 308 mg ($\pm$ 3) phosphorus led to net absorption of 186 mg ($\pm$ 35) in HD patients. In HD patients with calcitriol therapy, net absorption of a meal with 315 mg ($\pm$ 4) phosphorus content was 272 mg ($\pm$ 16).

A limiting factor for a structural mathematical model is that phosphate absorption is hard to quantify. Phosphorus is a natural and abundant food component available as either inorganic phosphate salts or as a constituent of phosphoproteins. While the absorption of phosphorus of plant-origin is below 40%, the net gastrointestinal absorption

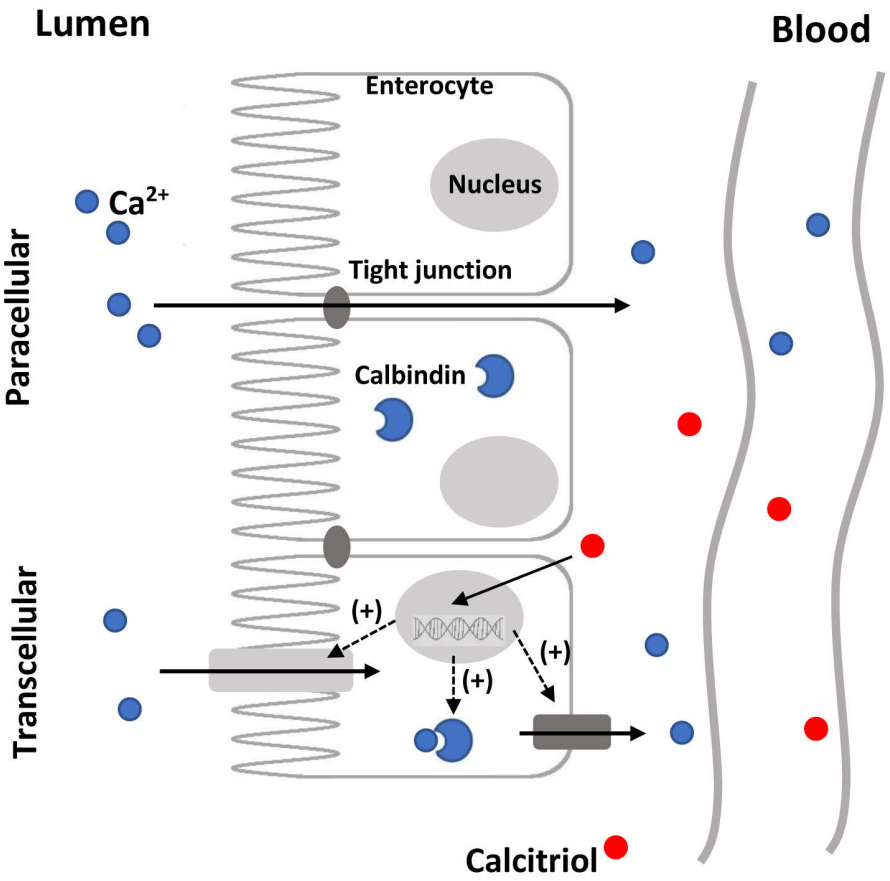

Figure 3.3 Paracellular and transcellular calcium transport. Transcription is indicated by the dotted line. Calcium can diffuse passively via the tight junctions. Active transport involves the entry across the brush border of enterocytes, binding to calbindin and intracellular diffusion, and extrusion.

of inorganic-phosphorus-containing preservatives is approaching 100% (156). Since the exact diet is generally unknown, it is inefficacious to model phosphate absorption in great detail. On average, the net absorption of phosphorus in healthy subjects is around 60%.

Calcium absorption is not easy to quantify, either. Calcium is absorbed more efficiently if the calcium content in the diet is low. Therefore, it makes a significant difference whether daily calcium is consumed, for example, in 8 small or 2 large meals (93). If we assume relatively constant eating preferences, a simplified absorption model might be the better choice for the integrated calcium and phosphate homeostasis model.

Balance studies are mostly based on one meal after a fast with smaller or larger calcium or phosphate contents. Therefore, we cannot quantitatively compare predictions

of daily absorptions with this type of study. Thus, we refrain from fitting data and instead calibrate the absorption models based on the following basic assumptions: a calcium diet of 25 mmol/day leads to net absorption of approximately 4 mmol/day, a phosphate diet of 38 mmol/day leads to net absorption of about 22 mmol/day (30, 189).

3.4 RENAL REGULATION OF CALCIUM AND PHOSPHATE

3.4.1 Physiology of renal calcium handling

In healthy subjects, intestinal absorption of calcium and phosphate is balanced by renal excretion. Various feedback systems regulate renal regulation of phosphate and calcium excretion and reabsorption.

Ionized and complexed fractions of calcium are ultrafilterable, while protein-bound calcium is not. Therefore, approximately 55 - 60% of calcium can be filtrated by the kidneys (17, 166). In healthy subjects, about 220 mmol calcium is filtered per day. The kidneys reabsorb around 98% of the filtered calcium load, and only about 3-5 mmol are excreted daily (17, 166, 183). Approximately 60 - 70% of filtered calcium is reabsorbed in the proximal convoluted tubule, 20% in the Henle's loopy, 10% in the distal convoluted tubule (Fig. 3.4). Around 80% of proximal tubular calcium reabsorption occurs paracellular, 20% transcellular. While paracellular and transcellular pathways are present in the Henle's loop, the distal tubule reabsorbs calcium exclusively via the transcellular route (166) (Fig. 3.5). PTH regulates transcellular transport (17).

Besides, the CaSR regulates calcium reabsorption. Inhibition of the CaSR increased the permeability to the paracellular pathway's calcium, thereby increasing calcium absorption and blood calcium concentration independently of PTH (142).

The relationship between serum calcium and renal calcium excretion is non-linear. There is a renal threshold for calcium, which corresponds to the plasma concentration of calcium above which calcium is detectable in the urine. Another crucial parameter is the maximum rate with which actively reabsorbed calcium is transported by the tubular cells, T_m. Since some channels might reach their full capacity before others do, the renal threshold is generally smaller than T_m/GFR, where GFR is the glomerular filtration rate. The difference between the maximal renal resorption (T_m/GFR) and the renal threshold is called splay. For concentrations above the maximal renal resorption, the slope of renal Ca^{2+}excretion is equal to the filtration rate. In the absence of PTH and calcitriol, the maximal renal resorption is decreased, resulting in a shift of the excretion curve towards lower calcium concentrations. In loss-of-function mutations of the CaSR, the slope is significantly smaller (95). The renal threshold for calcium is around 1.875-2.25 mMol.

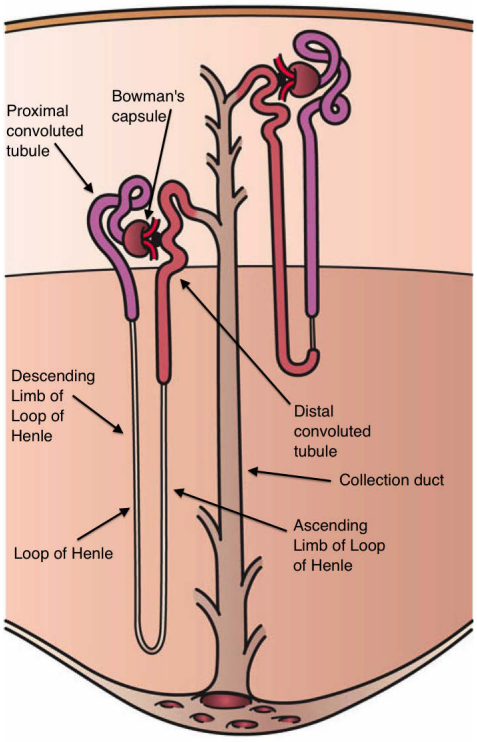

Figure 3.4 Artwork by Holly Fischer / CC BY. The sketch shows the structure of a nephron, including the proximal tubule, the Henle's loop, and the distal tubule.

3.4.2 Physiology of renal phosphate handling

The kidney freely filters ionized and ion-bound forms of phosphate. These forms represent approximately 85-90% of total plasma phosphate (191). About 75 - 85% of the daily filtered phosphate load is reabsorbed by the renal tubules (183). Approximately 85% of phosphate reabsorption occurs in the proximal tubule, while about 10% occurs in the Henle's loop. Only 3% of phosphate reabsorption occurs in the distal convoluted tubule (Fig. 3.4). There are two reabsorption pathways: transcellular reabsorption as well as the paracellular reabsorption. Transcellular reabsorption via co-transporter NaPi-IIa and NaPi-IIc is dominant in the proximal tubule, which accounts for approximately 80%. Transcellular reabsorption is down-regulated by PTH since high levels of PTH cause a decrease in the number of transporters (17, 69).

Again, the relationship between phosphate excretion and plasma phosphate levels is non-linear. The renal threshold of phosphate is roughly between 1.14 and 1.25 mMol. Under phosphate homeostasis, approximately 210 mmol are filtered daily, of which 22 mmol are excreted daily.

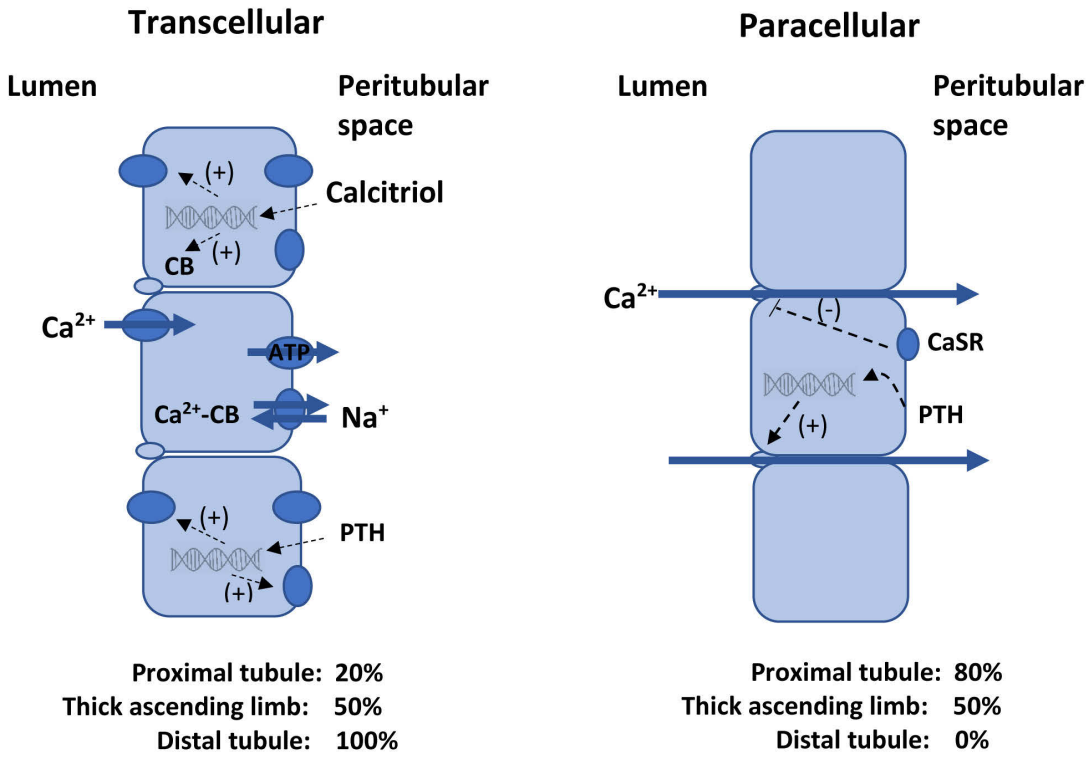

Figure 3.5 Renal calcium handling. The different segments of a nephron reabsorb calcium via paracellular and transcellular pathways. Activation of the CaSR down-regulates paracellular transport. PTH increases calcium reabsorption in both pathways; calcitriol enhances active reabsorption via transcriptional activities. CB denotes calbindin.

3.5 CALCITRIOL

Calcitriol is the most potent bio-active form of vitamin D (14, 60). Systemically, calcitriol binds to the VDR in the PTG, kidney, intestine, and bone. Vitamin D_3 is produced in the epidermis and hydroxylated to 25(OH)D_3 in the liver (14, 60). 25(OH)D_3 is the primary storage form of vitamin D (172). 25(OH)D_3 is converted to calcitriol in the proximal tubule of the nephron by the enzyme 25OHD-1α hydroxylase (CYP27B1) (172) (Fig. 3.6). Knock-out animal models of this gene produce rickets, growth retardation, hypophosphatemia, hypocalcemia, hyperparathyroidism (53).

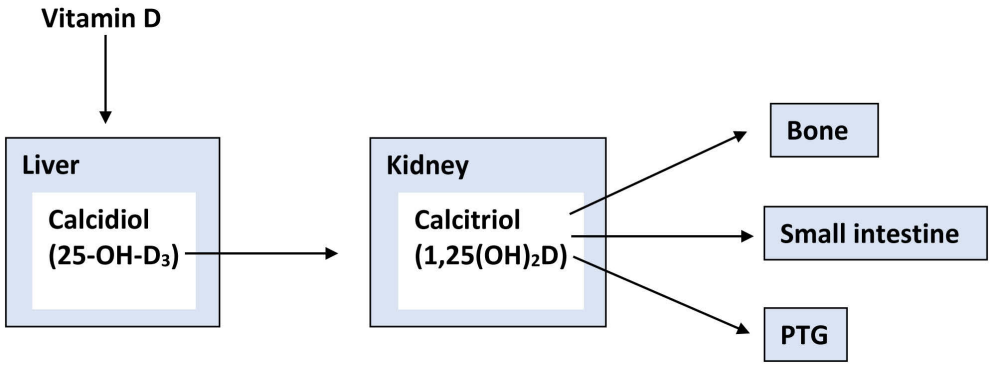

Figure 3.6 In the liver, Vitamin D is hydroxylated to 25(OH)D_3. 25(OH)D_3 is hydroxylated to calcitriol in the kidneys. The parathyroid gland, the small intestines, the bone, and the kidney itself are the main target organs of calcitriol.

Several factors, such as calcitonin, estrogens, and cytokines, regulate calcitriol synthesis (139). Moreover, the conversion from 25(OH)D_3 to calcitriol is stimulated by PTH and down-regulated by high $Ca^{2+}$and phosphate concentrations and high levels of calcitriol itself (Fig. 3.7). The plasma concentration of calcitriol is about 1000 times less than the concentration of 25(OH)D_3 (172). High PTH concentrations suppress 24-OHase resulting in a lower 1,25D clearance rate (172). Due to the positive feedback loop between the CaSR and VDR (37) and the calcitriol dependent increase of intestinal calcium absorption (199), calcitriol generally lowers PTH levels. Due to the loss of kidney function, calcitriol synthesis is impaired in CKD patients (136). However, calcitriol is produced outside the kidney in small amounts by other tissue (3). Its half-life is measured in hours, the half-life of its precursor 25(OH)D_3 is measured in weeks (139, 172).

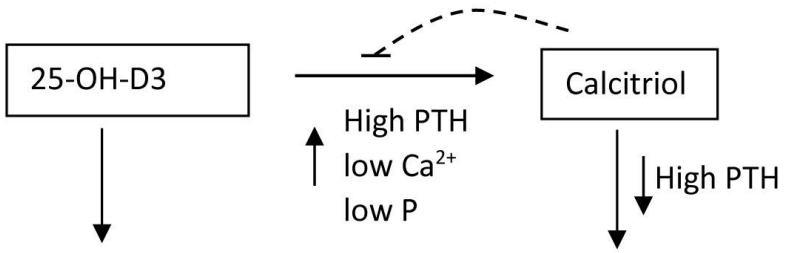

Figure 3.7 High PTH concentrations up-regulate calcitriol synthesis. Moreover, the synthesis rate is up-regulated under hypocalcemic or hypophosphatemic conditions. High PTH concentrations decrease the clearance rate of calcitriol.

3.6 INTRACELLULAR PHOSPHATE

In contrast to calcium, intracellular phosphate is not neglectable. In a 70kg person, around 15% or roughly 3.4 moles / 100 mMol of the total body phosphate content are intracellular (191). Only a small fraction of intracellular phosphate is free; most of it is complexed or bound to proteins or lipids. Phosphate ions attach and detach from different molecules as a response to phosphatases or kinases (103). Therefore, the free and complexed or bound intracellular phosphate pools are continually shifting.

Intracellular phosphate is essential for most cellular processes. For example, phosphate groups and sugar build the DNA and RNA backbone (223). The energy for many processes in cells is provided by adenosine triphosphate (ATP) and its hydrolysis and release of inorganic phosphate (122), and phosphorylation is an essential regulator of the activities of various proteins (103).

Since the intracellular concentration of phosphate is greater than the extracellular concentration, phosphate entry into cells requires an active transport (11, 13, 40, 117, 118). In (13), the authors reported that while plasma phosphate concentration spanned fourfold, the corresponding intramuscular phosphate concentration increased by only 70%. A similar effect was observed in erythrocytes indicating that the cells can buffer intracellular phosphate concentrations when extracellular concentration is disturbed.

The presence of a complex IC-ECF regulation is also observed during a hemodialysis session. While the amount of phosphate removed during an HD session increased linearly with time, Lemoine et al. (134) reported a three phasic decline in phosphate plasma concentration: a steep decline within the first 50 minutes of phosphate removal and a smaller decline within the next 100 minutes and a plateau region/recovery of phosphate concentrations for the remaining HD time. The same behavior - steep decline consistent with IC-ECF diffusion followed by a small decline/plateau region despite continuing phosphate removal - has been observed in other studies as well, e.g., (101, 211).

In many models of calcium and phosphate homeostasis, the authors assume a pure diffusion between intracellular and extracellular phosphate (45, 85, 174), e.g.

$$\frac{d}{dt}P_{ic} = k_p^{ic} \cdot P_p - k_{ic}^p \cdot P_{ic},$$

where ic denotes intracellular and p denotes plasma. The linear model implicates that a linear removal of phosphate from the plasma results in a linear decline in phosphate concentration (Fig. 3.8). These results are contradicting clinical findings (101, 134, 211). Moreover, the linear relationship cannot explain intracellular phosphate buffer capacity

regarding disturbances of plasma phosphate concentration (117).

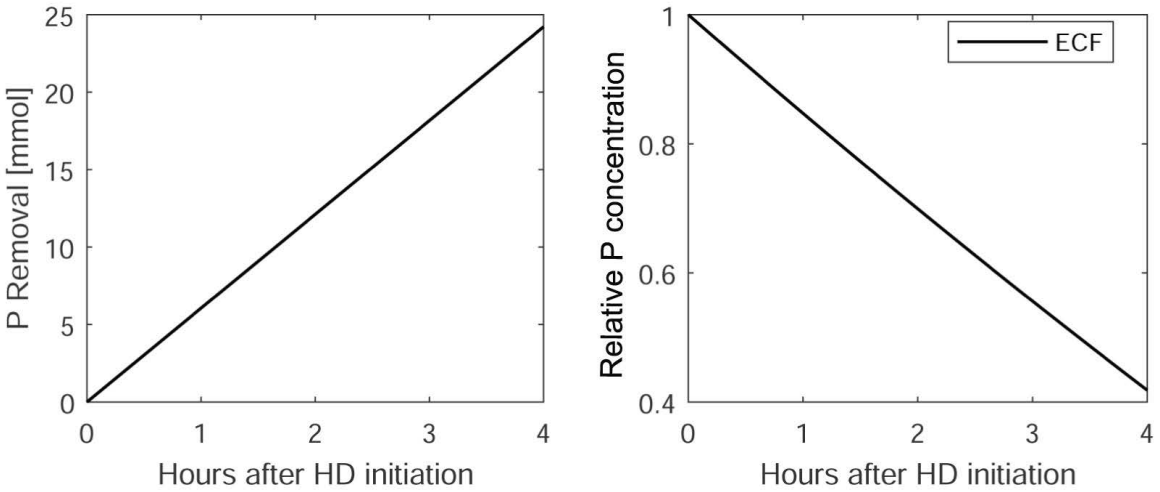

Figure 3.8 Predictions based on the simple diffusion model: Linear removal of phosphate during hemodialysis leads to a linear decline in plasma phosphate concentration.

Several more sophisticated models can be found in literature, mostly in the context of phosphate removal during hemodialysis. In (213), the authors used an undefined phosphate reserve, mobilized when phosphate reaches a patient's minimum. Another approach reported in (4) engaged two compartments. One compartment is an accessible pool from which phosphate is removed by dialysis. A second compartment is not directly accessible by dialysis, but phosphate is mobilized from the second to the first compartment. Spalding and co-workers (211) proposed a four-compartment model. The four compartments represent extracellular fluid, intracellular space, a third compartment allowing an additional flux to the ECF to maintain individual phosphate levels within a narrow range, and a hysteresis element located in the intracellular space preventing intracellular phosphate from decreasing below a certain threshold. An overview of current modeling phosphate during HD approaches is provided in a review by Laursen et al. (128).

3.7 CALCIUM-PHOSPHATE PRECIPITATION

Plasma calcium and phosphate can form $CaHPO_4$ and CaH_2PO_4 salts. Since most uremic patients develop hyperphosphatemia, calcium-phosphate precipitation is a major factor in this patient group and is associated with vascular calcification (150, 171). While human smooth muscle cells containing normal serum phosphate levels accumulate very little calcium, the presence of high phosphate levels ($\geq$ 2 mMol) triggers a significant increase in calcium deposition in *in-vitro* studies (113).

With $CaPO_4$, we denote the total concentration of calcium-phosphate salts. The formation of $CaPO_4$ is readily reversible under physiological conditions (143). Moreover, $CaPO_4$ is freely filtered by the kidneys and excreted or reabsorbed as calcium and phosphate. The plasma concentration of $CaPO_4$ is roughly 10% of the Ca^{2+}concentration (143). $CaPO_4$ can undergo four fates:

(1) $CaPO_4$ formation is reversed, and calcium and phosphate are released back to their respective plasma pools.

(2) Fetuin-A, a protein synthesized in the liver, binds the salts to form calciprotein particles (CPP), which are cleared swiftly (41, 99). CPP concentrations can be measured indirectly as the Fetuin-A reduction ratio (RR). In healthy subjects, RR is below the detection limit (210). In CKD, the RR rises to 12.4% ($\pm$ 7.3%) and in HD patients to 37.5% ($\pm$ 13.2%). Fetuin-A decreases with decreased kidney function. While the average concentration in healthy subjects reported in (210) was 0.28 g/l ($\pm$ 0.048 g/l), the concentration is reduced to 0.218 g/l ($\pm$ 0.036) in CKD patients and 0.167 g/l ($\pm$ 0.059 g/l) in HD patients. Therefore, as a first step, we assume that Fetuin-A is a function of GFR. At this stage, we ignore other inhibitors, such as pyrophosphate (PPi) (141).

(3) $CaPO_4$ can be spontaneously hydrolyzed to solid forms (165). We assume that the likelihood of hydrolyses is zero under physiological conditions. However, if the concentration of $CaPO_4$ is high, the chance that a part of $CaPO_4$ converts to calcification preforms is increasing (132). The conversion from $CaPO_4$ to calcification preforms is assumed to be irreversible; the corresponding compartment is called depot.

(4) $CaPO_4$ is freely filtered by the kidneys. Its renal excretion is governed by the renal excretion of $Ca^{2+}$and phosphate and part of the corresponding equations.

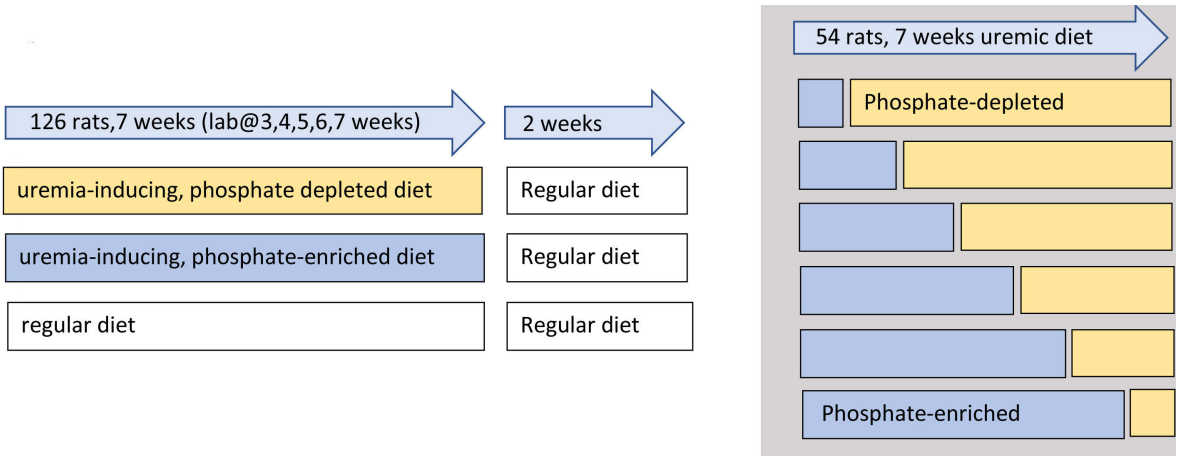

Figure 3.9 Experimental setup reported in (204). 126 rates were divided into three groups according to the diet they received for 7 weeks (uremia-inducing and phosphate depleted diet, uremia-inducing and phosphate enriched diet, or regular diet). Moreover, the authors studied 54 rats for 7 weeks fed a uremic-inducing and phosphate enriched diet for different periods before switching to the phosphate depleted diet.

Furthermore, we propose a hypothesis based on experimental results and as well as model predictions:
There is a point of no return for the formation of $CaPO_4$ under hyperphosphatemic conditions (204, 226). After this point, the formation process is detached from the actual phosphate and Ca^{2+}concentrations. This assumption is based on a study published in 2019, in which the authors studied 170 rats (204). 126 rats were either fed with a phosphate-enriched uremic diet, a phosphate-depleted uremic diet, or a regular diet for 7 weeks. The authors assessed aortic valve calcification at different time points. The authors also studied 54 rats that were first fed a phosphate-enriched diet for one to six weeks and subsequently switched to a phosphate-depleted diet to complete 7 weeks of uremic diet (Fig. 3.9). The results are the following:

- Osteoblast-like phenotype, inflammation, and eventually, valve calcification could only be observed in rats that were fed a phosphate-enriched diet.
- The authors observed significant valve calcification only if the animals were on the phosphate-enriched diet for at least four weeks.
- Valve calcification was only observed when the switch to phosphate-depleted regimen occurred after osteoblast markers and intracellular downstream signaling associated with vascular calcification have been found in the valve.
- Phosphate depletion did not affect valve calcification once osteoblast markers

were already expressed in valve tissue. However, at this time point, calcification was not yet apparent. Therefore, there seems to be a point of no return regarding the effect of hyperphosphatemia on vascular calcification, which occurs significantly before the clinical manifestation of vascular calcification.

If we assume that $CaPO_4$ eventually converts to calcification preforms, the results presented above justify a point of no return under hyperphosphatemic conditions for $CaPO_4$ formation.

This assumption is crucial for model predictions when it comes to cinacalcet. Clinical studies with HD patients reported that cinacalcet reduces PTH and Ca^{2+}levels, and lowers or even normalizes phosphate levels in HD patients, e.g., (19, 21). While the decline in PTH and Ca^{2+}levels can be predicted, the classical bone model cannot predict the phosphate decline. In healthy subjects, net calcium absorption is roughly 4 mmol/day, while around 15 mmol/day are released from the bone. In phosphate homeostasis, the net absorption is approximately 22 mmol/day; about 8 mmol/day are released from the bone. While mineral homeostasis is severely disturbed in stage 3-5 CKD patients (136), the flux of phosphate from the bone is determined by the flux of calcium from the bone and the stoichiometric ratio between calcium and phosphate in hydroxyapatite (102). Therefore, the reduction in PTH due to calcimimetics, resulting in a decline of osteoclastic activity, is sufficient for lowering Ca^{2+}levels but might not be enough to predict a decline in phosphate.

Recently, an article was published on the pre-print server bioRxiv (219) investigating vascular calcification. The authors argued that calcifying arteries change the systemic disposition of phosphate, i.e., substantial phosphate is actively recruited by calcification processes. This argument would translate to the point-of-no return hypothesis.

3.8 BONE

The bone is the primary storage for calcium and phosphate. Approximately 99% of calcium and roughly 85% of phosphate is stored in the bone, mostly in the form of hydroxyapatite crystals ($Ca_{10}(PO_4)_6(OH)_2$) (165, 173). In adults, the percentage weight of calcium in the bone is roughly 37-38%; the percentage weight of phosphate is around 16.5% (162).

The bone is continuously remodeled. The rate of bone turnover is about 4% in cortical bone and approximately 28% in the trabecular bone (148). Since about 75% of the skeleton consists of cortical bone and 25% of trabecular bone, the skeleton's turnover rate is approximately 10% per year (148). A specific location is remodeled every 2-5 years (148). The remodeling process provides continuous regeneration of the bone; it also plays an essential role in regulating phosphate and calcium homeostasis. The remodeling process involves four steps (46, 173):

(1) Activation of osteoclast precursor from the circulation.

(2) Osteoclast-mediated bone resorption, thereby releasing calcium and phosphate from the bone to the extracellular fluid. The resorption phase about 2-4 weeks. At the end of the resorption phase, osteoclasts undergo apoptosis.

(3) Recruitment of pre-osteoblasts.

(4) Formation of new bone via osteoblasts within 4-6 months. Osteoblasts synthesize a new collagen structure and regulate the mineralization of the matrix. Osteoblasts trapped within the matrix become osteocytes with a life-span of approximately 50 years. The remaining osteoblasts undergo apoptosis after bone formation. Therefore, the mean life-span of active osteoblasts is roughly 3 months (148).

Any imbalance in the remodeling process may reduce bone mineral density associated with an increased risk of fracture and cardiovascular calcification in hemodialysis patients (5).

Many different factors regulate bone resorption, formation, and mineralization. A comprehensive table of these factors is provided in (205). The central regulators relevant for the model are the following (Fig. 3.10):

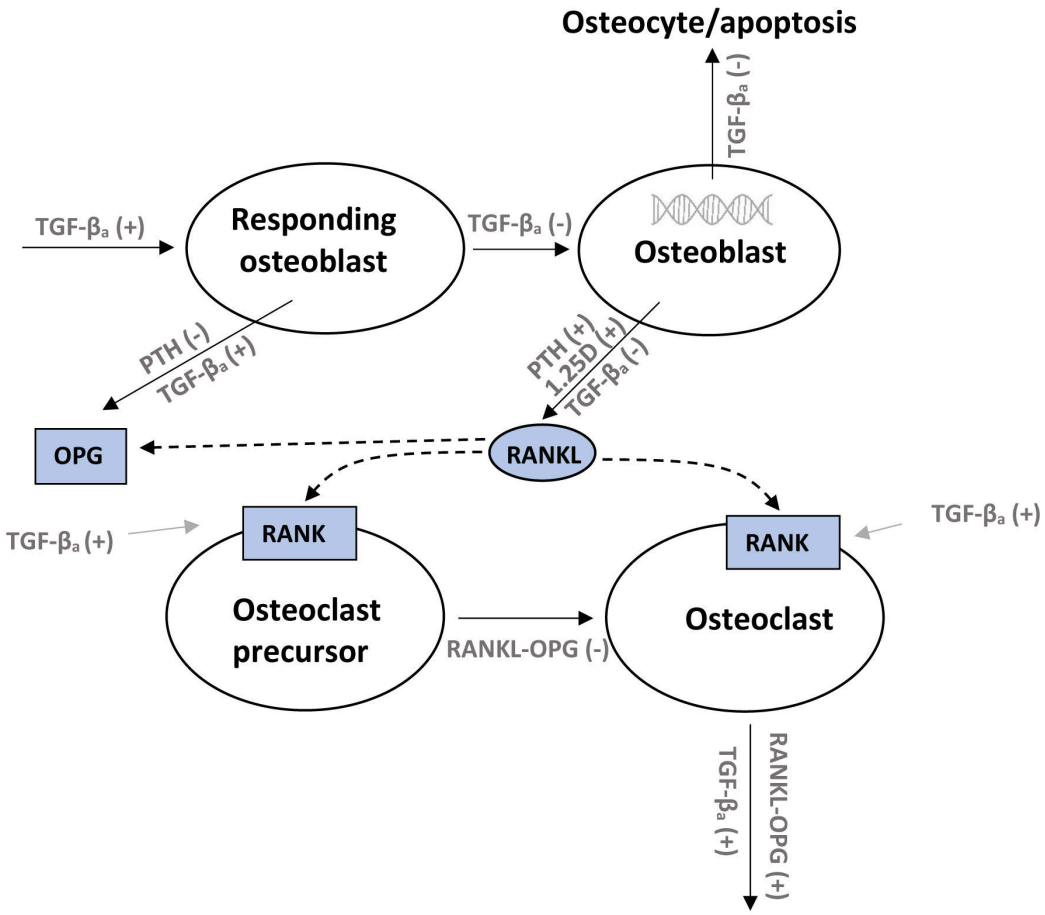

Figure 3.10 RANK-RANKL-OPG regulation of bone turnover. Intracellular regulation regulating osteoblastic apoptosis comprises Runx-2-CREB-Bcl-2 axis.

- Osteoclast recruitment and resorption phase: RANK-RANKL-OPG
  RANKL (Receptor activator of nuclear factor kappa-B ligand) is a protein expressed by osteoblasts (25, 73, 120, 215, 221). RANK (Receptor activator of nuclear factor kappa-B) is a receptor for RANKL. RANK is located on osteoclast precursors and mature osteoclasts (25, 73, 120, 215, 221). Briefly, osteoblasts release RANKL. The binding of RANKL to RANK initiates the differentiation of osteoclast precursors to osteoclasts (25, 73, 120, 215, 221). Mature osteoclasts express RANK receptors as well. The binding of RANKL on the RANK receptor results in the activation of mature osteoclasts.

  Also, osteoblasts express osteoprotegerin (OPG) (104, 120), which acts as a decoy receptor for RANKL. OPG which binds RANKL with an around 500-fold higher affinity than RANK (104, 163). Therefore, OPG prevents the binding of RANKL to

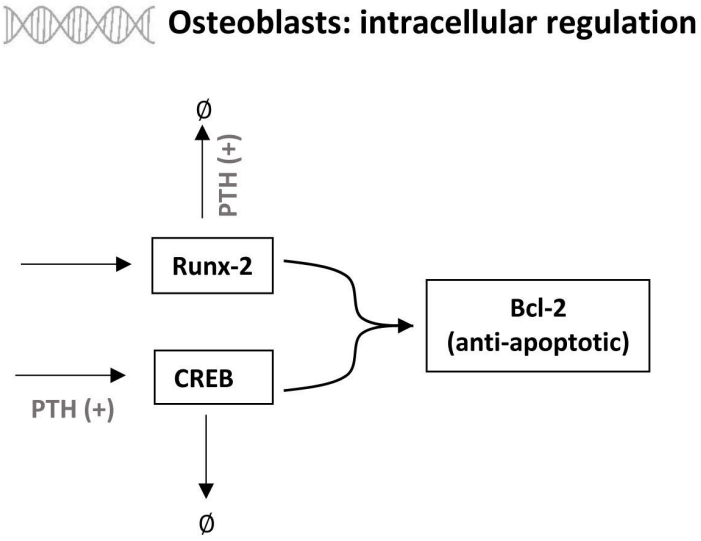

Figure 3.11 Intracellular regulation of osteoblastic apoptosis. PTH enhances the expression of CREB and the synthesis of Runx-2 degrading enzymes. The effect on CREB is kinetically faster than the effect on Runx-2 degradation. CREB and Runx-2 are critical for activating survival genes and synthesizing the anti-apoptotic protein Bcl-2.

RANK and is protective against bone resorption.

A key regulator of the RANK-RANKL-OPG interplay is PTH (74, 144). While it has no direct effect on osteoclasts, PTH stimulates bone resorption via the enhanced synthesis of RANKL and the inhibitory effect on OPG synthesis (74, 144). Besides, calcitriol increases RANKL release, thereby stimulating bone resorption (121, 161, 227).

- Formation phase: Runx2-CREB-Bcl-2
  Continuous administration of PTH stimulates bone resorption, whereas intermittently administered PTH stimulates bone formation (7). In mice, daily injections of PTH decreased osteoblast apoptosis, thereby increasing the number of osteoblasts (7) while the number of osteoclasts was not affected. In (7), the authors showed that PTH increases the transcription of the survival gene B-cell lymphoma 2 (Bcl-2) by the enhanced synthesis of the transcription factors cAMP response element-binding protein (CREB) and runt-related transcription factor 2 (Runx2). However, Runx2 is also a key regulator in osteoblastic differentiation (225), and PTH enhances its proteolysis. Therefore, PTH's anti-apoptotic effect is only present as long as PTH has not significantly decreased Runx2 via proteasomal proteolysis.

- Coupling between resorption and formation phase: Transforming growth factor-beta (TGF-β)

  TGF-β is essential for the coupling of bone resorption by osteoclasts and bone formation by osteoblasts. It is synthesized in a latent form and stored in the extracellular matrix (115). Its activation is regulated by osteoclastic bone resorption (51, 115, 178). Active TGF-β promotes early differentiation and proliferation of osteoprogenitors while inhibiting the transition of osteoblasts into osteocytes.
  Moreover, active TGF-β increases OPG expression and down-regulates RANKL expression. It also increases RANK expression, thereby stimulating osteoclast maturation in isolated bone cells (107, 115).

Other prominent factors are calcitonin and estrogen. If the model was to be applied to study osteoporosis in older women, estrogen has to be included in the model.

3.8.1 Phosphate and calcium homeostasis

Bone is a crucial regulator of phosphate and calcium homeostasis. During bone resorption, calcium and phosphate are released from the bone to the extracellular fluid (EFC) (46). During bone resorption, calcium and phosphate are used for mineralization of the newly formed tissue matrix. The exchange rate between bone and ECF due to bone resorption and formation is about 10 -15 mmol calcium per day.

In addition to these slow processes, there is a rapid regulation of Ca^{2+}via an exchange mechanism between plasma and pool. It has been hypothesized that a labile calcium pool on the bone surface can either rapidly supply calcium in acute hypocalcemia or store excess calcium (175). The basal exchange rate between the extracellular fluid and the labile calcium pool is supposedly around 150 mmol daily(175). Therefore, the flux between the ECF and the labile and stable bone pools dramatically exceeds all other fluxes (both net absorption and renal excretion are approximately 4 mmol daily), showing the bone's importance for calcium and phosphate homeostasis. Since the dominant form of calcium and phosphate in the bone is hydroxyapatite, the ratio of calcium and phosphate released by bone resorption is approximately 10/6 (148, 165).

3.9 FGF-23

Another regulator of phosphate and calcium homeostasis in healthy subjects is fibroblast growth factor 23 (FGF-23) (114, 116, 201). FGF-23 down-regulates renal phosphate reabsorption. Since there is a negative feedback loop with calcitriol, FGF-23 indirectly regulates intestinal phosphate and calcium absorption (140, 177, 200). Moreover, there is a negative feedback loop between PTH and FGF-23 since FGF-23 inhibits PTH secretion and synthesis (9) whereas PTH stimulates FGF-23 (116).

At the onset of CKD, FGF-23 might prevent hyperphosphatemia by promoting phosphaturia and down-regulating calcitriol (87, 105). However, in patients suffering from end-stage renal disease, renal phosphate excretion becomes negligible, and the role of FGF-23 is not clear. In hemodialysis patients, FGF-23 levels are frequently elevated by factor 100. Despite these high levels, most of these patients develop severe secondary hyperparathyroidism (123). Furthermore, Mace and co-workers (145) showed that while FGF-23 inhibits PTH synthesis and secretion in normocalcemia, it does not have a lowering effect during hypocalcemia when high PTH levels are needed to resolve the condition. Summarizing, FGF-23 has a crucial role in phosphate homeostasis in healthy subjects. However, due to the decline in kidney function and the failing down-regulation of PTH, it will most likely be less important in hemodialysis patients. Therefore, FGF-23 is omitted in this model.

3.10 CURRENT MODEL APPROACHES

The system of regulators of calcium and phosphate homeostasis is multi-dimensional. Furthermore, various subsystems act significantly different timescales. Since the control loops are interwoven, a small change in one subsystem triggers a cascade of (patho)physiological effects in other dimensions.

Due to the complexity of mineral homeostasis, there have been several approaches to translating the regulators' key features into mathematical models to gain inside into the multi-dimensional system. Various approaches include models of subunits such as PTH release in response to calcium changes (32, 157, 203) or the prediction of phosphate concentrations as a response to phosphate removal during hemodialysis (4, 128, 213). Moreover, there are several mathematical models of bone formation and bone resorption based on RANK-RANKL-OPG interaction and PTH (126, 133).

There are also comprehensive calcium and phosphate homeostasis models, including many key regulators (45, 85, 174, 181). In 2002, Raposo et al. proposed an 11-compartment model, including the intestine, bone, kidney, and parathyroid gland (45). The authors modelled the effect of calcitriol on bone turnover but not on intestinal absorption. The main issue is that the authors assume that renal calcium excretion is inhibited by calcium and increased by calcitriol. The complex interplay between osteoblasts and osteoclasts is not taken into account.

Peterson and Riggs chose a more elaborate approach (174). In 2010 they published a calcium and phosphate homeostasis model consisting of 28 coupled ordinary differential equations (174). The model included a detailed description of the bone regulation based on the RANK-RANKL-OPG axis, including TGF-β as well as the Runx2-CREB-Bcl2 axis. They predicted that intermittently administered PTH would result in bone formation, while constantly elevated PTH concentrations would result in bone resorption. However, they did not take the phosphaturic effect of PTH into account. Moreover, the authors assumed that osteoclasts are regulated by the relative expression of RANKL*RANK instead of the relative expression of RANKL*OPG. The authors employed an interchangeable or fast calcium/phosphate pool and a slow calcium /phosphate pool. However, they assumed that calcium and phosphate diffuse between the slow and the fast pool, and bone resorption and formation are responsible for around 10% exchange between the ECF and the fast pool. Besides, the feedback of calcium on renal calcium reabsorption and calcium-phosphate precipitation is missing.

A model based on (174) published in 2014 studied the effect of vitamin D deficiency and simulated, for example, primary hyperparathyroidism (45). However, their simula-

tions predicted hypocalciuria instead of hypercalciuria in primary hyperparathyroidism.

Recently, Granjon et al. published a comprehensive calcium and phosphate homeostasis model in rats (85). The model included calcium-protein binding, sodium-phosphate complexes, calcium-phosphate precipitation, Fetuin-A, and CPPs, as well as FGF-23 and a more detailed description of renal phosphate and calcium handling. However, they did not model bone resorption and formation in detail. Moreover, the parathyroid gland's description is not sophisticated enough to capture parathyroid gland biology's adaptation mechanisms. Finally, intracellular-extracellular phosphate exchange is linear, not reflecting clinical results (128).

3.11 AIM OF THESIS

The aim of this thesis was to translate the critical properties of the regulators of calcium and phosphate homeostasis into mathematical models to allow the study of CKD-MBD development. Since the models should be physiology-based, adaptation to different scenarios, such as lifestyle changes regarding phosphate reduced diet, should be straight forward.

The main focus lied on a sophisticated model of parathyroid gland biology as well as bone metabolism. The models should predict clinical or experimental manifestation in acute and chronic disturbances of calcium and phosphate homeostasis. In particular, the model should predict the development of chronic kidney disease-bone mineral disorder (CKD-MBD) in patients suffering from end-stage renal disease. The hallmarks of CKD-MBD is secondary hyperparathyroidism, PTG hyperplasia, bone loss, and vascular calcification. Moreover, we indicated possible future applications by conducting a virtual clinical trial regarding the off-label use of cinacalcet.

In contrast to previous models, we proposed a detailed mathematical model of PTG biology, including varying adaptation mechanisms acting on different timelines (seconds to years). Moreover, we used a detailed bone model, including key-regulators of basic multicellular units (BMU). We introduced a new approach for intracellular- extracellular phosphate regulation based on physiological assumptions. Finally, we introduced a new hypothesis involving the point of no return for calcium-phosphate precipitation. We performed a sensitivity analysis for critical model parts.

In chapter 4, we introduce the translation of crucial physiological properties into mathematical models. If possible, we provide the validation or results of stand-alone sub-models, such as the parathyroid gland model. In chapter 5, we present the results of the integrated bone and mineral metabolism model. In chapter 6, we discuss possible shortcomings for our approach and future steps.

4 Mathematical models

All simulations were performed with Matlab 2017b (Mathworks) with default 16 digits of precision. The time discretization for the numerical differential equations solver (ode23s) was in general in the order of a second. To increase numerical stability, all derivatives with an absolute value smaller than 10^{-10} were set to zero. We used the method of least squares for all parameter estimations.

4.1 PARATHYROID GLAND

As discussed in the introduction, it is not sufficient to know the current calcium, phosphate, and calcitriol concentrations to determine the system's state, and we need to know the whole history of the condition (Fig. 3.1). The key to overcoming this obstacle is to model the condition of the CaSR in response to different stimuli. We published the model and its critical predictions in (192).

4.1.1 CaSR expression

A structural CaSR model would involve activation of the receptor, G-protein binding, ligand binding, structural changes of the G-protein, and the intracellular signaling cascade. The black-box model is a dose-response model (2, 28, 185, 198). Since the exact mechanisms of CaSR signaling are still a matter of debate, we choose a stimulation based model which can be validated by experimental or clinical data. Moreover, the model can be easily adjusted to various genetic pathologies, e.g., (98, 164).

Therefore, the PTG model's core is the dimensionless CaSR expression ($CaSR$) and the dimensionless VDR expression (VDR). These functions govern the receptors' sensitivity to $Ca^{2+}$and calcitriol concentrations and thereby PTH release and PTG adaptation mechanism if a steady state is disturbed. The optimal value is set to 1 for both variables; values lower than 1 correspond to a loss of CaSR or VDR expression.

Receptor expressions are up-regulated by the positive feedback between the two receptors and high levels of $Ca^{2+}$and calcitriol. High levels of phosphate suppress the expression. However, alterations in Ca^{2+}, calcitriol, and phosphate plasma levels do not alter the receptor expression immediately. Instead, alterations have to be present for a critical amount of time (31, 80, 187). Therefore, we need a mathematical model that includes delays accounting for the necessary amount of time for the system's reaction to

disturbances in Ca^{2+}, calcitriol, and phosphate. Moreover, we want to filter input signals such that resolved disturbances within the necessary amount of time do not change receptor expression.

Therefore, we assume that $CaSR$ are VDR, are governed by the following system of differential equations:

$$\frac{dCaSR}{dt} = p_{Ca} \cdot (Ca^{in} + (VDR - 1) - P^{in}) \cdot CaSR + n_{Ca} \cdot (1 - CaSR) \tag{4.1}$$

$$\frac{dVDR}{dt} = p_D \cdot (D^{in} + (CaSR - 1) - P^{in}) \cdot VDR + n_D \cdot (1 - VDR) \tag{4.2}$$

$$\frac{dCa^{in}}{dt} = (\mathrm{stim}_C(C - Ca_{opt}) \cdot \big(1 - \mathrm{sign}(\mathrm{stim}_C(C - Ca_{opt}))Ca^{in}\big) - Ca^{in}) \cdot \tau_C \tag{4.3}$$

$$\frac{dD^{in}}{dt} = (\mathrm{stim}_D(D - D_{opt}) \cdot \big(1 - \mathrm{sign}(\mathrm{stim}_D(D - D_{opt}))D^{in}\big) - D^{in}) \cdot \tau_D \tag{4.4}$$

$$\frac{dP^{in}}{dt} = (\mathrm{stim}_P(P - P_{opt}) \cdot \big(1 - \mathrm{sign}(\mathrm{stim}_P(P - P_{opt}))P^{in}\big) - P^{in}) \cdot \tau_P \tag{4.5}$$

where Ca_{opt}, D_{opt}, and P_{opt} are the individual optimal serum values of Ca^{2+}, calcitriol, and phosphate. C, D and P are plasma Ca^{2+}, calcitriol, and phosphate concentration, respectively. The time constants $\tau.$ are associated with the critical time after which the system starts to react to stepwise changes in Ca^{2+}, calcitriol, or phosphate. The relationship between p and n determines the system's equilibrium value, while p governs the intensity of the stimulus. Ca^{in}, D^{in}, and P^{in} are factors determining the effect of the stimulus on the $CaSR$ and VDR.

Under healthy conditions, the stimulus functions,

$$\mathrm{stim}_\lambda(x) = \frac{1}{1 + \exp(-K_\lambda(x - \lambda_1))} + \frac{1}{1 + \exp(-K_\lambda(x + \lambda_1))} - 1, \quad \text{and} \quad \lambda \in (C, D, P),$$

with constants K and λ_1, are zero and CaSR and VDR expressions are not altered. Moreover, if a deviation from the optimal value is present shorter than the critical time associated with the time constants, the stimulus will be too small to change Ca^{in} significantly. In this case, CaSR and VDR expressions are not altered either. However, if there is a chronic deviation from the optimal value, even a slight one, CaSR expression

will slowly change. The stimulus function is depicted in Fig. 4.1.

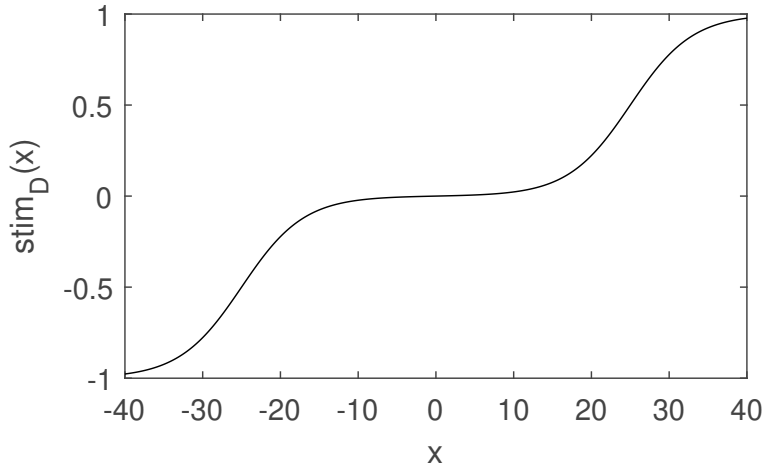

Figure 4.1 Exemplar stimulus function ($\lambda = D, D_1 = 25$ pMol, $K_D = 0.25$ 1/pMol). The slope around $x = 0$ is small to account for the presence of insignificant fluctuations around the optimal value. The function is approaching 1 or -1 for large deviations.

4.1.2 CaSR and VDR sensitivity

It is not the measured Ca^{2+}level that determines the response of the PTG but the sensed calcium concentration CS. If the receptor expression is reduced, the receptor's sensitivity to $Ca^{2+}$is decreased (82, 194). We model the sensed calcium and calcitriol concentration via the following equations:

$$\frac{dCS}{dt} = \text{sens}(CaSR + VDR) \cdot C - CS \tag{4.6}$$

$$\frac{dDS}{dt} = \text{sens}(CaSR + VDR) \cdot D - DS \tag{4.7}$$

$$\text{sens}(x) = A_S + (1 - A_S) \cdot \frac{x}{2} \tag{4.8}$$

C is the actual (measured or simulated) plasma ionized calcium concentration and D is the actual (measured or simulated) calcitriol concentration. CS and DS are calcium and calcitriol concentrations sensed by CaSR and VDR. At a healthy steady state, $CaSR$ and VDR are equal 1, and CS and DS equilibrates to C and D. If CaSR expression starts to decline, CS declines as well but with a pre-defined delay. This effect is fully reversible

if the stimulus returns to optimal levels again, e.g., in the case of a low phosphate diet, calcitriol therapy or therapy with calcimimetics.

4.1.3 CaSR signaling

CS, the sensed calcium concentration, and the phosphate concentration (P) directly govern the CaSR signaling cascade (206).

$$\frac{dC_\lambda}{dt} = p_\lambda \cdot (Ca_\lambda^{in} - P_\lambda^{in}) \cdot C_\lambda + n_\lambda \cdot (1 - C_\lambda), \tag{4.9}$$

$$\frac{dCa_\lambda^{in}}{dt} = \left(\mathrm{stim}_{Ca}(CS - Ca_{opt}) \cdot \left(1 - \frac{\mathrm{stim}_{Ca}}{|\mathrm{stim}_{Ca}|} Ca_\lambda^{in}\right) - Ca_\lambda^{in}\right) \cdot \tau_{Ca}^\lambda, \tag{4.10}$$

$$\frac{dP_\lambda^{in}}{dt} = \left(\mathrm{stim}_P(P - P_{opt}) \cdot \left(1 - \frac{\mathrm{stim}_P}{|\mathrm{stim}_P|} P_\lambda^{in}\right) - P_\lambda^{in}\right) \cdot \tau_P^\lambda. \tag{4.11}$$

Again, p_λ and n_λ determine the steady state of the system. The time constants $\tau_\star^\lambda$ determine the critical time with which the system responses to the stimulus. These set of equations is used for all PTG adaptation mechanisms: intracellular degradation rate ($\lambda = d$), synthesis rate ($\lambda = p$), and cellular proliferation rate ($\lambda = pr$).

Cellular degradation rate

Under healthy conditions, the cellular degradation k_d is kept at a basal rate of A_d. If not regulated by the CaSR, the degradation rate will decrease to a minimum rate of $B_d = 0.5 \cdot A_d$ (33):

$$k_d = \begin{cases} B_d + (A_d - B_d) \cdot C_d & \text{for } C_d < 1 \\ A_d & \text{else} \end{cases} \tag{4.12}$$

PTH synthesis rate

Under healthy conditions, the synthesis rate of PTH is kept at a basal rate of A_p. If not regulated by the CaSR, the synthesis rate k_p will increase within minutes to hours to a maximum level of $B_p = 3 \cdot A_p$ (33):

$$k_p = \begin{cases} B_p + (A_p - B_p) \cdot C_p & \text{for } C_p < 1 \\ A_p & \text{else} \end{cases} \tag{4.13}$$

Cellular proliferation rate

If not down-regulated by the CaSR, the cellular proliferation rate k_{pr} increases from the basal level A_{pr} to a maximum rate of $B_{pr} = 2 \cdot A_{pr}$ (217, 224):

$$k_{pr} = \begin{cases} B_{pr} + (A_{pr} - B_{pr}) \cdot C_{pr} & \text{for } C_{pr} < 1 \\ A_{pr} & \text{else} \end{cases} \tag{4.14}$$

4.1.4 Glandular cells

Parathyroid gland cells cycle through the two states. Therefore, we employ two cell population in our mathematical model, cells in the quiescent state Q and secretory active cells S. Only cells in the quiescent state can undergo apoptosis or proliferate. If untreated, pathologic conditions resulting in SHPT and hyperplasia; the glandular volume will continue to increase. We capture this behavior by a tumor model with dynamic carrying capacity K (10, 184). The carrying capacity represents the gland vasculature. We assume that the carrying capacity is proportional to the PTG surface and the number of cells corresponds to the volume. Therefore, we formulate the PTG model by the following set of equations:

$$\frac{dS}{dt} = -k_{SQ}S + k_{QS}Q, \tag{4.15}$$

$$\frac{dQ}{dt} = k_{SQ}S - k_{QS}Q - k_aQ + k_{pr}Q\ln\left(K/(S+Q)\right), \tag{4.16}$$

$$\frac{dK}{dt} = k_k((S+Q)/(S(0)+Q(0)) - 1)_+^{2/3}. \tag{4.17}$$

The constants k_{SQ} and k_{QS} govern the cell cycle between the secretory active and quiescent state, and k_a is the constant apoptosis rate. The constant k_k determines how fast the carrying capacity K adjusts to the gland's size.

4.1.5 Parathyroid hormone

The relationship between between Ca^{2+} and PTH release rate is sigmoidal (68, 86, 224). Here, we employ a two-compartment model allowing the storage of PTH in the gland (32, 157, 181, 196, 203):

$$\begin{aligned} \frac{dPTG}{dt} &= k_p S - \text{release}(CS)PTG - k_d PTG, && (4.18)\\ \frac{dPTH}{dt} &= \text{release}(CS)PTG - k_{cl} PTH, && (4.19)\\ \text{release}(CS) &= B + (A-B)\frac{1}{1+(CS/S_r)^m}. && (4.20) \end{aligned}$$

PTG and PTH are the amounts of PTH in the gland serum, respectively. The release function is a classical Hill function. These types of functions are widely used to analyze ligand-receptor interactions and can be derived from the mass-balance equation for the concentration of free CaSR and CaSR activated by the binding of Ca^{2+}. The constant m corresponds to the number of Ca^{2+}atoms binding to one CaSR in order to activate the receptor. S_r is the nth-root of the dissociation equilibrium constant of the CaSR and Ca^{2+}reaction. A value of around 1.18 mMol ensures that PTG reacts quickly by releasing a high amount of pre-formed PTH in the case of a drop in Ca^{2+} or by suppressing the release of PTH in the case of excess Ca^{2+} concentrations in healthy subjects. In hemodialysis patients with pathological phosphate and calcitriol levels, CaSR sensitivity is reduced and, therefore, the release function is shifted. A shift in the set-point S_r has the same effect. Consequently, the gland cannot react appropriately to normal Ca^{2+}levels. If the CaSR sensitivity (i.e., expression) is significantly reduced, even higher Ca^{2+}concentrations might not be enough to suppress PTH release.

4.1.6 Parameters and sensitivity analysis

Most parameters are based on literature (Table 4.1). All parameters associated with the stimulus functions (Equations (4.1),(4.2),(4.6), and (4.9)) had to be estimated. We chose

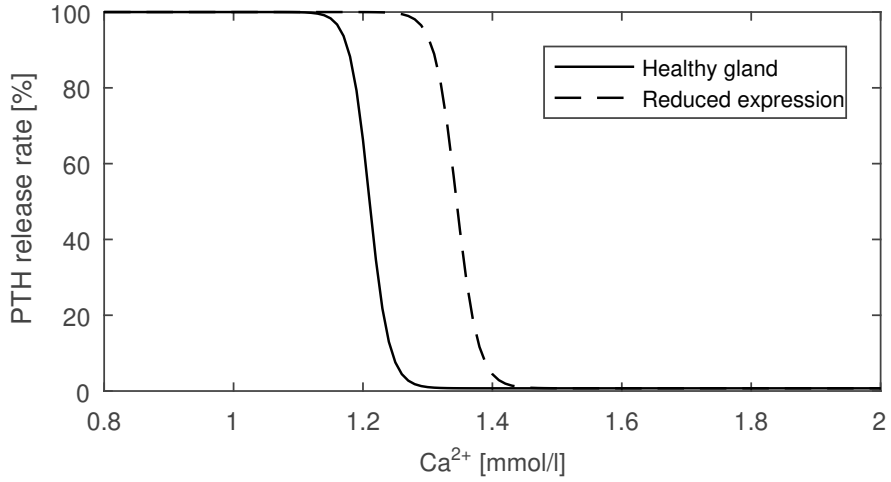

Figure 4.2 From Schappacher-Tilp et al. (192) under CC-BY. PTH release rate as a function of Ca^{2+}. Reduced sensitivity of the CaSR results in a shift of the release function. In this example, CS equals 90% of the actual ionized calcium concentration.

basic parameters for the stimulus functions (table 4.2) based on the following criteria:

- The derivative of the stimulus function is maximal around the critical values (Ca^{2+}(arterial blood ionized calcium): 1.4 mMol, calcitriol: 270 pMol, P: 2.2 mMol).
- The mean derivative in the reference range (Ca^{2+}: 1.15-1.35 mMol, calcitriol: 52-266 pMol, P: 0.84-1.45 mMol) is smaller than 0.08 for $Ca^{2+}$and P and 0.0035 for calcitriol (which is less controlled than $Ca^{2+}$and phosphate levels).

We chose the time constants such that the system reacts to stepwise changes in Ca^{2+}, phosphate, or calcitriol concentrations at the pre-defined critical time (Table 4.3). All adaptation mechanisms but cellular proliferation reach steady state. Therefore, only the time constant associated with cellular proliferation is of interest for long-term predictions. We assessed the sensitivity of the system to estimations of this time constant by multiplying or dividing the base values in equations (4.10) and (4.11) one at a time by a factor of 10. All other parameters were kept constant. The setting we chose for the sensitivity analysis was mild hypocalcemia and hyperphosphatemia, a scenario likely in CKD patients. The analysis of the corresponding PTH values revealed that the system does not react critically to changes in the time constants.; the difference in PTH is below 0.003% for changes in Ca^{2+}related values and 0.009% for changes in phosphate related values after 30 days.

Moreover, we assessed the system's sensitivity to uncertainties in estimating the intensities of the stimulation functions. In this case, base values were either multiplied

Table 4.1 Basic set of parameters for PTG biology

Compartment	Parameter	Value	Source
PTG	k_{SQ}	$2{\cdot}10^{-3}$ /min	(182)
	k_{QS}	$5{\cdot}10^{-4}$ min^{-1}	(182)
	k_p^0	$3{\cdot}10^{-3}$ /min	(224)
	k_a	0.001 min^{-1}	(224)
PTH release	A	0.12 pmol/min	(203)
	B	0.001 pmol/min	(203)
	S_r	1.1881 mMol	(203)
	m	50	(203)
Clearance	k_c	0.632/min	(203)
Degradation	A_d^0	0.012/min	(203)
Production	A_{pr}	132	(203)
Proliferation	A_p	0.003/min	(75)
	k_k	$5 \cdot 10^{-5}$	

At steady state, the fraction of active cells is 0.2.
The parameter k_{QS} was chosen accordingly.

or divided by a factor 2 one at a time. All other parameters were kept constant. The simulation scenario was normocalcemia, the onset of hyperphosphatemia, and a decline in calcitriol levels. The highest sensitivity was observed regarding changes in the parameters associated with the PTH degradation rate (Equations (4.9) and (4.13)). Moreover, the system was sensitive to changes of parameters associated with the CaSR (Equations (4.1) and (4.2)) which determine the steady state of the CaSR expression. The results are depicted in Fig. 4.3.

4.1.7 Results

We compared our model predictions with experimental or clinical data provided in the literature. Specifically, we were interested in the reaction of the system under prescribed disturbances, i.e.

- Rate dependency of PTH response to acutely induced hypocalcemia
- Mild but chronic hypocalcemia
- Hysteresis effects under subsequent hypocalcemic cycles

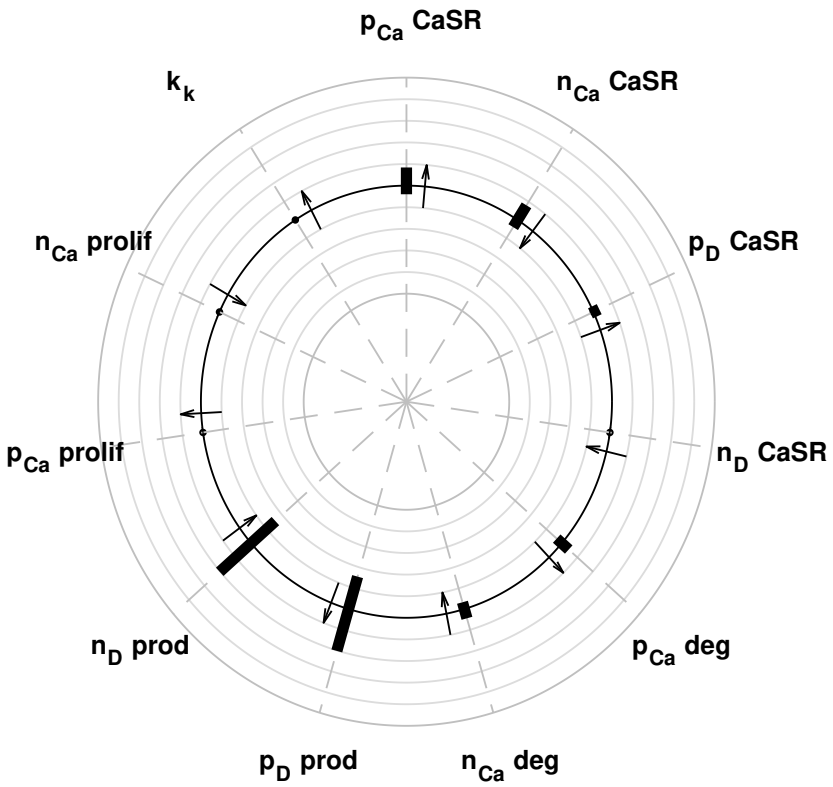

Figure 4.3 From Schappacher-Tilp et al. (192) under CC-BY. The maximum deviation from reference PTH values depicted as the ratio between the calculated PTH and the reference PTH. The inner-circle denotes a relative deviation of 0.5, the outer-circle a relative deviation of 1.5. If the arrows point outward, higher parameter values imply higher PTH values. If the arrows point inward, higher parameter values imply lower PTH values. Parameters were either multiplied by 2 or 0.5.

Table 4.2 Basic set of parameters for the stimulation functions.

	Parameter	Value
Optimal Values	C	1.2 mMol
	P	1.2 mMol
	D	90 mMol
Stimulus	C_1	0.5 mMol
	K_C	2 1/mMol
	D_1	30 pMol
	K_D	0.2 1/pMol
	P_1	0.8 mMol
	K_P	0.8 1/mmol

- effect of low phosphate diet on PTH

4.1.8 Rate dependency of PTH response to acutely induced hypocalcemia

Various studies have shown that PTH release depends on the rate of Ca^{2+}reduction (27, 48, 68, 86, 195). While a high rate of Ca^{2+}change will lead to a significant overshoot in PTH release, this effect is not observed if $Ca^{2+}$is changed at a low rate (27, 48, 68, 86, 195). More specifically, a significant linear drop of 1.6 mg/dl Ca^{2+}within 30 minutes in dogs produced a significant peak in PTH concentration (68). When Ca^{2+}concentration dropped by the same amount but within 120 minutes, there was no dramatic overshoot observable, but PTH concentrations after 60 minutes were higher than those from the high rate (68). The same results were reported in a study with rats (195). Moreover, when Ca^{2+}levels were slowly decreased in renal patients, there was no PTH overshoot observed either (152).

We assess the system's reaction to the rate of change of $Ca^{2+}$by starting from the system steady state and prescribing different changes of Ca^{2+}concentrations. Since PTH is stored in secretory active cells, the fast induction of hypocalcemia will result in an overshoot due to the quick release of stored PTH. Slow induction of hypocalcemia will eventually lead to the same steady state level but with a significantly smaller PTH overshoot (Fig. 4.4).

Table 4.3 Time constants and intensity parameters for stimulation functions.

Compartment	Parameter	Value
Degradation	τ_{Ca}	10^{-2}
	τ_P	$5 \cdot 10^{-2}$
	p_{Ca}	2.5
	n_{Ca}	0.5
Production	τ_{Ca}	10^{-3}
	τ_P	10^{-3}
	p_{Ca}	25
	n_{Ca}	0.5
Proliferation	τ_{Ca}	10^{-5}
	τ_P	10^{-4}
	p_{Ca}	5
	n_{Ca}	0.5
Expression	τ_{Ca}	10^{-4}
	τ_P	10^{-1}
	τ_D	10^{-4}
	p_{Ca}	$5{\cdot}10^{-4}$
	n_{Ca}	$5{\cdot}10^{-4}$
	p_D	$5{\cdot}10^{-7}$
	n_D	$5{\cdot}10^{-7}$

4.1.9 Mild but chronic hypocalcemia

Due to our model's structure, all PTG adaptation mechanisms will be present under mild but chronic hypocalcemia (Fig. 3.1). Specifically, we would observe the effects of decreased intracellular degradation within minutes (197) and increased synthesis rate within hours (89). Due to the enhanced proliferation rate, PTH concentration will not reach a steady state. To simulate chronic hypocalcemia, we prescribed a decrease in Ca^{2+}concentration by 0.25 mg/dl (0.0624 mmol/l) and kept Ca^{2+}concentration at this value for 200 days (Fig. 4.5).

4.1.10 Hysteresis effects under subsequent hypocalcemic cycles

PTH release shows hysteresis effects under subsequent hypocalcemic cycles. In (196), the authors quickly induced hypocalcemia within 30 minutes. After another 30 minutes, $Ca^{2+}$was briefly returned to normal values before another hypocalcemic condition was induces. During the first hypocalcemic condition, PTH levels increased dramatically. However, the authors could not observe another transient peak during the second hypocalcemic condition. We mimic the experimental protocol by prescribing comparable

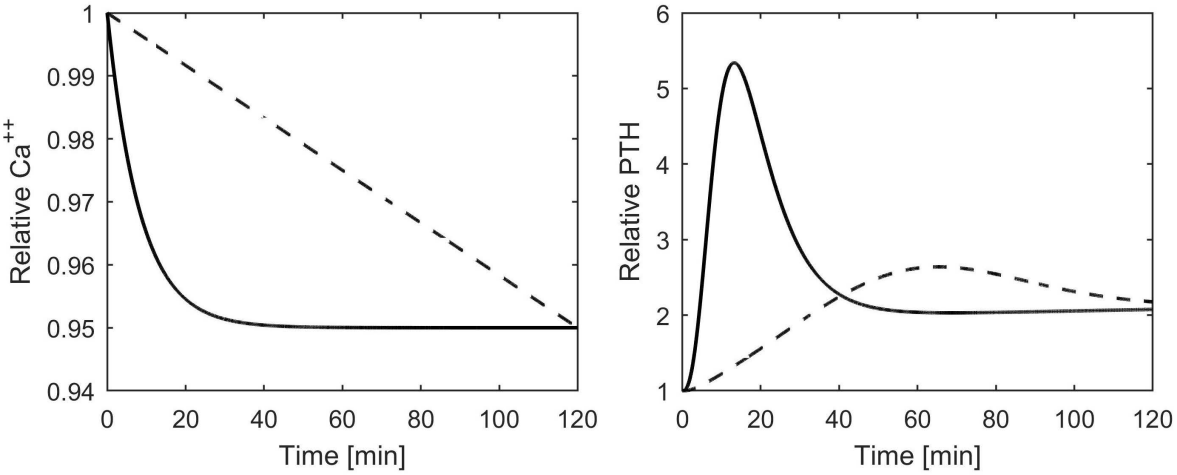

Figure 4.4 Time versus prescribed $Ca^{2+}$and corresponding predicted PTH concentrations. High rates of Ca^{2+}changes (solid line) lead to a prominent overshoot; at low rates, the peak is almost diminished (dashed line).

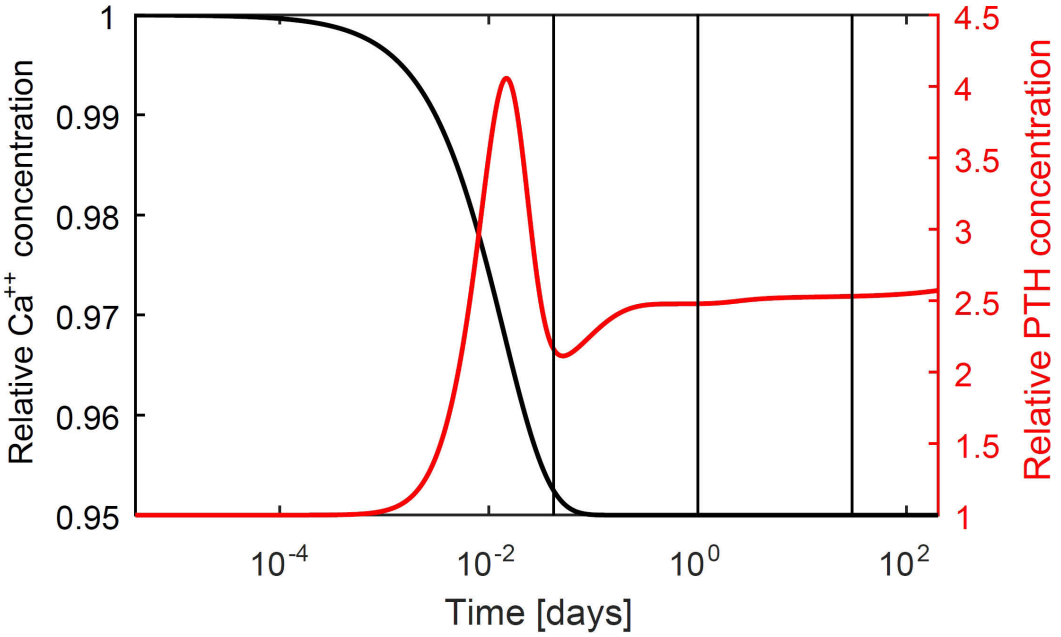

Figure 4.5 Time versus prescribed Ca^{2+}(black line) and corresponding simulated PTH concentrations (red line) during a fast induced mild but chronic hypocalcemia. The time scale is logarithmic; the black vertical lines indicate one hour, one day, and one month.

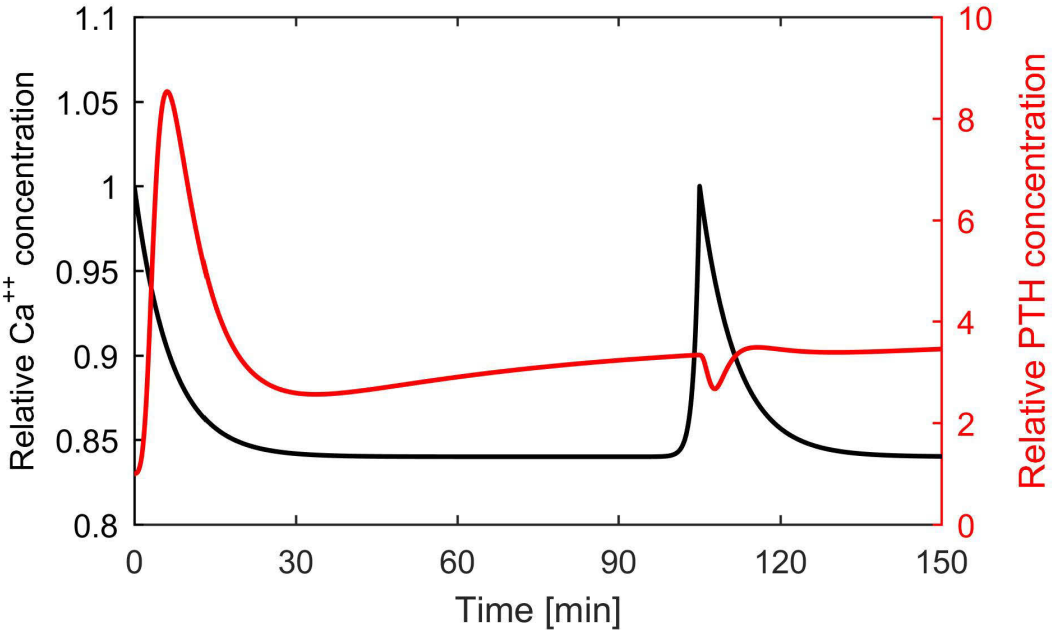

Figure 4.6 Time versus prescribed Ca^{2+}(black line) and corresponding simulated PTH (red line) concentrations during induced hypocalcemia, normocalcemia, and subsequent hypocalcemia.

Ca^{2+}concentrations. Since PTH is stored in secretory active cells, we observe a PTH overshoot. Since the return to normocalcemic conditions was too brief to recover the storage, PTH cannot overshoot during the second hypocalcemic cycle (Fig. 4.6).

4.1.11 Effect of low phosphate diet on PTH

Disturbances in phosphate and calcitriol levels will lead to PTG alterations due to the effect of phosphate on the CaSR (18, 55, 209) and the positive feedback loop between the CaSR and the VDR (37, 76, 187, 217). In CKD patients, renal phosphate excretion and calcitriol synthesis is impaired. Therefore, PTH will slowly increase over time, even if $Ca^{2+}$is kept at an optimal value. In (188), Rutherford et al. studied three groups of 5/6 nephrectomized dogs for 24 months. The first group of dogs received a regular phosphate diet. In the second group of dogs, phosphate intake was adjusted according to the declining kidney function. In the third group, the dogs received the adjusted phosphate diet and additional calcitriol supplements. Ca^{2+}concentrations were kept constant during the duration of the experiment. While PTH increased dramatically over 24 months in the first group of dogs, it was well controlled within the first 12 months in the second group and increased only slightly after that. PTH levels did not change significantly in

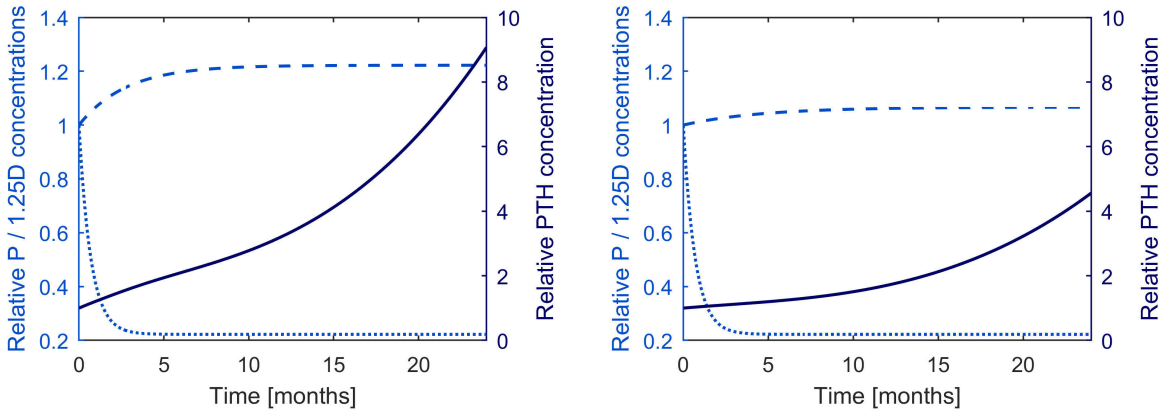

Figure 4.7 From Schappacher-Tilp et al. (192) under CC-BY. Time versus prescribed phosphate (dashed blue line) and calcitriol (1,25D) concentrations (dotted blue line), as well as the corresponding predicted PTH concentrations (solid line). The simulations mimic the experimental setup by Rutherford et al. (188). Regular diet resulting in elevated phosphate levels (left panel) to significantly higher PTH levels than the scenario with an adjusted phosphate diet (right panel).

the third group. We mimic the experimental setup by decreasing calcitriol and increasing phosphate levels. Specifically, phosphate levels were increased by 20% in the first group and only 5% in the second group. We see the same effect in our simulation: A low phosphate diet allows for PTH control in the first months. End-point PTH levels are significantly lower in the low-phosphate group.

4.2 CINACALCET

Cinacalcet is a calcimimetic that has been effectively used to treat secondary hyperparathyroidism (19, 20, 22, 58). It activates the CaSR via allosteric modulation (90, 168). It is commonly used in hemodialysis patients. In (193), we published a multi-compartment model capturing the pharmacokinetics of cinacalcet. Here, we present the model as well as its application in detail.

4.2.1 Pharmacokinetics of cinacalcet

- Maximum plasma concentrations following oral administration occurs within 2-6 hours (127).
- The absolute bio-availability is 20-25% indicating a high first-pass metabolism (67).
- Cinacalcet is highly protein-bound. Only about 5% of the drug in the systemic circulation is free (67, 127).
- The terminal elimination half-life is 30-40 hours, the distribution half-life approximately 6 hours (65).
- Steady-state concentrations are achieved within 7 to 8 days. The pharmacokinetics of cinacalcet is dose proportional over the dose range of 30-180 mg (90).
- Cinacalcet is primarily metabolized by the liver. Severe hepatic impairment increases the exposure by four-fold (169).
- Absorption saturates at around 200 mg (90).
- The apparent oral clearance rate V_D is around 1250 l, indicating a large distribution outside the systemic circulation (65). In studies with radioactively labeled cinacalcet, radioactivity was maximal in most tissues after 4-12 h; for some tissues, the peak occurred after 24-48 hours (67).
- The exposure AUC_∞ is increased 1.5 to 1.8 fold when cinacalcet is administered with meals (170).

4.2.2 Mathematical model

In (193), we proposed a physiology-based minimal multi-compartment model capturing all pharmacokinetics properties of cinacalcet comprises absorption, first-pass metabolism,

plasma protein binding, and tissue compartments (Fig. 4.8). Various tissue can be lumped in two distinct compartments, one with faster kinetics and slower kinetics. The tissue with the slower kinetics is of less importance for the pharmacokinetic properties of cinacalcet. However, since it comprises body fat, it was included in order to allow to study the effect of cinacalcet in obese patients.

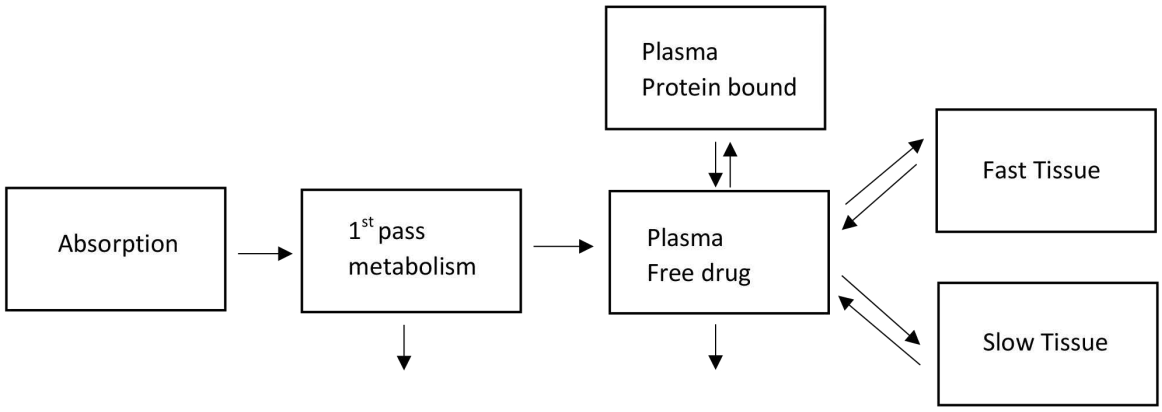

Figure 4.8 Structure of the multi-compartment pharmacokinetics model. From Schappacher-Tilp et al. (193) under CC-BY. The slow tissue compartment is only relevant for pathological situations, such es obesity.

Since we were interested in simulations over long periods, we chose a linear model. Numerics is reduced to the calculation of eigenvalues and eigenvectors.

$$\frac{d\vec{y}}{dt} = \begin{pmatrix} -k_a & 0 & 0 & 0 & 0 & 0 \\ k_a & -k_e - k_{lp} & 0 & 0 & 0 & 0 \\ 0 & k_{lp} & -k_b - k_{PTf} - k_{PTs} - k_e^P & k_f & k_{TPf} & k_{TPs} \\ 0 & 0 & k_b & -k_f & 0 & 0 \\ 0 & 0 & k_{PTf} & 0 & -k_{TPf} & 0 \\ 0 & 0 & k_{PTs} & 0 & 0 & -k_{TPs} \end{pmatrix} \vec{y},$$

where $\vec{y}(1)$ corresponds to the absorption compartment, $\vec{y}(2)$ to the first-pass metabolism, $\vec{y}(3)$ and $\vec{y}(4)$ to the plasma fee and protein-bound compartment. $\vec{y}(5)$ and $\vec{y}(6)$ corre-

spond to fast and slow tissue.

The initial dose of cinacalcet is delivered to the absorption compartment. Since the maximal daily dose approved by the Food and Drug Administration (FDA) is 180 mg and the available dose saturates at 200 mg, there is no need for saturable absorption equation. Since very little is known about the saturation process, we used a simple mechanistic model for dose-response assessment:

$$\vec{y}(1)(t_0) = \begin{cases} \text{Dose}, & \text{Dose} \leq 50 \text{ mg} \\ 200(1/(1+\exp(-0.02(\text{Dose}-50))) - 0.5) + 100, & \text{else} \end{cases}.$$

Exemplar model parameters

Plasma volume	3L
k_a	0.4 h^{-1}
k_e	0.266 h^{-1}
k_{lp}	0.09 h^{-1}
k_e^p	130 h^{-1}
k_b	$1 \cdot 10^3$ h^{-1}
k_{PTf}	550 h^{-1}
k_{TPf}	0.08 h^{-1}
k_{PTs}	50 h^{-1}
k_{TPs}	1 $\cdot 10^{-5}$ h^{-1}

We assume that 95% of the drug is protein-bound in the steady state. Therefore, $k_f = 0.0526 k_b$.

4.2.3 Main model predictions

The predicted cinacalcet concentration is the total plasma concentration, i.e., protein-bound and free drug concentration in the plasma. The main results are the following;

- The model can be adjusted to predict pharmacokinetic parameters such as C_{max}, t_{max}, V_D, and CL/F within a reasonable range (67, 90, 168). Parameter estimation was based on the method of least squares.

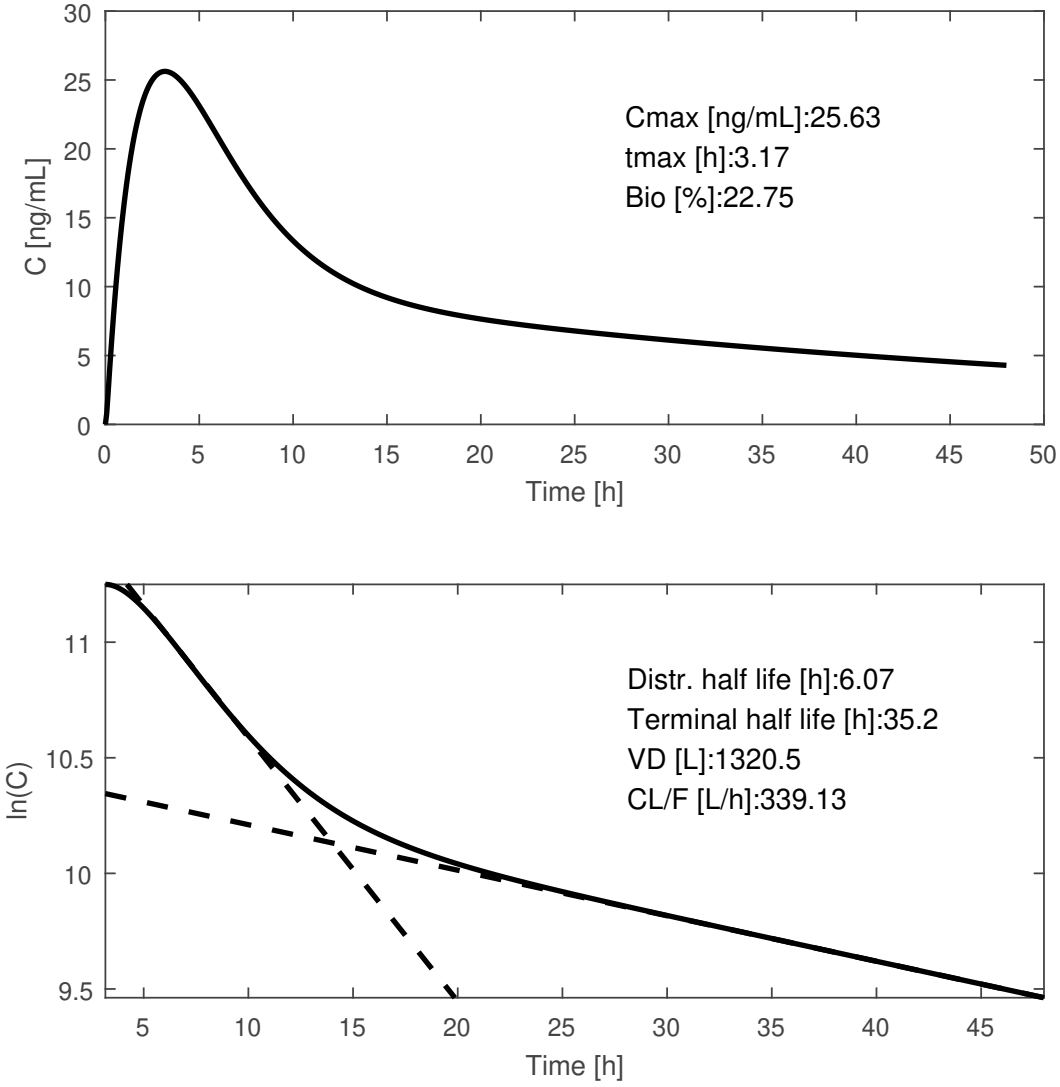

Figure 4.9 Upper panel: plasma concentration as a function of time after a single 75mg oral dose. Lower panel: the corresponding logarithmic concentration as a function of time. The slopes of the two regression lines correspond to the distribution half-life and the terminal half-life. Cmax, tmax, bio-availability (Bio), volume of distribution (VD), and apparent oral clearance rate (CL/F) are calculated from the upper panel.

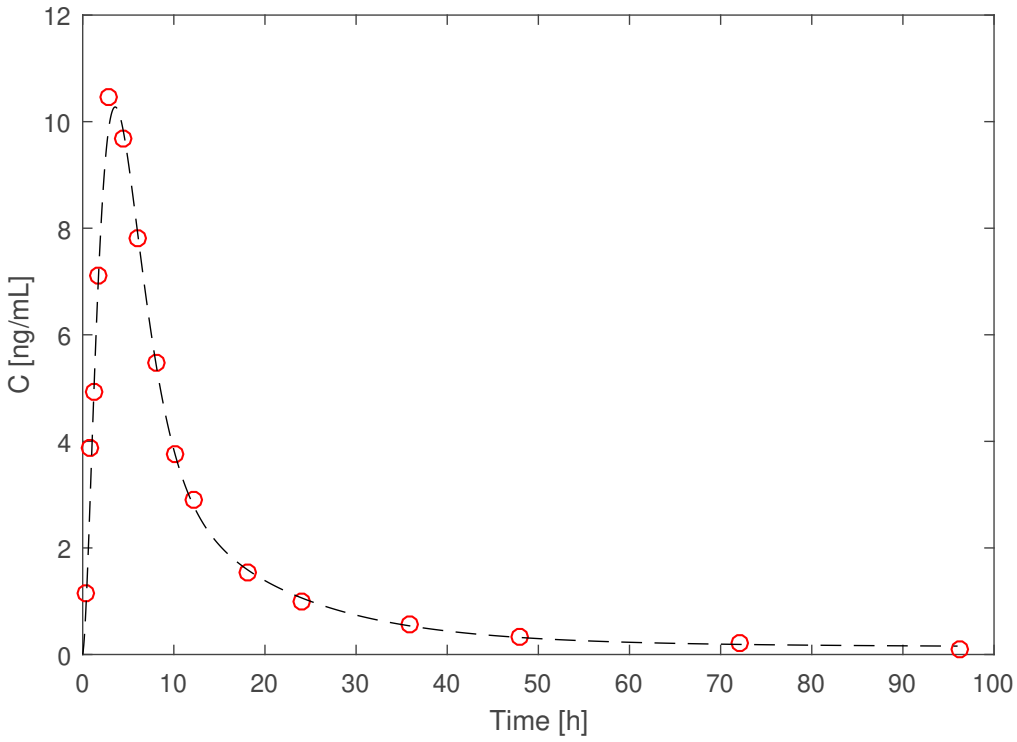

Figure 4.10 Plasma concentration vs. time after a single 75mg oral dose. Dots represent experimental results (digitized data from (127)), the dashed black line represents the model prediction.

- Steady state kinetics (i.e., daily intake of cinacalcet is in a dynamic equilibrium with its daily elimination) is reached within 7 days (Fig. 4.11).

- While C_{max} saturates at high oral doses, pharmacokinetics is linear to an oral dose of 180 mg (Fig. 4.12).

- The model parameters can be adjusted to follow individual plasma concentration curves, even with significantly different pharmacokinetic properties such as C_{max} (Fig. 4.10). Again, the parameter estimation was based on the method of the least squares.

- If cinacalcet is administered three times a week, there is a weekly kinetic steady state, i.e., a concentration profile on a specific day is equal to the profile 7 days later. However, due to the three days gap, there is no steady state between single administrations independent of the dose (Fig. 4.13 and Fig. 4.14).

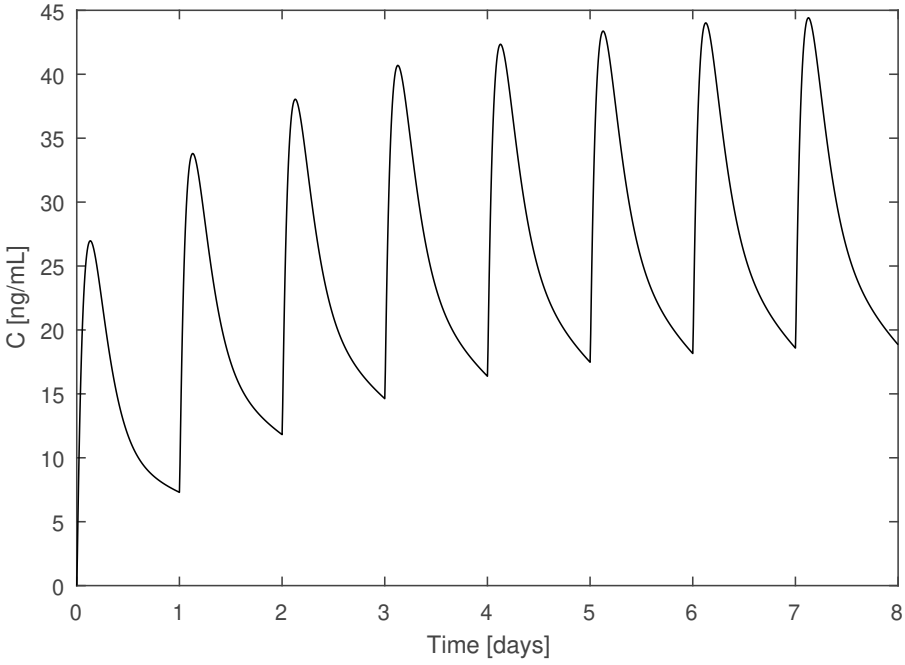

Figure 4.11 Plasma concentration as a function of time for daily doses of 75mg cinacalcet.

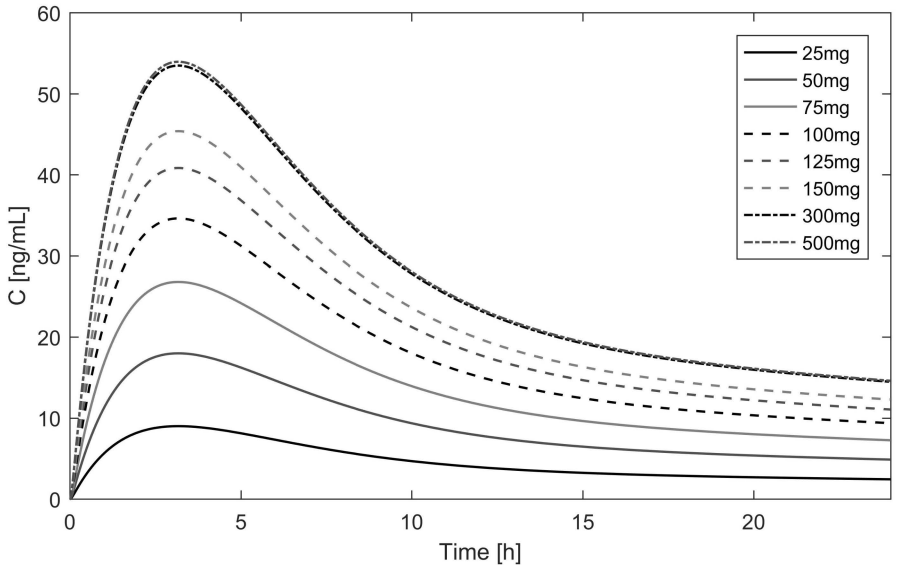

Figure 4.12 Plasma concentration as a function of time for different single doses of cinacalcet. C_{max} saturates at high oral doses while pharmacokinetic is linear for doses up to 200 mg.

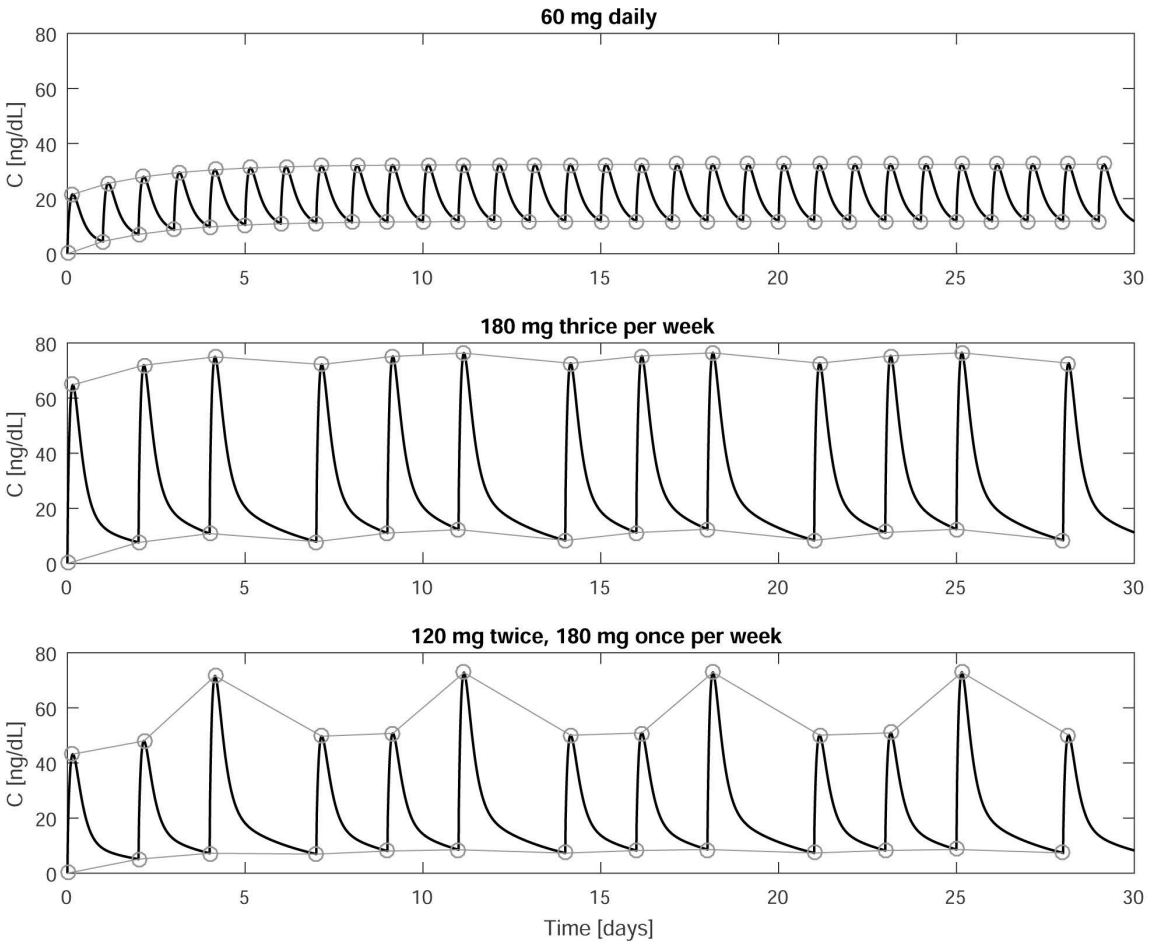

Figure 4.13 Plasma concentrations of cinacalcet as a function of time and administration regime. While the steady state is reached within 7-8 days in the daily administration regime, there is only a weekly kinetic steady state. The daily dose of cinacalcet is 60 mg; the dose of cinacalcet administered thrice weekly is chosen accordingly.

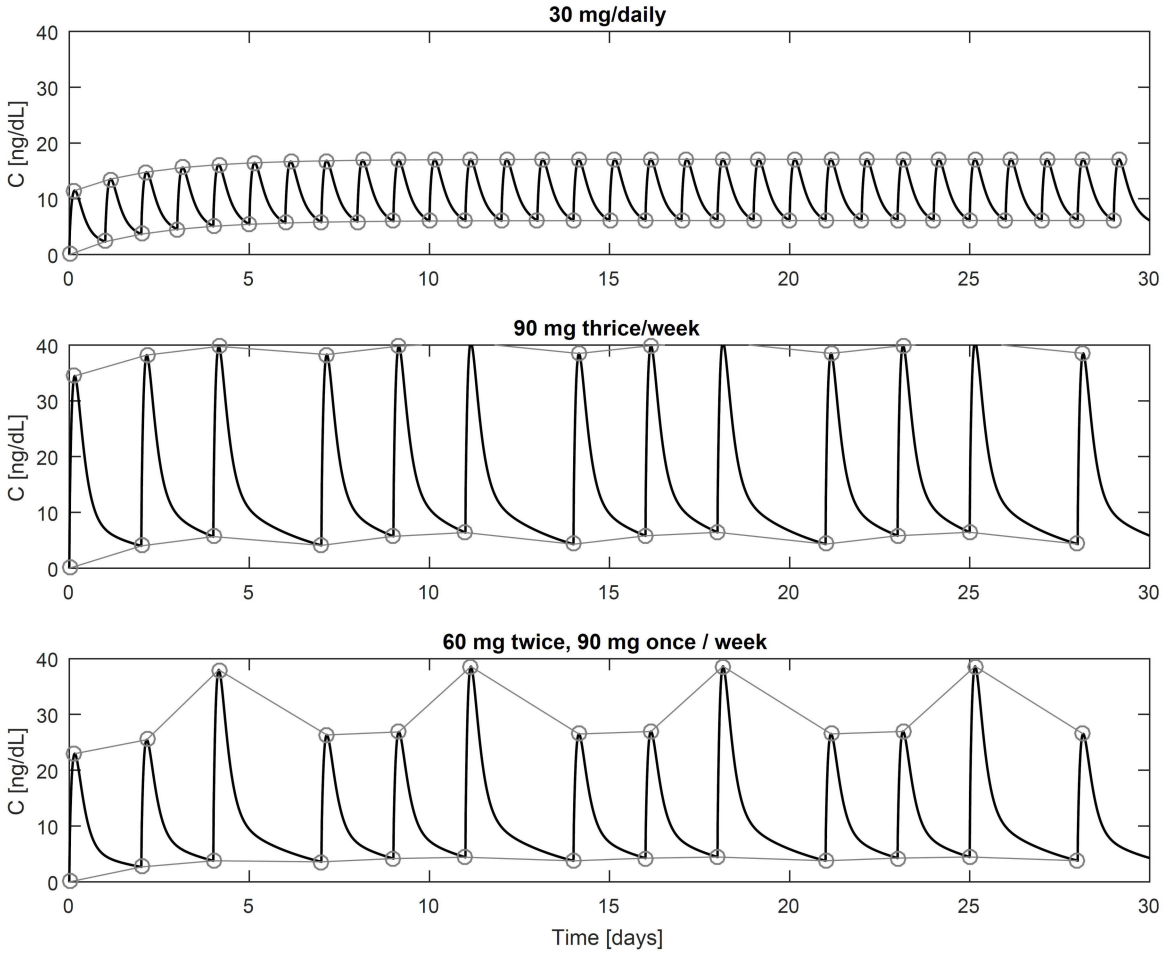

Figure 4.14 Plasma concentrations of cinacalcet as a function of time and administration regime. While the steady state is reached within 7-8 days in the daily administration regime, there is only a weekly kinetic steady state. The daily dose of cinacalcet is 30 mg; the dose of cinacalcet administered thrice weekly is chosen accordingly.

4.2.4 Sensitivity analysis cinacalcet

We fixed the parameter set in the overall sensitivity analysis and varied only the indicated variable from 50% to 150%. The single oral dose was 75mg. Error refers to the $\|$Predicted - opt values $\|^2$ normalized to the original set of parameters' error. From this term, we subtract one such that the error is zero for the original set of parameters. Optimal values are mean values from literature (67, 127):

Parameter	Opt. Value	Parameter	Opt. Value
C_{max}	25 ng/ml	$t^d_{1/2}$	6 h
t_{max}	3.5 h	$t_{1/2}$	35 h
V_D	1000 L	BIO	25 %

Sensitivity analysis reveals that overall errors (i.e., the sum of errors for all 6 parameters as described above) are most sensitive to changes in k_e and k_{lp} and least sensitive to changes of k_a and k_{TPs} (Fig. 4.15).

The sensitivity analysis of all estimated model parameters is presented in Fig. 4.16. The base values were either divided by 2 or multiplied by 2. The analysis shows that C_{max} is most sensitive to changes of k_e, k_{lp} and k_{PTf}. Moreover, C_{max} is sensitive to changes of k^p_e and k_b, but to a lesser degree. Bio-availability is most sensitive to changes of k_e and k_{lp}. There are only negligible effects by other rates. Terminal half-life $t_{1/2}$ is most sensitive to changes of k_{PTf}, k_{TPf}, and k_{PTs}. There is almost no effect of changes of k_a on the apparent volume of distribution V_D. Low protein binding rates k_b increase the error of distribution half-life $t^d_{1/2}$ substantially. t_{max} is sensitive to changes of k_b and k_e. Smaller values of both rates lead to greater errors.

4.2.5 Adaptation to specific patient groups

Due to the physiologically meaningful compartments, adaptation to specific patients groups is straight forward.

An example would be the simulation of the effect of cinacalcet administration with food. In (168), the authors showed that the bio-availability of a single 90 mg dose of cinacalcet is significantly increased if cinacalcet is administered with a high or low-fat meal. The corresponding increase of AUC_∞ was 68% (90% confidence interval: 48% to 89%) and 50% (90% confidence interval: 33% to 70%) for the high fat and low-fat meal. Terminal half-life did not change significantly, while t_{max} decreased from 6

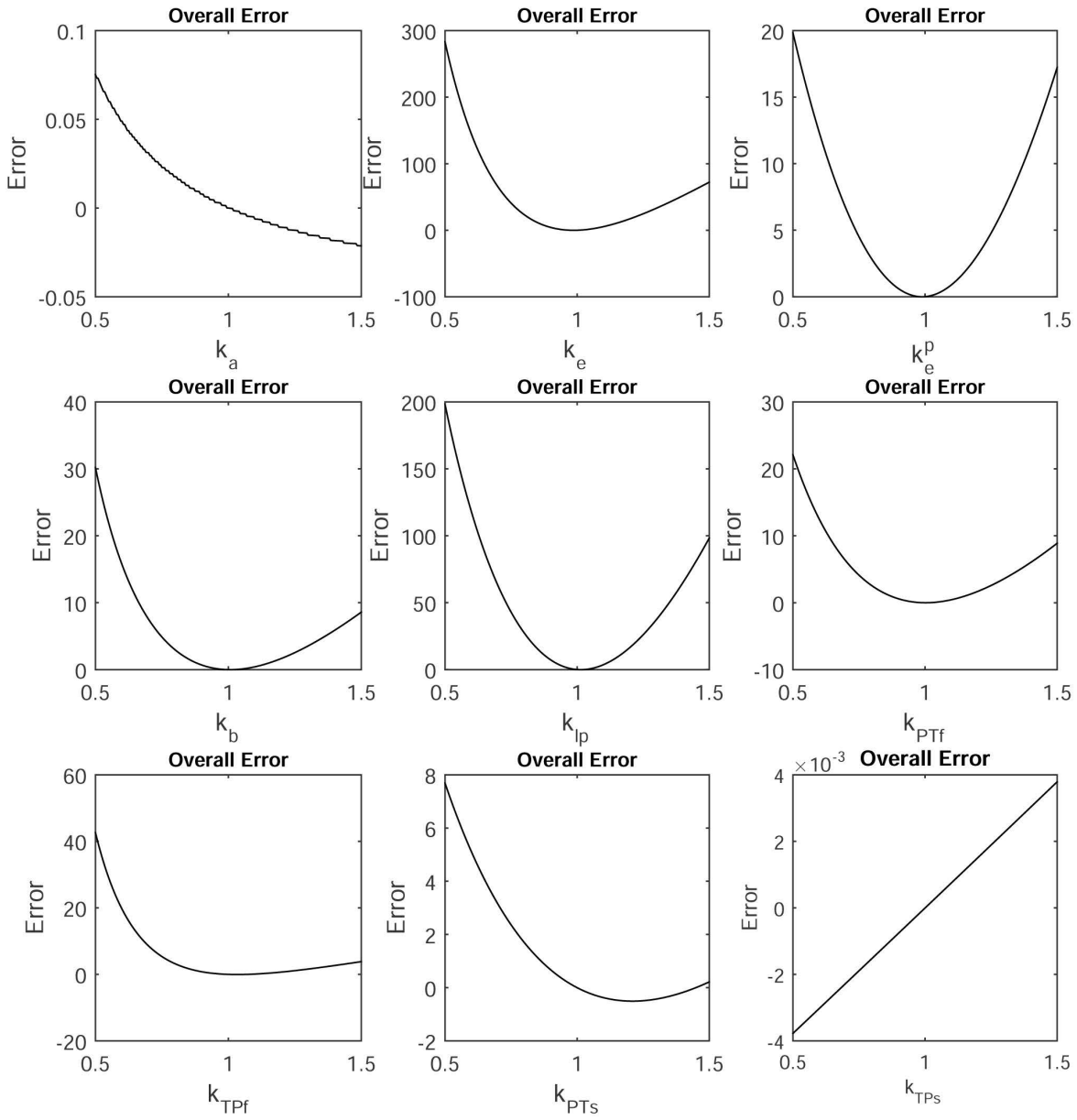

Figure 4.15 Overall error as a function of the rate constants.

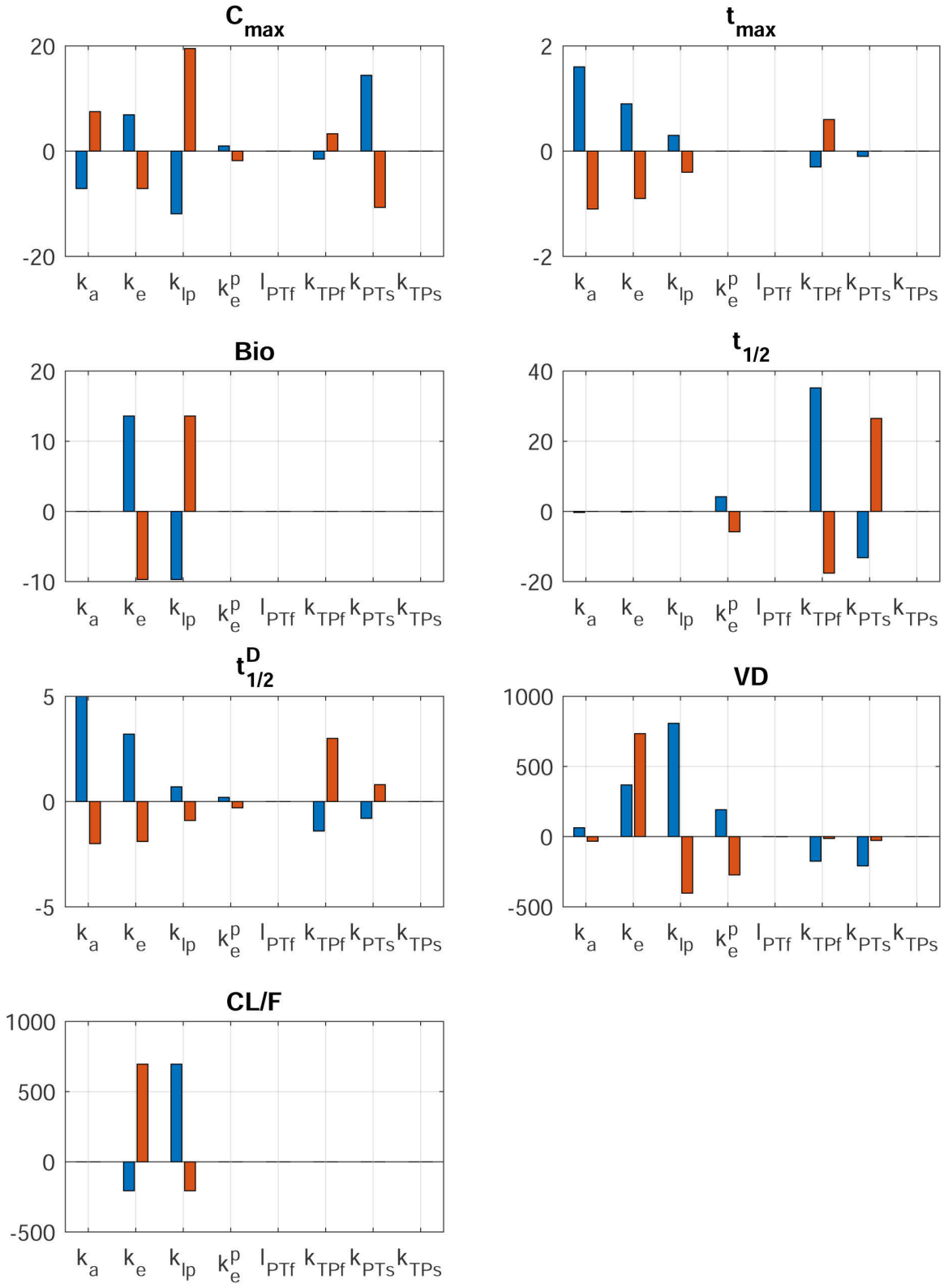

Figure 4.16 Sensitivity analysis. Base values were either divided by 2 (blue bar) or multiplied by 2 (orange bar).

hours in fastening subjects to 3.5-4 hours in subjects receiving high or low-fat meal with cinacalcet. Bio-availability is based on absorption and first-pass metabolism. Therefore, we have to adjust k_a, k_e and /or k_{lp}. Since bio-availability is most sensitive to changes in k_e and k_{lp}, we do not adjust k_a. Moreover, an increase in k_e would result in an increase of t_{max}. Therefore, we adjust only k_{lp}.

Another example would be hepatic impairment. If we want to adjust the model to patients with hepatic impairment, we have to adjust the parameters such that AUC_∞ is 2.4 and 4.2 times higher, and $t_{1/2}$ is roughly 1.2-1.8 times higher in patients with hepatic impairment than healthy control patients (169). C_{max} and t_{max} seemed not altered in patients with hepatic impairment. The parameters reflecting liver functions are parameter describing first-pass metabolism rates k_e and k_{lp} as well as metabolization and, therefore, elimination of the drug, k_e^P. Since, based on our sensitivity analysis, changes in k_e and k_{pl} result in changes of C_{max} and t_{max}, we will not adjust these parameters. Therefore, the only meaningful rate to adjust is k_e^P. Since the model is linear we can easily calculate AUC_∞:

$$AUC_\infty = \int_0^\infty C(\tau)d\tau = -\left(\sum_{i=1}^{6}(\frac{1}{\lambda_i}\Phi^{-1}\vec{y_0'})_i\vec{v_i}\right)_3 - \left(\sum_{i=1}^{6}(\frac{1}{\lambda_i}\Phi^{-1}\vec{y_0'})_i\vec{v_i}\right)_4,$$

where the subscripts 3 and 4 denote the third and fourth vector components, respectively. Furthermore, we estimate terminal half-life which is associated with the tissue compartments and the eigenvalue λ_k associated with the fast tissue compartment:

$$t_{1/2} \approx \frac{\ln(0.5)}{\lambda_k}.$$

Therefore, a reduction of k_l^P by 53% results in a 1.4 fold rise of the terminal half-life and a 2.2 fold rise of AUC_∞. If we reduced k_l^P by 76%, it would result in a 1.8 fold increase of $t_{1/2}$ and a 4.2 fold increase of AUC_∞.

4.2.6 Pharmacodynamics of cinacalcet

We combine the compartment model of cinacalcet with the PTG model by incorporating a simplified operational model of allosterism, i.e., we use the transformation

$$T(C) = \frac{(C(\beta + \alpha M) + \tau M K_d)}{\beta + M},$$

where C is the ionized Ca concentration in [mMol] and M the plasma concentration of unbound cinacalcet given in [pg/dL] (129, 130, 131, 186). The main assumption allowing the simplified formula is that $Ca^{2+}$is the main agonist for the CaSR. For all the following simulations, we used the following values:

$$\alpha = 1.3, \beta = 6.5 \text{ [pg/dl]}, \tau = 0.35, K_d = 1.1881 \text{ [mMol]}.$$

The values for α and β are based on published data (129), while τ was chosen such that a single dose of 60 mg cinacalcet reduces PTH by 50% in healthy subjects.

Remarks:

(-) Structural changes of the CaSR, as well as mutation, can be modeled by adjusting α and β values (129).

(-) In the combined bone and PTG model, we take the reduction of the gland size due to cinacalcet into account (59, 108, 124, 151). Specifically, we introduce another feedback mechanism ensuring that the apoptosis rate is decreasing over time with cinacalcet, i.e.,

$$\begin{aligned} k_a &= k_a^0 \cdot (1 + (\Phi_{Cina} \cdot \max(0, C_{Cina} - 1))) && (4.21) \\ \frac{dC_{Cina}}{dt} &= p_{Cina} \cdot (Cina^{in}) \cdot C_{Cina} + n_{Cina} \cdot (1 - C_{Cina}) && (4.22) \\ \frac{dCina^{in}}{dt} &= (\text{stim}_{Cina}(M) \cdot \left(1 - \frac{\text{stim}_{Cina}}{|\text{stim}_{Cina}|} Cina^{in}\right) - Cina^{in}) \cdot \tau_{Cina} && (4.23) \end{aligned}$$

where M is again the free drug concentration in the plasma. The parameter Φ_{Cina} determines the quasi-steady state reduction of the gland volume. Furthermore, we assume that the carrying capacity is not increasing during the treatment with cinacalcet.

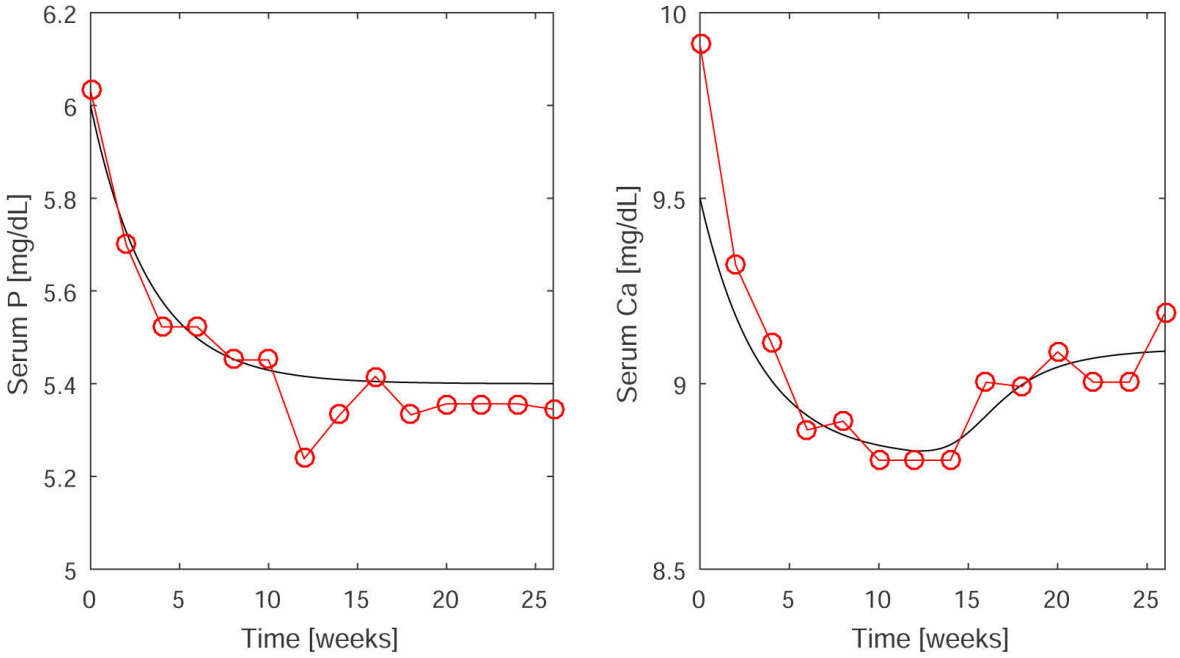

Figure 4.17 Temporal changes of phosphate and calcium as input functions for the virtual clinical trial. Red circles correspond to clinical data presented in (154). Time zero denotes the start of daily cinacalcet administration in the clinical trial. Within the first weeks of cinacalcet treatment, phosphate and calcium concentrations decline. Calcium slightly recovers after around 12 weeks.

4.2.7 Virtual clinical trial

Patient adherence to cinacalcet is very poor (78), most likely due to common gastrointestinal side effects and high pill burden. Refill data provided by the Data analytics unit at FMCNA showed a mean refill rate of 64.44%, which was based on 7,387 patients. Other published medication possession ratios are even lower (78). An easy way to overcome poor patient adherence would be to administer cinacalcet after each hemodialysis session three times a week. Cinacalcet administration would be observable and reliable. Since this would mean an off-label use, we employ our PTG and cinacalcet model to investigate whether thrice weekly (TIW) could be an easy to implement alternative.

The VCT was based on the PTG stand-alone model. Therefore, we had to assume the temporal changes of phosphate and calcium due to altered bone metabolism (Fig. 4.17). We determine the state of the PTG system at the onset of cinacalcet treatment by using the following simulation assumptions:

- The clearance rate of PTH is halved due to the impaired kidney function.

- At time zero, we slowly increase P from 4.5 to 6 mg/dL (1.45 to 1.93 mMol) and decrease $Ca^{2+}$from 5 to 4.75 mg/dL (1.25 to 1.18 mMol).
- We determine the state of the system after 200 days. This state is the initial condition for all following simulations.

For all predictions involving the administration of cinacalcet, we assume that phosphate and calcium concentrations decrease over time (20). The temporal changes of phosphate and calcium are presented in Fig. 4.17. We simulate two distinct patient populations:

(A) Cinacalcet naïve patients starting with either a daily cinacalcet prescription or with thrice-weekly in-center cinacalcet administration

(B) Patients who had a prescription for the daily administration of 30 mg or 60 mg for 12 weeks and subsequently either kept the daily prescription or switched to the thrice-weekly protocol

We further distinguish between full patient adherence and real-life (and, therefore, limited patient) adherence for both patient populations. The distinction is only relevant for the daily protocol as clinical staff administration in the thrice-weekly protocol should be flawless. Based on the refill ratio of 64.5% we assume that patients skip alternately 3 or 2 cinacalcet doses per week. The days with no drug administration are chosen randomly.

Cinacalcet naïve patients

(A.1) **60 mg daily or 60 mg TIW / Full patient adherence**
Weekly mean PTH as well as max/min values in cinacalcet naïve patients are shown in Fig. 4.18. While the administration of 60 mg daily (red line) leads to lower PTH values than 60 mg thrice a week (black line), both administration regimes lead to a decline in PTH and a mean value below or around 300 pg/ml. Steady state is reached after around 12 weeks. Notably, the PTH response variation is much higher in the daily protocol due to cinacalcet accumulation.

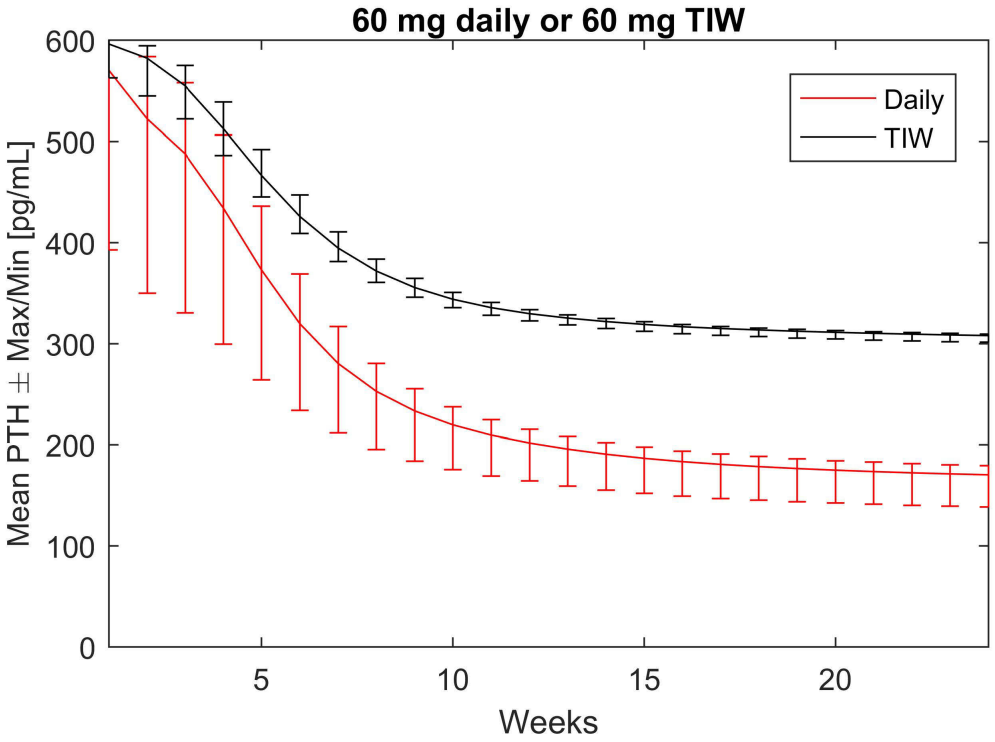

Figure 4.18 Weekly mean PTH as well as max/min values of cinacalcet naïve patients as a response to 60 mg daily or 60 mg TIW in patients with full adherence.

(A.2) **60 mg daily or 60 mg TIW / Real-life patient adherence**

Weekly mean PTH as well as max/min values of cinacalcet naïve patients based on real-life patient adherence are shown in Fig. 4.19. The administration of prescribed 60 mg daily (red line) results in PTH values compared to guaranteed 60 mg thrice weekly. However, the difference between the two protocols gets significantly smaller. Accumulation of cinacalcet is limited in real-life patient adherence. Therefore, the variation in PTH is smaller compared to the variation in patients with full adherence.

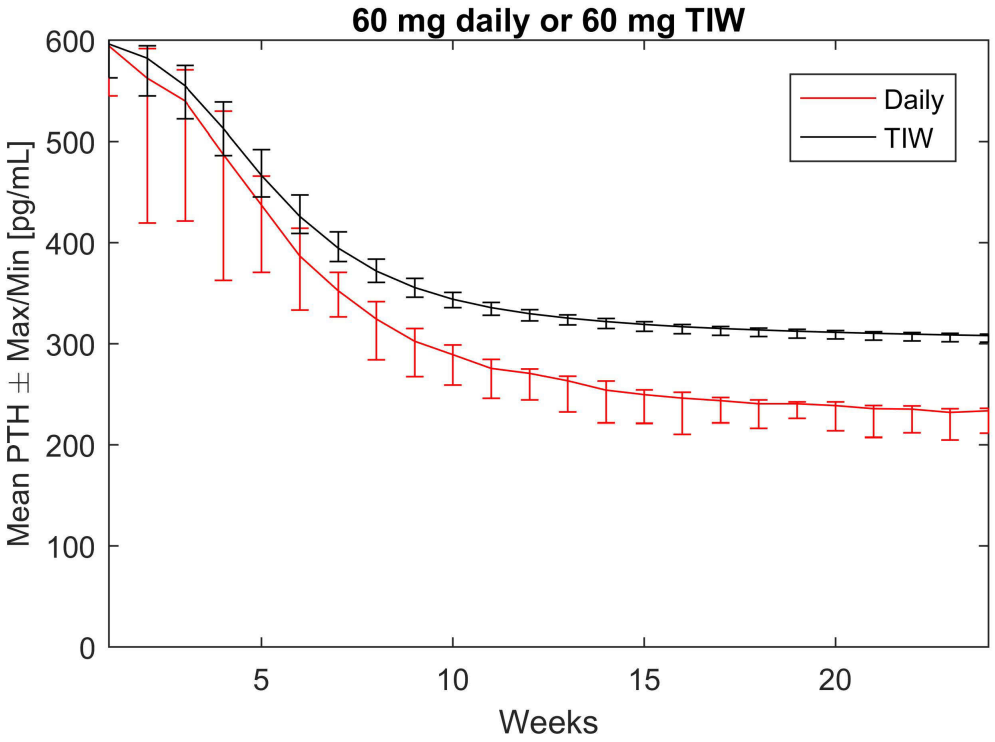

Figure 4.19 Weekly mean PTH as well as max/min values of cinacalcet naïve patients as a response to 60 mg daily or 60 mg TIW in patients with limited patient adherence.

(A.3) **30 mg daily or 60 mg TIW / Full patient adherence**

Weekly mean PTH as well as max/min values of cinacalcet naïve patients are shown in Fig. 4.20. While the administration of 30 mg daily (red line) leads to lower steady state PTH values of 60 mg thrice a week (black line), both administration regimes lead to a decline in PTH and a mean value of around 300 pg/ml. Steady state is reached after around 12 weeks. Notably, the PTH response is slightly higher in the TIW protocol due to the higher single cinacalcet dose.

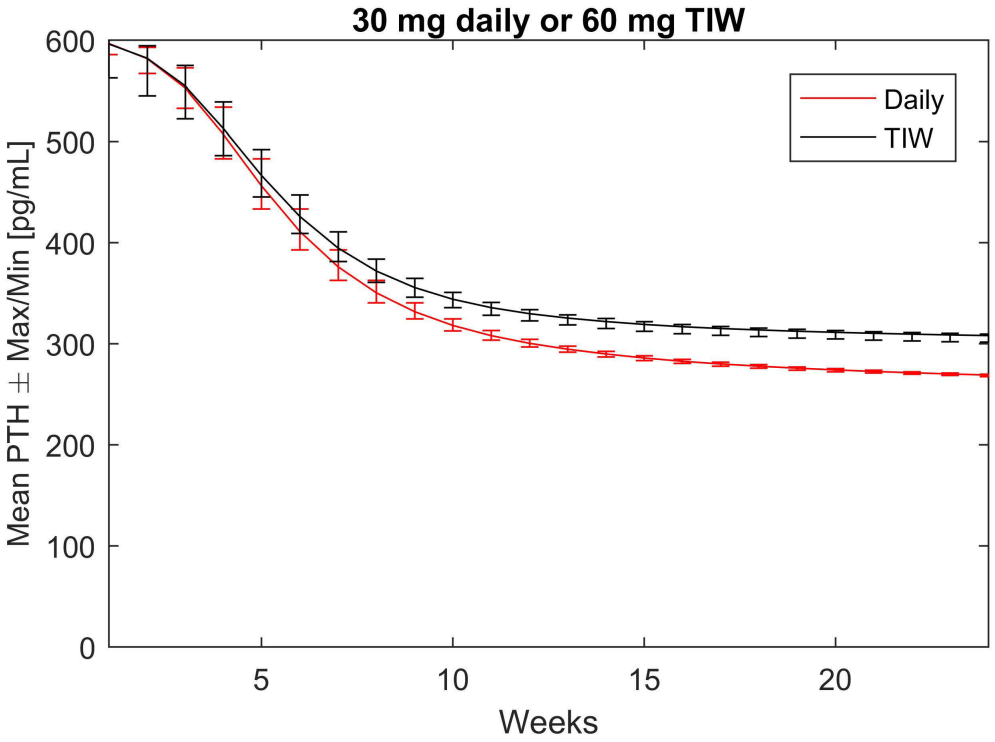

Figure 4.20 Weekly mean PTH as well as max/min values of cinacalcet naïve patients as a response to 30 mg daily or 60 mg TIW in patients with full adherence.

(A.4) **30 mg daily or 60 mg TIW / limited patient adherence**

Weekly mean PTH as well as max/min values of cinacalcet naïve patients based on real-life patient adherence are shown in Fig. 4.21. The administration of prescribed 30 mg daily (red line) leads to higher PTH values than the guaranteed administration 60 mg thrice weekly.

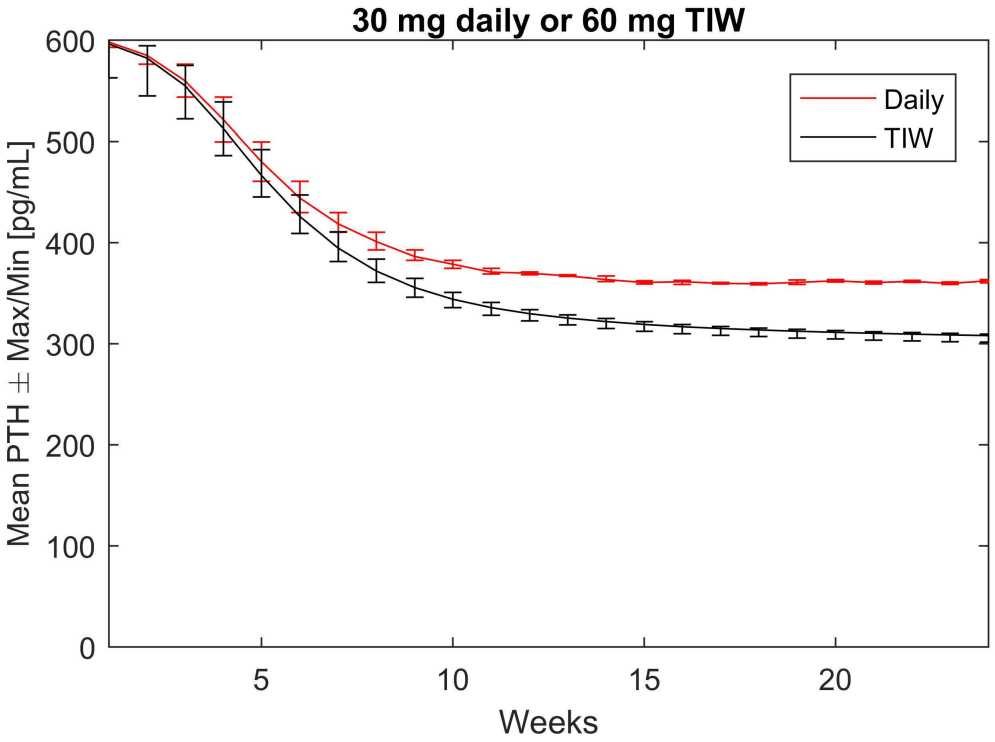

Figure 4.21 Weekly mean PTH as well as max/min values of cinacalcet naïve patients as a response to 30 mg daily or 60 mg TIW in patients based on real-life patient adherence.

Post run-in phase

(B.1) **60 mg daily or 60 mg TIW / Full patient adherence**

Fig. 4.22 shows weakly mean PTH as well as max/min values of patients who have already received 12 weeks 60 mg cinacalcet daily. The administration of 60 mg daily (red line) leads to lower PTH values and a prolonged decline in PTH due to the recovery of Ca^{2+}. When we switch the protocol to 60 mg thrice a week administration (black line), PTH will rise until it reaches a steady state after around 15 weeks. Both administration regimes keep mean PTH values below or around 300 pg/ml.

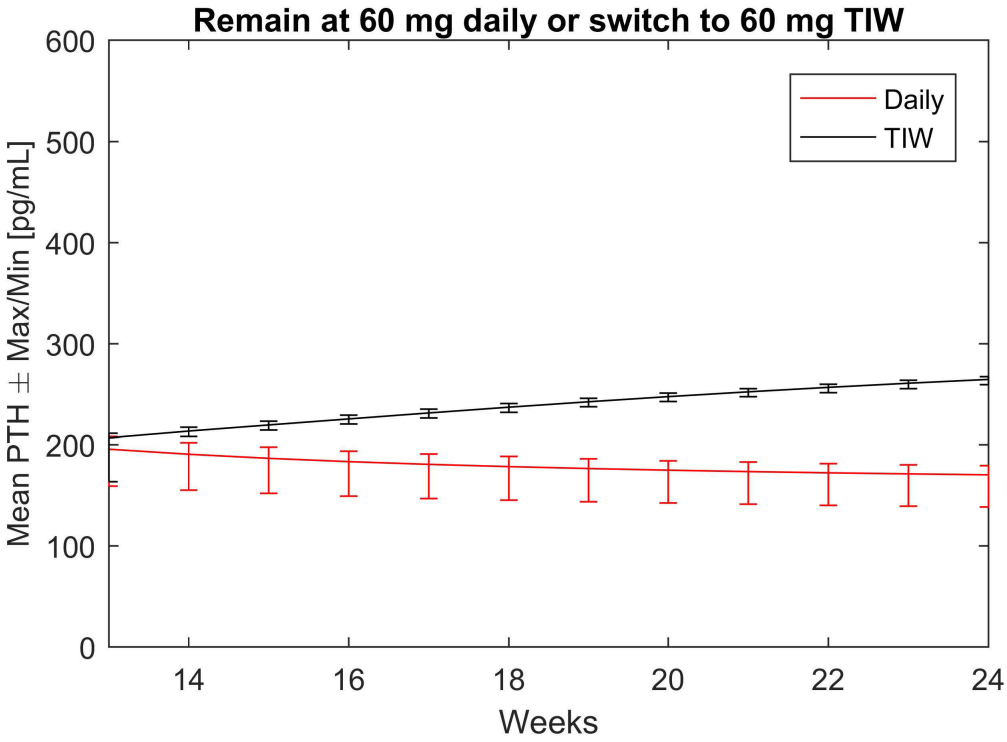

Figure 4.22 Weekly mean PTH as well as max/min values in the post run-in phase as a response to 60 mg daily or 60 mg TIW in patients with full adherence.

(B.2) **60 mg daily or 60 mg TIW / Real-life patient adherence**

Fig. 4.23 shows weakly mean PTH as well as max/min values of patients who have already received 12 weeks 60 mg cinacalcet daily. The administration of 60 mg daily (red line) still leads to lower PTH values than the administration of 60 mg TIW. However, the difference between the two administration regimes' mean values is within 60 pg/ml.

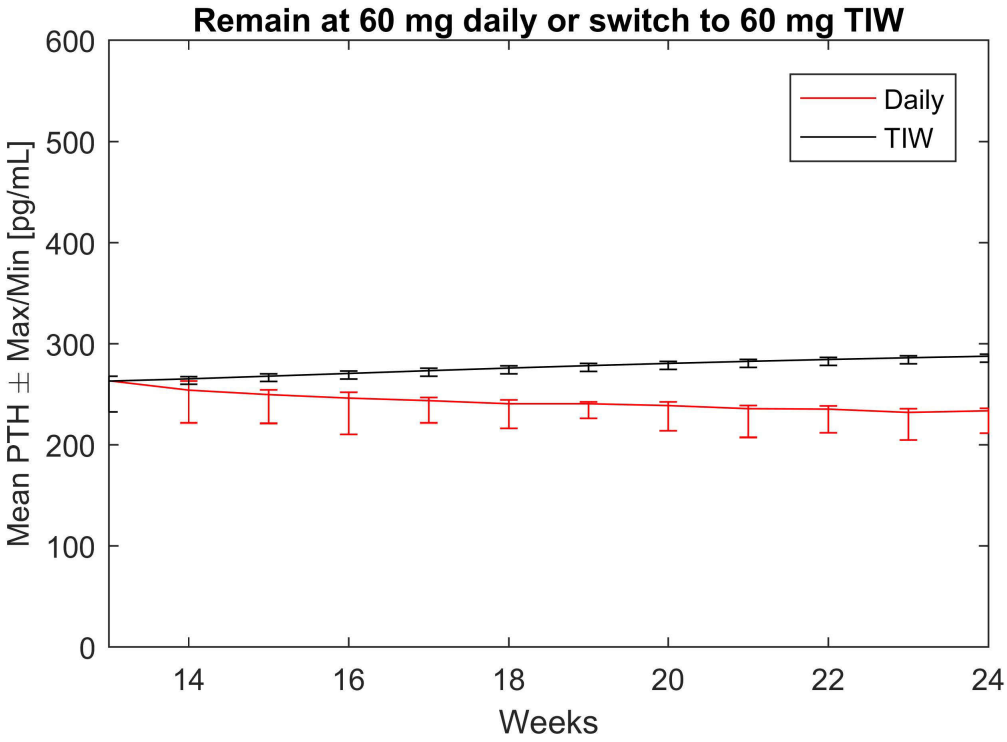

Figure 4.23 Weekly mean PTH as well as max/min values of cinacalcet naïve patients as a response to 60 mg daily or 60 mg TIW in patients with limited patient adherence.

(B.3) **30 mg daily or 60 mg TIW / Full patient adherence**

Fig. 4.22 shows weakly mean PTH as well as max/min values of patients who have already received 12 weeks 30 mg cinacalcet daily. The administration of 30 mg daily (red line) leads to slightly lower PTH values and a prolonged decline in PTH due to the recovery of Ca^{2+}. PTH values remain almost constant when the protocol is switched from 30 mg daily to 60 mg thrice a week (black line). Both administration regimes keep mean PTH values around 300 pg/ml.

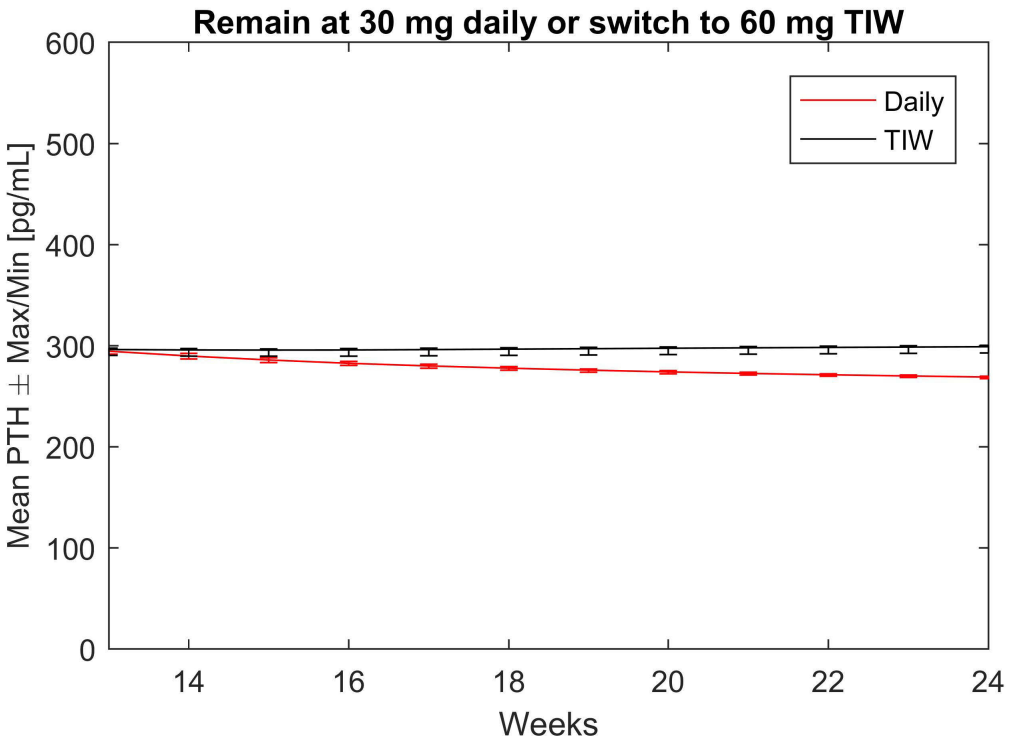

Figure 4.24 Weekly mean PTH and max/min values in the post run-in phase as a response to 30 mg daily or 60 mg TIW of patients with full adherence.

(B.4) **30 mg daily or 60 mg TIW / Real-life patient adherence**

Fig. 4.25 shows weakly mean PTH as well as max/min values of cinacalcet naïve patients with limited patient adherence. The administration of 30 mg daily (red line) leads to higher PTH values than the administration.

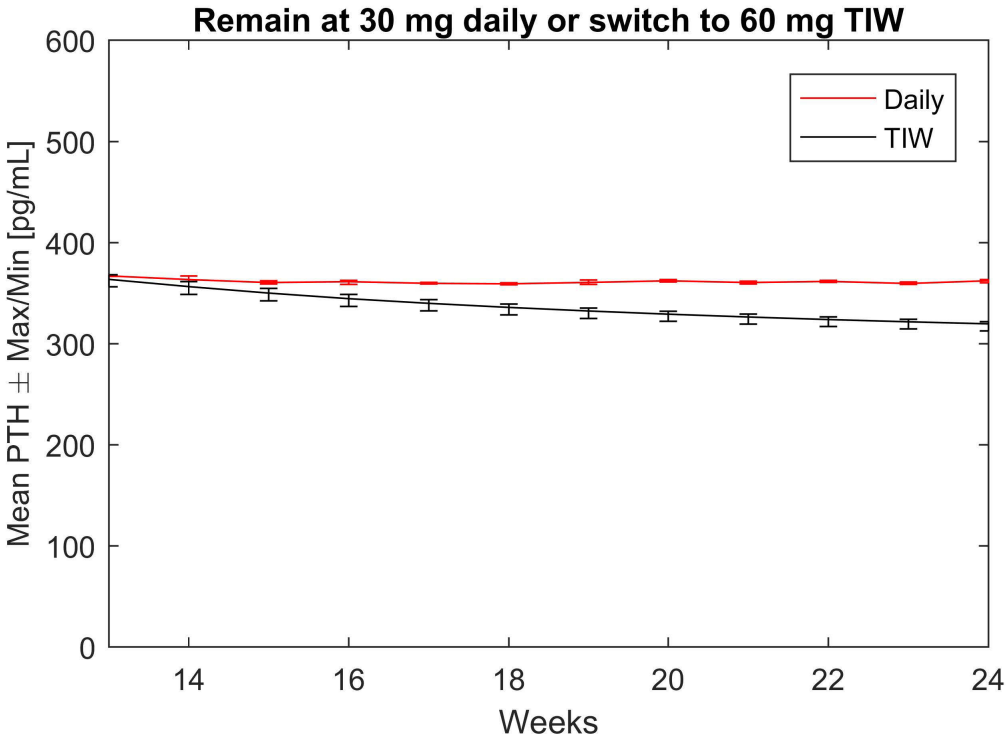

Figure 4.25 Weekly mean PTH as well as max/min values of the post run-in phase as a response to 30 mg daily or 60 mg TIW in patients with limited patient adherence.

4.2.8 Limitations and conclusion

The assumptions on the decline of phosphate and calcium due to cinacalcet administration are crucial for the model. The slower the decline in phosphate, the larger are the variations in PTH values, and the longer it takes to reach a steady state in PTH.

We assume that the decline in phosphate and calcium is independent of the administration regiment and the dose. We could not find any reference in the literature describing phosphate and calcium's response to cinacalcet administration for single patients. The mean values presented in literature might not be representative.

Large differences in min/max values of PTH in the run-in phase might indicate low patient adherence. Limited compliance with food intake would decrease the TIW protocol's disadvantage compared to the daily protocol even further.

Mutations in the CaSR lead to impaired responses to cinacalcet (129, 131, 186). We could easily adjust the parameters of the operational model for allosterism to capture known effects. Therefore, the model could be used to examine cinacalcet's effect on individual patients with genetic disorders in the CaSR.

Based on our assumptions, direct observable thrice-weekly cinacalcet with a com-

parable weekly dose is not performing inferior to daily administration based on real-life patient adherence.

4.3 INTESTINAL CALCIUM AND PHOSPHATE ABSORPTION

4.3.1 Simplified calcium absorption model

We take the transcellular (calcitriol dependent and saturable) as well as the paracellular pathway into account.

(1) Calcitriol dependency:

$$\Phi_{D,G}^{Ca}(D(0)) = \alpha_{D,G}^{Ca} + \rho_{D,G}^{Ca} \cdot \frac{D(0)^{\gamma_{D,G}^{Ca}}}{D(0)^{\gamma_{D,G}^{Ca}} + (\delta_{D,G}^{Ca})^{\gamma_{D,G}^{Ca}}} \tag{4.24}$$

$$\Phi_{D,G}^{Ca}(D) = \frac{1}{\Phi_{D,G}^{Ca}(D(0))} \cdot \left(\alpha_{D,G}^{Ca} + \rho_{D,G}^{Ca} \cdot \frac{D^{\gamma_{D,G}^{Ca}}}{D^{\gamma_{D,G}^{Ca}} + (\delta_{D,G}^{Ca})^{\gamma_{D,G}^{Ca}}} \right) \tag{4.25}$$

where D is the serum calcitriol concentration.

(2) Net calcium absorption:
Active transport which is modeled by a classic Michaelis-Menten equation:

$$J_{ac}^{Ca} = \Phi_{D,G}^{Ca} \cdot v_G^{Ca} \cdot \frac{\mathrm{OralCa}}{k_G^{Ca} + \mathrm{OralCa}}$$

Passive transport:

$$J_{pass}^{Ca} = c_G^{Ca} \cdot \mathrm{OralCa}$$

Total net calcium absorption:

$$J_G^{Ca} = \Phi_{D,G}^{Ca} \cdot v_G^{Ca} \cdot \frac{\mathrm{OralCa}}{k_G^{Ca} + \mathrm{OralCa}} + c_G^{Ca} \cdot \mathrm{OralCa} + d_G^{Ca} \tag{4.26}$$

d_G^{Ca} is an off-set to take endogenous calcium re-entering the gut into account. Furthermore, we use d_G^{Ca} to calibrate the system. At a steady state with a standard

calcium diet of 25 mmol per day, J_G^{Ca} should be around 4 mmol. OralCa is the amount of calcium intake in mmol per hour. Reduced calcium diets or enriched calcium diets can be simulated by adjusting OralCa .

Model predictions

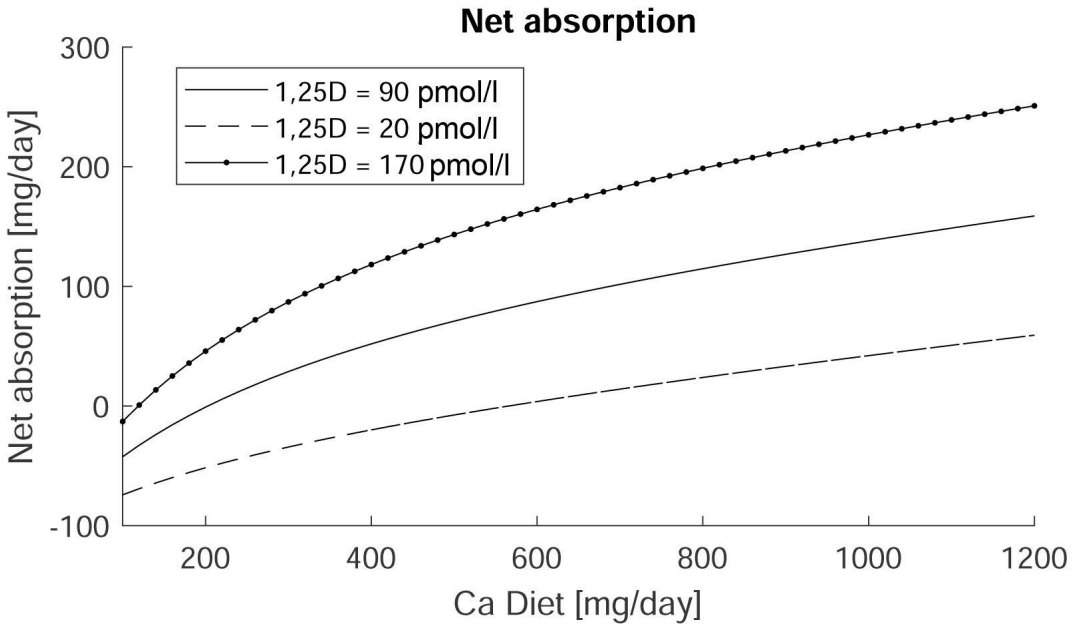

Figure 4.26 Predicted relationship between calcium diet and intestinal calcium net absorption. The absorption is significantly higher with higher calcitriol (1.25D) levels, while absorption is lower at low calcitriol levels following the literature, e.g.(199).

Model parameters

Table 4.4 Exemplar parameters for calcium absorption

Variable	Value	Variable	Value
$\alpha_{D,G}^{Ca}$	0.05	$\rho_{D,G}^{Ca}$	0.5
$\gamma_{D,G}^{Ca}$	2	$\delta_{D,G}^{Ca}$	90pMol
v_G^{Ca}	0.29 mmol h^{-1}	k_G^{Ca}	0.3 mmol
c_G^{Ca}	0.07 h^{-1}	d_G^{Ca}	-0.07 mmol

4.3.2 Simplified phosphate absorption model

Again, we take the transcellular (calcitriol and saturable) as well as the paracellular pathway into account.

(1) Calcitriol dependency:

$$\Phi^P_{D,G}(D(0)) = \alpha^P_{D,G} + \rho^P_{D,G} \cdot \frac{D(0)^{\gamma^P_{D,G}}}{D(0)^{\gamma^P_{D,G}} + (\delta^P_{D,G})^{\gamma^P_{D,G}}} \tag{4.27}$$

$$\Phi^P_{D,G}(D) = \frac{1}{\Phi^P_{D,G}(D(0))} \cdot \left(\alpha^P_{D,G} + \rho^P_{D,G} \cdot \frac{D^{\gamma^P_{D,G}}}{D^{\gamma^P_{D,G}} + (\delta^P_{D,G})^{\gamma^P_{D,G}}} \right) \tag{4.28}$$

where D is the serum calcitriol concentration.

(2) Net phosphate absorption:

$$J^P_G = \Phi^P_{D,G} \cdot v^P_G \cdot \frac{\mathrm{OralP}}{k^P_G + \mathrm{OralP}} + c^P_G \cdot \mathrm{OralP} + d^P_G \tag{4.29}$$

d^P_G is an off-set to take endogenous phosphate re-entering the gut into account. Furthermore, we use d^P_G to calibrate the system. At steady state with a standard phosphate diet of 32 mmol / day, J^P_G should be around 21 mmol. OralP is the amount of phosphate intake in mmol per hour. Reduced phosphate diets or enriched phosphate diets can be simulated by adjusting OralP .

Model predictions

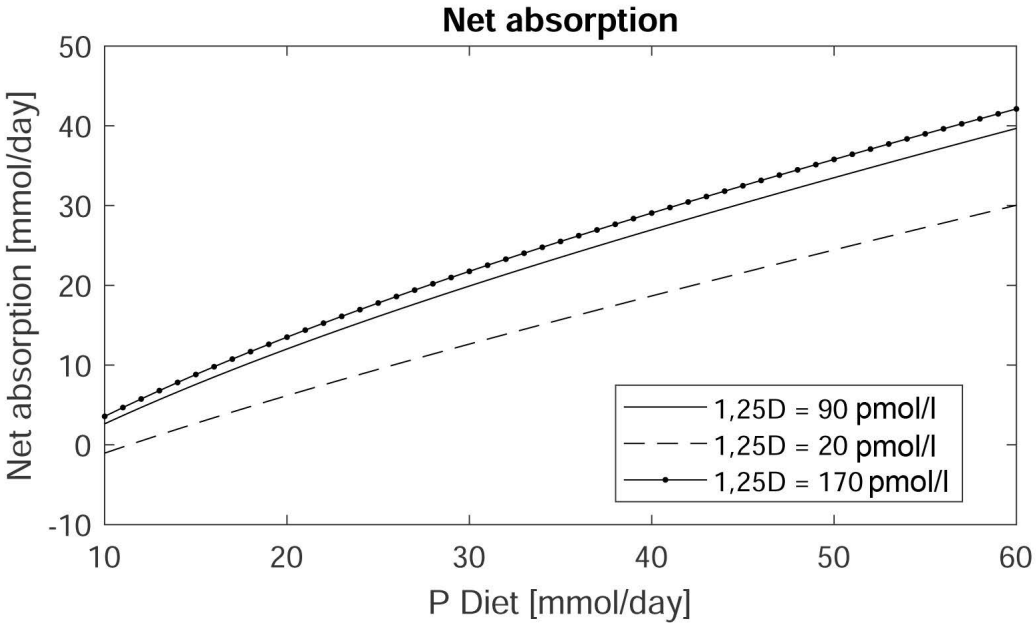

Figure 4.27 Predicted relationship between phosphate diet and intestinal phosphate net absorption. The absorption is higher with higher calcitriol levels; intestinal phosphate absorption is significantly lower at low calcitriol concentrations following the literature, e.g.(180).

Model parameters

Table 4.5 Exemplar parameters for phosphate absorption

Variable	Value	Variable	Value
$\alpha^P_{D,G}$	0.5	$\rho^P_{D,G}$	1.2
$\gamma^P_{D,G}$	3	$\delta^P_{D,G}$	60 pMol
v^P_G	1.2 mMol h^{-1}	k^P_G	1.2
c^P_G	0.07 h^{-1}		

4.4 RENAL HANDLING OF CALCIUM AND PHOSPHATE

4.4.1 Simplified model for renal calcium reabsorption and excretion

We use a simplified model for renal calcium excretion:
We fit three lines to the excretion curve: One line with a slope zero for calcium concentrations below the renal threshold, one line with a slope close to zero for the splay, and a line with a slope equal to the filtration rate for values larger than T_m/GFR. In order to have a smooth function, we use an exponential function approximation for the piecewise linear function (112). The maximal renal reabsorption T_m/GFR of calcium is a function of PTH: higher PTH concentrations (PTH) shift the value towards higher plasma calcium concentrations resulting in increased calcium reabsorption:

$$\Phi^{Ca}_{PTH,R}(0) = \alpha^{Ca}_{PTH,R} - (\alpha^{Ca}_{PTH,R} - \rho^{Ca}_{PTH,R}) \cdot \frac{PTH(0)^{\gamma^{Ca}_{PTH,R}}}{PTH(0)^{\gamma^{Ca}_{PTH,R}} + (\delta^{Ca}_{PTH,R})^{\gamma^{Ca}_{PTH,R}}} \quad (4.30)$$

$$\Phi^{Ca}_{PTH,R} = \Phi^{Ca}_{PTH,R}(0) \cdot \left(\alpha^{Ca}_{PTH,R} - (\alpha^{Ca}_{PTH,R} - \rho^{Ca}_{PTH,R}) \cdot \frac{PTH^{\gamma^{Ca}_{PTH,R}}}{PTH^{\gamma^{Ca}_{PTH,R}} + (\delta^{Ca}_{PTH,R})^{\gamma^{Ca}_{PTH,R}}} \right)^{-1} \quad (4.31)$$

Let B^0 be a vector of the two points where the pairs of two consecutive lines meet under calcium homeostasis and JCa a vector of the three values of the line slopes which is a function of filtration rate, i.e., $JCa_i = jCa_i \cdot GFRFunction(t) \cdot 0.6$ (under the assumption, that 60% of non-protein-bound calcium is freely filtrated). $B = B^0 \cdot \Phi^P_{PTH,R}$ corrects the maximal renal reabsorption concentration as a function of PTH. We use the following auxiliary functions:

$$bCa^0 = 0.5 \cdot (JCa^0(3) + JCa^0(1)) \qquad bCa = 0.5 \cdot (JCa(3) + JCa(1))$$
$$cCa^0 = 0.5 \cdot \sum_{i=1}^{2} (JCa^0(i+1) - JCa^0(i)) \qquad cCa = 0.5 \cdot \sum_{i=1}^{2} (JCa(i+1) - JCa(i))$$
$$aCa^0 = \sum_{i=1}^{2} cCa_i^0 \cdot |B_i^0| \qquad aP = \sum_{i=1}^{2} cCa_i \cdot |B_i|$$
$$ACa^0 = aCa^0 - \sum_{i=1}^{2} cCa_i^0 \cdot b_i^0 \qquad ACa = aCa - \sum_{i=1}^{2} cCa_i \cdot b_i$$
$$BCa^0 = bCa^0 + \sum_{i=1}^{2} cCa_i^0 \qquad BCa = bCa + \sum_{i=1}^{2} cCa_i$$

$$J_R^{Ca}(0) = ACa^0 + BCa^0 \cdot C(0) + \frac{2}{\alpha} \sum_{i=1}^{2} cCa_i^0 \cdot \ln(1 + \exp(-\alpha \cdot (C(0) - bCa^0))) \quad (4.32)$$

$$J_R^{Ca} = ACa + BCa \cdot C + \frac{2}{\alpha} \sum_{i=1}^{2} cCa_i \cdot \ln(1 + \exp(-\alpha \cdot (C - bCa))) \quad (4.33)$$

The parameter α regulates the smoothness of the approximation. C is the total calcium concentration (+ $CaHPO_4$ if taken into account).

Model predictions

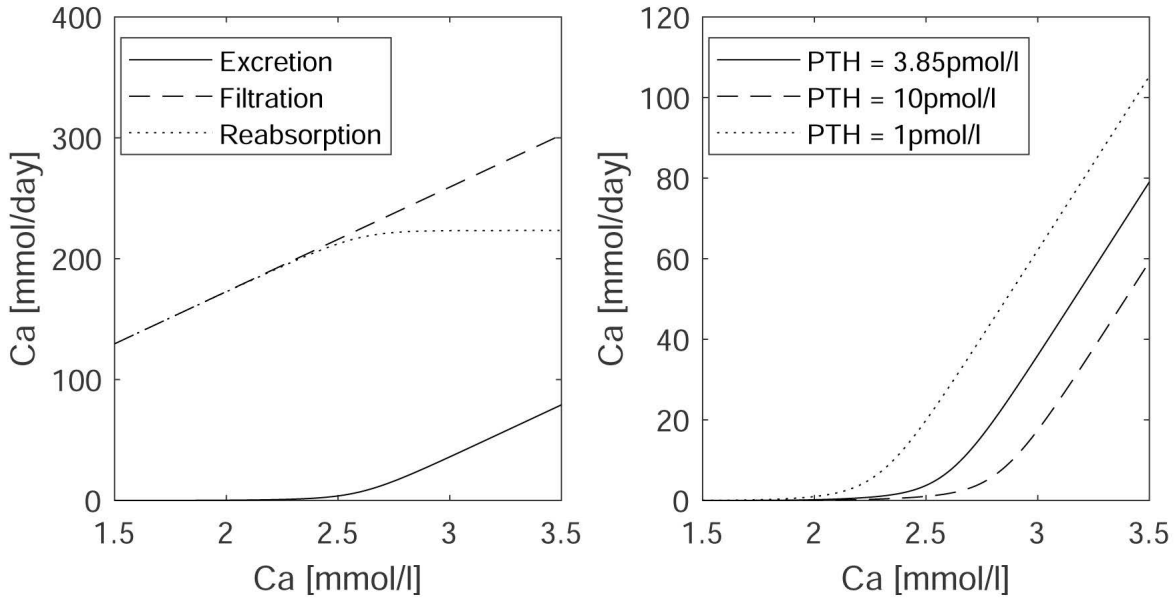

Figure 4.28 Left: predicted calcium filtration, excretion, and reabsorption as a function of plasma calcium concentration. Right: Predicted calcium excretion for different levels of PTH plasma concentration.

Model parameters

Table 4.6 Exemplar parameters for renal calcium handling. Parameters estimation is based on (166).

Variable	Value	Variable	Value
$\alpha^{Ca}_{PTH,R}$	0.98	$\rho^{Ca}_{PTH,R}$	1.02
$\delta^{Ca}_{PTH,R}$	$PTH(0)$ pMol	$\gamma^{Ca}_{PTH,R}$	2
B^0	$(2.1, 2.6)$ mMol	JCa	$(0, 0.1667, 1)$

4.4.2 Simplified model for renal phosphate excretion and reabsorption

We use the following simplified model for renal phosphate excretion:
Again, we fit three lines to the excretion curve: One line with a slope of zero for low phosphate concentrations, one line with a slope close to zero for values in the splay region, and one line with a slope equal to the filtration rate for values larger than the maximal renal reabsorption capacity. To have a smooth function, we use an exponential function approximation for a piecewise linear function (112). The renal threshold of phosphate is a function of PTH: higher values of PTH shift the renal threshold towards smaller plasma phosphate concentrations:

$$\begin{aligned}
\Phi^P_{PTH,R}(0) &= \alpha^P_{PTH,R} - \\
&\quad (\alpha^P_{PTH,R} - \rho^P_{PTH,R}) \cdot \frac{PTH(0)^{\gamma^P_{PTH,R}}}{PTH(0)^{\gamma^P_{PTH,R}} + (\delta^P_{PTH,R})^{\gamma^P_{PTH,R}}} \qquad (4.34)\\
\Phi^P_{PTH,R} &= \frac{1}{\Phi^P_{PTH,R}(0)} \cdot \\
&\quad \left(\alpha^P_{PTH,R} - (\alpha^P_{PTH,R} - \rho^P_{PTH,R}) \cdot \frac{PTH^{\gamma^P_{PTH,R}}}{PTH^{\gamma^P_{PTH,R}} + (\delta^P_{PTH,R})^{\gamma^P_{PTH,R}}}\right) \qquad (4.35)
\end{aligned}$$

Let b^0 be a vector of the two points where the pairs of two consecutive lines meet under phosphate homeostasis and J a vector of the three values of the line slopes, which is a function of filtration rate, i.e., $J_i = j_i \cdot GFRFunction(t) \cdot 0.85$ (under the assumption, that 85% of phosphate are freely filtrated). $b = b^0 \cdot \Phi^P_{PTH,R}$ corrects the renal threshold

as a function of PTH. We use the following auxiliary functions:

$$
\begin{array}{ll}
bP^0 = 0.5 \cdot (JP^0(3) + JP^0(1)) & bP = 0.5 \cdot (JP(3) + JP(1)) \\
cP^0 = 0.5 \cdot \sum_{i=1}^{2} (JP^0(i+1) - JP^0(i)) & cP = 0.5 \cdot \sum_{i=1}^{2} (JP(i+1) - JP(i)) \\
aP^0 = \sum_{i=1}^{2} cP_i^0 \cdot |b_i^0| & aP = \sum_{i=1}^{2} cP_i \cdot |b_i| \\
AP^0 = aP^0 - \sum_{i=1}^{2} cP_i^0 \cdot b_i^0 & AP = aP - \sum_{i=1}^{2} cP_i \cdot b_i \\
BP^0 = bP^0 + \sum_{i=1}^{2} cP_i^0 & BP = bP + \sum_{i=1}^{2} cP_i
\end{array}
$$

$$J_R^P(0) = AP^0 + BP^0 \cdot C(0) + \frac{2}{\alpha} \cdot \sum_{i=1}^{2} cP_i^0 \cdot \ln(1 + \exp(-\alpha \cdot (C(0) - bP^0))) \quad (4.36)$$

$$J_R^P = AP + BP \cdot C + \frac{2}{\alpha} \cdot \sum_{i=1}^{2} cP_i \cdot \ln(1 + \exp(-\alpha \cdot (C - b))) \quad (4.37)$$

The parameter α regulates the smoothness of the approximation. C is the total phosphate concentration (+ $CaHPO_4$ if taken into account).

Model predictions

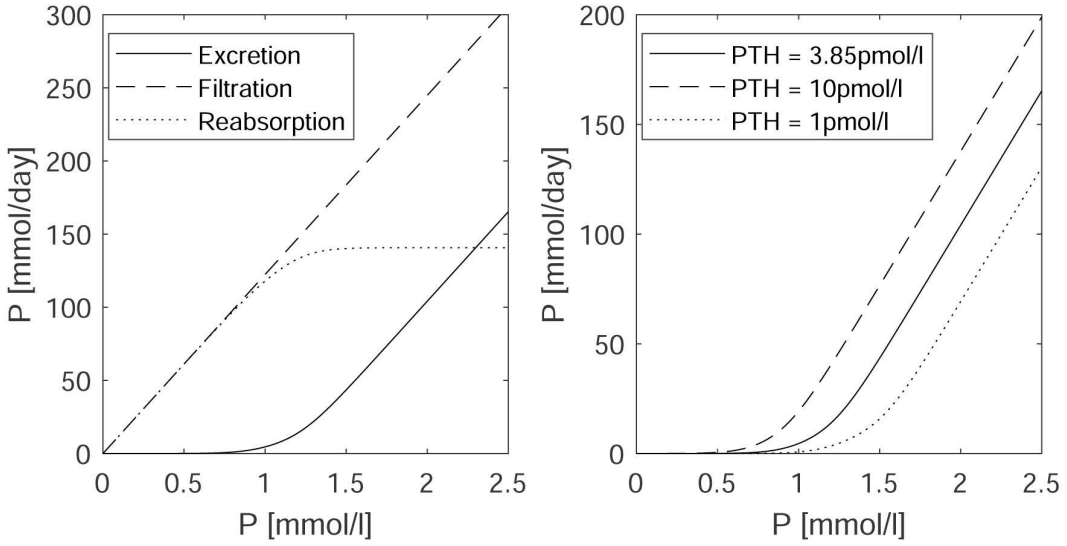

Figure 4.29 Left: predicted phosphate filtration, excretion, and reabsorption as a function of plasma phosphate concentration. Right: Predicted phosphate excretion for different levels of PTH plasma concentration.

Model parameters

Table 4.7 Exemplar parameters for renal phosphate handling. Parameter estimation is based on (119, 125).

Variable	Value	Variable	Value
$\alpha^P_{PTH,R}$	1	$\rho^P_{PTH,R}$	0.6
$\gamma^P_{PTH,R}$	4	$\delta^P_{PTH,R}$	$PTH(0)$ pMol
b^0	$(0.9, 1.22)$ mMol	J	$(0, 0.22, 1)$

4.5 CALCITRIOL

We use a two-compartment model for calcitriol levels. The first compartment corresponds to calcitriol synthesis (SD), the second to the serum calcitriol levels (D).

(1) The synthesis rate SR is a function of Ca^{2+}(Ca), phosphate (P), PTH (PTH) and calcitriol concentrations. Moreover, we assume that the synthesis ability of the kidneys is reflected by the GFR:

$$SR = \delta_D^{\min} + \delta_D^{\max} \cdot \frac{PTH^{\gamma_{D,PTH}}}{PTH^{\gamma_{D,PTH}} + K_{D,PTH}^{\gamma_{D,PTH}}} \cdot \frac{K_{D,P}}{P + K_{D,P}} \cdot \frac{K_{D,D}}{D + K_{D,D}} \cdot \frac{K_{D,Ca}}{Ca + K_{D,Ca}},$$

where $\delta_D^{\min}$ is the minimum synthesis rate.

(2) The dynamic equation for the synthesis can be written as

$$\frac{dSD}{dt} = SR \cdot (\phi_{GFR} + (1 - \phi_{GFR}) \cdot \mathrm{GFRFunction}(t)) - c_{SD} \cdot SD.$$

(3) The degradation rate of calcitriol in the plasma is partly down-regulated by PTH concentration:

$$c_D = cD \cdot \left(\phi_{D,PTH} + (1 - \phi_{D,PTH}) \cdot \frac{1 + PTH(0)}{1 + PTH} \right).$$

(4) The amount of calcitriol in the plasma (D) is determined by the following ordinary differential equation:

$$\frac{dD}{dt} = SD - c_D \cdot D.$$

Parameters

Table 4.8 Exemplar parameters for calcitriol dynamics. Parameter estimation is based on (14, 139, 172).

Variable	Value	Variable	Value
$\delta_D^{\min}$	6.299 pmol h^{-1}	$\delta_D^{\max}$	89.2 pmol h^{-1}
$K_{D,PTH}$	30 pMol	$\gamma_{D,PTH}$	4.8
$K_{D,D}$	200pMol	$K_{D,Ca}$	3.3 mMol
$K_{D,P}$	5 mMol	c_D	0.1 h^{-1}
ϕ_{GFR}	0.9	c_{SD}	0.05 / h
$\phi_{D,PTH}$	0.1		

4.6 INTRACELLULAR PHOSPHATE

We make the following assumptions for our physiology-based model approach:

(1) We have two intracellular compartments: One compartment represents the amount of free intracellular phosphate, P_{ic}^{f}. The second compartment represents the amount of bound intracellular phosphate, P_{ic}^{s}. The two compartments ensure the buffer ability of the cell.

(2) There is a fast passive transport between these two compartments.

(3) There are two ways for phosphate to transfer from the ECF to the intracellular compartment: it can diffuse, or it can be pumped actively into the cells.

(4) Phosphate diffuses from the cells to the ECF. However, transport is enhanced if the plasma concentration reaches a critical level.

Therefore, the new model reads as follows:

$$\frac{d}{dt}P_{ic}^{f} = k_{ecf}^{ic}P_{p}^{\gamma_P} + \frac{a_p P_p}{P_p^{\gamma_P} + \delta_p^{\gamma_P}} - H(P_p)\cdot P_{ic} + k_s^f P_{ic}^s - k_f^s P_{ic}^f \tag{4.38}$$

$$\frac{d}{dt}P_{ic}^{s} = -k_s^f P_{ic}^s + k_f^s P_{ic}^f, \tag{4.39}$$

where P_p is the plasma phosphate concentration and $H(P_p) = k_{ic}^{ecf} - \tau_P^{ic}\cdot P_p^{\gamma_P^{ic}}/(P_p^{\gamma_P^{ic}} + (\delta_P^{ic})^{\gamma_P^{ic}})$. The model predictions are close to the clinical findings (Fig 4.30).

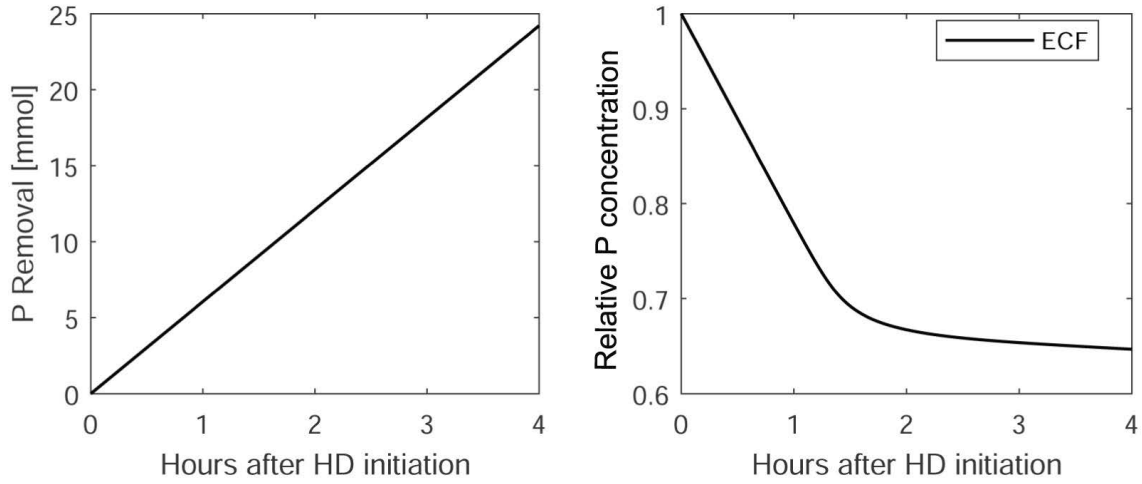

Figure 4.30 Predictions based on the new model: Linear removal of phosphate during hemodialysis (left panel) leads to a steep decline within the first hour of an HD session. The plasma phosphate concentration then plateaus despite continuing phosphate removal (right panel).

Parameters

Table 4.9 Exemplar parameters for IC-ECF phosphate exchange. Parameter estimation was based on (117, 134, 211).

Variable	Value	Variable	Value
a_P	5 h^{-1}	γ_P	5
δ_p	2.5 mMol	k_{ic}^{ecf}	100 h^{-1}
τ_P^{ic}	99.99 h^{-1}	γ_P^{ic}	40
δ_P^{ic}	0.9 mMol	k_{ecf}^{ic}	0.407 h^{-1}
k_s^f	10 h^{-1}	k_f^s	0.7143 h^{-1}
$P_{ic}^f(0)$	200 mMol	$P_{ic}^s(0)$	2800 mMol

4.6.1 Sensitivity analysis

We performed a sensitivity analysis by multiplying the corresponding parameters by 2 or 0.5 and analyzed the response of phosphate removal in a single dialysis session (Fig. 4.31 and Fig. 4.32). Since the relationship between extra and intracellular phosphate also determines the rise and fall of phosphate plasma concentrations under non-steady state conditions, we also simulated kidney function loss and regular hemodialysis (when GFR is below 5% of the healthy GFR) with the integrated calcium and phosphate homeostasis model. These results are presented in the Appendix.

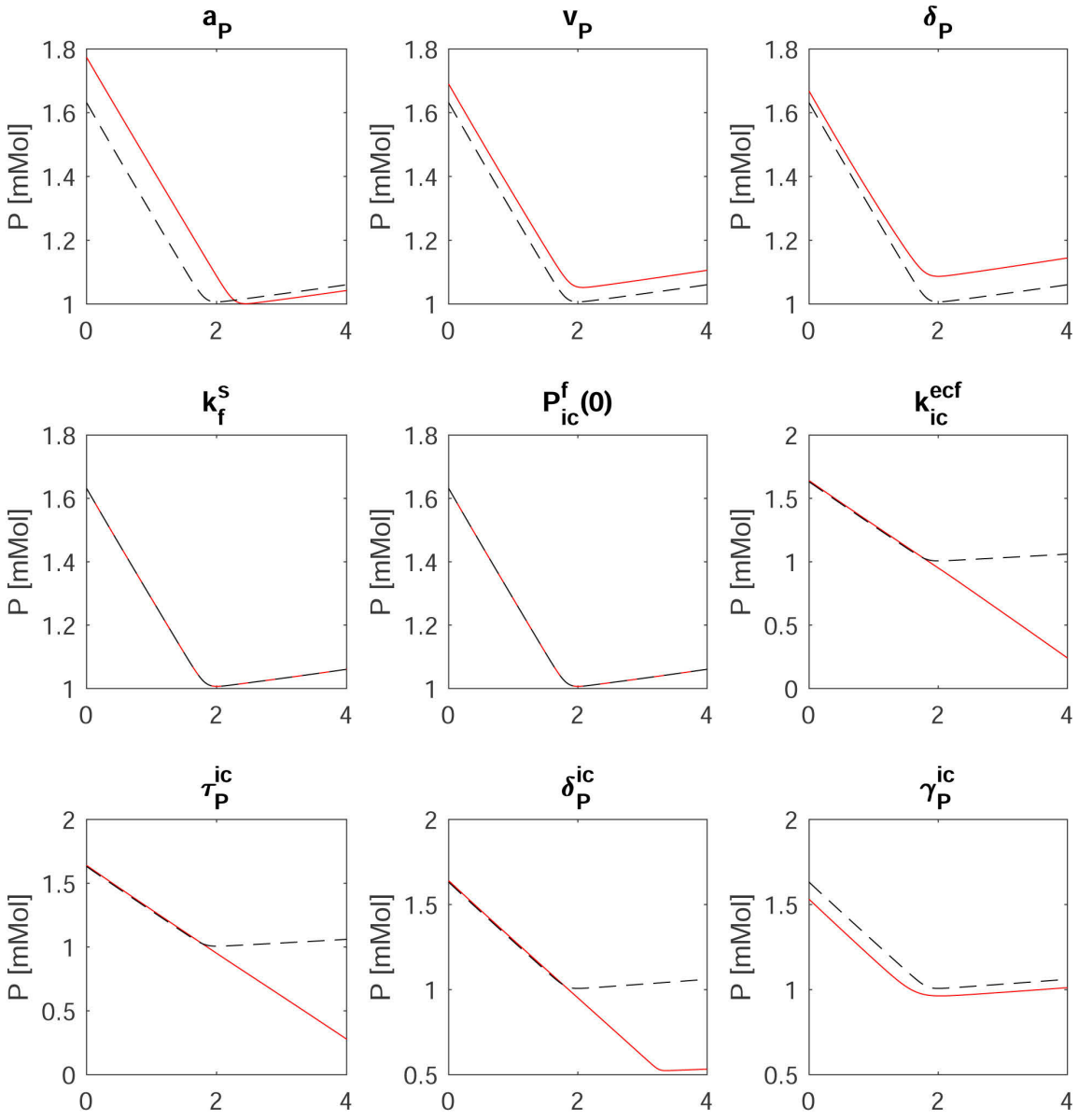

Figure 4.31 Predicted behavior during a single dialysis session with the standard parameter set (black line) and under the condition that a single parameter is multiplied by 0.5 (red line). While the qualitative prediction is not sensitive to changes in a_P, v_P, k_f^s, $P_{ic}^f(0)$, and γ_P^{ic}, the behavior changes significantly if k_{ic}^{ecf}, τ_P^{ic} or δ_P^{ic} are altered. Specifically, the flux from the IC compartment does not reach a significant level indicating that the point of recovery is not reached during the dialysis session. Changing one of these parameters implies that the other two parameters have to be adjusted as well.

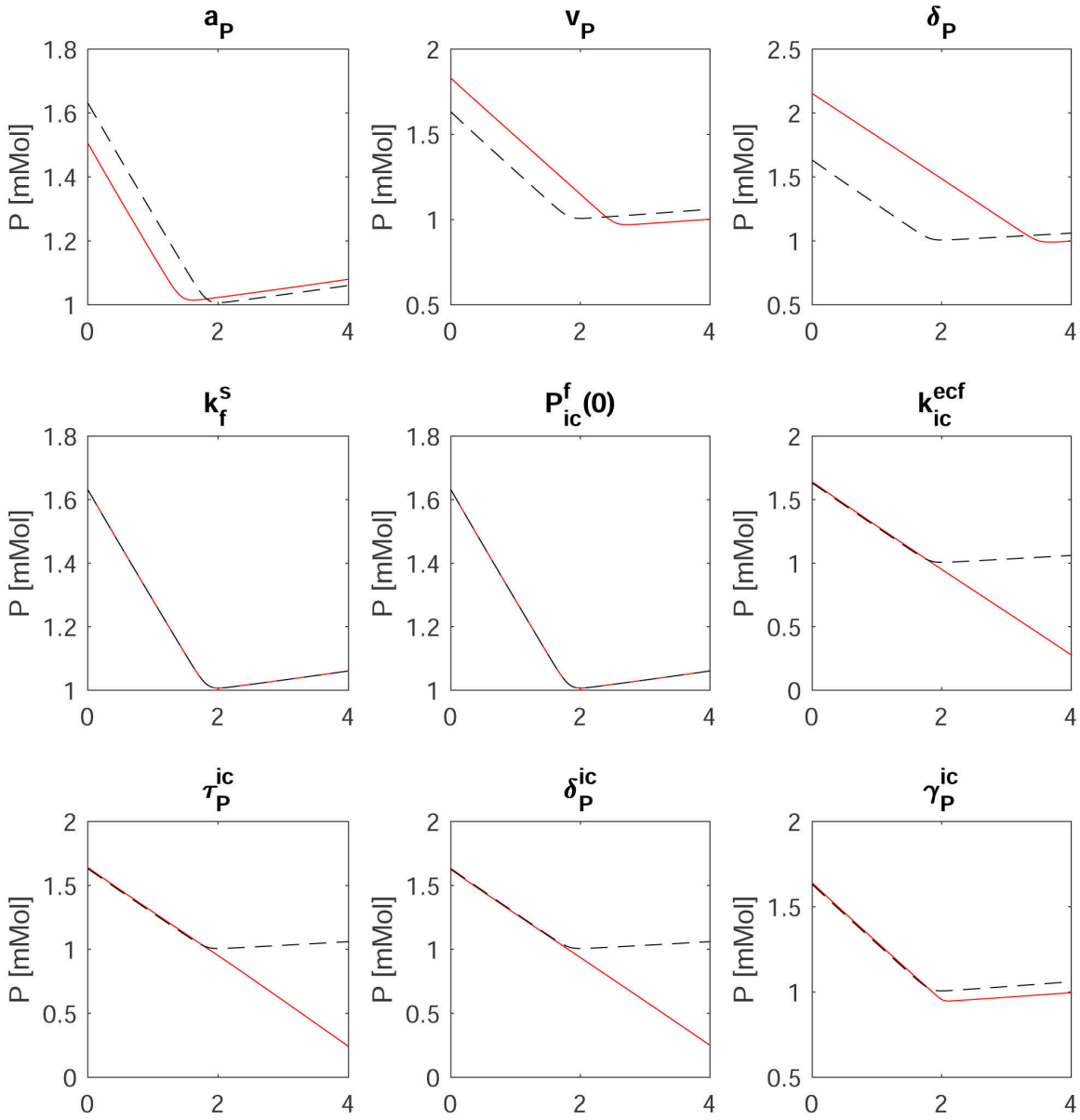

Figure 4.32 Predicted behavior during a single dialysis session with the standard parameter set (black line) and or under the condition that a parameter is multiplied by 2 (red line). Again, while the qualitative prediction is not sensitive to changes in a_P, v_P, k_f^s, $P_{ic}^f(0)$, and γ_P^{ic}, the behavior changes significantly if k_{ic}^{ecf}, τ_P^{ic} or δ_P^{ic} are altered.

4.7 CALCIUM-PHOSPHATE PRECIPITATION AND VASCULAR CALCIFICATION

We use the following model for $CaPO_4$ dynamics:

(1) Point of no return due to hyperphosphatemia:
We assume that it takes high levels of phosphate for a long time before the point of no return is reached. Again, we use a stimulus function to model the effect of hyperphosphatemia. This approach takes the critical amount of time necessary for the reaction of the system into account. Moreover, the stimulus function filters short-lived phosphate spikes. In our model, the point of no return is reached if the variable $PNR = 0$. However, while PNR declines exponentially under the presence of a long-lasting phosphate stimulus, it will not reach zero in a finite amount of time. In our numerical implementation, the point of no return is reached once PNR is sufficiently small. In this thesis, the numerical threshold for PNR is defined as 10^{-10}.

$$\frac{dPNR}{dt} = -k_{PNR} \cdot PNR_{stim} \cdot PNR \tag{4.40}$$

$$\frac{dPNR_{stim}}{dt} = (stim_P(P - P_{opt}) \cdot (1 - \text{sign}(stim_P(P - P_{opt})) \cdot PNR_{stim}) - PNR_{stim}) \cdot \tau_{PNR}, \tag{4.41}$$

$$\text{stim}_P(x) = \max(0, \frac{1}{1 + \exp(-K_P \cdot (x - x_1))} + \frac{1}{1 + \exp(-K_P(x + x_1))} - 1) \tag{4.42}$$

where $PNR(0) = 1$ and $PNR_{stim}(0) = 0$.

(2) Conversion rate k_{nr} from $CaPO_4$ to solid forms:
The conversion rate is zero at steady state and increases when a threshold level of $CaPO_4$ is reached. We estimate the rate by a piecewise linear function consisting of three lines and use a smooth approximation of the piecewise linear function. We assume that the lines meet in $b_{nr} = (b_{nr}^1, b_{nr}^2)$. J_{nr} is a vector comprising the slopes of the three lines:

$$
\begin{aligned}
k_{nr} &= (k_{nr}^0 + A_{nr} + B_{nr} \cdot CaPO_4 + \\
&\quad \frac{2}{\alpha_{nr}} \cdot \sum_{i=1}^{3} c_{nr}^i \cdot \ln(1 + \exp(-\alpha_{nr} \cdot (CaPO_4 - b_{nr})))) \qquad (4.43)
\end{aligned}
$$

where

$$
\begin{array}{ll}
\beta_{nr} = 0.5 \cdot (JP(3) + JP(1)) & c_{nr}^i = 0.5 \cdot (J_{nr}^{i+1} - J_{nr}^i) \\
a_{nr} = \sum_{i=1}^{2} c_{nr}^i \cdot |b_{nr}^i| & A_{nr} = a_{nr} - \sum_{i=1}^{2} c_{nr}^i \cdot b_{nr}^i \\
B_{nr} = \beta_{nr} + \sum_{i=1}^{2} c_{nr}^i, &
\end{array}
$$

where α_{nr} regulates the smoothness of the approximation.
We make the same parameter adjustment for d_{FetA}.

(2) Dynamic equations for $CaPO_4$, Fetuin A ($FetA$), CPPs (CPP) and solid forms $CaPO_4^s$:

$$
\begin{aligned}
J_{Ca,P}^{CaPO_4} &= k_{CaxP} \cdot PNR \cdot (C_{ECC}^{2+} - CaPO_4 \cdot V) \cdot (P_{ECC} - CaPO_4 \cdot V) \\
&\quad + (1 - PNR) \cdot k_{CaxP}^{PNR} \qquad (4.44) \\
J_{CaPO_4}^{Ca,P} &= d_{CaxP} \cdot CaPO_4 \qquad (4.45) \\
J_{CaPO_4}^{FetA} &= d_{FetA} \cdot (FetA - CPP) \cdot CaPO_4 \qquad (4.46) \\
J_{CaPO_4}^{depot} &= k_{nr} \cdot CaPO_4 \qquad (4.47) \\
\frac{dCaPO_4}{dt} &= J_{Ca,P}^{CaPO_4} - J_{CaPO_4}^{Ca,P} - J_{CaPO_4}^{FetA} - J_{CaPO_4}^{depot} \qquad (4.48) \\
\frac{dCPP}{dt} &= J_{CaPO_4}^{FetA} - c_{CPP} \cdot CPP \qquad (4.49) \\
\frac{dFetA}{dt} &= p_{FetA}(GFR) - c_{FetA} \cdot FetA \qquad (4.50)
\end{aligned}
$$

Here, we assume that C_{ECC}^{2+} is 55% of the total calcium concentration (29). When PNR is close to zero, the formation rate of $CaPO_4$ detaches from actual $Ca^{2+}$and phosphate concentrations. Furthermore, we adjust the total calcium and phosphate equa-

tions by taking the loss due to CPP formation and the loss to the depot ($CaPO_4^s$) into account.

In case the model should be studied without the point of no return concept, equation 4.48 reduces to

$$\begin{aligned}\frac{dCaPO_4}{dt} &= k_{CaxP} \cdot (C \cdot 0.55 - CaPO_4 \cdot V) \cdot (P - CaPO_4 \cdot V) - d_{CaxP} \cdot CaPO_4 \\ &\quad -d_{FetA} \cdot (FetA - CPP) \cdot CaPO_4 - k_{nr} \cdot CaPO_4.\end{aligned}$$

Parameters

c_{CPP} and c_{FetA} are estimated from the literature (41, 99). The slope of p_{FetA} is estimated from the literature (210). The steady state determines p_{FetA} and the basal value for d_{FetA}. k_{CaXP} and d_{CaxP} are based on literature data (85).

k_{nr} is zero at steady state and starts to increases after a certain threshold b_{nr}^1 is reached. The threshold (currently 0.13 mMol) is estimated. The other parameters are assumed to be $b_{nr}^2 = 0.2$ mMol and $J_{nr} = (0, 6, 0)$ (i.e., the slope is zero for values below b_{nr}^1. k_{nr} than rises quickly before reaching its maximum value at b_{nr}^2.)

The parameters regarding the point of no return for the detachment of $CaPO_4$ formation from $Ca^{2+}$and phosphate concentrations is estimated based on the simulations. Currently, $\tau_{PNR} = 10^{-5}$ and $k_{PNR} = 5$, $x_1 = 0.8$ mMol (i.e., the stimulus is almost zero for deviations smaller than 0.8 mMol from the steady state value and reaches its maximum with a deviation lager than approximately 1.357 mMol), and $K_P = 2.5$ / mMol.

Table 4.10 Exemplar parameters for $CaPO_4$ dynamics

Variable	Value	Variable	Value
b_{nr}	(0.15 0.5) mMol	J_{nr}	(0, 5, 0)
τ_{PNR}	10^{-6}	k_{PNR}	5
x_1	0.8 mMol	K_P	2.5/mMol
k_{PNR}	5	k_{CaxP}	121/(mMol·h)
c_{CPP}	0.9242 h^{-1}	c_{FetA}	0.2791 h^{-1}
k_{CaxP}^{PNR}	1.5·k_{CaXP}	d_{FetA}^0	7.4·10^{-3}
b_{FetA}	(0.062 0.07)	J_{FetA}	(0, 10, 0)

Sensitivity analysis

To analyze the sensitivity of model predictions to various parameters, we performed a sensitivity analysis. The respective parameters were either multiplied by 2 or divided

by 2. Since the effect of calcium-phosphate precipitation is systemic, we simulated the loss of kidney function over time. We assumed that regular dialysis started when the GFR was below 5% of the healthy GFR. In the sensitivity graphs, the black vertical line indicates the start of hemodialysis. The analysis shows that k_{CaxP}, is a crucial parameter (Fig. 4.34, Fig. 4.33). A wrong choice of k_{CaxP} might even lead to instabilities. The same is true for $J_{nr}(2)$ and $b_{nr}(1)$. If $J_{nr}(2)$ is too large, plasma calcium levels decline unrealistically. If $b_{nr}(1)$ is too large, plasma calcium levels rise unrealistically. The model is not sensitive to the other 6 parameters (their graphs are presented in the Appendix).

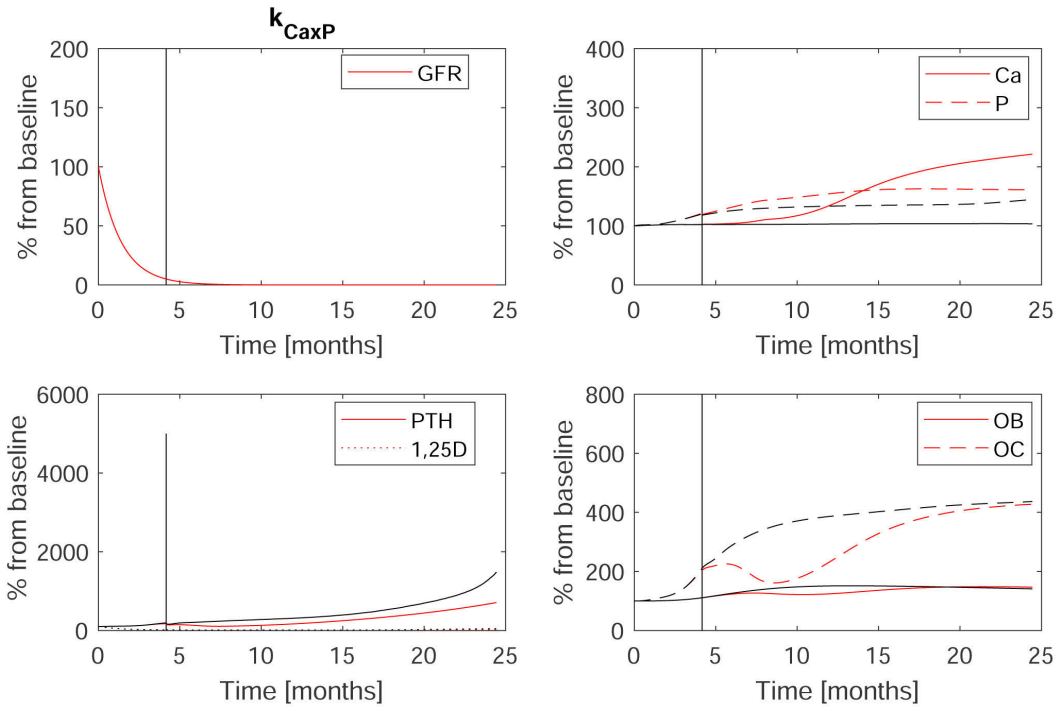

Figure 4.33 Red lines: k_{CaxP} is multiplied by 2, black lines: standard parameters.

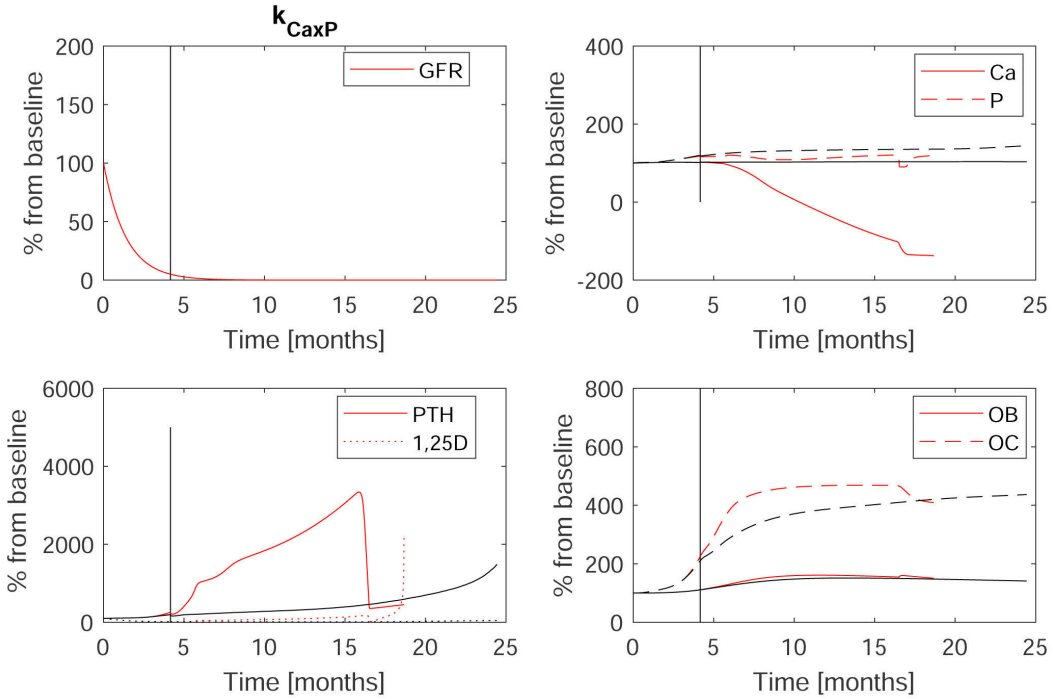

Figure 4.34 Red lines: k_{CaxP} is multiplied by 0.5, black lines: standard parameters.

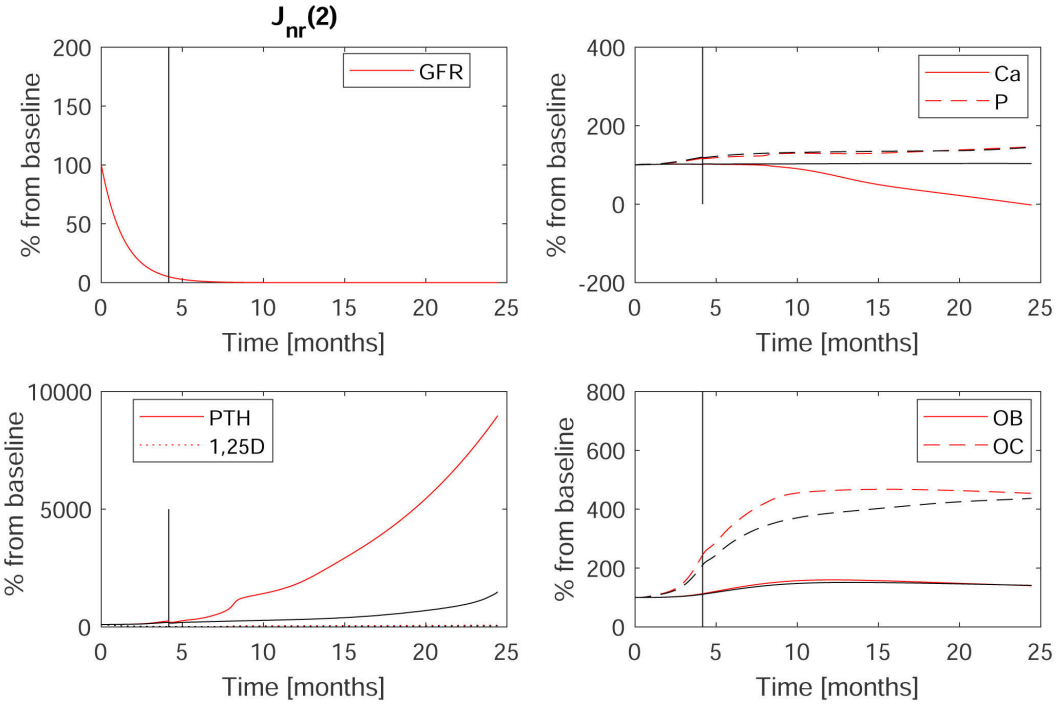

Figure 4.35 Red lines: $J_{nr}(2)$ is multiplied by two, black lines: standard parameters.

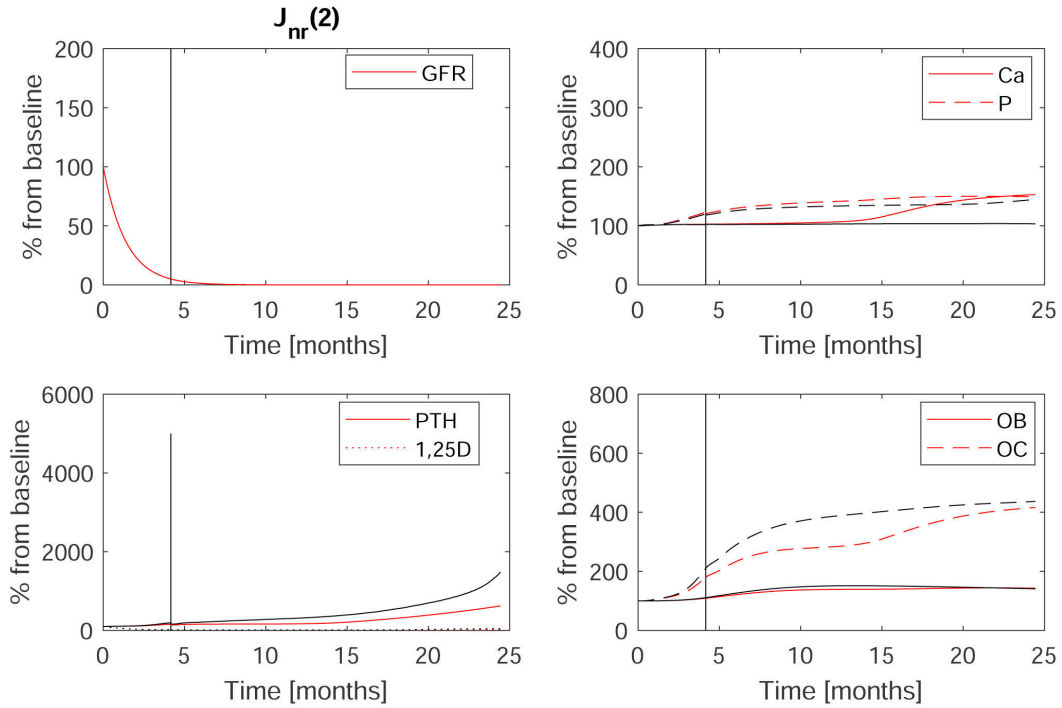

Figure 4.36 Red lines: $J_{nr}(2)$ is multiplied by 0.5, black lines: standard parameters.

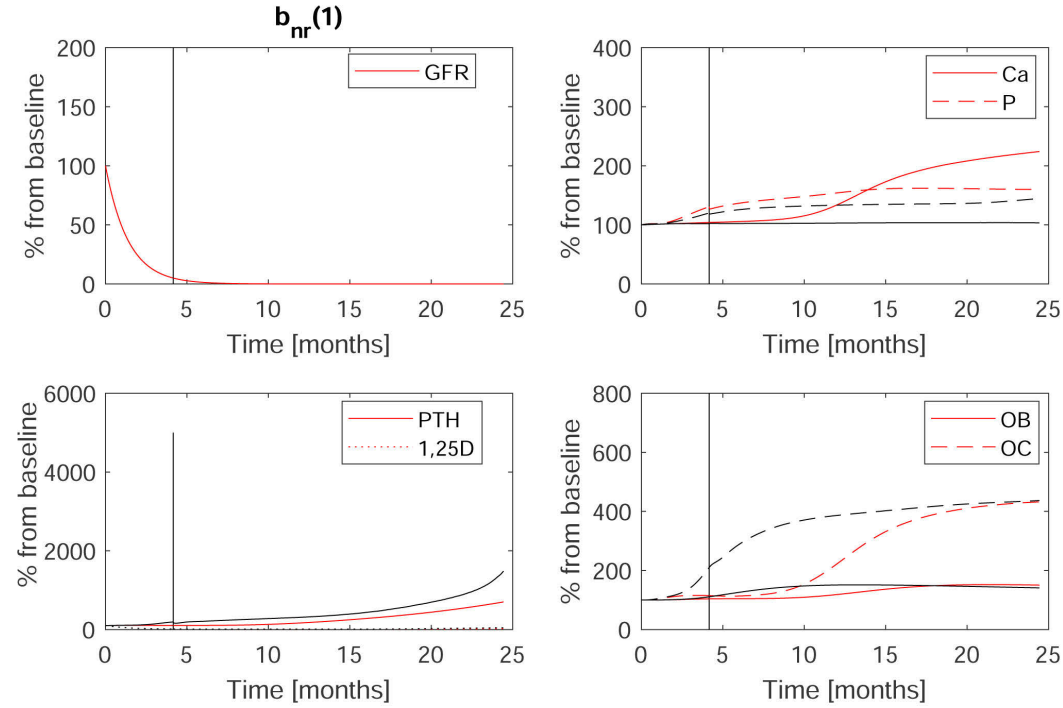

Figure 4.37 Red lines: $b_{nr}(1)$ is multiplied by two, black lines: standard parameters.

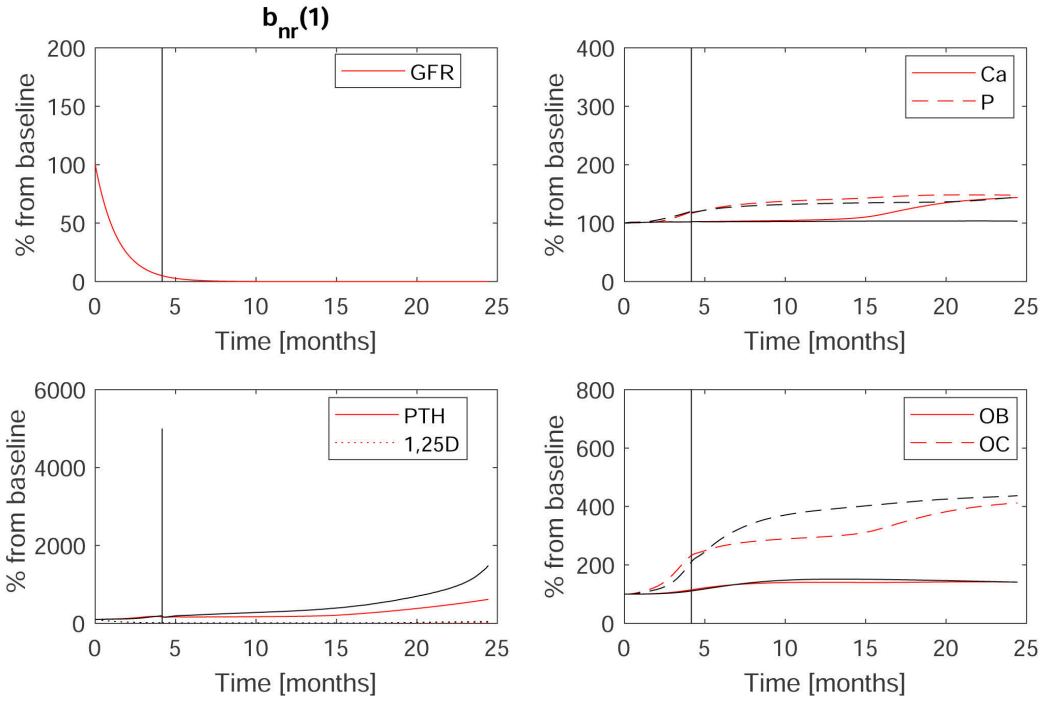

Figure 4.38 Red lines: $b_{nr}(1)$ is multiplied by 0.5, black lines: standard parameters.

4.8 BONE MODEL

The bone model is loosely based on the model introduced by Peterson and Riggs (174) and includes RANK-RANKL-OPG regulation, Runx-Bcl2-CREB regulation and TGF-β. The main differences include the regulation of the maturation of osteoclasts (104), the regulation of apoptosis and differentiation of osteoblasts, and the action of TGF-β on osteoclasts.

4.8.1 Main model assumptions

Based on bone physiology, we made the following model assumptions:

(1) RANK synthesis is inducible by active TGF-β (115). RANK degradation is assumed to be a first-order process.

(2) The synthesis rate of RANKL is a function PTH concentration (74, 144) and calcitriol (121, 161, 227). Since osteoblasts express RANKL, the synthesis rate includes a term for the fractional changes in osteoblasts. RANKL degradation is described as a first-order process.

(3) Binding rate constants account for association and dissociation of RANKL/RANK and RANKL/OPG. The association rate of RANKL and OPG is a factor 100 higher than the association rate of RANK and RANKL.

(4) Runx2 and CREB synthesis rates are assumed to follow first-order elimination. The Runx2 elimination rate and the CREB synthesis rate are functions of PTH concentrations. Bcl-2 affects osteoblast survival by decreasing the apoptosis rate of osteoblasts. Intermittent PTH administration is associated with an increase in Runx2-associated anti-apoptotic signaling. However, this effect is diminished by continuous PTH administration due to the increased production of Runx2 degrading enzyme (6, 8). Accordingly, the increase in the anti-apoptotic signaling is kinetically faster than the increase of the Runx2 degrading enzyme's synthesis rate.

(5) OPG synthesis is linearly affected by the amount of responding osteoblasts and is inversely related to PTH levels (74, 144).

(6) TGF-β is produced as a latent form by osteoblasts (51). The latent form is converted to its active form during bone resorption by the signaling of osteoclasts (52). Therefore, we assume that the latent form's production rate is a function

of the number of osteoblasts, the removal rate of the latent form is a function of the number of osteoclasts. The active form's removal rate is assumed to be 1000-fold higher than the removal rate of the latent form. Therefore, the amount of latent TGF-β is 1000-fold higher than the amount of the active form under healthy steady state (52).

(7) Mesenchymal progenitors are differentiated into responding osteoblasts. The differentiation rate is a function of active TGF-β. The elimination rate for responding osteoblasts is assumed to be of first-order. The input rate for active osteoblasts equals the output rate from the responding osteoblast compartment. Again, elimination is assumed to be of first-order. Osteoblasts have two fates: they can undergo apoptosis (roughly 70%) or differentiate to osteocytes (111).

(8) The ratio of osteoclasts to osteoblasts at a healthy steady state is approximately 4-5 osteoblasts per osteoclasts (110).

(9) RANKL is required for the production and survival of osteoclasts (178). The effect of RANKL on the production rate depends on the relative level of the OPG-RANKL complex. Apoptosis is assumed to be of first-order and inversely related to active TGF-β and RANKL (212).

(10) The availability of osteoblastic and osteoclastic precursors in unlimited.

Auxiliary functions

We use the following auxiliary functions:

$$H_p(x) = \alpha\left(\frac{x^\gamma}{\delta^\gamma + x^\gamma}\right) \tag{4.51}$$

$$H_p^-(x) = \alpha - (\alpha - \rho)\left(\frac{x^\gamma}{\delta^\gamma + x^\gamma}\right) \tag{4.52}$$

$$H_p^+(x) = \rho + (\alpha - \rho)\left(\frac{x^\gamma}{\delta^\gamma + x^\gamma}\right), \tag{4.53}$$

where p is either the parameter set (α, δ, γ) or the parameter set $(\alpha, \delta, \gamma, \rho)$.

Notation

G denotes the gut compartment, ECC the extracellular fluid compartment. I denotes intestinal, B denotes the bone compartment. IC denotes the intracellular compartment. The superscript $fast$ denotes the interchangeable pool in the bone, the superscript $slow$

the non-interchangeable pool. The symbol $*$ between two variables denotes the complex of the two variables, i.e., $RANKL*OPG$ is the RANKL-OPG complex.

Intracellular pathway: Runx2-CREB-Bcl2

The model of the Runx2-pathways is the same as the one introduced by (174). The mRNA for Runx2 ($RX2$) has a half-life of less than 2 hours (77), and we assume that the entire Runx2-pathway responds on a similar time scale. Bcl-2 (Bcl) and CREB ($Creb$) are assumed to follow first-order elimination. The corresponding parameters are provided in table 4.12.

$$\begin{aligned}
\frac{d}{dt}RX2 &= c_{RX2} \cdot RX2(0) - H^{+}_{PTH,RX2}(PTH_{ECC}/V_{ECC}) \cdot RX2 && (4.54)\\
\frac{d}{dt}Creb &= c_{Creb} \cdot Creb(0) \cdot H^{+}_{PTH,Creb}(PTH_{ECC}/V_{ECC}) - c_{Creb} \cdot Creb && (4.55)\\
\frac{d}{dt}Bcl &= c_{Bcl} \cdot RX2 \cdot Creb - c_{Bcl} \cdot Bcl && (4.56)
\end{aligned}$$

RANK-RANKL pathway

The parameters are provided in table 4.13.

$$\begin{aligned}
\frac{d}{dt}RANKL &= k_{RANKL} - c_{RANKL} \cdot RANKL - k_{RANKL,RANKL*OPG} \cdot OPG \cdot RANKL \\
&\quad + k_{RANKL*OPG,RANKL} \cdot RANKL*OPG \\
&\quad - k_{RANKL,RANKL*RANK} \cdot RANK \cdot RANKL \\
&\quad + k_{RANKL*RANK,RANKL} \cdot RANKL*RANK, && (4.57)
\end{aligned}$$

where $PTHc = PTH_{ECC}/V_{ECC}$, D is the calcitriol concentration and

$$\begin{aligned}
k_{RANKL} &= k^{0}_{RANKL} \cdot \left(\frac{OB}{OB(0)}\right)^{\gamma_{OEff}} \cdot \frac{\alpha_{PTH,RANKL} \cdot PTHc}{\delta_{PTH,RANKL} \cdot (OB/OB(0))^{\gamma_{OEff}} + PTHc} \cdot \\
&\quad H^{+}_{D,RANKL}(D) \cdot H^{+}_{TGFBact,RANKL}(TGFBact) && (4.58)
\end{aligned}$$

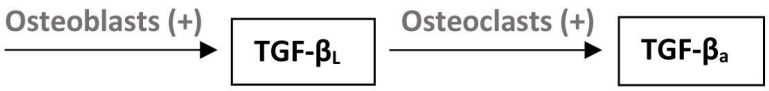

Figure 4.39 TGF-β is produced in a latent form by osteoblasts and activated by osteoclasts.

$$\begin{aligned}
\frac{d}{dt}RANK &= k_{RANK} \cdot TGFBact^{\gamma_{TGFBact,RANK}} - c_{RANK} \cdot RANK && (4.59)\\
&\quad - k_{RANKL,RANKL*RANK} \cdot RANK \cdot RANKL\\
&\quad + k_{RANKL*RANK,RANKL} \cdot RANKL * RANK\\
\frac{d}{dt}RANKL * RANK &= k_{RANKL,RANKL*RANK} \cdot RANK \cdot RANKL && (4.60)\\
&\quad - k_{RANKL*RANK,RANKL} \cdot RANKL * RANK\\
\frac{d}{dt}RANKL * OPG &= k_{RANKL,RANKL*OPG} \cdot OPG \cdot RANKL && (4.61)\\
&\quad k_{RANKL*OPG,RANKL} \cdot RANKL * OPG\\
\frac{d}{dt}OPG &= c_{OPG} \cdot OPG(0) \cdot (OBres/OBres(0)) \cdot\\
&\quad PTHonOPG \cdot H^{+}_{TGFBact,OPG}(TGFBact) && (4.62)\\
&\quad - k_{RANKL,RANKL*OPG} \cdot OPG \cdot RANKL\\
&\quad + k_{RANKL*OPG,RANKL} \cdot RANKL * OPG\\
&\quad - c_{OPG} OPG,
\end{aligned}$$

where

$$PTHonOPG = \frac{PTHc + PTHc(0) \cdot OBres/OBres(0)}{2 \cdot PTHc}.$$

TGF-β

The following set of ordinary differential equations describes the dynamics TGF-β in its latent ($TGFB$) and active form ($TGFBact$). The parameters are provided in table 4.14.

$$\frac{d}{dt}TGFB = c_{TGFB} \cdot TGFB(0) \cdot \left(\frac{OB}{OB(0)}\right)^{\gamma_{OB,TGFB}} - c_{TGFB} \cdot TGFB \quad (4.63)$$

$$\frac{d}{dt}TGFBact = c_{TGFB} \cdot TGFB \cdot \left(\frac{OC}{OC(0)}\right)^{\gamma_{OC,TGFB}} - 10^3 \cdot c_{TGFB} \cdot TGFBact \quad (4.64)$$

Osteoblasts

We model responding osteoblasts ($OBres$), which mature to active osteoblasts. Active osteoblasts (OB) can undergo apoptosis or transform into osteocytes. The parameters used in the simulations are provided in table 4.15.

$$\frac{d}{dt}OBres = k_{OBres} \cdot H^{+}_{TGFB,OBres}(TGFBact) - \frac{c_{OBres}}{H^{+}_{TGFB,OB}(TGFBact)} \cdot OBres \quad (4.65)$$

$$\frac{d}{dt}OB = \frac{c_{OBres}}{H^{+}_{TGFB,OB}(TGFBact)} \cdot OBres - \left(\frac{c_{apo}}{H_{RX,OB}(RX)} + \frac{c_{diff}}{TGFB}\right) \cdot OB \quad (4.66)$$

where $RX = \max(10, Bcl - 90)$.

Osteoclasts

The production of osteoclasts depends on the relative level of RANK in complex with OPG compared to RANKL. The removal rate is inversely related to active TGF-β. The survival of osteoclasts also depends on RANKL due to its anti-apoptotic function (212).

$$\frac{d}{dt}OC = k_{OC} \cdot H^{+}_{RANK*OPG,OC}(RANK*OPG) - c_{OC} \cdot H^{-}_{OPG,OC}(RANK*OPG) \cdot OC \quad (4.67)$$

(4.68)

Initial conditions

The initial conditions used in the simulations are provided in table 4.11.

Table 4.11 Initial conditions for the bone model.

Ca fast pool	150 mmol (175)
Ca slow pool	24850 mmol (175)
PO4 fast pool	100 mmol (165)
PO4 slow pool	1500 mmol (165)
Responding Osteoblast	0.001
Osteoblast	0.005
Osteoclast	0.001
Latent TGF-β	200
Active TGF-β	0.2
RANK	10 (174)
RANKL	0.4 (174)
OPG	4 (174)
Runx2	10 (174)
CREB	10 (174)
Bcl-2	100 (174)

Table 4.12 BCL2-CREB-Runx2-pathway. All other parameters are calculated from the initial conditions and a steady state assumption.

Compartment	Parameter	Value
Runx2	c_{RX2}	0.7 h^{-1}
	$\alpha_{PTH,RX2}$	2
	$\gamma_{PTH,RX2}$	1
	$\rho_{PTH,RX2}$	0.125
Creb	c_{Creb}	0.003 h^{-1}
	$\alpha_{PTH,RX2}$	4
	$\gamma_{PTH,RX2}$	1
	$\rho_{PTH,RX2}$	0.5
BCL2	c_{BCL}	0.7 h^{-1}

4.8.2 Results

A key result regarding osteoblast regulation is that intermittently elevated PTH concentrations reduce osteoblast apoptosis rate, while continuously elevated PTH concentrations don't alter the apoptosis rate (6, 8, 225). In both scenarios, PTH up-regulates bone turnover. We test the model's ability to predict such behavior by prescribing either continuously rising PTH concentrations are intermittently elevated PTH concentrations. The results are presented in Fig. 4.40. While the apoptosis rate is not altered if PTH rises continuously, the daily average apoptosis rate declines if PTH is administered intermittently. Since PTH is enhancing bone turnover, the number of osteoblasts is rising

Table 4.13 RANK-RANKL-OPG pathway. All other parameters are calculated from the initial conditions and a steady state assumption.

Compartment	Parameter	Value
RANKL	c_{RANKL}	0.003 h^{-1}
	γ_{OEff}	0.18
	$\alpha_{PTH,RANKL}$	1.3
	$\alpha_{D,RANKL}$	1.2
	$\gamma_{D,RANKL}$	2
	$\rho_{D,RANKL}$	2
	$\delta_{TGFBact,RANKL}$	1.5$\cdot TGFBact(0)$
	$\gamma_{TGFBact,RANKL}$	0.2
	$\alpha_{TGFBact,RANKL}$	1.2
	$k_{RANKL,RANKL*OPG}$	3.12$\cdot$ 10^{-3} h^{-1}
	$k_{RANKL,RANKL*RANK}$	6.5 $\cdot$ 10^{-6} h^{-1}
	$k_{RANKL*OPG,RANKL}$	5.6$\cdot$ 10^{1} h^{-1}
	$k_{RANKL*RANK,RANKL}$	1.12 $\cdot$ 10^{-1} h^{-1}
RANK	c_{RANK}	0.0032 h^{-1}
	$\gamma_{TGFBact,RANK}$	0.1518
OPG	c_{OPG}	16 h^{-1}
	$\delta_{TGFBact,OPG}$	1.5$\cdot TGFBact(0)$
	$\gamma_{TGFBact,OPG}$	0.2
	$\rho_{TGFBact,OPG}$	0.8

Table 4.14 Parameters TGF-β.

Parameter	Value
c_{TGFB}	3$\cdot 10^{-5}$ h^{-1}
$\gamma_{OB,TGFB}$	0.01
$\gamma_{OC,TGFB}$	0.6

in both scenarios. However, the rise is more prominent in the case PTH is administered intermittently.

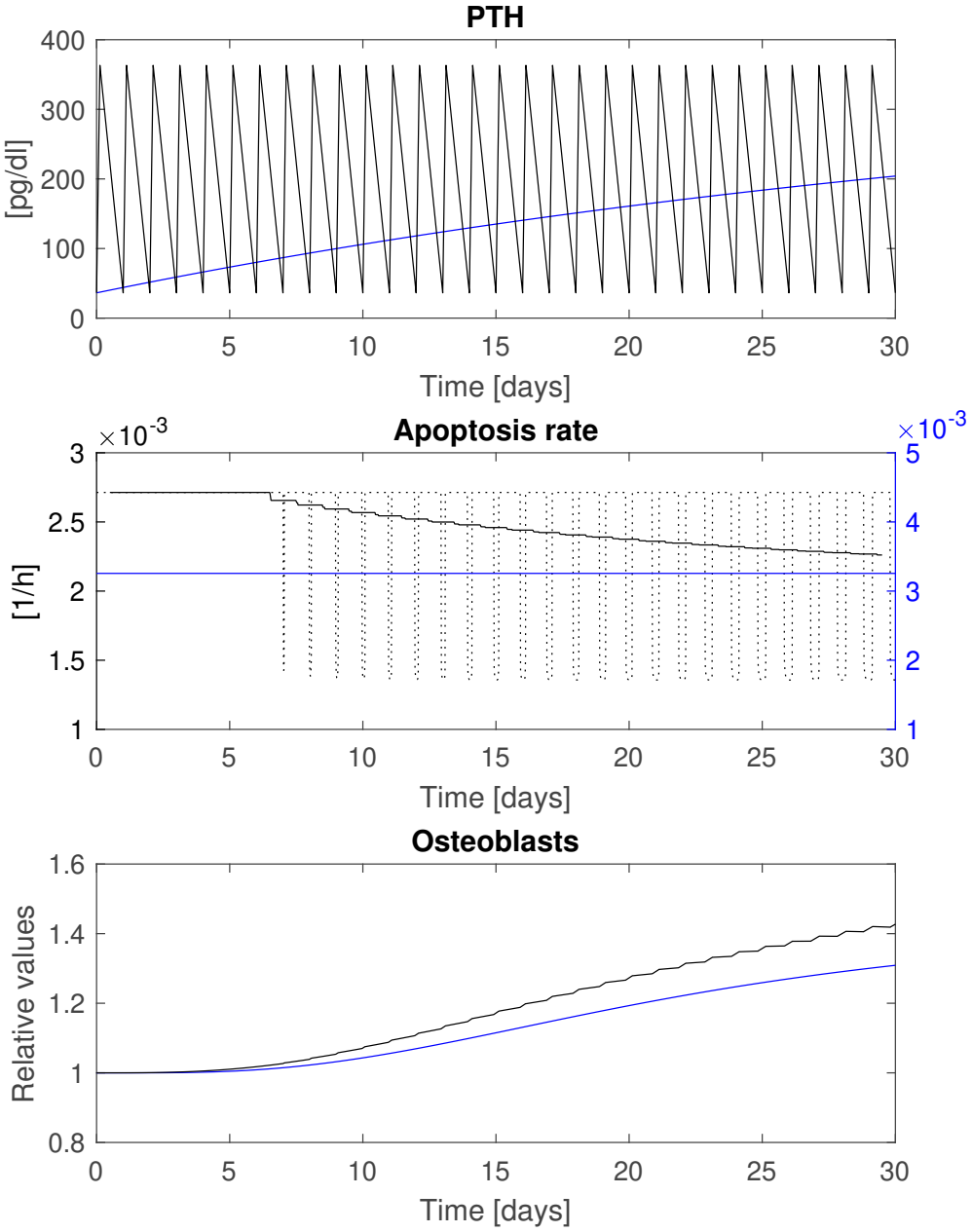

Figure 4.40 Upper panel: We prescribed either intermittently elevated PTH concentrations (black line) or continuously rising PTH concentrations (blue line). Middle panel: Daily average apoptosis rate (solid black line) declines if PTH is administered intermittently (left y-axis) while the apoptosis rate is unchanged if PTH rises continuously (right y-axis). The lower panels shows the corresponding dynamics of osteoblasts for intermittently elevated PTH concentrations (black line) and continuously rising PTH concentrations (blue line).

Table 4.15 Parameters for the osteoblast and osteoclast model. Apoptosis rates are chosen such that the mean lifetime at a healthy steady state of osteoblasts is three months, the mean lifetime of osteoclasts is two weeks. All parameters not presented in this table are calculated from the initial conditions and a steady state assumption.

Compartment	Parameter	Value
Responding OB	k_{OBres}	$1.5 \cdot 10^{-5}$ h^{-1}
	c_{OBres}	$3.3 \cdot 10^{-3}$ h^{-1}
	$\gamma^0_{TGFB,Res}$	1.8
	$\alpha_{TGFB,Res}$	15
	$\rho_{TGFB,Res}$	0.2
OB	c_{apo}	$2.7 \cdot 10^{-3}$ h^{-1}
	ϕ_{OB0}	0.764
	ϕ_{kb}	0.3132
	$\gamma_{RX,OB}$	3.6780
OC	ϕ_{OC}	0.0292
	$\rho_{RANKL*RANK,OC}$	0.3883
	$\alpha_{RANKL*RANK,OC}$	3.1567+$\rho_{RANKL*RANK,OC}$
	$\gamma_{RANKL*RANK,OC}$	8.5306
	$\phi_{RANKL*RANK}$	0.3883
	$\rho_{TGFB,OC}$	0.2004
	$\alpha_{TGFB,OC}$	1.9746 + $\rho_{TGFB,OC}$
	$\gamma_{TGFB,OC}$	1.0168

4.9 INTEGRATED MODEL OF CALCIUM AND PHOSPHATE HOMEOSTASIS

4.9.1 $Ca^{2+}$and phosphate fluxes from and to the bone pools

We employ two bone pools, a labile or interchangeable bone pool, and a slow bone pool. Since the labile bone pool is thought to be on the bone surface, we assume that calcium and phosphate diffuse between ECF and the labile bone pool (85). Due to mineralization governed by osteoblasts, calcium and phosphate are transported to the slow bone pool. Bone resorption by osteoclasts is responsible for transferring calcium and phosphate from the solid bone to the ECF (Fig. 4.41). At a healthy steady state, 15 mmol calcium per day is exchanged between the ECF and the bone due to bone resorption and formation (175).

With J_{ECC}^{Bf} we denote the flux from the ECF to the fast calcium bone pool, with J_{Bf}^{ECC} the flux from the fast calcium bone pool (Bf) to the ECF. J_{Bf}^{Bs} denotes the flux from the fast calcium bone pool to the slow calcium bone pool (Bs) and J_{Bs}^{ECC} the flux from the slow bone pool to the ECF.

$$
\begin{aligned}
JCa_{ECC}^{Bf} &= k_{pB} \cdot C_{ECC} && (4.69)\\
JCa_{Bf}^{ECC} &= k_{Bp} \cdot Bf_{Ca} && (4.70)\\
JCa_{Bf}^{Bs} &= C_{ECC} \cdot (M_{min} + M) && (4.71)\\
\frac{d}{dt}M &= k_M \cdot OB - c_M \cdot M, && (4.72)
\end{aligned}
$$

where M is a dummy variable describing mineralization in response to changes in osteoblasts.

$$
\begin{aligned}
JCa_{Bs}^{ECC} &= Bs \cdot (Basal + Resorp(RANK{*}OPG, OC)) && (4.73)\\
Resorp &= k_{sp} \cdot \left(\frac{RANK{*}OPG_0}{RANK{*}OPG} \cdot \frac{OC}{OC(0)} \right)^{\gamma_{RROC}} \cdot H_{OC,ECC}(OC) && (4.74)
\end{aligned}
$$

The same equations hold for the fast and slow phosphate bone pool. While the molar

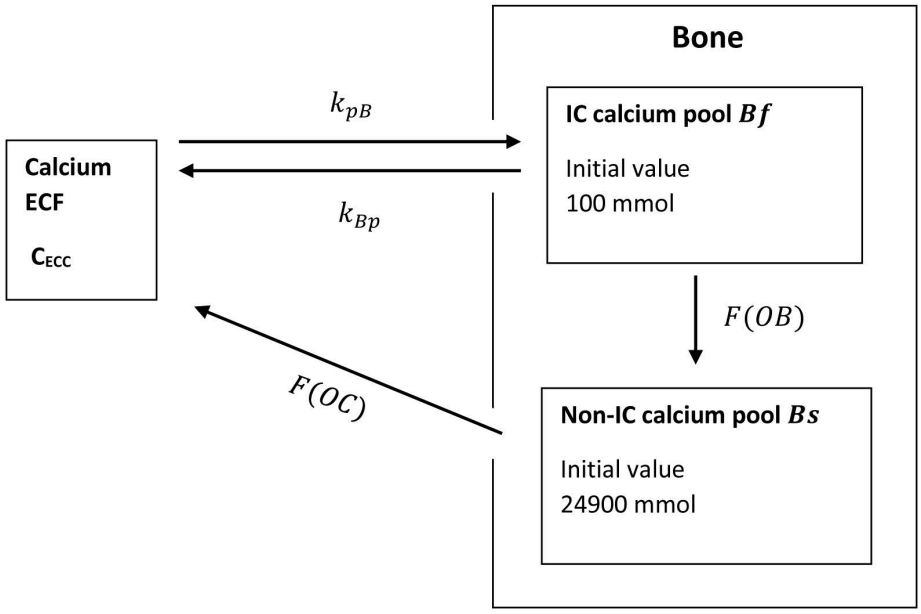

Figure 4.41 Calcium entering and leaving the bone compartments. There is a rapid (passive) exchange between ECF and the fast bone pool. Osteoblasts are responsible for bone formation and the transformation between the fast and the slow bone pool. Osteoclasts are responsible for bone resorption.

ratio of hydroxyapatite determines the ratio of calcium and phosphate release from the bone, the daily exchange rate between the interchangeable bone pool can be chosen according to calcium-phosphate salts in the labile bone layer.

Parameters

The parameters k_{pB} and $Basal + k_{sp}$ are chosen such that the daily flux from the fast bone pool to the ECF under healthy steady state is 100 mmol and the daily flux from the ECF to the fast bone pool is 115 mmol (175). Moreover, we assume 15 mmol calcium is shifted from the fast bone pool to the slow bone pool and from the slow bone pool to the ECF due to osteoblast regulated mineralization and osteoclast regulated resorption (173, 175).

Table 4.16 Parameters used for the simulations

Compartment	Parameter	Value
Mineralization	k_M	55.3 h^{-1}
	M_0	1
Resorption	$\gamma_{OC,ECC}$	1.15
	$\alpha_{OC,ECC}$	0.5
	γ_{RROC}	0.6
	$Basal$	2.26·10^{-5} mmol
	ksp	0.1 mmol

5 Results

We provide a sketch of the integrated model of calcium and phosphate homeostasis in Fig. 5.1. Fluxes between the different compartments are described in the corresponding chapters.

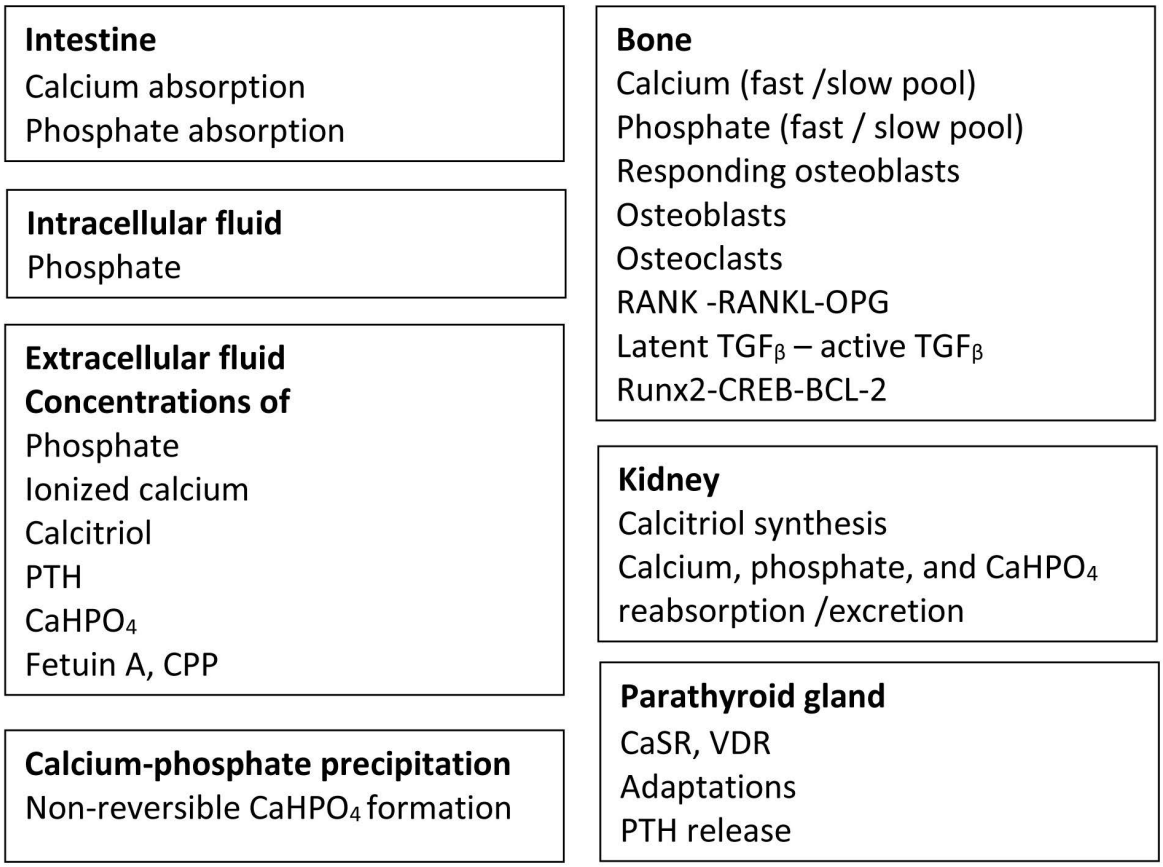

Figure 5.1 Block diagram of the integrated calcium and phosphate homeostasis model. The main compartments are the intestine, intracellular fluid, extracellular fluid, calcium-phosphate precipitation, bone kidney, and parathyroid gland. There is an exquisite network of regulators and feedback loops between and within the various compartments triggering a cascade of alterations if calcium and phosphate homeostasis is disturbed. Calcium and phosphate fluxes between the compartments and the fluxes' regulations are described in the corresponding chapters.

5.1 RESTORATION OF CALCIUM AND PHOSPHATE HOMEOSTASIS

An integrated model of calcium and phosphate homeostasis must predict the fast restoration of calcium and phosphate homeostasis in the case of non-chronic disturbances. We chose days with different calcium diets as well as intravenous phosphate load as test scenarios.

(I) Intravenous phosphate load:
We assume a rapid rise in the phosphate concentration due to a phosphate injection. In (216), the authors studied the effect of an intravenous phosphate load on PTH, renal response, and calcium and phosphate levels in rats. Phosphate infusion of 0.5 mmol led to a transient rise in plasma phosphate levels and phosphaturia within 10 minutes. Calcium levels declined, and PTH levels increased within 10 minutes. Our model predicts the same behavior (Fig. 5.2). The prominent rise in phosphate leads to a sharp increase in $CaHPO_4$ formation. Due to the increase in calcium-phosphate precipitation, Ca^{2+}declines, and the PTG responses with pre-formed PTH release. PTH triggers renal phosphate excretion resulting in phosphaturia quickly.

(II) Lifestyle effects: A single day without any calcium in the diet
The body must have the ability to restore calcium homeostasis and prevent drops in Ca^{2+}concentrations if the calcium diet is disturbed. Here, we assume no calcium was the diet on day 1 (i.e., calcium net absorption is negative, and calcium diet was back to a standard content of 25 mmol/day on day 2. The simulations predict that the system is back to a quasi homeostatic state at the end of day 2. The nadir of $Ca^{2+}$is less than 2%. PTG response with a quick release of preformed and stored PTH. Phosphate decreases to the phosphaturic effect of PTH. Therefore, $CaPO_4$ salt formation is impaired, ensuring higher Ca^{2+}concentrations compared to total calcium concentration.

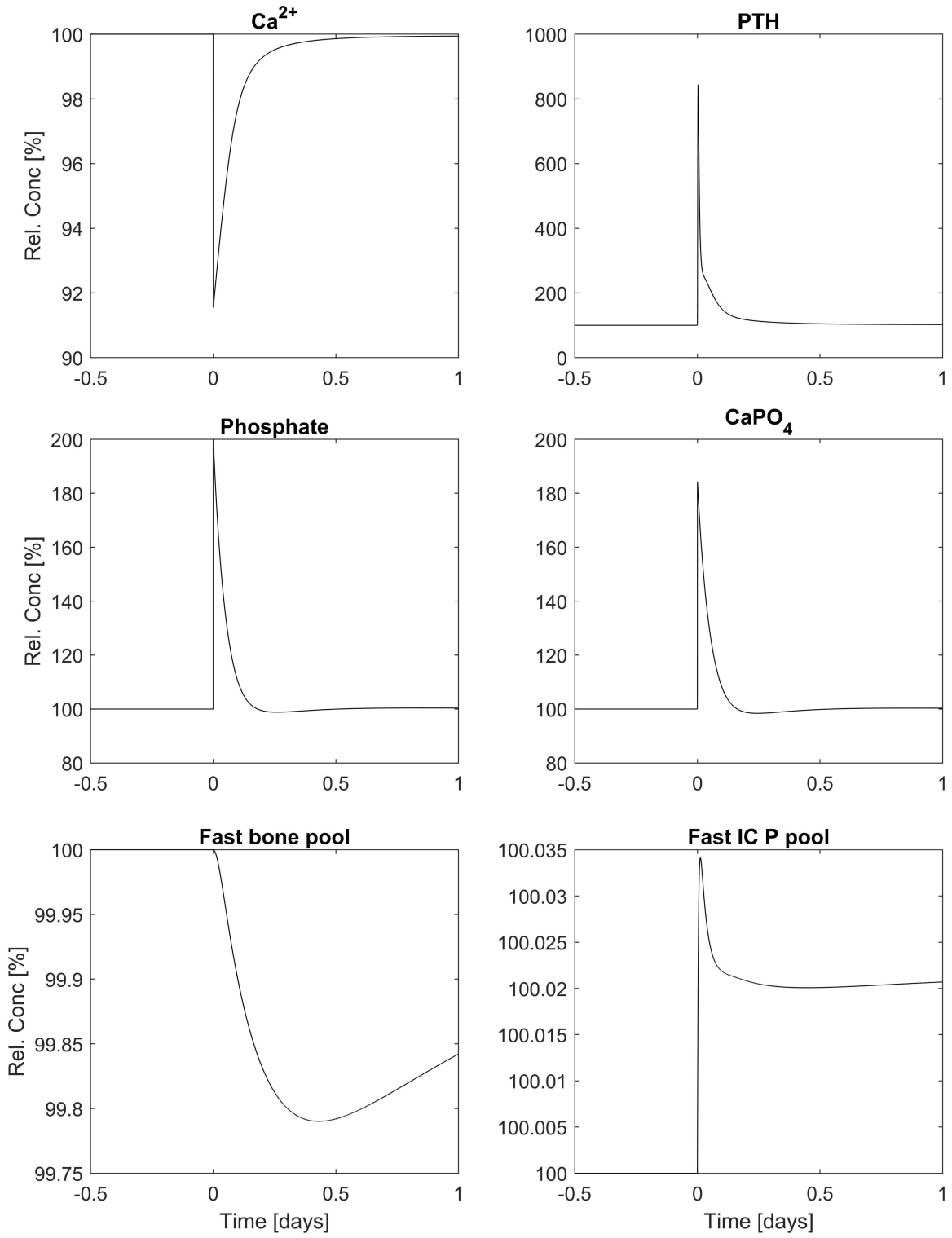

Figure 5.2 The sharp rise in phosphate leads to a sharp rise in the formation of $CaHPO_4$ salts. The resulting drop in Ca^{2+}which triggers a sharp rise in PTH. PTH enhances renal phosphate excretion. Homeostasis is restored within 5 hours.

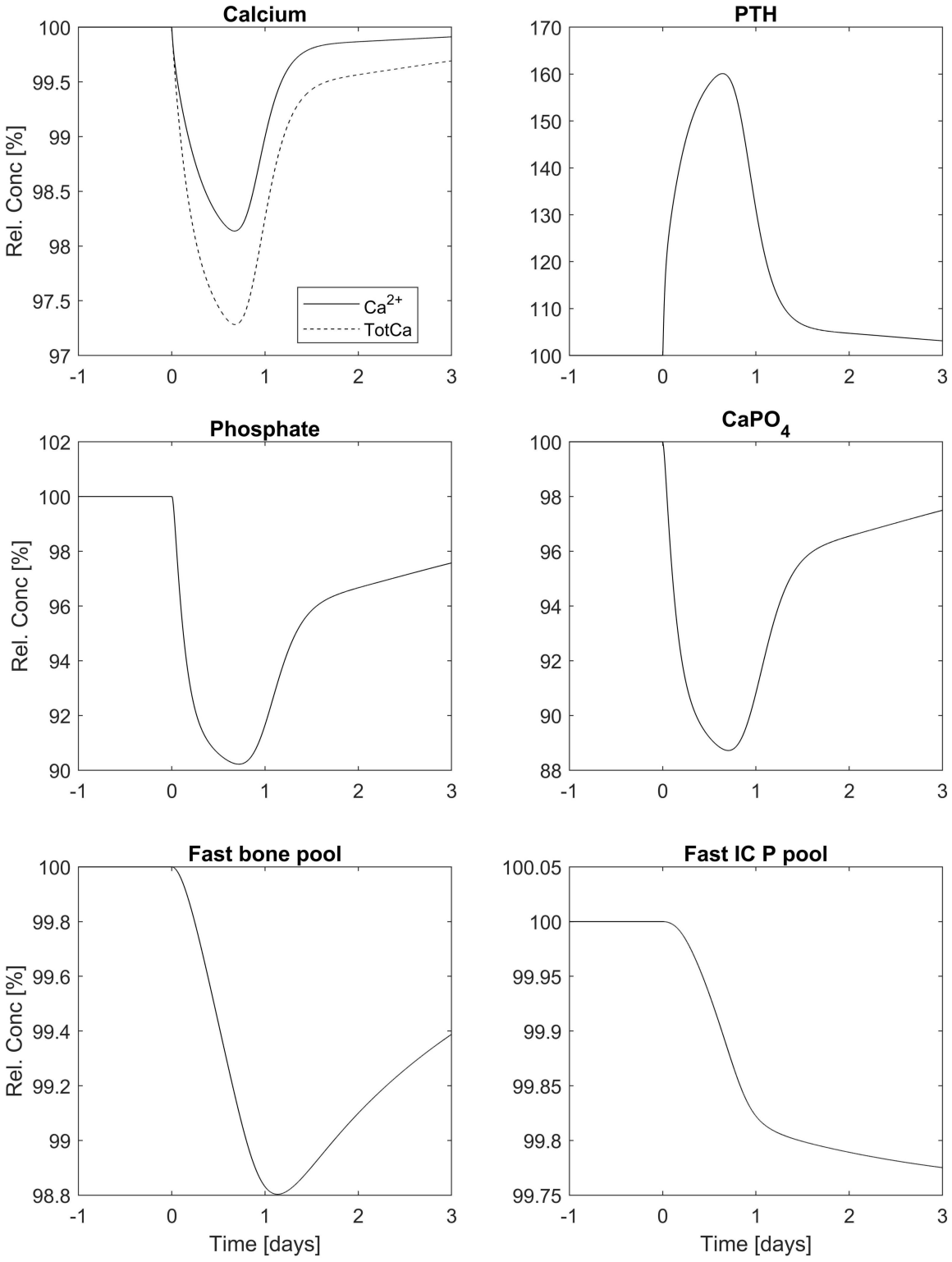

Figure 5.3 Response of various concentrations to a day without any calcium in the diet. We assume that no calcium was in the diet on day 1. The diet content was back to the regular diet (25 mmol / day) on day 2. The PTH response to lower calcium levels triggers the renal excretion of phosphate and renal reabsorption of calcium. Fluxes from $CaPO_4$ and the fast bone pool also buffer the ionized calcium concentration.

5.2 PRIMARY HYPERPARATHYROIDISM

A tumor in the PTG is usually the cause of primary hyperparathyroidism (PHP). PHP commonly results in hypercalcemia and hypophosphatemia (207). Moreover, PHP commonly leads to bone loss (167). Patients suffering from primary hyperparathyroidism usually suffer from hypercalciuria, which often results in renal stone formation. Renal stone formation is the indication for parathyroidectomy in most patients (57, 214). We mimic PHP by increasing the PTH synthesis rate such that the PTH concentration increases roughly five-fold. Our results reflect the clinical manifestations of primary hyperparathyroidism (Fig. 5.4). While calcium levels are elevated, phosphate declines despite an increase in calcitriol. The numbers of osteoblasts and osteoclasts increase. However, osteoclasts' increase exceeds the increase in osteoblasts, disturbing the balance between bone formation and bone resorption in favor of bone resorption. Moreover, we observe hypercalciuria (Fig. 5.5).

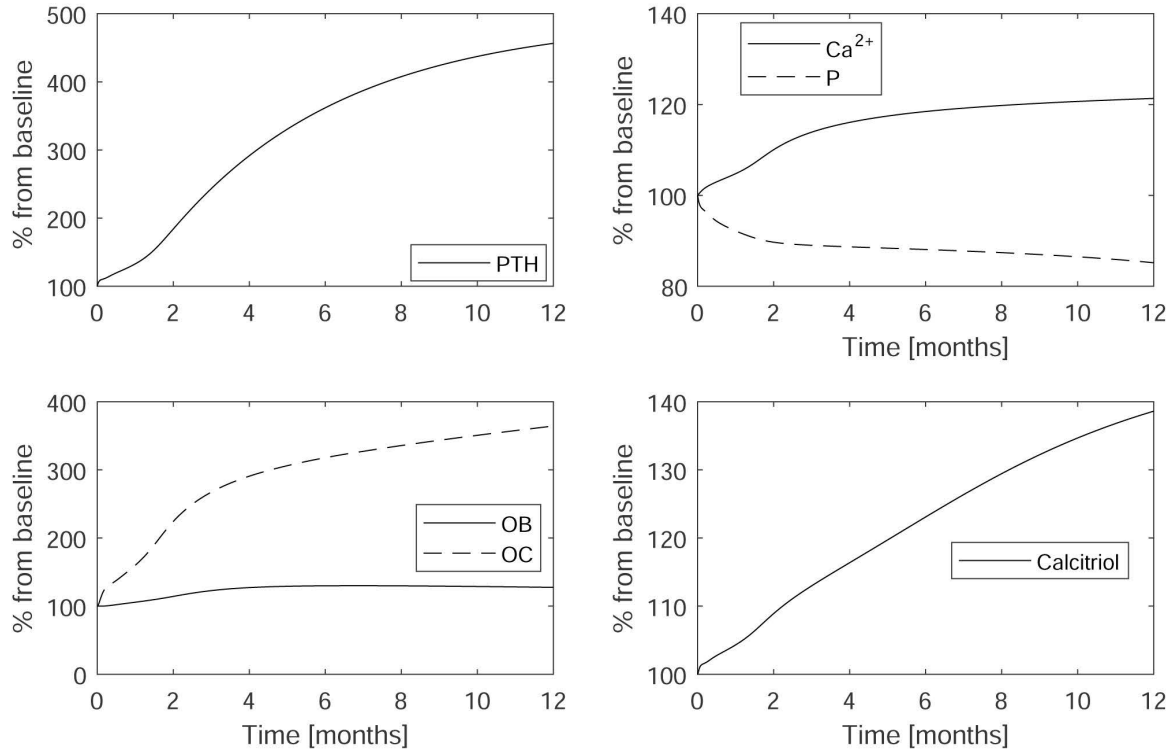

Figure 5.4 Simulated primary hyperparathyroidism based on elevated PTH synthesis rates. High PTH levels lead to a higher increase in osteoclasts than in osteoblasts and, therefore, bone resorption. Calcium levels increase significantly. Despite the rise in calcitriol levels, phosphate decreases due to the phosphaturic effect of PTH.

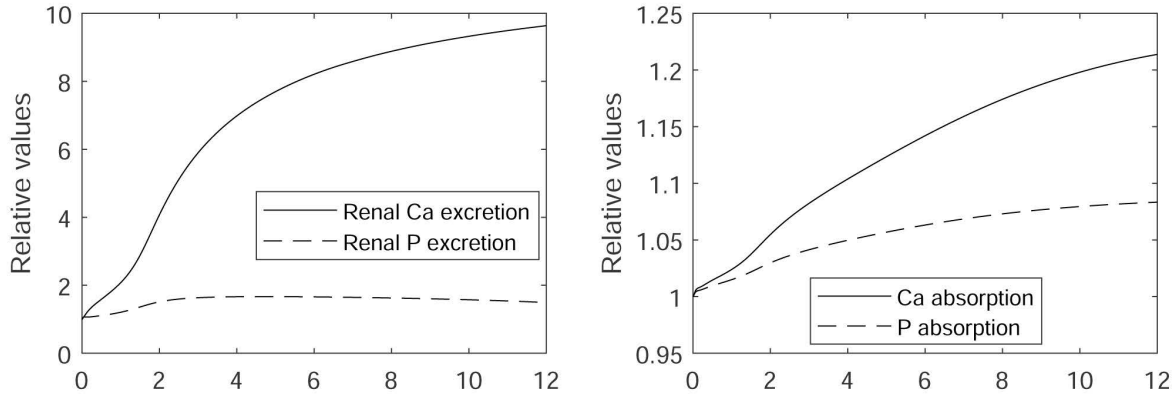

Figure 5.5 Renal excretion and intestinal absorption of calcium and phosphate during simulated primary hyperparathyroidism (Fig. 5.4). The high calcium load results in hypercalciuria despite significantly elevated PTH concentrations.

5.3 HYPOPARATHYROIDISM

Hypoparathyroidism is a severe abnormality of calcium and phosphate homeostasis characterized by low PTH levels despite hypocalcemia (15, 202). Some hypoparathyroidism forms are associated with activating mutations in the calcium-sensing receptor gene (98, 164). For our simulations, we reduced the PTH synthesis rate such that PTH levels drop by 50%. We observe a drop in calcium and decreased bone turnover (Fig. 5.6). It is worth noting that calcium is very well regulated, and PTH will eventually recover if the decline in PTH is too steep. Therefore, it is insufficient to lower the production rate to simulate severe hypoparathyroidism, but one would have to lower all the parathyroid gland's adaptation mechanisms. To adjust the model to different CaSR mutations, we would change the PTH release set-point in equation 4.20 (62).

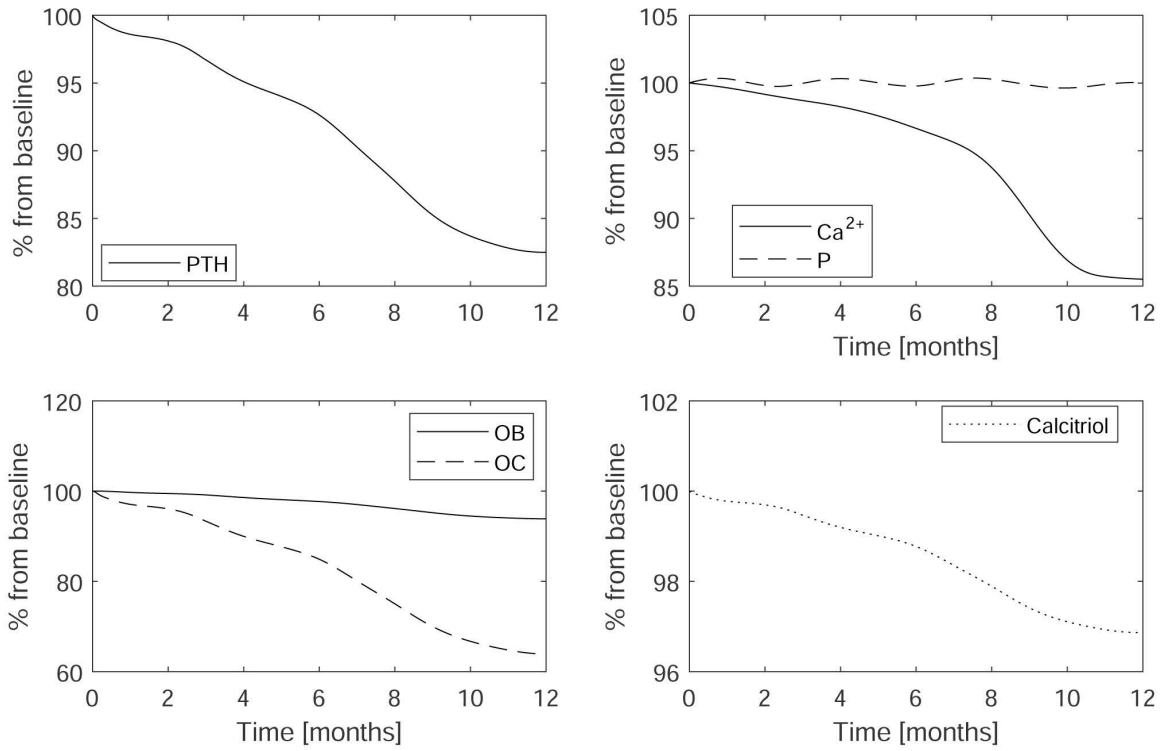

Figure 5.6 Simulated hypoparathyroidism. While ionized calcium levels drop, resulting in hypocalcemia, phosphate levels are only slightly elevated. The number of osteoclasts and osteoblasts is declining, resulting in significantly reduced bone turnover.

5.4 BONE MINERAL METABOLISM IN CKD PATIENTS

5.4.1 Loss of kidney function in CKD patients

We simulate progressive renal failure by reducing the GFR to zero over 24 months. We simulate phosphate removal due to dialysis once the GFR is below 5%. The removal is a continuous function of plasma phosphate concentration. We assume that the maximum of phosphate removal during a single hemodialysis session is 25 mmol (64). The predictions of our model (Fig. 5.7) are in close accordance with the clinical data (136):

- The regulatory system keeps ionized calcium within a narrow range, even under the gradual kidney function loss. The body can balance impaired calcium absorption due to impaired calcitriol synthesis and significantly impaired renal calcium excretion with the help of the bone and $CaHPO_4$ formation remarkably well.
- PTH concentrations are rising due to rising phosphate concentrations, declining calcitriol concentrations, and impaired kidney clearance, eventually resulting in secondary hyperparathyroidism.
- Phosphate rises continuously due to impaired kidney clearance. Rising PTH levels at the onset of CKD results in higher renal phosphate clearance. With declining kidney function, phosphate removal is impaired and, therefore, the influence of PTH on renal phosphate excretion is of less importance. The slope of phosphate's progression changes once we start to simulate hemodialysis.
- The reduced kidney function and rising phosphate concentrations, resulting in a declining calcitriol concentration. PTH would enhance the synthesis of calcitriol in healthy kidneys.
- The numbers of osteoclasts and osteoblasts are rising, resulting in enhanced bone turnover. Since the number of osteoclasts rises more prominently than the number of osteoblasts, the model correctly predicts bone resorption (155, 171).
- The risk for vascular calcification, which is hypothesized to be reflected by non-solvable $CaHPO_4$, rises continuously with the onset of hemodialysis.

5.4.2 Hypocalcemia and recovery during cinacalcet treatment

In the section before, we simulate progressive renal failure by reducing the GFR to zero over 24 months. We simulate phosphate removal due to dialysis as a constant once the

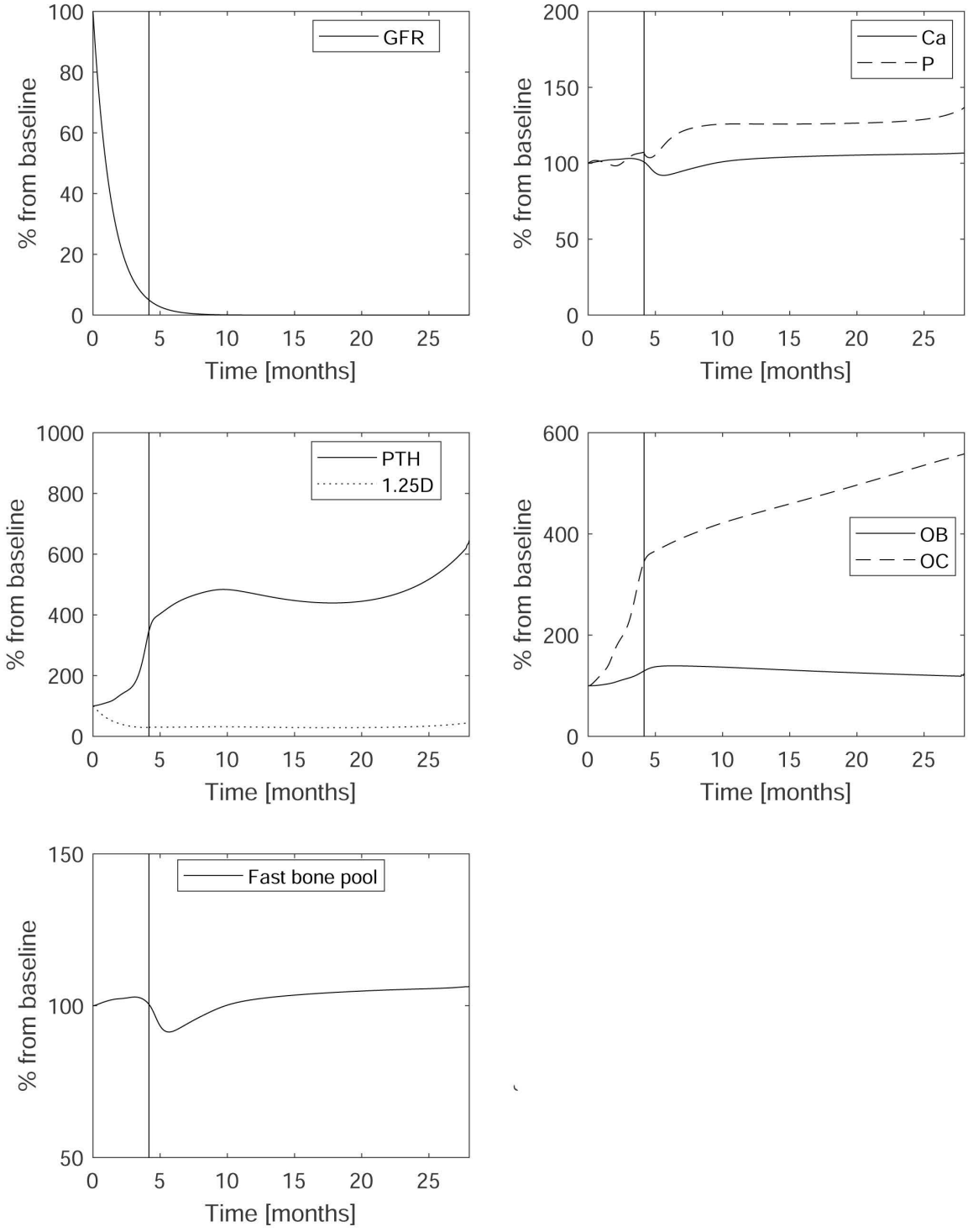

Figure 5.7 Simulated progressive renal insufficiency mimicked by the decline in GFR from a healthy state to zero within 24 months. The horizontal line indicates the start of hemodialysis. We predict a decline of calcitriol levels with declining GFR, rising phosphate levels with declining GFR, and quasi constant calcium levels with declining GFR. PTH is rising with declining kidney function. Bone turnover is elevated with significantly more bone resorption than formation.

GFR is below 5%. However, this time we start to reduce PTH after 2 years of hemodialysis mimicking the administration of cinacalcet for 12 weeks. In accordance to clinical studies, we observe a decline in calcium and phosphate due to reduced bone resorption and increasing bone formation (Fig. 5.8). Calcium and phosphate both recover after around 10 weeks (19, 21, 154). The same results would be predicted when simulating the hungry bone syndrome after parathyroidectomy in patients with severe primary or secondary hyperparathyroidism (26, 81). Due to the decline in PTH, bone resorption is reduced while bone formation is increased resulting in a net flux from the plasma to the bone compartment.

5.4.3 Phosphate reduced diet in the onset of CKD

In the section before, we simulate progressive renal failure by reducing the GFR to zero over 24 months. We simulate phosphate removal due to dialysis as a constant once the GFR is below 5%. However, this time we radically adjust the phosphate diet with the glomerular filtration rate. When GFR is close to zero, the daily phosphate intake is halved. PTH increases moderately due to impaired renal clearance, calcitriol declines due to impaired synthesis. However, due to the adaption of the phosphate diet, PTH is rising only slightly. Bone turnover increases slightly. Again, osteoclasts are more elevated than osteoclasts. However, the difference between the two is significantly smaller in the phosphate adjusted diet than in the regular diet (Fig. 5.9). A factor of approximately 5.65 reduces the risk for vascular calcification associated with the amount of non-solvable $CaHPO_4$. While the dietary change is extreme, it shows the potential of life-style changes in CKD patients. Moreover, it reflects clinical results where dialysis vintage and hyperphosphatemia, particularly combined with hypercalcemia, is a significant risk factor for vascular calcification (50, 220).

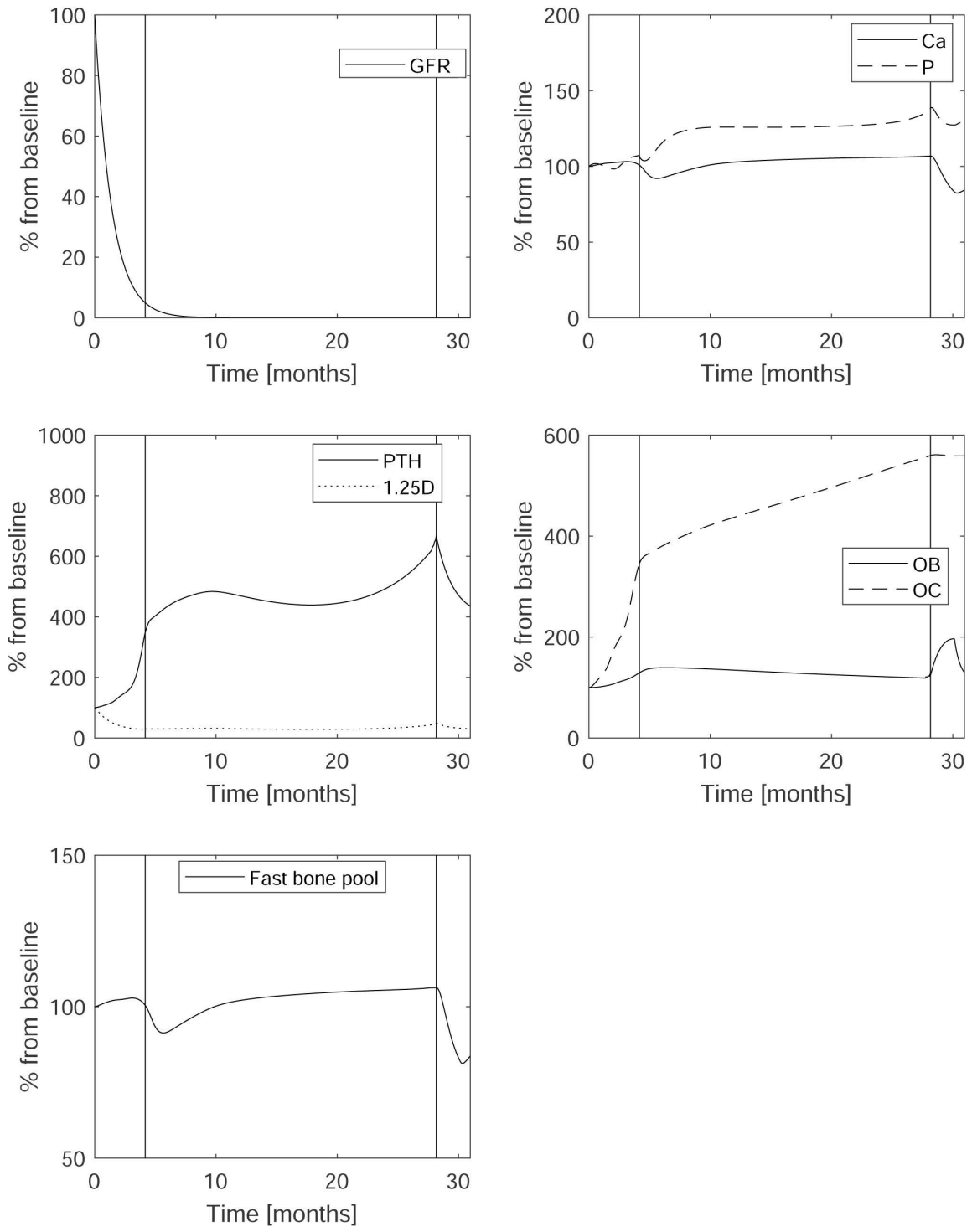

Figure 5.8 Simulated progressive renal insufficiency mimicked by the decline in GFR healthy state to zero within 24 months. The first horizontal line indicates the start of hemodialysis, the second horizontal line indicates the start of cinacalcet treatment. We predict a decline of calcitriol levels with declining GFR, rising phosphate levels with declining GFR and quasi constant calcium levels with declining GFR. PTH is rising with declining kidney function. Bone turnover is elevated with significantly more bone resorption than formation.

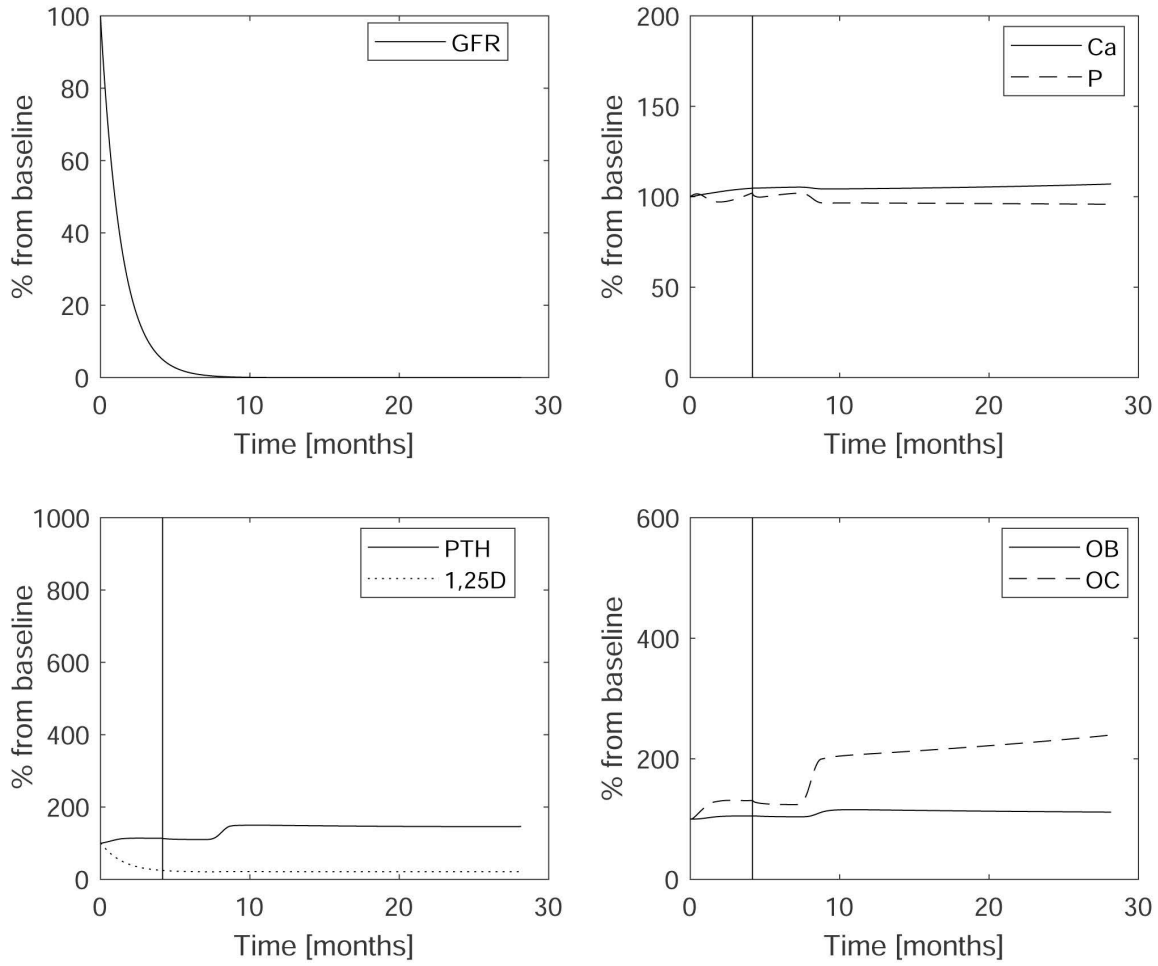

Figure 5.9 Simulated decrease of phosphate intake in response to impaired kidney function. Phosphate is well controlled. While osteoclasts are still rising due to PTH's impaired clearance, the increase is significantly smaller compared to a regular phosphate diet (Fig. 5.7).

6 Discussion

Disorders of mineral and bone metabolism (CKD-MBD) affect most CKD patients, which make up for around 14% of the world's population (63). CKD-MBD is diagnosed by the manifestation of one or a combination of the following (155):

- Abnormalities in bone turnover, bone mineralization, bone volume
- Abnormalities of Ca^{2+}, phosphate, PTH or calcitriol concentrations
- Soft tissue calcification

CKD-MBD evolves due to an imbalance in the complex regulatory system, which ensures calcium and phosphate homeostasis. This regulatory system is highly complex and multidimensional and involves many hormones and ions and their actions on the kidney, bone, intestine, and parathyroid gland. Due to impaired kidney function, the equilibrium between mineral and endocrine functions comes off balance, triggering a cascade of (patho) physiological reactions. As a result, bone abnormalities are found in the vast majority of end-stage renal disease patients (155, 171). Moreover, there is an association between mineral metabolism disorders and fractures, vascular calcification, and mortality (155).

Due to the complexity of CKD-MBD, mathematical models might provide a helpful tool to study the mechanisms resulting in CKD-MBD and find the optimal treatment strategy that is not straight forward due to the coupling of the regulatory effects. For example, secondary hyperparathyroidism could be treated with calcitriol. However, calcitriol enhances intestinal phosphate (and calcium) absorption, and rising phosphate could depending on the state of the parathyroid gland, result in rising PTH concentrations.

Mathematical models developed in the last 60 years were applied to gain insight into the complex regulation of calcium and phosphate homeostasis. One example would be the sub-model predicting PTH release as a function of Ca^{2+}plasma concentration. In 1983, Brown published a simple 4-parameter model that captured the sigmoidal response of PTH to Ca^{2+}changes (32).The four parameters where the maximum and minimum PTH release rate, the set-point (i.e., the calcium concentration causing half-maximal PTH secretion), and the slope of the curve at the set-point. This simple model was used in the following years to analyze experimental and clinical results. Experiments involving subsequent cycles of hypocalcemia, normocalcemia, and hypercalcemia revealed a hysteresis effect in PTH release (196). This effect can be correctly predicted

by two coupled ordinary differential equations allowing to take PTH storage into account (157, 203).

Today we know that parathyroid gland biology is complex. PTG adaptation mechanisms work on significantly different timelines, and the state of the system is history-dependent. To capture PTG biology, one must employ a more sophisticated model allowing for responses within seconds in the case of acute hypocalcemia and long-term adaptations, which might even result in hyperplasia. However, most models capturing PTH dynamics under different conditions are still based on the classic 4-parameter model (32).

This thesis's main goal was to build a mathematical model of mineral and bone metabolism in patients with end-stage renal disease. However, we refrained from building a phenomenological model of CKD-MBD, which would allow mimicking CKD-MBD but would not provide any insight into CKD-MBD's driving mechanisms. The model should instead translate the regulatory system of calcium and phosphate homeostasis's critical physiological properties into mathematical models. This approach allowed us to assess the integrated model of mineral and bone metabolism regarding its predictive value in different scenarios.

Previously published models of calcium and phosphate homeostasis and bone turnover had some shortcomings or were not appropriate for our aim. Nevertheless, they have been beneficial in building our model (85, 133, 174, 181, 182). In this thesis, we tried to find the right balance between simplifying physiological and pathophysiological properties and the complexity of the model. Oversimplified models might not be complex enough to capture the critical physiological properties of the regulators. Oversimplification resulting in non-physiological predictions were, for instance, present in (174), where primary hyperparathyroidism would imply hyperphosphatemia due to missing regulatory effects of renal phosphate excretion and reabsorption. Another example would be the simple linear relationship between intracellular and extracellular phosphate concentrations (85, 133, 174, 181). This simplification neither allows us to predict the non-linear behavior of phosphate plasma concentration as a response to linear phosphate removal during a single hemodialysis session nor the phosphate buffer capacity of cells.

On the other hand, models should only be as complex as necessary to capture the key features. Otherwise, it might prove impossible to identify parameters or simulate, for instance, the slow progression of chronic kidney disease and the development of CKD-MBD, which will take several years. In (85), the authors presented a comprehensive model of calcium and phosphate homeostasis, including FGF-23, calcium-protein binding, and phosphate binding to different ions. However, the trade-off for the complexity in

calcium and phosphate species and an additional regulator is the black box model for the bone and a simple two-compartment model for the parathyroid gland. For our purpose, we omitted FGF-23 as discussed in the introduction and different phosphate species and calcium-protein binding for the sake of a sophisticated PTG and bone model. The model's complexity also has a cost regarding the interpretation of the results and the model adaption to different situations. In (174), the authors introduced a complex model of two species of osteoblasts. The main result regarding the anabolic effect of intermittently administered PTH and the catabolic effect of continuously elevated PTH levels on bone are flawless. However, the two species and the corresponding model equations are not interpretable in a physiological sense.

6.1 BENEFITS OF THE NOVEL MODEL

Our model translates key properties of the regulatory system of calcium and phosphate homeostasis into mathematical equations allowing the study of various disturbances. In contrast to phenomenological models, we can study the mechanisms underlying CKD-MBD development since the only input parameter of importance is the kidney function. We assume that the glomerular filtration rate reflects kidney function.

Our model of bone mineral metabolisms employed a detailed model of parathyroid gland biology and bone turnover. Most calcium and phosphate homeostasis models represent the parathyroid gland (85, 133, 174) as well as the bone (85, 182) as black box compartments. Here, we employed a sophisticated parathyroid gland biology model based on the expression of the calcium-sensing receptor. The main challenge for a mathematical model of PTG biology is the history dependence of the parathyroid gland's state.

Our PTG model is based on the CaSR and VDR expression and takes the history of a disturbance in calcium and phosphate homeostasis into account. It can address the evolution of PTG physiology and pathophysiology over several time scales, ranging from seconds to month. Evolution mechanisms involve enhanced PTH synthesis and PTH mRNA stability or increased PTG proliferation rate. We can accurately predict secondary hyperparathyroidism in patients suffering from chronic kidney disease. We also aimed at developing a mathematical model that can be adapted to mutations of the CaSR and VDR. These predictions could be employed to predict experimental results in knock-out models, for instance. Due to the structure of the PTG model, these adaptations are straight forward. Since the model is based on the CaSR expression, it can be coupled with a pharmacodynamics/pharmacokinetics model of calcimimetics or calcitic, which act as antagonists at the CaSR, thereby increasing PTH release. In combination with a cinacalcet six-compartment model, we employed the PTG model to perform a virtual clinical trial. While cinacalcet decreases PTH efficiently and might even lead to decreased hyperplasia (19, 154), patient adherence is a great challenge. The virtual clinical trial's goal was to address whether thrice-weekly observed in-center cinacalcet intake was non-inferior to daily prescription if real-life patient adherence is taken into consideration. The three times weekly off-label use of cinacalcet is a convenient way to administer cinacalcet in-center after each hemodialysis session. The new administration scheme has found its way into clinical practice. Currently, we are evaluating the results of this treatment scheme in two large U.S. hemodialysis patient populations.

The model of bone resorption and formation is detailed as well. We take several

regulatory mechanisms into account. While these regulation mechanisms where already part in previous models of calcium and phosphate homeostasis (45, 174), we simplified the description of osteoblast apoptosis and differentiation. Moreover, we corrected the regulation of osteoclasts activation and introduced calcitriol as a stimulating factor for the release of RANKL (121, 161, 227). While there are markers for bone resorption and bone formation, the model provides insight into the dynamics of parameters not readily available to clinicians such as RANK-RANKL-OPG.

Other sub-models, such as intestinal calcium and phosphate absorption, are highly simplified models. However, they are complex enough to capture the main physiological features such as paracellular and transcellular transport in the intestine and the regulation of the transcellular transport by calcitriol. The same is true for renal calcium and phosphate excretion, where we take the regulatory effects of PTH, calcitriol as well as calcium and phosphate themselves into account.

Whereas most calcium and phosphate homeostasis models take a linear relationship between intracellular and extracellular phosphate concentrations into account, we introduced a physiology-based model involving active transport into the cells, the buffer capacity of the cells as well as an emergency mechanism in case of pathologically low plasma phosphate concentrations. This model is a significant step towards a unified model of mineral and bone metabolism as it can accurately predict the phosphate buffer capacity of cells and phosphate plasma concentrations as a response to phosphate removal during a hemodialysis session. While other sophisticated models aimed at predicting this behavior (see (128) for a comprehensive review), we translate physiological properties into our model and refrain from using compartments and mechanisms that cannot be easily explained.

Wherever possible, we provided sub-model validations allowing us to adjust the sub-models independently from the integrated mineral and bone metabolism model. This approach allows us to study primary regulators separately and ensure that we do not overfit the integrated model's model parameters. Since calcium and phosphate homeostasis is tightly regulated, many unknown parameters can be estimated from small disturbances and homeostasis restoration.

Finally, the model could allow personalized treatment strategies based on the parathyroid gland's state, the sensitivity of the calcium-sensing receptor. An example could be the administration of calcimimetics. If the CaSR sensitivity is significantly reduced, the patients might not be susceptible to cinacalcet treatment. On the other hand, we can use the model to estimate how early in CKD progression we should start with the administration of calcimimetics even combined with calcitriol therapy and dietary changes

to slow down the development of CKD-MBD. The state of the parathyroid gland can be estimated, for instance, from a calcium mass balance study during single hemodialysis with a dialyzate with 1.75 mMol calcium (175).

6.2 LIMITATIONS

There are certain limitations of our model approach we have to discuss. The main limitation is that we do not take calcium-protein binding explicitly into account. Calcium in the extracellular fluid comes in three flavors: ionized, which is biologically essential, complexed to anions such as phosphate, or protein-bound and, therefore, not filterable by the kidneys. The main part of protein-bound calcium is bound to albumin. As a general rule, 1 g/dl albumin binds about 0.2 mMol of calcium. Calcium-albumin binding is affected by the pH. Lower pH results in decreased protein binding and, therefore, increased ionized calcium concentration. If pH decreases by 0.1 pH, ionized calcium will rise by about 0.05 mMol (36). Poor diet, proteinuria, liver disease, or inflammation may cause albumin deficiency and shifted ratios between ionized and total calcium concentration. During hemodialysis, bicarbonate replacement often corrects metabolic acidosis. Therefore, if we attempt to couple the integrated model with a previously published calcium mass transfer model during hemodialysis (146), we need to introduce albumin and bicarbonate to the model. To this extent, one could also think about separating interstitial fluid and plasma in different compartments.

Another limitation is that we did not introduce FGF-23 in the model. Since we were interested in patients receiving maintenance hemodialysis, the regulatory effect of FGF-23 was of less importance for this thesis, as discussed in the Introduction. However, FGF-23 might be critical when studying calcium and phosphate homeostasis in healthy subjects.

Finally, there are general limitations to mathematical modeling. Besides the trade-off between simplification and complexity, we can only model known regulators and calibrate the model based on physiological assumptions. It is very well possible that regulators that are unknown today play an essential role in calcium and phosphate homeostasis. For instance, FGF-23 has only been discovered in 2000 and has gained significant attention as a regulator of phosphate homeostasis.

6.3 NEXT STEPS AND CONCLUSION

Besides the inclusion of albumin and albumin-calcium binding in mathematical modeling, another promising next step would be to include calcium-phosphate precipitation in the kidneys to predict kidney stone formation. To this extent, a structural kidney model could be useful. In (23), the authors introduced a detailed model of renal calcium reabsorption across single cells. A similar detailed model would allow to include $CaHPO_4$ explicitly in the renal model.

The present model can study the effect of different medications, such as calcitriol therapy or long-term dietary changes. It was, for example, used to study the effect of a low phosphate diet on the development of CKD-MBD. Future studies would involve mutations of the calcium-sensing receptors allowing individualized therapy of hemodialysis patients (98, 164).

Finally, the point of no return for continuous mineralization of vascular tissue should be confirmed in more experimental setups. experimentally, for example, on the tissue level. Specifically, vascular calcification could be induced in human vascular smooth muscle cells by elevated phosphate levels. Once vascular calcification is measurable, normophosphatemia is induced, and ongoing calcification deposition (i.e., calcium- phosphate content in the smooth muscle cells) is monitored. This experimental setup would also determine the time point of the proposed point of no return for calcium and phosphate precipitation by analyzing the critical time after which the switch from hyperphosphatemia to normophosphatemia does not induce calcification deposition.

In conclusion, this work allowed us to elucidate the mechanism which results in chronic kidney disease mineral and bone metabolism disorder. Furthermore, it allowed us to introduce a new hypothesis regarding calcium-phosphate precipitation, which could be tested in future research. Bone mineral metabolism is highly complex, and we hope that the mathematical model of calcium and phosphate homeostasis presented in this thesis might serve for future work in this field.

Bibliography

1. **Abbona G, Papotti M, Gasparri G, Bussolati G**. Proliferative activity in parathyroid tumors as detected by Ki-67 immunostaining. *Human Pathology* 26:135–138, 1995. doi:{10.1016/0046-8177(95)90028-4}.

2. **Adams J, Omann G, Linderman J**. A mathematical model for ligand/receptor/G-protein dynamics and actin polymerization in human neutrophils. *Journal of Theoretical Biology* 193:543–560, 1998. doi:{10.1006/jtbi.1998.0721}.

3. **Adams JS, Hewison M**. Extrarenal expression of the 25-hydroxyvitamin D-1-hydroxylase. *Archives of Biochemistry and Biophysics* 523:95–102, 2012. doi:{10.1016/j.abb.2012.02.016}.

4. **Agar BU, Akonur A, Lo YC, Cheung AK, Leypoldt JK**. Kinetic Model of Phosphorus Mobilization during and after Short and Conventional Hemodialysis. *Clinical Journal of the American Society of Nephrology* 6:2854–2860, 2011. doi:{10.2215/CJN.03860411}.

5. **Barreto DV, Barreto FdC, de Carvalho AB, Cuppari L, Draibe SA, Dalboni MA, Affonso Moyses RM, Neves KR, Jorgetti V, Miname M, Santos RD, Canziani MEF**. Association of Changes in Bone Remodeling and Coronary Calcification in Hemodialysis Patients: A Prospective Study. *American Journal of Kidney Diseases* 52:1139–1150, 2008. doi:{10.1053/j.ajkd.2008.06.024}.

6. **Bellido T, Ali A, Gubrij I, Plotkin L, Fu Q, O'Brien C, Manolagas S, Jilka R**. Chronic elevation of parathyroid hormone in mice reduces expression of sclerostin by osteocytes: A novel mechanism for hormonal control of osteoblastogenesis. *Endocrinology* 146:4577–4583, 2005. doi:{10.1210/en.2005-0239}.

7. **Bellido T, Ali A, Plotkin L, Fu Q, Gubrij I, Roberson P, Weinstein R, O'Brien C, Manolagas S, Jilka R**. Proteasomal degradation of Runx2 shortens parathyroid hormone-induced anti-apoptotic signaling in osteoblasts. *Journal of Biological Chemistry* 278:50259–50272, 2003. doi:{10.1074/jbc.M307444200}.

8. **Bellido T, Ali A, Plotkin L, Fu Q, Gubrij I, Roberson P, Weinstein R, O'Brien C, Manolagas S, Jilka R**. Proteasomal degradation of Runx2 shortens parathyroid hormone-induced anti-apoptotic signaling in osteoblasts - A putative explanation

for why intermittent administration is needed for bone anabolism. *Journal of Biological Chemistry* 278:50259–50272, 2003. doi:{10.1074/jbc.M307444200}.

9. **Ben-Dov IZ, Galitzer H, Lavi-Moshayoff V, Goetz R, Kuro-o M, Mohammadi M, Sirkis R, Naveh-Many T, Silver J**. The parathyroid is a target organ for FGF23 in rats. *Journal of Clinical Investigation* 117:4003–4008, 2007. doi:{10.1172/JCI32409}.

10. **Benzekry S, Lamont C, Beheshti A, Tracz A, Ebos JML, Hlatky L, Hahnfeldt P**. Classical Mathematical Models for Description and Prediction of Experimental Tumor Growth. *PLoS Computational biology* 10, 2014. doi:{10.1371/journal.pcbi.1003800}.

11. **Bergwitz C, Jueppner H**. Phosphate Sensing. *Advances in Chronic Kidney Disease* 18:132–144, 2011. doi:{10.1053/j.ackd.2011.01.004}.

12. **Berndt T, Kumar R**. Phosphatonins and the regulation of phosphate homeostasis. *Annual Review of Physiology* 69:341–359, 2007. doi:{10.1146/annurev.physiol.69.040705.141729}.

13. **Bevington A, Mundy K, Yates A, Kanis J, Russell R, Taylor D, Rajagopalan B, Radda G**. A study of intracellular ortho-phosphate concentration in human-muscle and erythrocytes by P-31 nuclear-magnetic-resonance spectroscopy and selective chemical-assay. *Clinical Science* 71:729–735, 1986. doi:{10.1042/cs0710729}.

14. **Bikle DD**. Vitamin D and the skin: Physiology and pathophysiology. *Reviews in Endocrine & Metabolic Disorders* 13:3–19, 2012. doi:{10.1007/s11154-011-9194-0}.

15. **Bilezikian JP, Khan A, Potts JT Jr, Brandi ML, Clarke BL, Shoback D, Jueppner H, D'Amour P, Fox J, Rejnmark L, Mosekilde L, Rubin MR, Dempster D, Gafni R, Collins MT, Sliney J, Sanders J**. Hypoparathyroidism in the Adult: Epidemiology, Diagnosis, Pathophysiology, Target-Organ Involvement, Treatment, and Challenges for Future Research. *Journal of Bone and Mineral Research* 26:2317–2337, 2011. doi:{10.1002/jbmr.483}.

16. **Black J, Bonhamcarter R**. Association between aortic stenosis and facies of severe infantile hypercalcaemia. *Lancet* 2:745–&, 1963.

17. **Blaine J, Chonchol M, Levi M**. Renal Control of Calcium, Phosphate, and Magnesium Homeostasis. *Clinical Journal of the American Society of Nephrology* 10:1257–1272, 2015. doi:{10.2215/CJN.09750913}.

18. **Block G, Do TP, Collins AJ, Cooper KC, Bradbury BD**. Co-trending of parathyroid hormone and phosphate in patients receiving hemodialysis. *Clinical Nephrology* 85:142–151, 2016. doi:{10.5414/CN108629}.

19. **Block G, Martin K, de Francisco A, Turner S, Avram M, Suranyi M, Hercz G, Cunningham J, Abu-Alfa A, Messa P, Coyne D, Locatelli F, Cohen R, Evenepoel P, Moe S, Fournier A, Braun J, McCary L, Zani V, Olson K, Drueke T, Goodman W**. Cinacalcet for secondary hyperparathyroidism in patients receiving hemodialysis. *New England Journal of Medicine* 350:1516–1525, 2004. doi:{10.1056/NEJMoa031633}.

20. **Block G, Port F**. Re-evaluation of risks associated with hyperphosphatemia and hyperparathyroidism in dialysis patients: Recommendations for a change in management. *American Journal of Kidney Diseases* 35:1226–1237, 2000. doi:{10.1016/S0272-6386(00)70064-3}.

21. **Block GA, Bushinsky DA, Cheng S, Cunningham J, Dehmel B, Drueke TB, Ketteler M, Kewalramani R, Martin KJ, Moe SM, Patel UD, Silver J, Sun Y, Wang H, Chertow GM**. Effect of Etelcalcetide vs Cinacalcet on Serum Parathyroid Hormone in Patients Receiving Hemodialysis With Secondary Hyperparathyroidism A Randomized Clinical Trial. *JAMA-Journal of the American Medical Association* 317:156–164, 2017. doi:{10.1001/jama.2016.19468}.

22. **Block GA, Zaun D, Smits G, Persky M, Brillhart S, Nieman K, Liu J, St Peter WL**. Cinacalcet hydrochloride treatment significantly improves all-cause and cardiovascular survival in a large cohort of hemodialysis patients. *Kidney International* 78:578–589, 2010. doi:{10.1038/ki.2010.167}.

23. **Bonny O, Edwards A**. Calcium reabsorption in the distal tubule: regulation by sodium, pH, and flow. *American Journal of Physiology - Renal Physiology* 304:F585–F600, 2013. doi:{10.1152/ajprenal.00493.2012}.

24. **Borrego M, Felsenfeld A, MartinMalo A, Almaden Y, Concepcion M, Aljama P, Rodriguez M**. Evidence for adaptation of the entire PTH-calcium curve to sustained changes in the serum calcium in haemodialysis patients. *Nephrology Dialysis Transplantation* 12:505–513, 1997. doi:{10.1093/ndt/12.3.505}.

25. **Boyce BF, Xing L**. Functions of RANKL/RANK/OPG in bone modeling and remodeling. *Archives of Biochemistry and Biophysics* 473:139–146, 2008. doi:{10.1016/j.abb.2008.03.018}.

26. **Brasier A, Nussbaum S**. Hungry bone syndrome - clinical and biochemical predictors of its occurrence after parathyroid surgery. *American Journal of Medicine* 84:654–660, 1988. doi:{10.1016/0002-9343(88)90100-3}.

27. **Brent G, Leboff M, Seely E, Conlin P, Brown E**. Relationship between the concentration and rate of change of calcium and serum intact parathyroid-hormone levels in normal humans. *Journal of Clinical Endocrinology & Metabolism* 67:944–950, 1988. doi:{10.1210/jcem-67-5-944}.

28. **Bridge LJ, King JR, Hill SJ, Owen MR**. Mathematical modelling of signalling in a two-ligand G-protein coupled receptor system: Agonist-antagonist competition. *Mathematical Biosciences* 223:115–132, 2010. doi:{10.1016/j.mbs.2009.11.005}.

29. **Bronner F**. Gastrointestinal absorption of calcium. In *Calcium in human biology*, edited by B Nordin, chapter 5, 93–123. Berlin: Springer-Verlag, 1988. doi:{10.1007/978-1-4471-1437-6}.

30. **Bronner F**. Mechanisms of intestinal calcium absorption. *Journal of Cellular Biochemistry* 88:387–393, 2003. doi:{10.1002/jcb.10330}.

31. **Brown A, Ritter C, Finch J, Slatopolsky E**. Decreased calcium-sensing receptor expression in hyperplastic parathyroid glands of uremic rats: Role of dietary phosphate. *Kidney International* 55:1284–1292, 1999. doi:{10.1046/j.1523-1755.1999.00386.x}.

32. **Brown E**. 4-parameter model of the sigmoidal relationship between parathyroid-hormone release and extracellular calcium-concentration in normal and abnormal parathyroid tissue. *Journal of Clinical Endocrinology & Metabolism* 56:572–581, 1983. doi:{10.1210/jcem-56-3-572}.

33. **Brown E**. Control of parathyroid hormone secretion by its key physiological regulators. In *The Parathyroids: Basic and Clinical Concepts*, edited by Bilezikian, J, 101–118. Elsevier, 2015.

34. **Brown E, Leombruno R, Thatcher J, Burrowes M**. The acute secretory response to alterations in extracellular calcium-concentration and dopamine in perifused bovine parathyroid cells. *Endocrinology* 116:1123–1132, 1985. doi:{10.1210/endo-116-3-1123}.

35. **Brown EM**. Clinical lessons from the calcium-sensing receptor. *Nature Clinical Practice Endocrinology & Metabolism* 3:122–133, 2007. doi:{10.1038/ncpendmet0388}.

36. **Bushinsky DA, Monk RD**. Electrolyte quintet: Calcium. *Lancet* 352:306–311, 1998. doi:10.1016/s0140-6736(97)12331-5.

37. **Canalejo A, Almaden Y, Torregrosa V, Gomez-Villamandos J, Ramos B, Campistol J, Felsenfeld A, Rodriguez M**. The in vitro effect of calcitriol on parathyroid cell proliferation and apoptosis. *Journal of the American Society of Nephrology* 11:1865–1872, 2000.

38. **Centeno PP, Herberger A, Mun HC, Tu C, Nemeth EF, Chang W, Conigrave AD, Ward DT**. Phosphate acts directly on the calcium-sensing receptor to stimulate parathyroid hormone secretion. *Nature Communications* 10, 2019. doi:{10.1038/s41467-019-12399-9}.

39. **Chakravarti B, Chattopadhyay N, Brown EM**. Signaling Through the Extracellular Calcium-Sensing Receptor (CaSR). In *Calcium Signaling*, edited by Islam, MS, volume 740, 103–142. Advances in Experimental Medicine and Biology, 2012. doi:{10.1007/978-94-007-2888-2_5}.

40. **Chande S, Bergwitz C**. Role of phosphate sensing in bone and mineral metabolism. *Nature Reviews Endocrinology* 14:637–655, 2018. doi:{10.1038/s41574-018-0076-3}.

41. **Chen NX, O'Neill KD, Chen X, Duan D, Wang E, Sturek MS, Edwards JM, Moe SM**. Fetuin-A uptake in bovine vascular smooth muscle cells is calcium dependent and mediated by annexins. *American Journal of Physiology Renal Physiology* 292:F599–F606, 2007. doi:{10.1152/ajprenal.00303.2006}.

42. **Chen R, Goodman W**. Role of the calcium-sensing receptor in parathyroid gland physiology. *American Journal of Physiology-Renal Physiology* 286:F1005–F1011, 2004. doi:{10.1152/ajprenal.00013.2004}.

43. **Chertow GM, Block GA, Correa-Rotter R, Drueeke TB, Floege J, Goodman WG, Herzog CA, Kubo Y, London GM, Mahaffey KW, Mix TCH, Moe SM, Trotman ML, Wheeler DC, Parfrey PS, Investigators ET**. Effect of Cinacalcet on Cardiovascular Disease in Patients Undergoing Dialysis. *New England Journal of Medicine* 367:2482–2494, 2012. doi:{10.1056/NEJMoa1205624}.

44. **Cheung A, Sarnak M, Yan G, Dwyer J, Heyka R, Rocco M, Teehan B, Levey A, Study HH**. Atherosclerotic cardiovascular disease risks in chronic hemodialysis patients. *Kidney International* 58:353–362, 2000. doi:{10.1046/j.1523-1755.2000.00173.x}.

45. **Christie CR, Achenie LEK, Ogunnaike BA**. A Control Engineering Model of Calcium Regulation. *Journal of Clinical Endocrinology & Metabolism* 99:2844–2853, 2014. doi:{10.1210/jc.2013-3451}.

46. **Clarke B**. Normal Bone Anatomy and Physiology. *Clinical Journal of the American Society of Nephrology* 3:S131–S139, 2008. doi:{10.2215/CJN.04151206}.

47. **Conigrave AD, Ward DT**. Calcium-sensing receptor (CaSR): Pharmacological properties and signaling pathways. *Best Practice& Research Clinical Endocrinology & Metabolism* 27:315–331, 2013. doi:{10.1016/j.beem.2013.05.010}.

48. **Conlin P, Fajtova V, Mortensen R, Leboff M, Brown E**. Hysteresis in the relationship between serum ionized calcium and intact parathyroid-hormone during recovery from induced hypercalcemia and hypocalcemia in normal humans. *Journal of Clinical Endocrinology and Metabolism* 69:593–599, 1989. doi:{10.1210/jcem-69-3-593}.

49. **Cooper MS, Gittoes NJL**. Diagnosis and management of hypocalcaemia. *British Medical Journal* 336:1298–1302, 2008. doi:{10.1136/bmj.39582.589433.BE}.

50. **Cozzolino M, Ciceri P, Galassi A, Mangano M, Carugo S, Capelli I, Cianciolo G**. The Key Role of Phosphate on Vascular Calcification. *Toxins* 11, 2019. doi:{10.3390/toxins11040213}.

51. **Dallas S, Parksnyder S, Miyazono K, Twardzik D, Mundy G, Bonewald L**. Characterization and autoregulation of latent transforming growth-factor-beta (TGF-Beta) complexes in osteoblast-like cell-lines - production of a latent complex lacking the latent TGF-Beta-binding protein. *Journal of Biological Chemistry* 269:6815–6822, 1994.

52. **Dallas S, Rosser J, Mundy G, Bonewald L**. Proteolysis of latent transforming growth factor-beta (TGF-beta)-binding protein-1 by osteoclasts - A cellular mechanism for release of TGF-beta from bone matrix. *Journal of Biological Chemistry* 277:21352–21360, 2002. doi:{10.1074/jbc.M111663200}.

53. **Dardenne O, Prud'homme J, Arabian A, Glorieux F, St-Arnaud R**. Targeted inactivation of the 25-hydroxyvitamin D-3-1 alpha-hydroxylase gene (CYP27B1) creates an animal model of pseudovitamin D-deficiency rickets. *Endocrinology* 142:3135–3141, 2001. doi:{10.1210/en.142.7.3135}.

54. **Davies K, Rafferty K, Heaney R**. Determinants of endogenous calcium entry into the gut. *American Journal of Clinical Nutrition* 80:919–923, 2004. doi:{10.1093/ajcn/80.4.919.}

55. **Denda M, Finch J, Slatopolsky E**. Phosphorus accelerates the development of parathyroid hyperplasia and secondary hyperparathyroidism in rats with renal failure. *American Journal of Kidney Diseases* 28:596–602, 1996. doi:{10.1016/S0272-6386(96)90473-4}.

56. **Diamond J**. Quantitative evolutionary design. *Journal of Physiology-London* 542:337–345, 2002. doi:{10.1113/jphysiol.2002.018366}.

57. **Dolores Arenas M, de la Fuente V, Delgado P, Teresa Gil M, Gutierrez P, Ribero J, Rodriguez M, Almaden Y**. Pharmacodynamics of Cinacalcet Over 48 Hours in Patients With Controlled Secondary Hyperparathyroidism: Useful Data in Clinical Practice. *Journal of Clinical Endocrinology & Metabolism* 98:1718–1725, 2013. doi:{10.1210/jc.2012-4003}.

58. **Dong B**. Cinacalcet: An oral calcimimetic agent for the management of hyperparathyroidism. *Clinical Therapeutics* 27:1725–1751, 2005. doi:{10.1016/j.clinthera.2005.11.015}.

59. **Drueke T, Martin D, Rodriguez M**. Can calcimimetics inhibit parathyroid hyperplasia? Evidence from preclinical studies. *Nephrology Dialysis Transplantation* 22:1828–1839, 2007. doi:{10.1093/ndt/gfm177}.

60. **Dusso A, Brown A, Slatopolsky E**. Vitamin D. *American Journal of Physiology-Renal Physiology* 289:F8–F28, 2005. doi:{10.1152/ajprenal.00336.2004}.

61. **Eastell R, Vieira N, Yergey A, Riggs B**. One-day test using stable isotopes to measure true fractional calcium-absorption. *Journal of Bone and Mineral Research* 4:463–468, 1989.

62. **Egbuna OI, Brown EM**. Hypercalcaemic and hypocalcaemic conditions due to calcium-sensing receptor mutations. *Best Practive & Research in Clinical Rheumatology* 22:129–148, 2008. doi:{10.1016/j.berh.2007.11.006}.

63. **Eknoyan G, Lameire N, Barsoum R, Eckardt K, Levin A, Levin N, Locatelli F, MacLeod A, Vanholder R, Walker R, Wang H**. The burden of kidney disease: Improving global outcomes. *Kidney International* 66:1310–1314, 2004. doi:{10.1111/j.1523-1755.2004.00894.x}.

64. **Elias RM, Alvares VRC, Moyses RMA**. Phosphate Removal During Conventional Hemodialysis: a Decades-Old Misconception. *Kidney % Blood Pressure Research* 43:110–114, 2018. doi:{10.1159/000487108}.

65. **EMA**. *Mimpara, European Medicines Agency*, 2009, (accessed 2017-05-09). https://www.ema.europa.eu/en/documents/product-information/mimpara-epar-product-information_en.pdf.

66. **Evans M, Methven S, Gasparini A, Barany P, Birnie K, MacNeill S, May MT, Caskey FJ, Carrero JJ**. Cinacalcet use and the risk of cardiovascular events, fractures and mortality in chronic kidney disease patients with secondary hyperparathyroidism. *Scientific Reports* 8, 2018. doi:{10.1038/s41598-018-20552-5}.

67. **FDA**. *Sensipar, Food and Drug Administration*, 2004, (accessed 2017-12-06). https://www.accessdata.fda.gov/drugsatfda_docs/nda/2004/21-688.pdf_Sensipar_Pharmr_P1.pdf.

68. **Felsenfeld AJ, Rodriguez M, Aguilera-Tejero E**. Dynamics of parathyroid hormone secretion in health and secondary hyperparathyroidism. *Clinical Journal of the American Society of Nephrology* 2:1283–1305, 2007. doi:{10.2215/CJN.01520407}.

69. **Fenton RA, Murray F, Rieg JAD, Tang T, Levi M, Rieg T**. Renal Phosphate Wasting in the Absence of Adenylyl Cyclase 6. *Journal of the American Society of Nephrology* 25:2822–2834, 2014. doi:{10.1681/ASN.2013101102}.

70. **Fitzpatrick L, Leong D**. Individual parathyroid cells are more sensitive to calcium than a parathyroid cell-population. *Endocrinology* 126:1720–1727, 1990.

71. **Fleet JC, Schoch RD**. Molecular mechanisms for regulation of intestinal calcium absorption by vitamin D and other factors. *Critical Reviews in Clinical Laboratory Sciences* 47:181–195, 2010. doi:{10.3109/10408363.2010.536429}.

72. **Foundation NK**. *Kidney Disease: The Basics*, accessed 2020-09-06. https://www.kidney.org/news/newsroom/factsheets/KidneyDiseaseBasics#:

~:text=An%20estimated%2037%20million%20American,t%20know%20they%20have%20CKD.

73. **Frick K, LaPlante K, Bushinsky D**. RANK ligand and TNF-alpha mediate acid-induced bone calcium efflux in vitro. *American Journal of Physiology - Renal Physiology* 289:F1005–F1011, 2005. doi:{10.1152/ajprenal.00420.2004}.

74. **Fu Q, Jilka R, Manolagas S, O'Brien C**. Parathyroid hormone stimulates receptor activator of NF kappa B ligand and inhibits osteoprotegerin expression via protein kinase A activation of cAMP-response element-binding protein. *Journal of Biological Chemistry* 277:48868–48875, 2002. doi:{10.1074/jbc.M208494200}.

75. **Fukagawa M, Nakanishi S, Kazama JJ**. Basic and clinical aspects of parathyroid hyperplasia in chronic kidney disease. *Kidney International* 70:S3–S7, 2006. doi:{10.1038/sj.ki.5001594}.

76. **Fukagawa M, Okazaki R, Takano K, Kaname S, Ogata E, Kitaoka M, Harada S, Sekine N, Matsumoto T, Kurokawa K**. Regression of parathyroid hyperplasia by calcitriol-pulse therapy in patients on long-term dialysis. *New England Journal of Medicine* 323:421–422, 1990.

77. **Gilbert L, He X, Farmer P, Rubin J, Drissi H, van Wijnen A, Lian J, Stein G, Nanes M**. Expression of the osteoblast differentiation factor RUNX2 (Cbfa1/AML3/Pebp2 alpha A) is inhibited by tumor necrosis factor-alpha. *Journal of Biological Chemistry* 277:2695–2701, 2002. doi:{10.1074/jbc.M106339200}.

78. **Gincherman Y, Moloney K, McKee C, Coyne DW**. Assessment of adherence to cinacalcet by prescription refill rates in hemodialysis patients. *Hemodialysis International* 14:68–72, 2010. doi:{10.1111/j.1542-4758.2009.00397.x}.

79. **Go A, Chertow G, Fan D, McCulloch C, Hsu C**. Chronic kidney disease and the risks of death, cardiovascular events, and hospitalization. *New England Journal of Medicine* 351:1296–1305, 2004. doi:{10.1056/NEJMoa041031}. 36th Annual Meeting of the American-Society-of-Nephrology, SAN DIEGO, CA, NOV 12-17, 2003.

80. **Gogusev J, Duchambon P, Hory B, Giovannini M, Goureau Y, Sarfati E, Drueke T**. Depressed expression of calcium receptor in parathyroid gland tissue of patients with hyperparathyroidism. *Kidney International* 51:328–336, 1997. doi:{10.1038/ki.1997.41}.

81. **Goldfarb M, Gondek SS, Lim SM, Farra JC, Nose V, Lew JI**. Postoperative Hungry Bone Syndrome in Patients with Secondary Hyperparathyroidism of Renal Origin. *World Journal of Surgery* 36:1314–1319, 2012. doi:{10.1007/s00268-012-1560-x}.

82. **Goodman W, Veldhuis J, Belin T, Van Herle A, Juppner H, Salusky I**. Calcium-sensing by parathyroid glands in secondary hyperparathyroidism. *Journal of Clinical Endocrinology & Metabolism* 83:2765–2772, 1998. doi:{10.1210/jc.83.8.2765}.

83. **Goodman WG, Quarles LD**. Development and progression of secondary hyperparathyroidism in chronic kidney disease: lessons from molecular genetics. *Kidney International* 74:276–288, 2008. doi:{10.1038/sj.ki.5002287}.

84. **Graciolli FG, Neves KR, Barreto F, Barreto DV, dos Reis LM, Canziani ME, Sabbagh Y, Carvalho AB, Jorgetti V, Elias RM, Schiavi S, Moyses RMA**. The complexity of chronic kidney disease-mineral and bone disorder across stages of chronic kidney disease. *Kidney International* 91:1436–1446, 2017. doi:{10.1016/j.kint.2016.12.029}.

85. **Granjon D, Bonny O, Edwards1 A**. Coupling between phosphate and calcium homeostasis: a mathematical model. *American Journal of Physiology - Renal Physiology* 313: F1181–F1199, 2017. doi:{10.1152/ajprenal.00271.2017}.

86. **Grant F, Conlin P, Brown E**. Rate and concentration-dependence of parathyroid-hormone dynamics during stepwise changes in serum ionized calcium in normal humans. *Journal of Clinical Endocrinology & Metabolism* 71:370–378, 1990.

87. **Gutierrez O, Isakova T, Rhee E, Shah A, Holmes J, Collerone G, Juppner H, Wolf M**. Fibroblast growth factor-23 mitigates hyperphosphatemia but accentuates calcitriol deficiency in chronic kidney disease. *Journal of the American Society of Nephrology* 16:2205–2215, 2005. doi:{10.1681/ASN.2005010052}.

88. **Gutierrez OM, Muntner P, Rizk DV, McClellan WM, Warnock DG, Newby PK, Judd SE**. Dietary Patterns and Risk of Death and Progression to ESRD in Individuals With CKD: A Cohort Study. *American Journal of Kidney Diseases* 64:204–213, 2014. doi:{10.1053/j.ajkd.2014.02.013}.

89. **Habener J**. Regulation of parathyroid-hormone screation and biosythnesis. *Annual Review of Physiology* 43:211–223, 1981. doi:{10.1146/annurev.ph.43.030181.001235}.

90. **Harris R, Padhi D, Marbury T, Noveck R, Salfi M, Sullivan J**. Pharmacokinetics, pharmacodynamics, and safety of cinacalcet hydrochloride in hemodialysis patients at doses up to 200 mg once daily. *American Journal of Kidney Diseases* 44:1070–1076, 2004. doi:{10.1053/j.ajkd.2004.08.029}.

91. **Harrison H, Harrison H**. Intestinal transport of phosphate - action of vitamin D, calcium, and potassium. *American Journal of Physiology* 201:1007–&, 1961.

92. **Hattenhauer O, Traebert M, Murer H, Biber J**. Regulation of small intestinal Na-P-i type IIb cotransporter by dietary phosphate intake. *American Journal of Physiology - Gastrointestinal and Liver Physiology* 277:G756–G762, 1999.

93. **Heaney R, Berner B, Louie-Helm J**. Dosing regimen for calcium supplementation. *Journal of Bone and Mineral Research* 15:2291, 2000. doi:{10.1359/jbmr.2000.15.11.2291}.

94. **Heaney R, Recker R**. Determinants of endogenous fecal calcium in healthy women. *Journal of Bone and Mineral Research* 9:1621–1627, 1994.

95. **Hebert S**. Calcium and salinity sensing by the thick ascending limb: A journey from mammals to fish and back again. *Kidney International* 66:S28–S33, 2004. doi:{10.1111/j.1523-1755.2004.09105.x}.

96. **Hebert S, Brown E, Harris H**. Role of the Ca2+-sensing receptor in divalent mineral ion homeostasis. *Journal of Experimental Biology* 200:295–302, 1997.

97. **Heiwe S, Jacobson SH**. Exercise Training in Adults With CKD: A Systematic Review and Meta-analysis. *American Journal of Kidney Diseases* 64:383–393, 2014. doi:{10.1053/j.ajkd.2014.03.020}.

98. **Hendy G, D'Souza-Li L, Yang B, Canaff L, Cole D**. Mutations of the calcium-sensing receptor (CASR) in familial hypocalciuric hypercalcemia, neonatal severe hyperparathyroidism, and autosomal dominant hypocalcemia. *Human Mutation* 16:281–296, 2000. doi:{10.1002/1098-1004(200010)16:4\textless281::AID-HUMU1\textgreater3.0.CO;2-A}.

99. **Herrmann M, Schaefer C, Heiss A, Graeber S, Kinkeldey A, Buescher A, Schmitt MMN, Bornemann J, Nimmerjahn F, Herrmann M, Helming L, Gordon S, Jahnen-Dechent W**. Clearance of Fetuin-A-Containing Calciprotein Particles Is Mediated by Scavenger Receptor-A. *Circulation Research* 111:575–U304, 2012. doi:{10.1161/CIRCRESAHA.111.261479}.

100. **Hill NR, Fatoba ST, Oke JL, Hirst JA, O'Callaghan CA, Lasserson DS, Hobbs FDR**. Global Prevalence of Chronic Kidney Disease - A Systematic Review and Meta-Analysis. *PLoS One* 11, 2016. doi:{10.1371/journal.pone.0158765}.

101. **Hou S, Zhao J, Ellman C, Hu J, Griffin Z, Spiegel D, Bourdeau J**. Calcium and phosphorus fluxes during hemodialysis with low calcium dialysate. *American Journal of Kidney Diseases* 18:217–224, 1991. doi:{10.1016/S0272-6386(12)80882-1}.

102. **Hruska K, Korkor A, Martin K, Slatopolsky E**. The fallacy of the calcium-phosphorus product. *Kidney International* 72:792–796, 2007. doi:{10.1038/sj.ki.5002412}.

103. **Hunter T**. Protein-kinases and phosphatases - the ying and yang of protein-phosphorylation and signaling. *Cell* 80:225–236, 1995. doi:{10.1016/0092-8674(95)90405-0}.

104. **Ikeda F, Nishimura R, Matsubara T, Tanaka S, Inoue J, Reddy S, Hata K, Yamashita K, Hiraga T, Watanabe T, Kukita T, Yoshioka K, Rao A, Yoneda T**. Critical roles of c-Jun signaling in regulation of NFAT family and RANKL-regulated osteoclast differentiation. *Journal of Clinical Investigation* 114:475–484, 2004. doi:{10.1172/JCI200419657}.

105. **Isakova T, Craven TE, Lee J, Scialla JJ, Xie H, Wahl P, Marcovina SM, Byington RP, Wolf M**. Fibroblast Growth Factor 23 and Incident CKD in Type 2 Diabetes. *Clinical Journal of the American Society of Nephrology* 10:29–38, 2015. doi:{10.2215/CJN.06190614}.

106. **Iseki K, Ikemiya Y, Kinjo K, Inoue T, Iseki C, Takishita S**. Body mass index and the risk of development of end-stage renal disease in a screened cohort. *Kidney International* 65:1870–1876, 2004. doi:{10.1111/j.1523-1755.2004.00582.x}. Symposium on Immunology in Renal Disease, Berlin, GERMANY, JUN 02-05, 2003.

107. **Janssens K, ten Dijke P, Janssens S, Van Hul W**. Transforming growth factor-beta 1 to the bone. *Endocrine Reviews* 26:743–774, 2005. doi:{10.1210/er.2004-0001}.

108. **Jean G, Chazot C, Charra B**. Six cases of successful cinacalcet cessation in haemodialysis patients treated for secondary hyperparathyroidism. *Nephrology Dialysis Transplantation* 22:2102–2103, 2007. doi:{10.1093/ndt/gfm172}.

109. **Jha V, Garcia-Garcia G, Iseki K, Li Z, Naicker S, Plattner B, Saran R, Wang AYM, Yang CW**. Chronic kidney disease: global dimension and perspectives. *Lancet* 382:260–272, 2013. doi:{10.1016/S0140-6736(13)60687-X}.

110. **Jia D, O'Brien CA, Stewart SA, Manolagas SC, Weinstein RS**. Glucocorticoids act directly on osteoclasts to increase their life span and reduce bone density. *Endocrinology* 147:5592–5599, 2006. doi:{10.1210/en.2006-0459}.

111. **Jilka R, Weinstein R, Bellido T, Parfitt A, Manolagas S**. Osteoblast programmed cell death (apoptosis): Modulation by growth factors and cytokines. *Journal of Bone and Mineral Research* 13:793–802, 1998. doi:{10.1359/jbmr.1998.13.5.793}.

112. **Jimenez-Fernandez VM, Jimenez-Fernandez M, Vazquez-Leal H, Munoz-Aguirre E, Cerecedo-Nunez HH, Filobello-Nino UA, Castro-Gonzalez FJ**. Transforming the canonical piecewise-linear model into a smooth-piecewise representation. *SpringerPlus* 5, 2016. doi:{10.1186/s40064-016-3278-y}.

113. **Jono S, McKee M, Murry C, Shioi A, Nishizawa Y, Mori K, Morii H, Giachelli C**. Phosphate regulation of vascular smooth muscle cell calcification. *Circulation Research* 87:E10–E17, 2000. doi:{10.1161/01.RES.87.7.e10}.

114. **Jueppner H, Wolf M, Salusky IB**. FGF-23: More Than a Regulator of Renal Phosphate Handling? *Journal of Bone and Mineral Research* 25:2091–2097, 2010. doi:{10.1002/jbmr.170}.

115. **Karsdal M, Hjorth P, Henriksen K, Kirkegaard T, Nielsen K, Lou H, Delaisse J, Foged N**. Transforming growth factor-beta controls human osteoclastogenesis through the p38 MAPK and regulation of RANK expression. *Journal of Biological Chemistry* 278:44975–44987, 2003. doi:{10.1074/jbc.M303905200}.

116. **Kawata T, Imanishi Y, Kobayashi K, Miki T, Arnold A, Inaba M, Nishizawa Y**. Parathyroid hormone regulates fibroblast growth factor-23 in a mouse model of primary hyperparathyroidism. *Journal of the American Society of Nephrology* 18:2683–2688, 2007. doi:{10.1681/ASN.2006070783}.

117. **Kemp G, Bevington A**. How could a cell regulate its internal Pi concentration. *Biochemical Society Transactions* 17:1092, 1989. doi:{10.1042/bst0171092}.

118. **Kemp G, Khouja H, Bevington A, Ahmado A, Russell R**. Cellular Pi concentration and Pi uptake do not always change in parallel in cultured fibroblasts and osteoblasts. *Biochemical Society Transaction* 17:522–523, 1989. doi: {10.1042/bst0170522}.

119. **Kempson S, Lotscher M, Kassling B, Biber J, Murer H, Levi M**. Parathyroid-hormone action on phosphate transporter mRNA and protein in rat renal proximal tubulus. *American Journal of Physiology - Renal Fluid and Electrolyte Phyisology* 268:F784–F791, 1995.

120. **Khosla S**. Minireview: The OPG/RANKL/RANK system. *Endocrinology* 142:5050–5055, 2001. doi:{10.1210/en.142.12.5050}.

121. **Kim S, Yamazaki M, Zella LA, Meyer MB, Fretz JA, Shevde NK, Pike JW**. Multiple enhancer regions located at significant distances upstream of the transcriptional start site mediate RANKL gene expression in response to 1,25-dihydroxyvitamin D-3. *Journal of Steroid Biochemistry and Molecular Biology* 103:430–434, 2007. doi:{10.1016/j.jsbmb.2006.12.020}. 13th Workshop on Vitamin D, Victoria, CANADA, APR 07-12, 2006.

122. **Knowles J**. Enzyme-catalyzed phosphoryl transfer-reactions. *Annual Review of Biochemistry* 49:877–919, 1980. doi:{10.1146/annurev.bi.49.070180.004305}.

123. **Komaba H, Fukagawa M**. The role of FGF23 in CKD-with or without Klotho. *Nature Reviews Nephrology* 8:484–490, 2012. doi:{10.1038/nrneph.2012.116}.

124. **Komaba H, Nakanishi S, Fujimori A, Tanaka M, Shin J, Shibuya K, Nishioka M, Hasegawa H, Kurosawa T, Fukagawa M**. Cinacalcet Effectively Reduces Parathyroid Hormone Secretion and Gland Volume Regardless of Pretreatment Gland Size in Patients with Secondary Hyperparathyroidism. *Clinial Journal of the American Society of Nephrology* 5:2305–2314, 2010. doi:{10.2215/CJN.02110310}.

125. **Krapf R, Glatz M, Hulter H**. Neutral phosphate administration generates and maintains renal metabolic alkalosis and hyperparathyroidism. *American Journal of Physiology - Renal Physiology* 268:F802–F807, 1995.

126. **Kroll M**. Parathyroid hormone temporal effects on bone formation and resorption. *Bulletin of Mathematical Biology* 62:163–188, 2000. doi:{10.1006/bulm.1999.0146}.

127. **Kumar G, Sproul C, Poppe L, Turner S, Gohdes M, Ghoborah H, Padhi D, Roskos L**. Metabolism and disposition of calcimimetic agent cinacalcet HCL in humans and animal models. *Drug Metabolism and Disposition* 32:1491–1500, 2004. doi:{10.1124/dmd.104.000604}.

128. **Laursen SH, Vestergaard P, Hejlesen OK**. Phosphate Kinetic Models in Hemodialysis: A Systematic Review. *American Journal of Kidney Diseases* 71:75–90, 2018. doi:{10.1053/j.ajkd.2017.07.016}.

129. **Leach K, Gregory KJ, Kufareva I, Khajehali E, Cook AE, Abagyan R, Conigrave AD, Sexton PM, Christopoulos A**. Towards a structural understanding of allosteric drugs at the human calcium-sensing receptor. *Cell Research* 26:574–592, 2016. doi:{10.1038/cr.2016.36}.

130. **Leach K, Loiacono RE, Felder CC, McKinzie DL, Mogg A, Shaw DB, Sexton PM, Christopoulos A**. Molecular Mechanisms of Action and In Vivo Validation of an M-4 Muscarinic Acetylcholine Receptor Allosteric Modulator with Potential Antipsychotic Properties. *Neuropsychopharmacology* 35:855–869, 2010. doi:{10.1038/npp.2009.194}.

131. **Leach K, Sexton PM, Christopoulos A**. Allosteric GPCR modulators: taking advantage of permissive receptor pharmacology. *Trends in Pharmacological Sciences* 28:382–389, 2007. doi:{10.1016/j.tips.2007.06.004}.

132. **LeGeros R**. Formation and transformation of calcium phosphates: Relevance to vascular calcification. *Zeitschrift fuer Kardiologie* 90:116–124, 2001.

133. **Lemaire V, Tobin F, Greller L, Cho C, Suva L**. Modeling the interactions between osteoblast and osteoclast activities in bone remodeling. *Journal of Theoretical Biology* 229:293–309, 2004. doi:{10.1016/j.jtbi.2004.03.023}.

134. **Lemoine S, Fournier T, Kocevar G, Belloi A, Normand G, Ibarrola D, Sappey-Marinier D, Juillard L**. Intracellular Phosphate Dynamics in Muscle Measured by Magnetic Resonance Spectroscopy during Hemodialysis. *Journal of the American Society of Nephrology* 27:2062–2068, 2016. doi:{10.1681/ASN.2015050546}.

135. **Levey A, Eckardt K, Tsukamoto Y, Levin A, Coresh J, Rossert J, de Zeeuw D, Hostetter T, Lameire N, Eknoyan G**. Definition and classification of chronic kidney disease: A position statement from Kidney Disease: Improving Global Outcomes (KDIGO). *Kidney International* 67:2089–2100, 2005. doi:{10.1111/j.1523-1755.2005.00365.x}.

136. **Levin A, Bakris GL, Molitch M, Smulders M, Tian J, Williams LA, Andress DL**. Prevalence of abnormal serum vitamin D, PTH, calcium, and phosphorus in patients with chronic kidney disease: Results of the study to evaluate early kidney disease. *Kidney International* 71:31–38, 2007. doi:{10.1038/sj.ki.5002009}.

137. **Lin J, Curhan GC**. Associations of Sugar and Artificially Sweetened Soda with Albuminuria and Kidney Function Decline in Women. *Clinical Journal of the American Society of Nephrology* 6:160–166, 2011. doi:{10.2215/CJN.03260410}.

138. **Lin J, Hu FB, Curhan GC**. Associations of Diet with Albuminuria and Kidney Function Decline. *Clinical Journal of the American Society of Nephrology* 5:836–843, 2010. doi:{10.2215/CJN.08001109}.

139. **Lips P**. Vitamin D physiology. *Progress in Biophysics & Molecular Biology* 92:4–8, 2006. doi:{10.1016/j.pbiomolbio.2006.02.016}. Workshop of the International-Commission-on-Non-Ionizing Radiation-Protection, Munich, Germany, Oct 17-18, 2005.

140. **Liu S, Tang W, Zhou J, Stubbs J, Luo Q, Pi M, Quarles L**. Fibroblast growth factor 23 is a counter-regulatory phosphaturic hormone for vitamin D. *Journal of the American Society of Nephrology* 17:1305–1315, 2006. doi:{10.1681/ASN.2005111185}. 37th Annual Meeting of the American-Society-of-Nephrology, St Louis, MO, Oct 27-Nov 01, 2004.

141. **Lomashvili K, Khawandi W, O'Neill W**. Reduced plasma pyrophosphate levels in hemodialysis patients. *Journal of the American Society of Nephrology* 16:2495–2500, 2005. doi:{10.1681/ASN.2004080694}.

142. **Loupy A, Ramakrishnan SK, Wootla B, Chambrey R, de la Faille R, Bourgeois S, Bruneval P, Mandet C, Christensen EI, Faure H, Cheval L, Laghmani K, Collet C, Eladari D, Dodd RH, Ruat M, Houillier P**. PTH-independent regulation of blood calcium concentration by the calcium-sensing receptor. *Journal of Clinical Investigation* 122:3355–3367, 2012. doi:{10.1172/JCI57407}.

143. **Lu X, Leng Y**. Theoretical analysis of calcium phosphate precipitation in simulated body fluid. *Biomaterials* 26:1097–1108, 2005. doi:{10.1016/j.biomaterials.2004.05.034}.

144. **Ma Y, Cain R, Halladay D, Yang X, Zeng Q, Miles R, Chandrasekhar S, Martin T, Onyia J**. Catabolic effects of continuous human PTH (1-38) in vivo is associated

with sustained stimulation of RANKL and inhibition of osteoprotegerin and gene-associated bone formation. *Endocrinology* 142:4047–4054, 2001. doi:{10.1210/en.142.9.4047}.

145. **Mace ML, Gravesen E, Nordholm A, Olgaard K, Lewin E**. Fibroblast Growth Factor (FGF) 23 Regulates the Plasma Levels of Parathyroid Hormone In Vivo Through the FGF Receptor in Normocalcemia, But Not in Hypocalcemia. *Calcified Tissue International* 102:85–92, 2018. doi:{10.1007/s00223-017-0333-9}.

146. **Maheshwari V, Cherif A, Fuertinger D, Schappacher-Tilp G, Preciado P, Thijssen S, Bushinsky DA, Kotanko P**. An in silico method to predict net calcium transfer during hemodialysis. *Conference proceedings : Annual International Conference of the IEEE Engineering in Medicine and Biology Society IEEE Engineering in Medicine and Biology Society Annual Conference* 2017:2740–2743, 2017. doi:10.1109/EMBC.2017.8037424.

147. **Manghat P, Sodi R, Swaminathan R**. Phosphate homeostasis and disorders. *Annals of Clinical Biochemistry* 51:631–656, 2014. doi:{10.1177/0004563214521399}.

148. **Manolagas S**. Birth and death of bone cells: Basic regulatory mechanisms and implications for the pathogenesis and treatment of osteoporosis. *Endocrine Reviews* 21:115–137, 2000. doi:{10.1210/er.21.2.115}.

149. **Marks J, Srai S, Biber J, Murer H, Unwin R, Debnam E**. Intestinal phosphate absorption and the effect of vitamin D: a comparison of rats with mice. *Experimental Physiology* 91:531–537, 2006. doi:{10.1113/expphysiol.2005.032516}.

150. **Melamed ML, Eustace JA, Plantinga L, Jaar BG, Fink NE, Coresh J, Klag MJ, Powe NR**. Changes in serum calcium, phosphate, and PTH and the risk of death in incident dialysis patients: A longitudinal study. *Kidney International* 70:351–357, 2006. doi:{10.1038/sj.ki.5001542}. 37th Annual Meeting of the American-Society-of-Nephrology, St Louis, MO, OCT 27-NOV 01, 2004.

151. **Meola M, Petrucci I, Barsotti G**. Long-term treatment with cinacalcet and conventional therapy reduces parathyroid hyperplasia in severe secondary hyperparathyroidism. *Nephrology Dialysis Transplantation* 24:982–989, 2009. doi:{10.1093/ndt/gfn654}.

152. **Messam P, Vallone C, Mioni G, Geatti O, Turrin D, Passoni N, Cruciatti A**. Direct in-vivo assessment of parathyroid hormone-calcium relationship curve in

renal patients. *Kidney International* 46:1713–1720, 1994. doi:{10.1038/ki.1994.473}.

153. **Michishita R, Matsuda T, Kawakami S, Tanaka S, Kiyonaga A, Tanaka H, Morito N, Higaki Y**. The association between changes in lifestyle behaviors and the incidence of chronic kidney disease (CKD) in middle-aged and older men. *Journal of Epidemiology* 27:389–397, 2017. doi:{10.1016/j.je.2016.08.013}.

154. **Moe S, Chertow G, Coburn J, Quarles L, Goodman W, Block G, Drueke T, Cunningham J, Sherrard D, McCary L, Olson K, Turner S, Martin K**. Achieving NKF-K/DOQI (TM) bone metabolism and disease treatment goals with cinacalcet HCl. *Kidney International* 67:760–771, 2005. doi:{10.1111/j.1523-1755.2005.67139.x}.

155. **Moe S, Drueke T, Cunningham J, Goodman W, Martin K, Olgaard K, Ott S, Sprague S, Lameire N, Eknoyan G**. Definition, evaluation, and classification of renal osteodystrophy: A position statement from kidney disease: Improving global outcomes (KDIGO). *Kidney International* 69:1945–1953, 2006. doi:{10.1038/sj.ki.5000414}.

156. **Moe SM, Zidehsarai MP, Chambers MA, Jackman LA, Radcliffe JS, Trevino LL, Donahue SE, Asplin JR**. Vegetarian Compared with Meat Dietary Protein Source and Phosphorus Homeostasis in Chronic Kidney Disease. *Clinical Journal of the American Society of Nephrology* 6:257–264, 2011. doi:{10.2215/CJN.05040610}.

157. **Momsen G, Schwarz P**. A mathematical/physiological model of parathyroid hormone secretion in response to blood-ionized calcium lowering in vivo. *Scandinavian Journal of Clinical & Laboratory Investigation* 57:381–394, 1997. doi:{10.3109/00365519709084585}.

158. **Murer H, Hildmann B**. Trans-cellular transport of calcium and inorganic-phosphate in the small intestinal epithelium. *American Journal of Physiology* 240:G409–G416, 1981.

159. **Nagasawa Y, Yamamoto R, Rakugi H, Isaka Y**. Cigarette smoking and chronic kidney diseases. *Hypertension Research* 35:261–265, 2012. doi:{10.1038/hr.2011.205}.

160. **Navehmany T, Rahamimov R, Livni N, Silver J**. Parathyroid cell-proliferation in normal and chronic-renal-failure rats - the effect of calcium phosphate, and

vitamin-D. *Journal of Clinical Investigation* 96:1786–1793, 1995. doi:{10.1172/JCI118224}.

161. **Neale S, Smith R, Wass J, Athanasou N**. Osteoclast differentiation from circulating mononuclear precursors in Paget's disease is hypersensitive to 1,25-dihydroxyvitamin D-3 and RANKL. *Bone* 27:409–416, 2000. doi:{10.1016/S8756-3282(00)00345-8}.

162. **Nelp W, Murano R, Williams J, Rudd T, Hinn G, Denney J, Palmer H**. Absolute measurement of total-bod calcium (bone mass) in vivo. *Journal of Laboratory and Clinical Medicine* 79:430–&, 1972.

163. **Nelson CA, Warren JT, Wang MWH, Teitelbaum SL, Fremont DH**. RANKL Employs Distinct Binding Modes to Engage RANK and the Osteoprotegerin Decoy Receptor. *Structure* 20:1971–1982, 2012. doi:{10.1016/j.str.2012.08.030}.

164. **Nesbit MA, Hannan FM, Howles SA, Babinsky VN, Head RA, Cranston T, Rust N, Hobbs MR, Heath H III, Thakker RV**. Mutations Affecting G-Protein Subunit alpha(11) in Hypercalcemia and Hypocalcemia. *New England Journal of Medicine* 368:2476–2486, 2013. doi:{10.1056/NEJMoa1300253}.

165. **Neuman W, Neuman M**. *The chemical dynamics of bone mineral*. University of Chicago Press, 1958.

166. **Nordin B, Peacock M**. Role of kindey in regulation of plasma-calcium. *Lancet* 2:1280–&, 1969.

167. **P BJ**. Primary Hyperparathyroidism. *The Journal of Clinical Endocrinology and Metabolism* 103:3993–4004, 2018. doi:{10.1210/jc.2018-01225}.

168. **Padhi D, Harris R**. Clinical Pharmacokinetic and Pharmacodynamic Profile of Cinacalcet Hydrochloride. *Clinical Pharmacokinetics* 48:303–311, 2009.

169. **Padhi D, Harris RZ, Salfi M, Noveck RJ, Sullivan JT**. Pharmacokinetics and pharmacodynamics of cinacalcet in hepatic impairment - Phase I, open-label, parallel-group, single-dose, single-centre study. *Clinical Drug Investigation* 28:635–643, 2008. doi:{10.2165/00044011-200828100-00004}.

170. **Padhi D, Salfi M, Harris R**. The pharmacokinetics of cinacalcet are unaffected following consumption of high- and low-fat meals. *American Journal of Therapeutics* 14:235–240, 2007. doi:{10.1097/01.mjt.0000212703.71625.26}.

171. **Palmer SC, Hayen A, Macaskill P, Pellegrini F, Craig JC, Elder GJ, Strippoli GFM**. Serum Levels of Phosphorus, Parathyroid Hormone, and Calcium and Risks of Death and Cardiovascular Disease in Individuals With Chronic Kidney Disease A Systematic Review and Meta-analysis. *JAMA-Journal of the American Medical Association* 305:1119–1127, 2011. doi:{10.1001/jama.2011.308}.

172. **Pasquali M, Tartaglione L, Rotondi S, Muci ML, Mandanici G, Farcomeni A, Marangella M, Mazzaferro S**. Calcitriol/calcifediol ratio: An indicator of vitamin D hydroxylation efficiency? *BBA Clinical* 3:251–256, 2015. doi:{10.1016/j.bbacli.2015.03.004}.

173. **Peacock M**. Calcium Metabolism in Health and Disease. *Clinical Journal of the American Society of Nephrology* 5:S23–S30, 2010. doi:{10.2215/CJN.05910809}.

174. **Peterson MC, Riggs MM**. A physiologically based mathematical model of integrated calcium homeostasis and bone remodeling. *Bone* 46:49–63, 2010. doi:{10.1016/j.bone.2009.08.053}.

175. **Pirklbauer M, Mayer G**. The exchangeable calcium pool: physiology and pathophysiology in chronic kidney disease. *Nephrology Dialysis Transplantation* 26:2438–2444, 2011. doi:{10.1093/ndt/gfr207}.

176. **Pocotte S, Ehrenstein G, Fitzpatrick L**. Regulation of parathyroid-hormone secretion. *Endocrine Reviews* 12:291–301, 1991.

177. **Quarles LD**. Skeletal secretion of FGF-23 regulates phosphate and vitamin D metabolism. *Nature Reviews Endocrinology* 8:276–286, 2012. doi:{10.1038/nrendo.2011.218}.

178. **Quinn J, Itoh K, Udagawa N, Hausler K, Yasuda H, Shima N, Mizuno A, Higashio K, Takahashi N, Suda T, Martin T, Gillespie M**. Transforming growth factor beta affects osteoclast differentiation via direct and indirect actions. *Journal of Bone and Mineral Research* 16:1787–1794, 2001. doi:{10.1359/jbmr.2001.16.10.1787}.

179. **Raggi P, Boulay A, Chasan-Taber S, Amin N, Dillon M, Burke S, Chertow G**. Cardiac calcification in adult Hemodialysis patients - A link between end-stage renal disease and cardiovascular disease? *Journal of the American College of Cardiology* 39:695–701, 2002. doi:{10.1016/S0735-1097(01)01781-8}.

180. **Ramirez J, Emmett M, White M, Fathi N, Ana C, Morawski S, Fordtran J**. The absorption of dietary phosphorus and calcium in hemodialysis-patients. *Kidney International* 30:753–759, 1986. doi:{10.1038/ki.1986.252}.

181. **Raposo J, Sobrinho L, Ferreira H**. A minimal mathematical model of calcium homeostasis. *Journal of Clinical Endocrinology & Metabolism* 87:4330–4340, 2002. doi:{10.1210/jc.2002-011870}.

182. **Raposo JF, Pires A, Yokota H, Ferreira HG**. A mathematical model of calcium and phosphorus metabolism in two forms of hyperparathyroidism. *Endocrine* 41:309–319, 2012. doi:{10.1007/s12020-011-9521-y}.

183. **Renkema KY, Alexander RT, Bindels RJ, Hoenderop JG**. Calcium and phosphate homeostasis: Concerted interplay of new regulators. *Annals of Medicine* 40:82–91, 2008. doi:{10.1080/07853890701689645}.

184. **Ribba B, Watkin E, Tod M, Girard P, Grenier E, You B, Giraudo E, Freyer G**. A model of vascular tumour growth in mice combining longitudinal tumour size data with histological biomarkers. *European Journal of Cancer* 47:479–490, 2011. doi:{10.1016/j.ejca.2010.10.003}.

185. **Riccobene T, Omann G, Linderman J**. Modeling activation and desensitization of G-protein coupled receptors - Provides insight into ligand efficacy. *Journal of Theoretical Biology* 200:207–222, 1999. doi:{10.1006/jtbi.1999.0988}.

186. **Roche D, Gil D, Giraldo J**. Mechanistic analysis of the function of agonists and allosteric modulators: reconciling two-state and operational models. *British Journal of Pharmacology* 169:1189–1202, 2013. doi:{10.1111/bph.12231}.

187. **Rodriguez ME, Almaden Y, Canadillas S, Canalejo A, Siendones E, Lopez I, Aguilera-Tejero E, Martin D, Rodriguez M**. The calcimimetic R-568 increases vitamin D receptor expression in rat parathyroid glands. *American Journal of Physiology-Renal Physiology* 292:F1390–F1395, 2007. doi:{10.1152/ajprenal.00262.2006}. National Congress of the Spanish-Society-of-Nephrology, Tenerife, SPAIN, 2004.

188. **Rutherford W, Bordier P, Marie P, Hruska K, Harter H, Greenwalt A, Blondin J, Haddad J, Bricker N, Slatopolsky E**. Phosphate control and 25-Hydroxycholecalciferol administration in preventing experimental renal osteodystrophy in dog. *Journal of Clinical Investigation* 60:332–341, 1977. doi:{10.1172/JCI108781}.

189. **Sabbagh Y, Giral H, Caldas Y, Levi M, Schiavi SC**. Intestinal Phosphate Transport. *Advances in Chronic Kidney Disease* 18:85–90, 2011. doi:{10.1053/j.ackd.2010.11.004}.

190. **Sarnak M, Levey A, Schoolwerth A, Coresh J, Culleton B, Hamm L, McCullough P, Kasiske B, Kelepouris E, Klag M, Parfrey P, Pfeffer M, Raij L, Spinosa D, Wilson P**. Kidney disease as a risk factor for development of cardiovascular disease - A statement from the American Heart Association councils on kidney in cardiovascular disease, high blood pressure research, clinical cardiology, and epidemiology and prevention. *Circulation* 108:2154–2169, 2003. doi:{10.1161/01.CIR.0000095676.90936.80}.

191. **SB B, LI W**. The essentials of calcium, magnesium and phosphate metabolism: part I. Physiology. *Critical Care Resuscitation* 4:301–306, 2002.

192. **Schappacher-Tilp G, Cherif A, Fuertinger DH, Bushinsky D, Kotanko P**. A mathematical model of parathyroid gland biology. *Physiological Reports* 7, 2019. doi:{10.14814/phy2.14045}.

193. **Schappacher-Tilp G, Fuertinger D, Kotanko P**. A Multi-Compartment Model Capturing the Pharmacokinetics of the Calcimimetic Cinacalcet. *Cellular Physiology and Biochemistry* 53:429–438, 2019. doi:{10.33594/000000148}.

194. **Schmitt C, Schaefer F**. Calcium sensitivity of the parathyroid in renal failure: another look with new methodology. *Nephrology Dialysis Transplantation* 14:2815–2818, 1999. doi:{10.1093/ndt/14.12.2815}.

195. **Schmitt C, Schaefer F, Bruch A, Veldhuis J, SchmidtGayk H, Stein G, Ritz E, Mehls O**. Control of pulsatile and tonic parathyroid hormone secretion by ionized calcium. *Journal of Clinical Endocrinology & Metabolism* 81:4236–4243, 1996. doi:{10.1210/jc.81.12.4236}.

196. **Schwarz P, Madsen J, Rasmussen A, Transbol I, Brown E**. Evidence for a role of intracellular stored parathyroid hormone in producing hysteresis of the PTH-calcium relationship in normal humans. *Clinical Endocrinology* 48:725–732, 1998. doi:{10.1046/j.1365-2265.1998.00414.x}.

197. **Schwarz P, Sorensen H, McNair P, Transbol I**. Cica-clamp technique - a method for quantifying parathyroid-hormone secreation - a sequential critrate and calcium clamp study. *European Journal of Clinical Investigation* 23:546–553, 1993. doi:{10.1111/j.1365-2362.1993.tb00964.x}.

198. **Shea L, Linderman J**. Mechanistic model of G-protein signal transduction - Determinants of efficacy and effect of precoupled receptors. *Biochemical Pharmacology* 53:519–530, 1997. doi:{10.1016/S0006-2952(96)00768-X}.

199. **Sheikh M, Ramirez A, Emmett M, Ana C, Schiller L, Frdtran J**. Role of vitamin-D-dependent and vitamin-D-independent mechanisms in absorption of food calcium. *Journal of Clinical Investigation* 81:126–132, 1988.

200. **Shimada T, Hasegawa H, Yamazaki Y, Muto T, Hino R, Takeuchi Y, Fujita T, Nakahara K, Fukumoto S, Yamashita T**. FGF-23 is a potent regulator of vitamin D metabolism and phosphate homeostasis. *Journal of Bone and Mineral Research* 19:429–435, 2004. doi:{10.1359/JBMR.0301264}.

201. **Shimada T, Mizutani S, Muto T, Yoneya T, Hino R, Takeda S, Takeuchi Y, Fujita T, Fukumoto S, Yamashita T**. Cloning and characterization of FGF23 as a causative factor of tumor-induced osteomalacia. *Proceedings of the National Academy of Sciences of the United States of Amercia* 98:6500–6505, 2001. doi:{10.1073/pnas.101545198}.

202. **Shoback D**. Hypoparathyroidism. *New England Journal of Medicine* 359:391–403, 2008. doi:{10.1056/NEJMcp0803050}.

203. **Shrestha RP, Hollot CV, Chipkin SR, Schmitt CP, Chait Y**. A mathematical model of parathyroid hormone response to acute changes in plasma ionized calcium concentration in humans. *Mathematical Biosciences* 226:46–57, 2010. doi:{10.1016/j.mbs.2010.04.001}.

204. **Shuvy M, Abedat S, Eliaz R, Abu-Rmeileh I, Abu-Snieneh A, Ben-Dov IZ, Meir K, Pereg D, Beeri R, Lotan C**. Hyperphosphatemia is required for initiation but not propagation of kidney failure-induced calcific aortic valve disease. *American Journal of Physiology - Heart and Circulatory Physiolgy* 317:H695–H704, 2019. doi:{10.1152/ajpheart.00765.2018}.

205. **Siddiqui JA, Partridge NC**. Physiological Bone Remodeling: Systemic Regulation and Growth Factor Involvement. *Physiology* 31:233–245, 2016. doi:{10.1152/physiol.00061.2014}.

206. **Silver J, Naveh-Many T**. Phosphate and the parathyroid. *Kidney International* 75:898–905, 2009. doi:{10.1038/ki.2008.642}.

207. **Silverberg S, Shane E, Jacobs T, Siris E, Bilezikian J**. A 10-year prospective study of primary hyperparathyroidism with or without parathyroid surgery. *New England Journal of Medicine* 341:1249–1255, 1999. doi:{10.1056/NEJM199910213411701}.

208. **Slatopolsky E, Dusso A, Brown A**. The role of phosphorus in the of secondary hyperparathyroidism and parathyroid cell proliferation in chronic renal failure. *American Journal of the Medical Sciences* 317:370–376, 1999. doi:{10.1097/00000441-199906000-00004}.

209. **Slatopolsky E, Finch J, Denda M, Ritter C, Zhong M, Dusso A, MacDonald P, Brown A**. Phosphorus restriction prevents parathyroid gland growth - High phosphorus directly stimulates PTH secretion in vitro. *Journal of Clinical Investigation* 97:2534–2540, 1996. doi:{10.1172/JCI118701}.

210. **Smith ER, Cai MM, McMahon LP, Pedagogos E, Toussaint ND, Brumby C, Holt SG**. Serum fetuin-A concentration and fetuin-A-containing calciprotein particles in patients with chronic inflammatory disease and renal failure. *Nephrology* 18:215–221, 2013. doi:{10.1111/nep.12021}.

211. **Spalding E, Chamney P, Farrington K**. Phosphate kinetics during hemodialysis: Evidence for biphasic regulation. *Kidney International* 61:655–667, 2002. doi:{10.1046/j.1523-1755.2002.00146.x}. Autumn Meeting of the Renal-Association, Cambridge, England, Sep, 2000.

212. **Suda T, Takahashi N, Udagawa N, Jimi E, Gillespie M, Martin T**. Modulation of osteoclast differentiation and function by the new members of the tumor necrosis factor receptor and ligand families. *Endocrine Reviews* 20:345–357, 1999. doi:{10.1210/er.20.3.345}.

213. **Sugisaki H, Onohara M, Kunitomo T**. Phosphate in dialysis patients. *Transactions American Society for Artificial Internal Organs* 29:38–43, 1983.

214. **Suh JM, Cronan JJ, Monchik JM**. Primary hyperparathyroidism: Is there an increased prevalence of renal stone disease? *American Journal of Roentgenology* 191:908–911, 2008. doi:{10.2214/AJR.07.3160}.

215. **Theoleyre S, Wittrant Y, Tat S, Fortun Y, Redini F, Heymann D**. The molecular triad OPG/RANK/RANKL: involvement in the orchestration of pathophysiological bone remodeling. *Cytokine & Growth Factor Reviews* 15:457–475, 2004. doi:{10.1016/j.cytogfr.2004.06.004}.

216. **Thomas L, Bettoni C, Knopfel T, Hernando N, Biber J, Wagner CA**. Acute Adaption to Oral or Intravenous Phosphate Requires Parathyroid Hormone. *Journal of the American Society of Nephrology* 28:903–914, 2017. doi:{10.1681/ASN.2016010082}.

217. **Tokumoto M, Taniguchi M, Matsuo D, Tsuruya K, Hirakata H, Iida M**. Parathyroid cell growth in patients with advanced secondary hyperparathyroidism: Vitamin D receptor, calcium sensing receptor, and cell cycle regulating factors. *Therapeutic Apheresis and Dialysis* 9:S27–S34, 2005. doi:{10.1111/j.1744-9987.2005.00302.x}. 16th Meeting of the Japanese-Society-for-Kidney-Disease-and-Vitamin-D-Therapy, Tokyo, Japan, Feb 26, 2005.

218. **Tonelli M, Wiebe N, Culleton B, House A, Rabbat C, Fok M, McAlister F, Garg AX**. Chronic kidney disease and mortality risk: A systematic review. *Journal of the American Society of Nephrology* 17:2034–2047, 2006. doi:{10.1681/ASN.2005101085}.

219. **Turner M, Lansing A, Jeronimo P, Lee L, Svajger B, Zelt J, Forster C, Petkovich M, Holden R, MA A**. Vascular calcification has a role in acute non-renal phosphate clearance. doi:{https://doi.org/10.1101/2020.07.29.225532}.

220. **Vervloet MC, Sezer S, Massy ZA, Johansson L, Cozzolino M, Fouque D, Kidney EEWGC, Grp ERNW**. The role of phosphate in kidney disease. *Nature Reviews Nephrology* 13:27–38, 2017. doi:{10.1038/nrneph.2016.164}.

221. **Wada T, Nakashima T, Hiroshi N, Penninger J**. RANKL-RANK signaling in osteoclastogenesis and bone disease. *Trend in Molecular Medicine* 12:17–25, 2006. doi:{10.1016/j.molmed.2005.11.007}.

222. **Walling M**. Intestinal calcium and phosphate transport - differential responses to vitamin-D3 metabolites. *American Journal of Physiology* 233:E488–E494, 1977.

223. **Wang A, Qigley G, Kolpak F, Vandermarel G, Vanboom J, Rich A**. Left-handed double helical DNA-variations in the backbone conformation. *Science* 211:171–176, 1981. doi:{10.1126/science.7444458}.

224. **Wang Q, Palnitkar S, Parfitt A**. The basal rate of cell proliferation in normal human parathyroid tissue: Implications for the pathogenesis of hyperparathyroidism. *Clinical Endocrinology* 46:343–349, 1997. doi:{10.1046/j.1365-2265.1997.1420959.x}.

225. **Wysokinski D, Pawlowska E, Blasiak J**. RUNX2: A master bone growth regulator that may be involved in the DNA damage response. *DNA and Cell Biology* 34:305–315, 2015. doi:{10.1089/dna.2014.2688}.

226. **Yamada S, Tokumoto M, Tatsumoto N, Taniguchi M, Noguchi H, Nakano T, Masutani K, Ooboshi H, Tsuruya K, Kitazono T**. Phosphate overload directly induces systemic inflammation and malnutrition as well as vascular calcification in uremia. *American Journal of Physiology - Renal Physiology* 306:F1418–F1428, 2014. doi:{10.1152/ajprenal.00633.2013}.

227. **Yasuda H, Shima N, Nakagawa N, Yamaguchi K, Kinosaki M, Mochizuki S, Tomoyasu A, Yano K, Goto M, Murakami A, Tsuda E, Morinaga T, Higashio K, Udagawa N, Takahashi N, Suda T**. Osteoclast differentiation factor is a ligand for osteoprotegerin osteoclastogenesis-inhibitory factor and is identical to TRANCE/RANKL. *Proceedings of the National Academy of Sciences of the United States of America* 95:3597–3602, 1998. doi:{10.1073/pnas.95.7.3597}.

228. **Yergey A, Abrams S, Vieira N, Aldroubi A, Marini J, Sidbury J**. Determination of fractional absorption of dietary calcium in humans. *Journal of Nutrition* 124:674–682, 1994.

Appendix

SENSITIVITY GRAPHS FOR INTRACELLULAR-EXTRACELLULAR PHOSPHATE

The corresponding parameters are either multiplied by 2 or 0.5. Here, we were interested in the effect of changes in the parameters on the long-term predictions. We simulate the loss of kidney function and hemodialysis as soon as the GFR is below 5% of the healthy GFR.

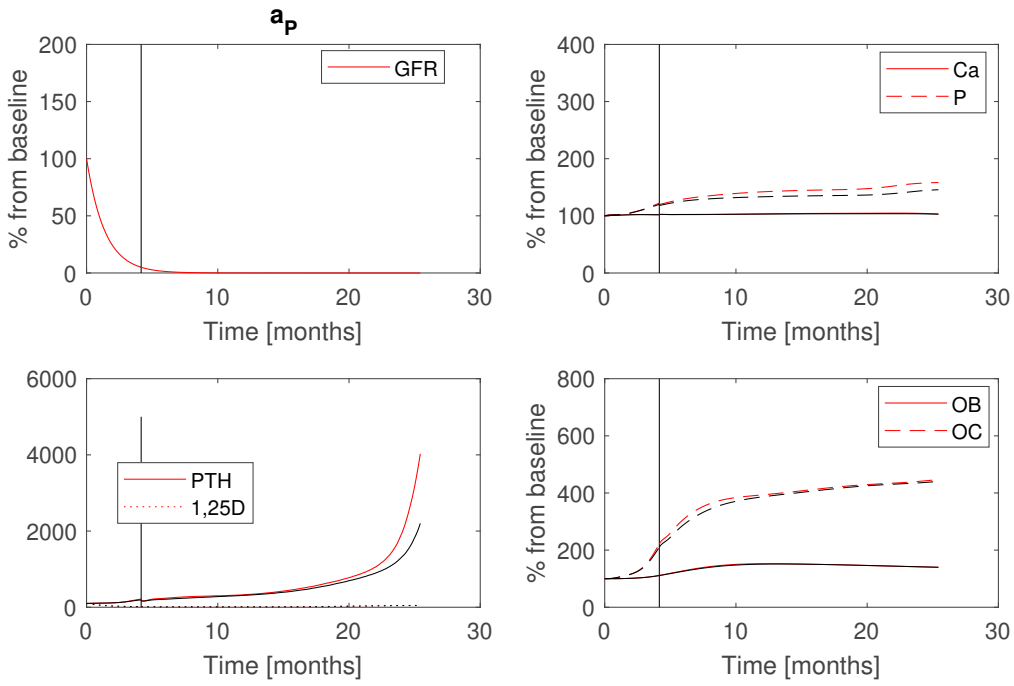

Figure 6.1 Red lines: Parameter a_P is multiplied by 0.5, black lines: standard parameters.

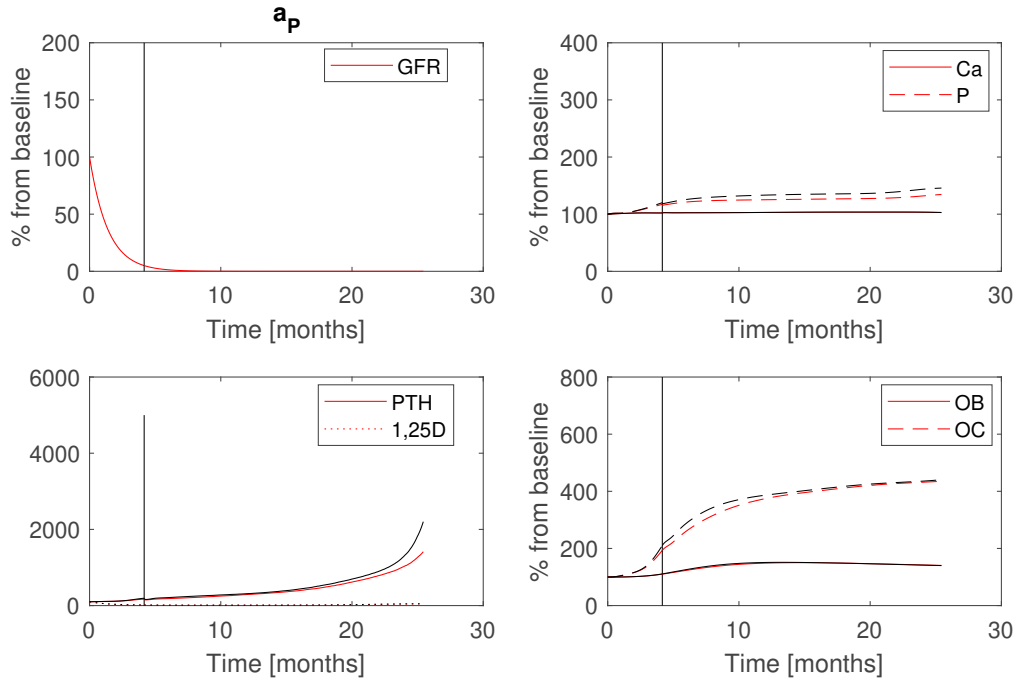

Figure 6.2 Red lines: Parameter a_P is multiplied by 2, black lines: standard parameters.

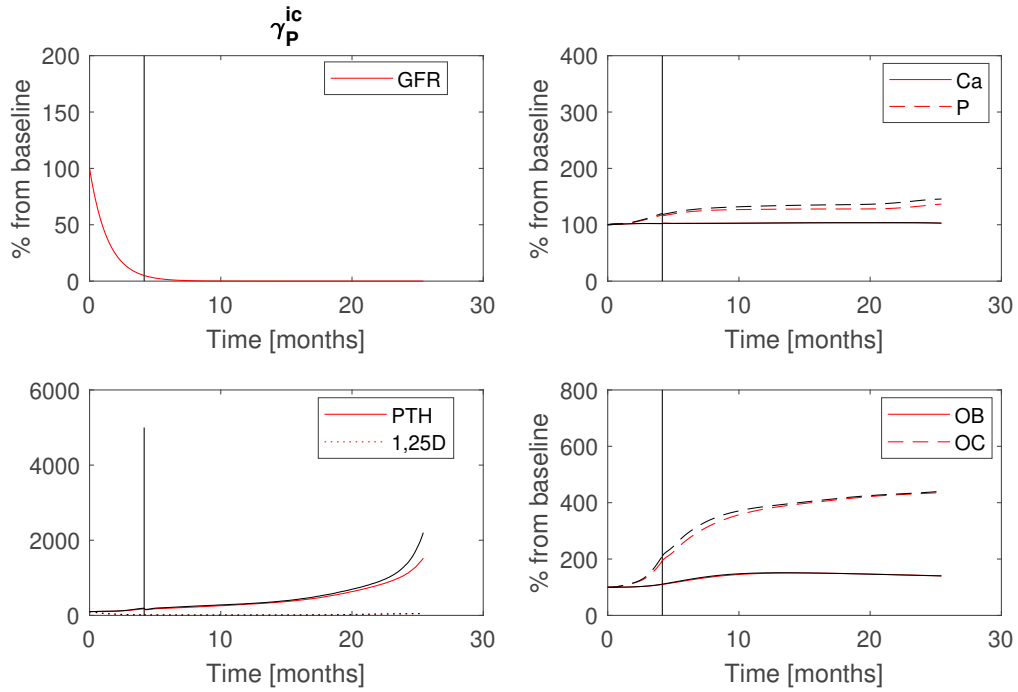

Figure 6.3 Red lines: Parameter γ_P^{ic} is multiplied by 0.5, black lines: standard parameters.

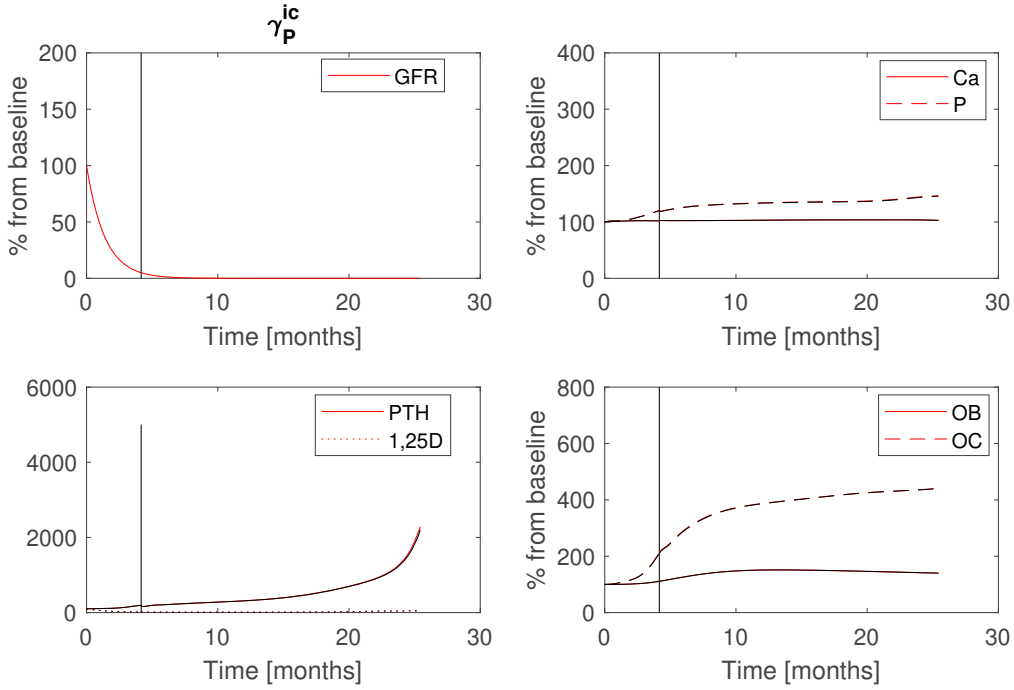

Figure 6.4 Red lines: Parameter γ_P^{ic} is multiplied by 2, black lines: standard parameters.

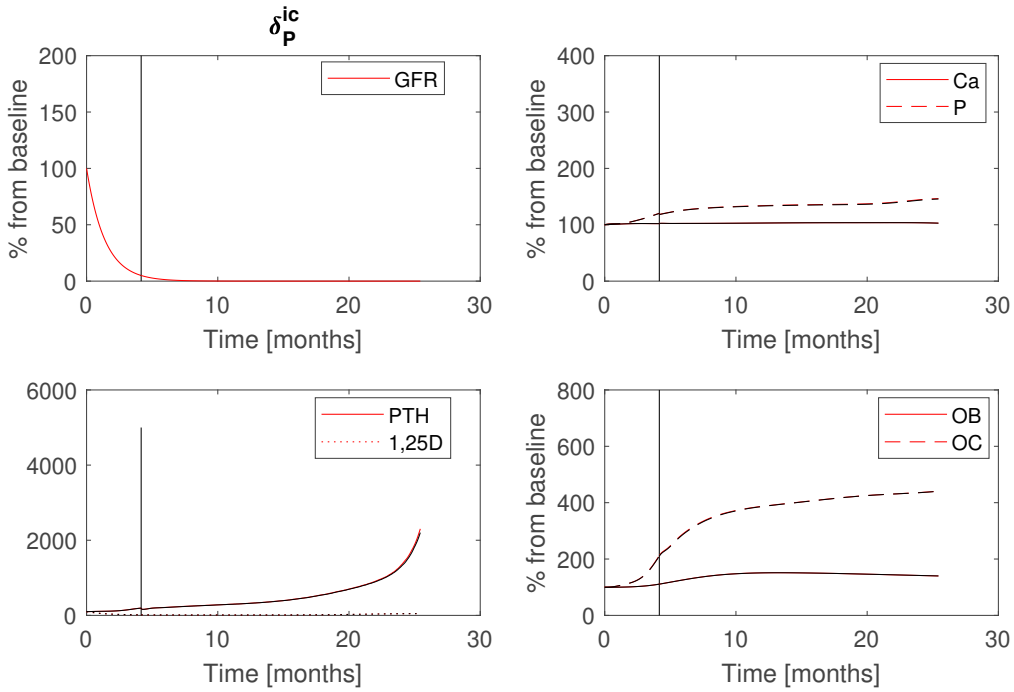

Figure 6.5 Red lines: Parameter δ_P^{ic} is multiplied by 0.5, black lines: standard parameters.

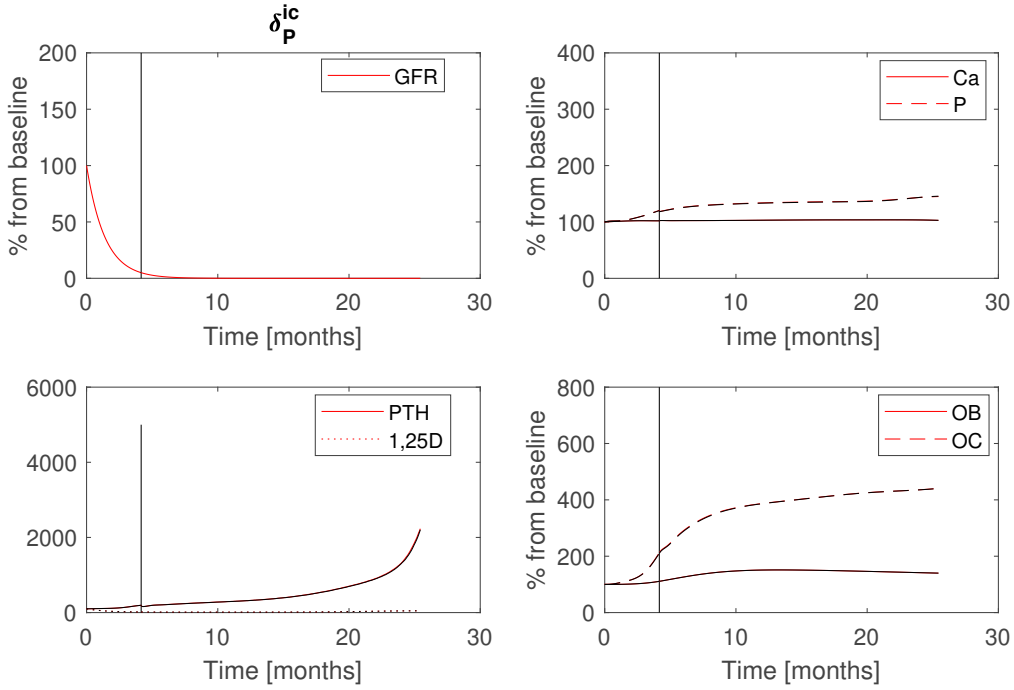

Figure 6.6 Red lines: Parameter δ_P^{ic} is multiplied by 2, black lines: standard parameters.

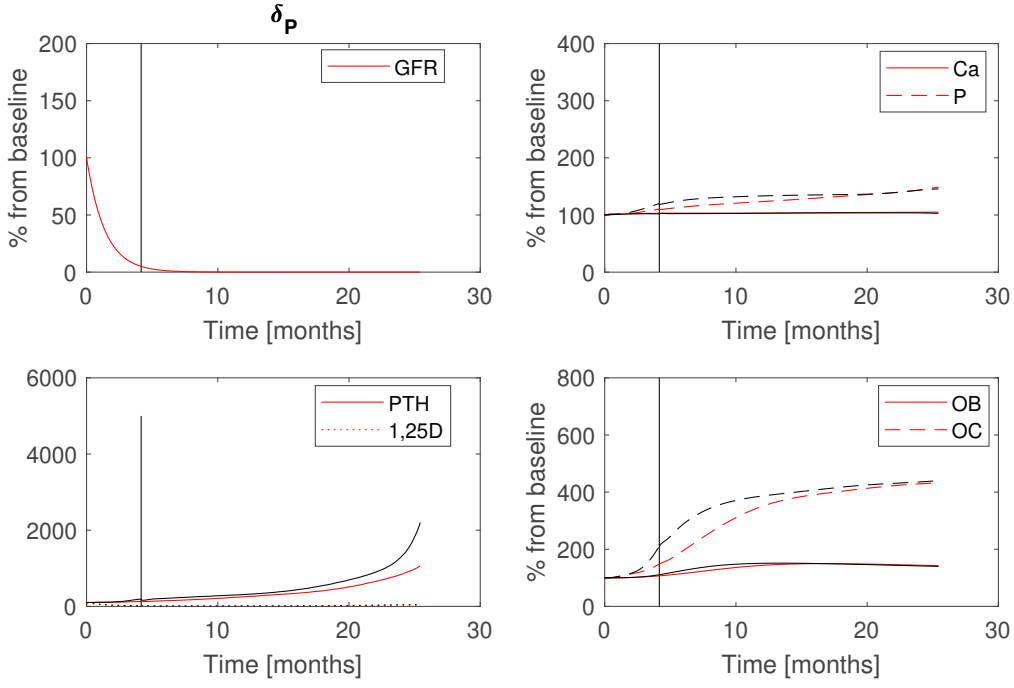

Figure 6.7 Red lines: Parameter δ_P is multiplied by 0.5, black lines: standard parameters. δ_P is the only parameter able to regulate the slope of the rise of phosphate over time.

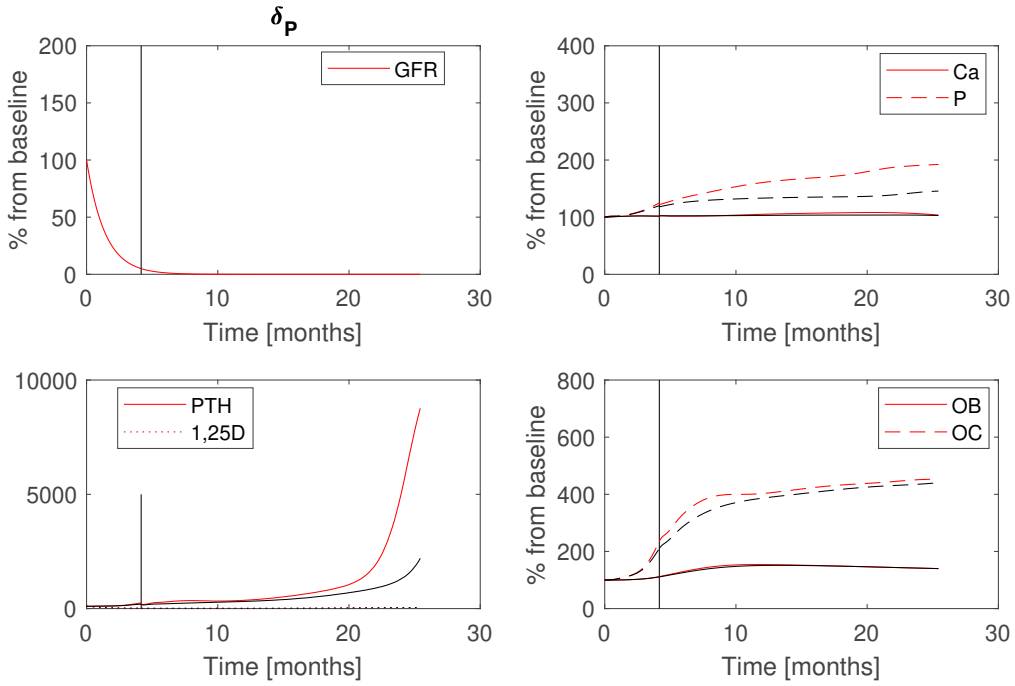

Figure 6.8 Red lines: Parameter δ_P is multiplied by 2, black lines: standard parameters. δ_P is the only parameter able to strongly regulate the slope of the rise of phosphate over time.

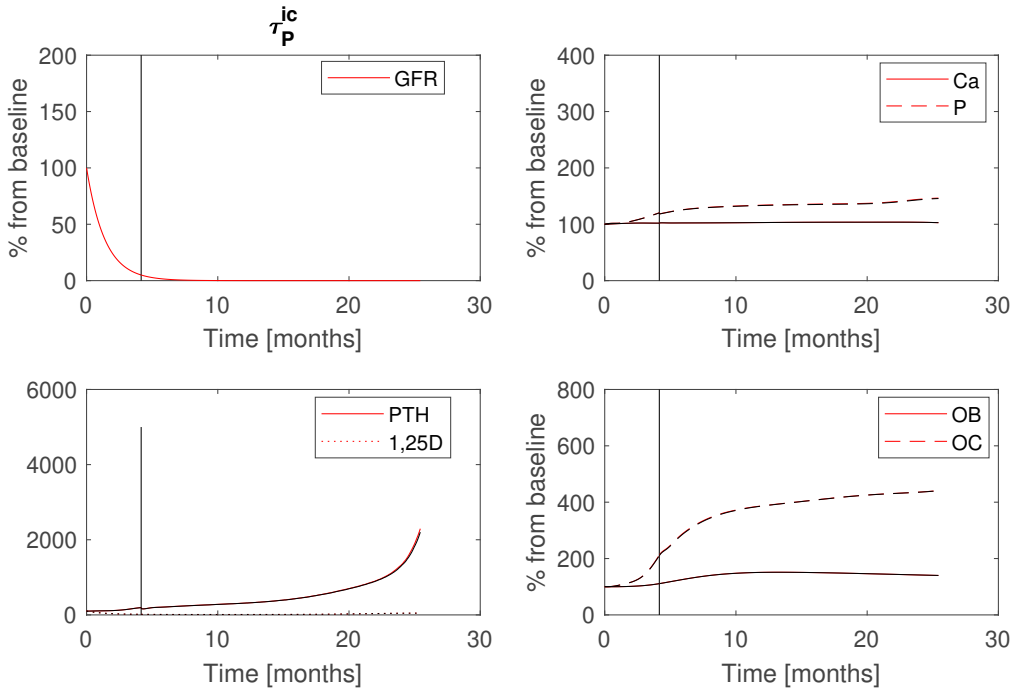

Figure 6.9 Red lines: Parameter τ_P^{ic} is multiplied by 0.5, black lines: standard parameters.

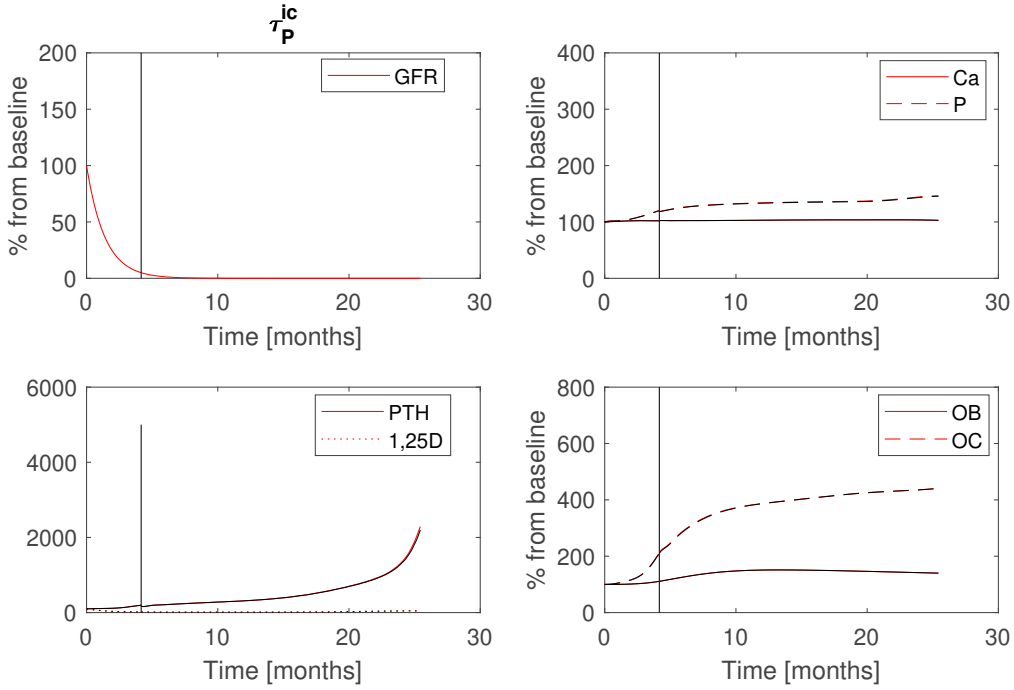

Figure 6.10 Red lines: Parameter τ_P^{ic} is multiplied by 2, black lines: standard parameters.

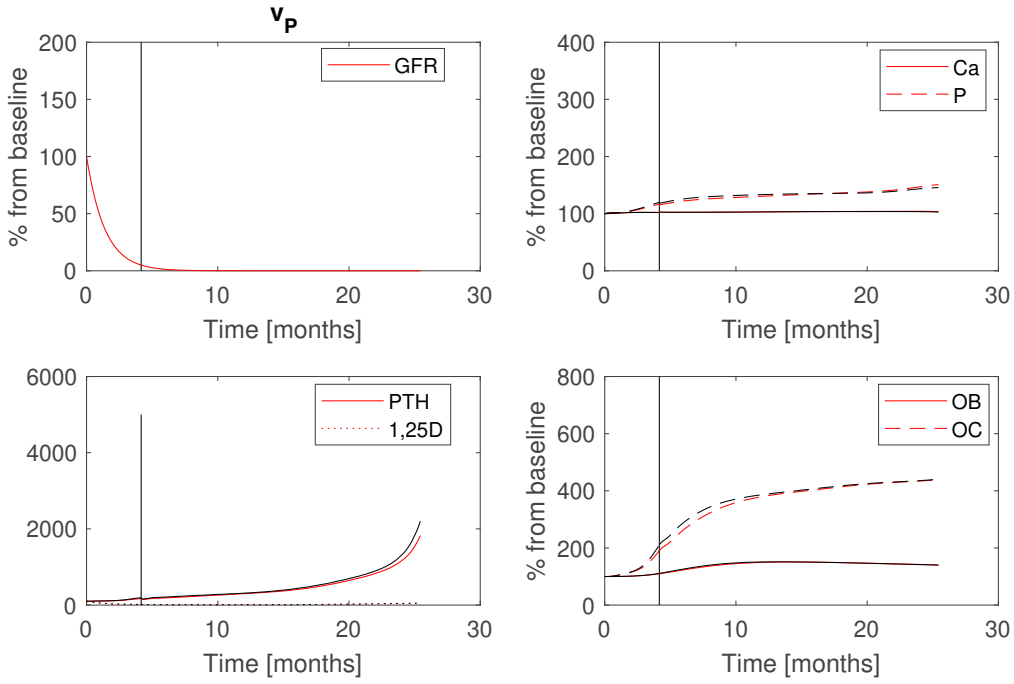

Figure 6.11 Red lines: Parameter v_P is multiplied by 0.5, black lines: standard parameters.

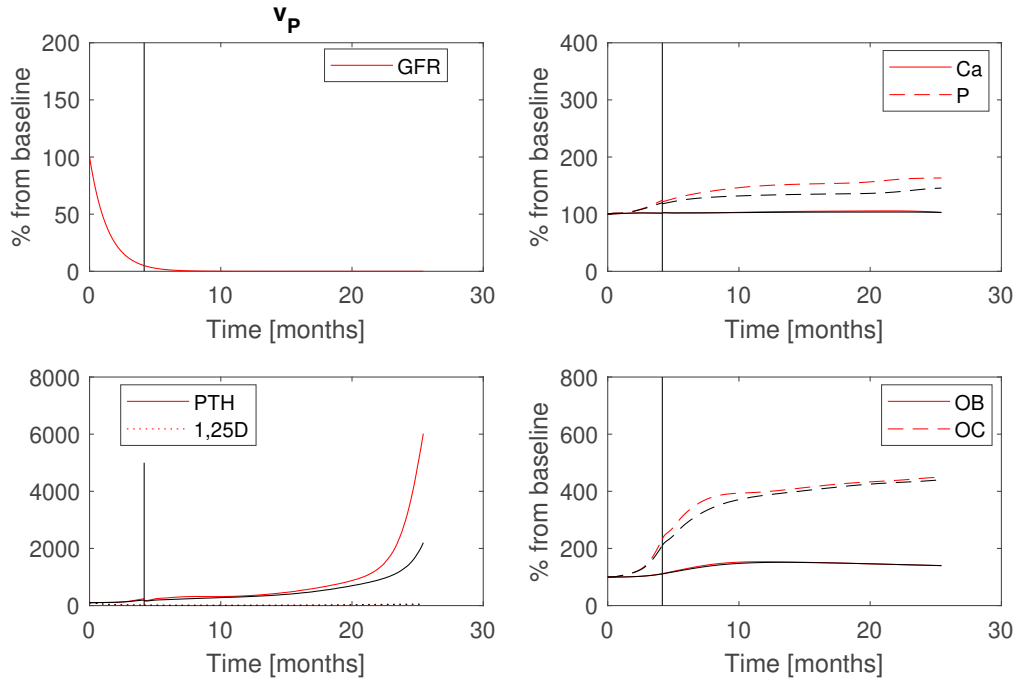

Figure 6.12 Red lines: Parameter v_P is multiplied by 2, black lines: standard parameters.

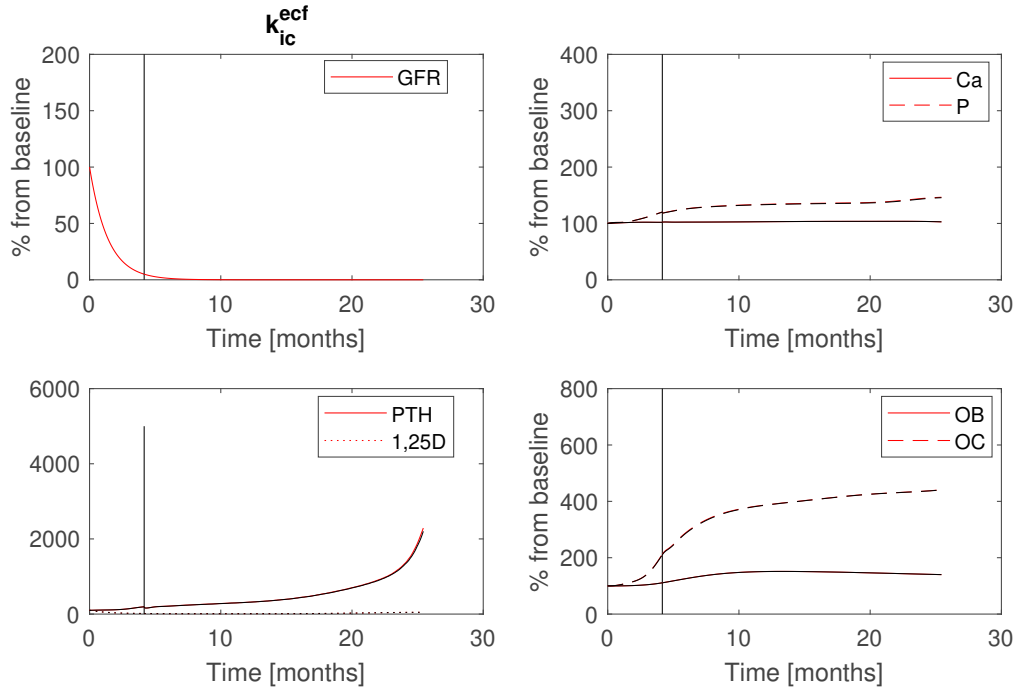

Figure 6.13 Red lines: Parameter k_{ic}^{ecf} is multiplied by 0.5, black lines: standard parameters.

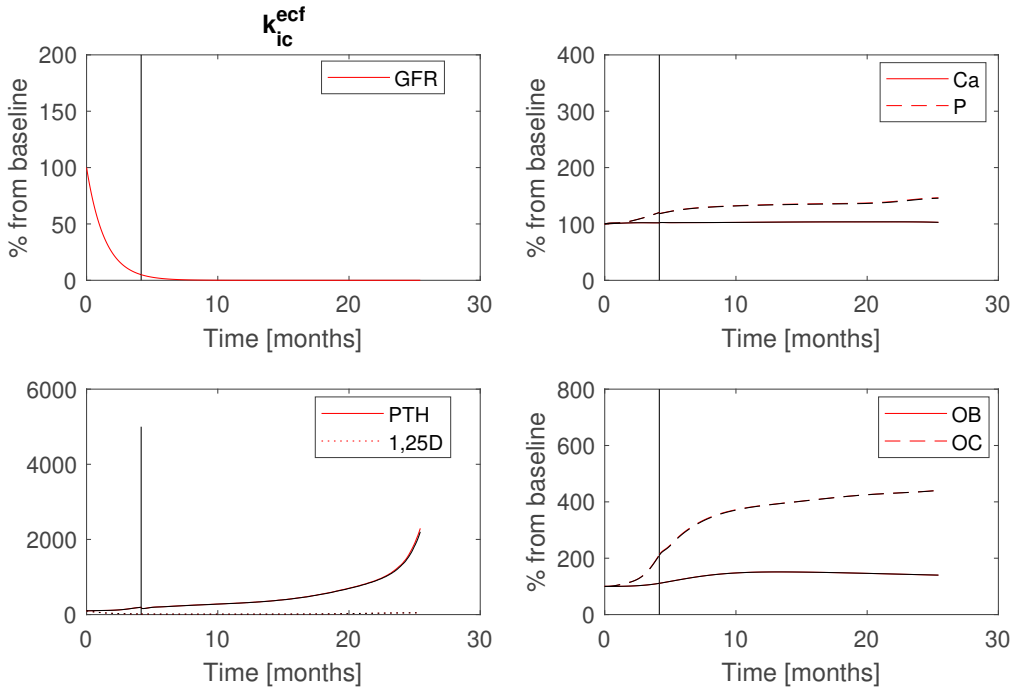

Figure 6.14 Red lines: Parameter k_{ic}^{ecf} is multiplied by 2, black lines: standard parameters.

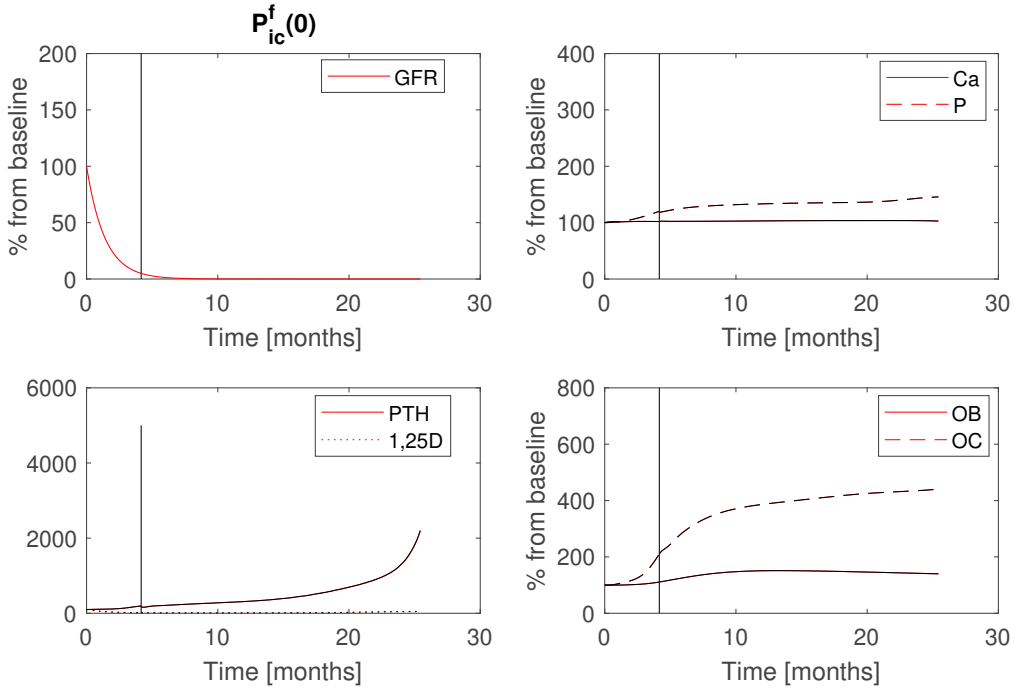

Figure 6.15 Red lines: Parameter $P_{ic}^{f}(0)$ is multiplied by 0.5, black lines: standard parameters.

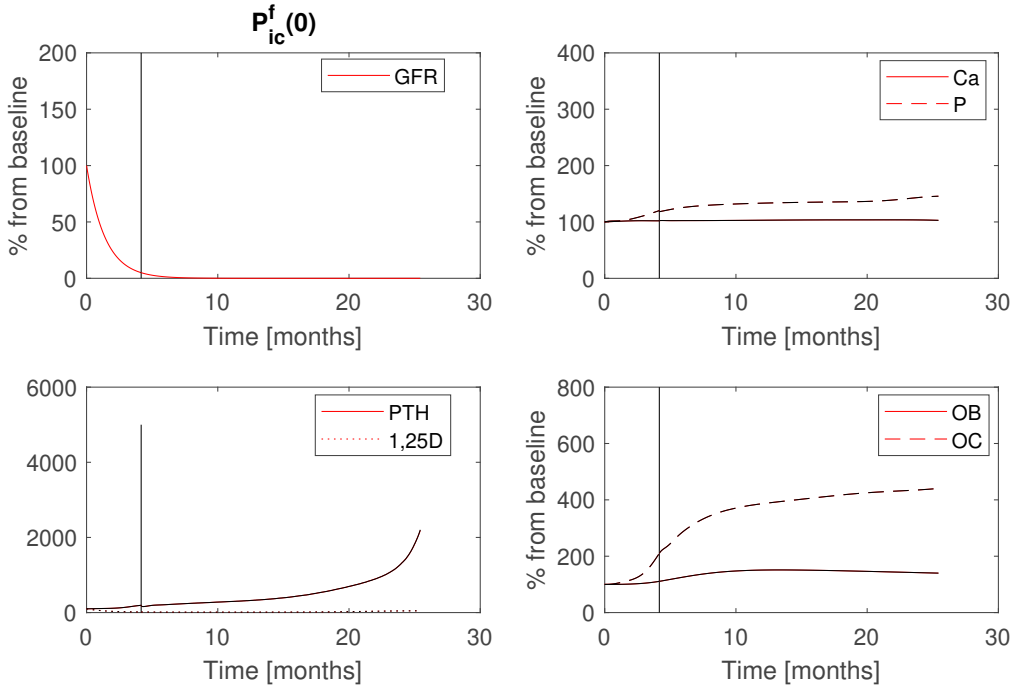

Figure 6.16 Red lines: Parameter $P_{ic}^{f}(0)$ is multiplied by 2, black lines: standard parameters.

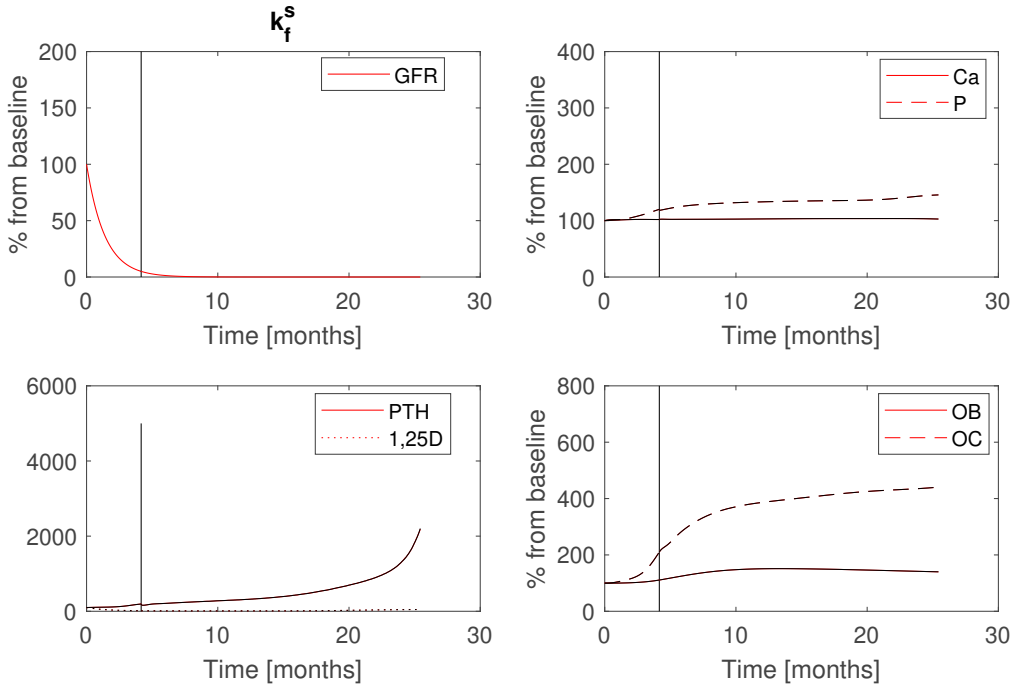

Figure 6.17 Red lines: Parameter k_f^s is multiplied by 0.5, black lines: standard parameters.

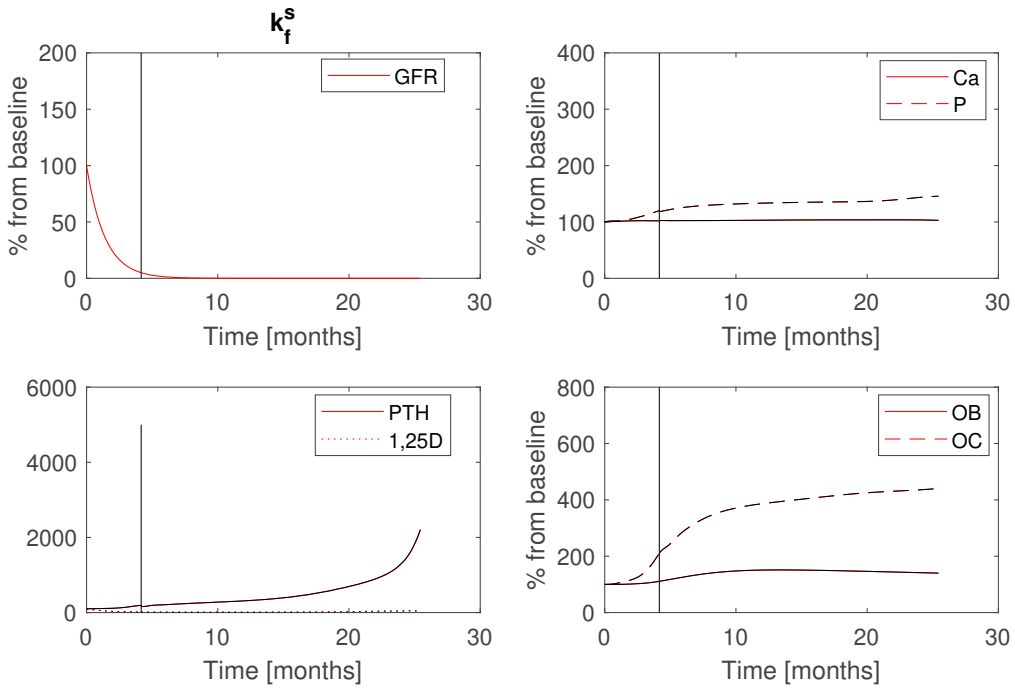

Figure 6.18 Red lines: Parameter k_f^s is multiplied by 2, black lines: standard parameters.

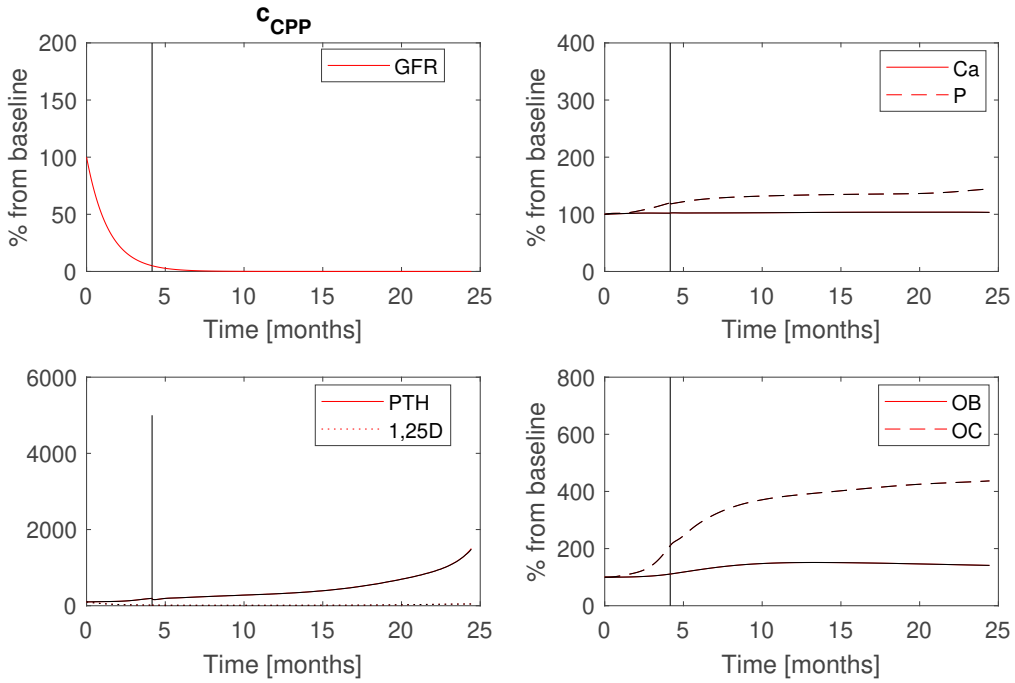

Figure 6.19 Red lines: c_{CPP} is multiplied by 0.5, black lines: standard parameters.

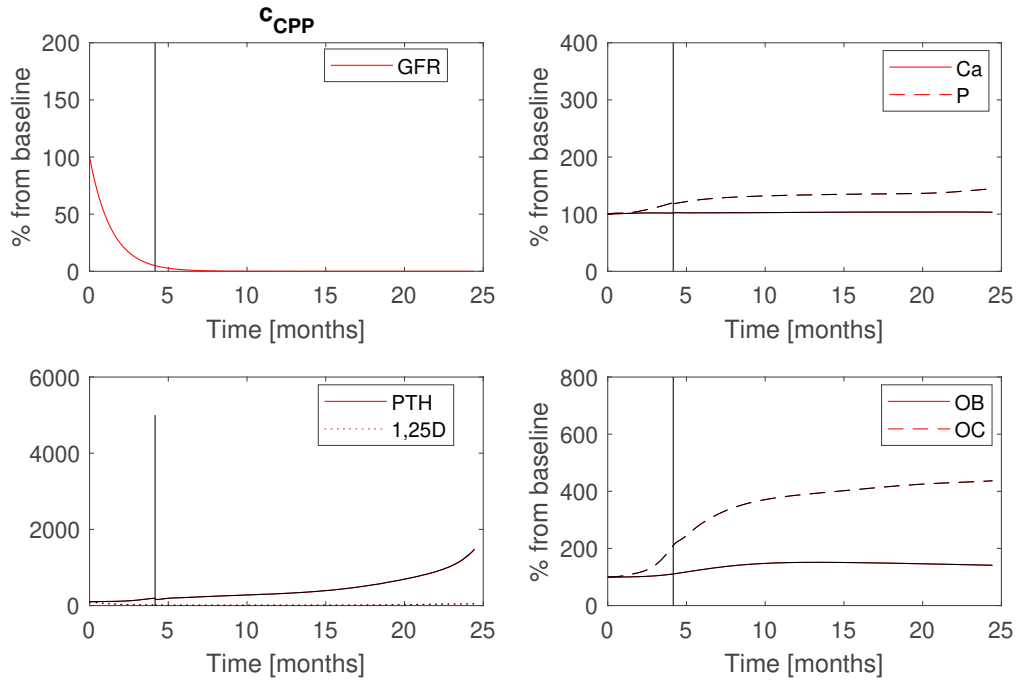

Figure 6.20 Red lines: c_{CPP} is multiplied by two, black lines: standard parameters.

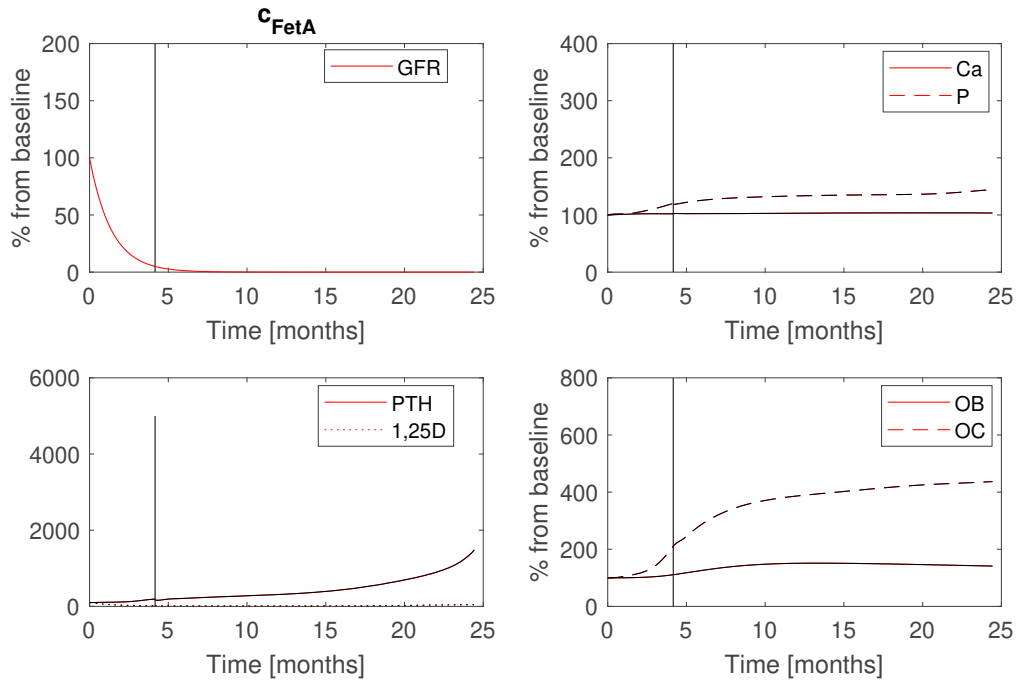

Figure 6.21 Red lines: c_{FetA} is multiplied by 0.5, black lines: standard parameters.

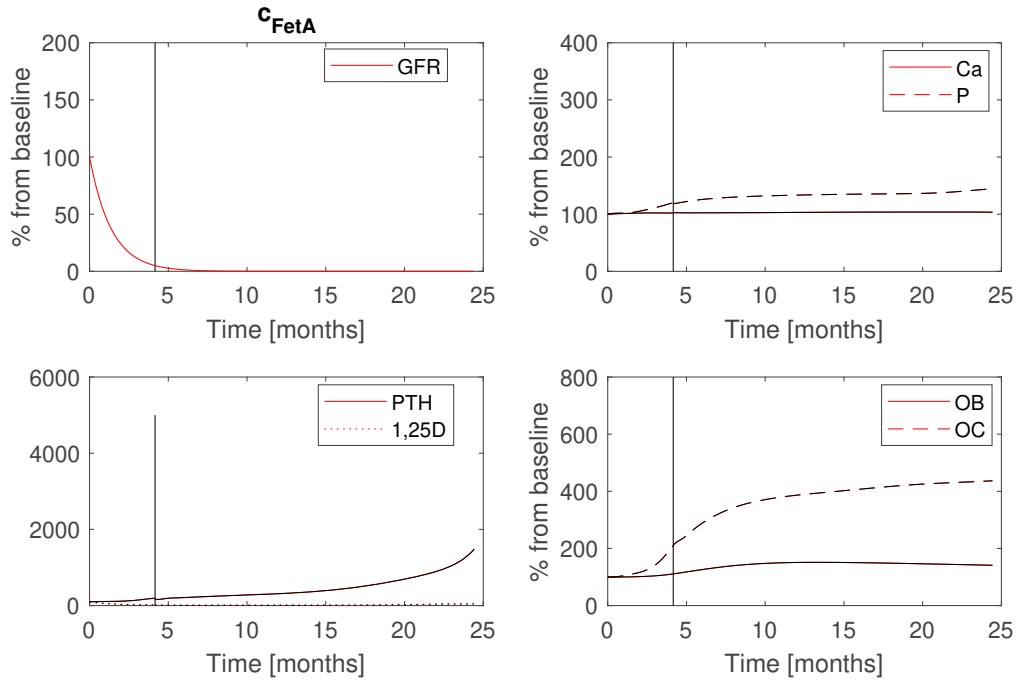

Figure 6.22 Red lines: c_{FetA} is multiplied by two, black lines: standard parameters.

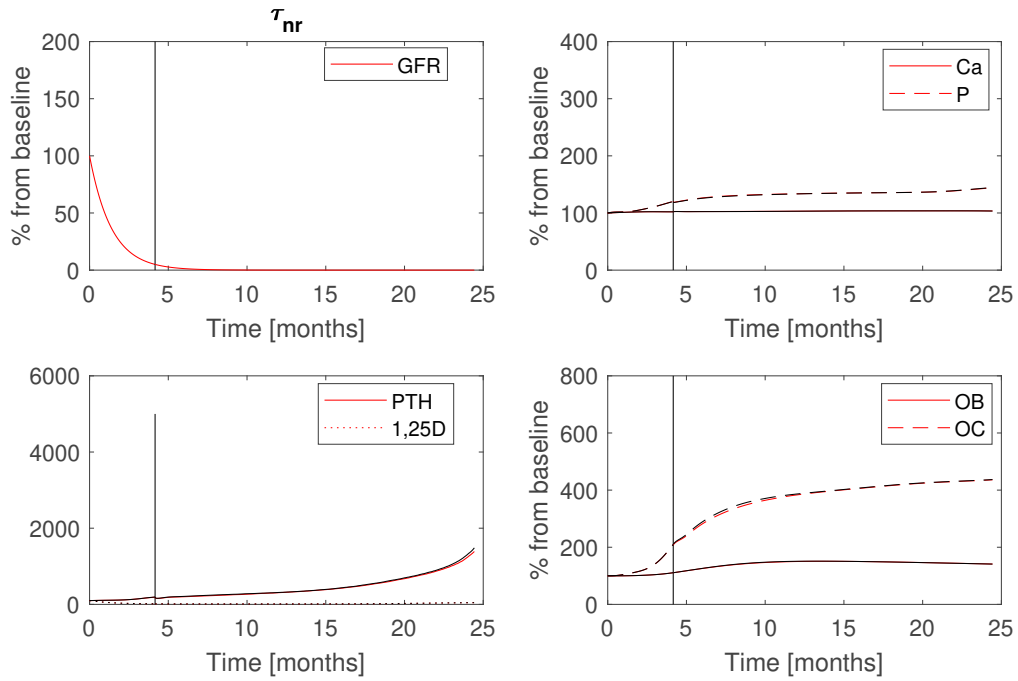

Figure 6.23 Red lines: τ_{nr} is multiplied by 0.5, black lines: standard parameters.

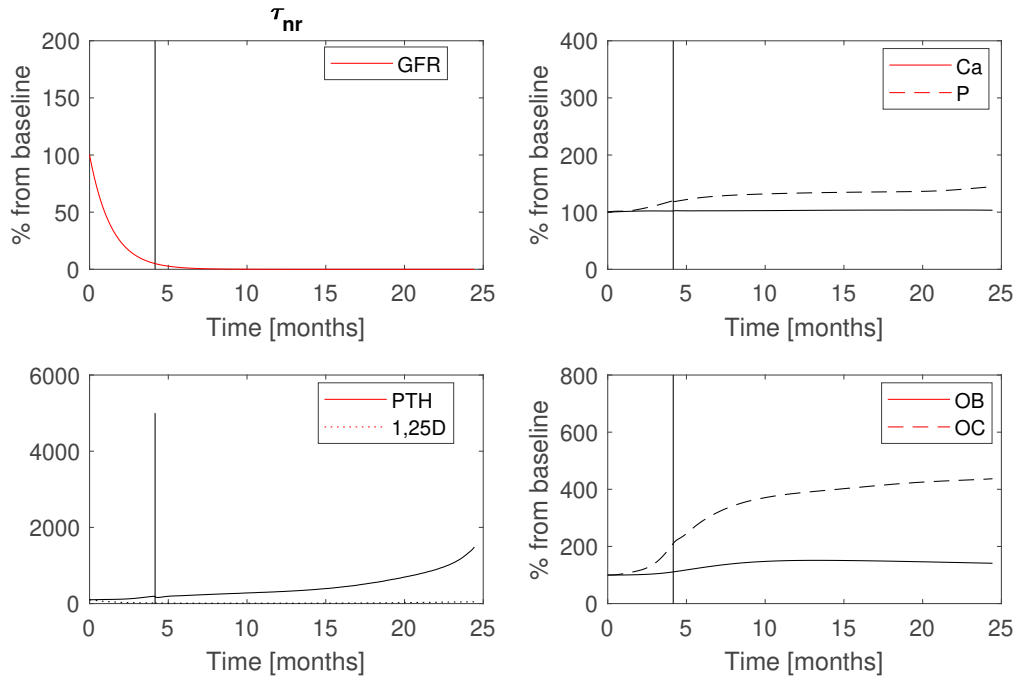

Figure 6.24 Red lines: τ_{nr} is multiplied by 2, black lines: standard parameters.

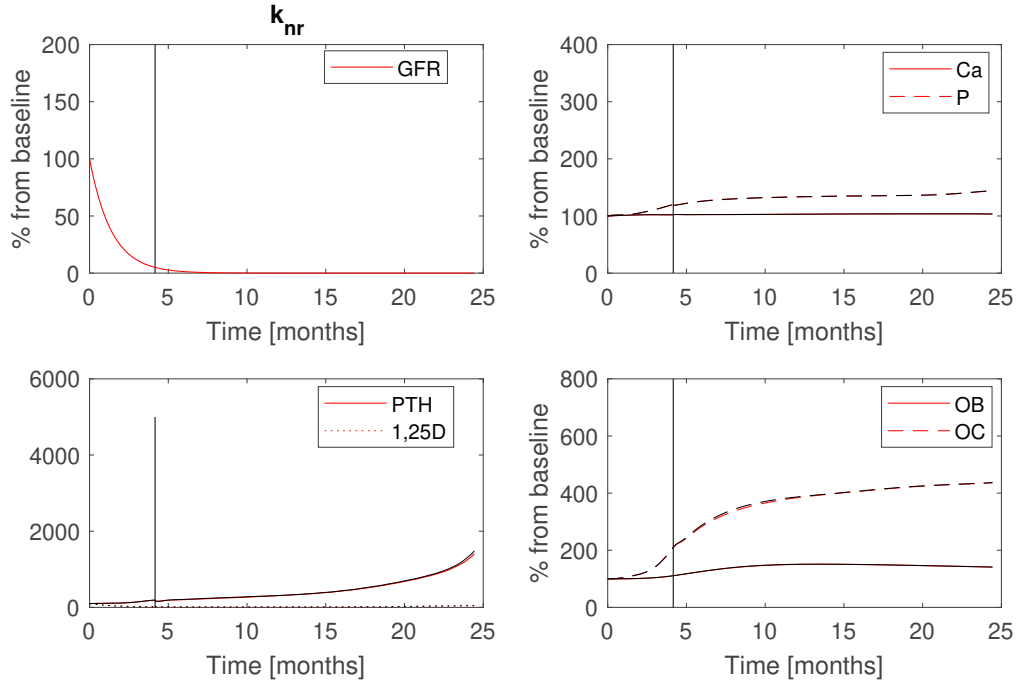

Figure 6.25 Red lines: k_{nr} is multiplied by 0.5, black lines: standard parameters.

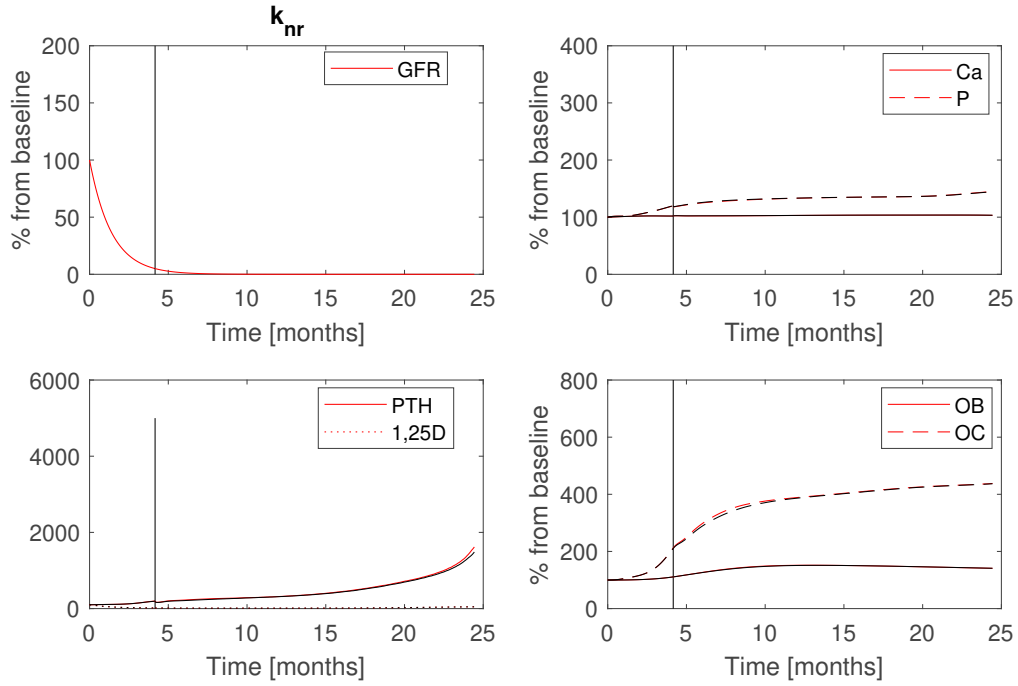

Figure 6.26 Red lines: k_{nr} is multiplied by two, black lines: standard parameters.

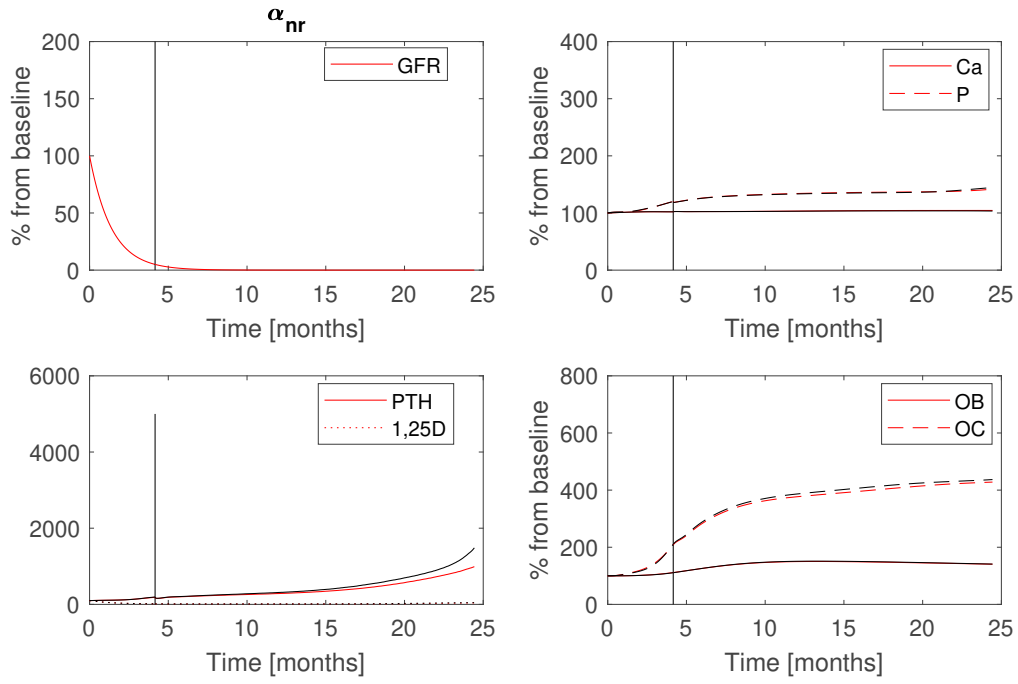

Figure 6.27 Red lines: α_{nr} is multiplied by 0.5, black lines: standard parameters.

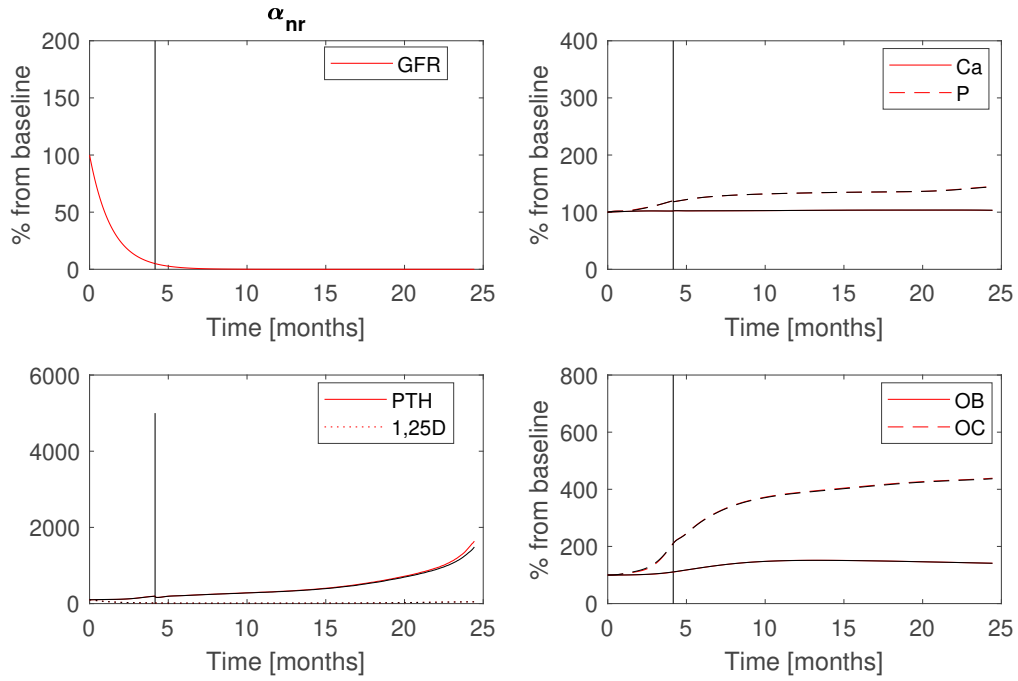

Figure 6.28 Red lines: α_{nr} is multiplied by two, black lines: standard parameters.

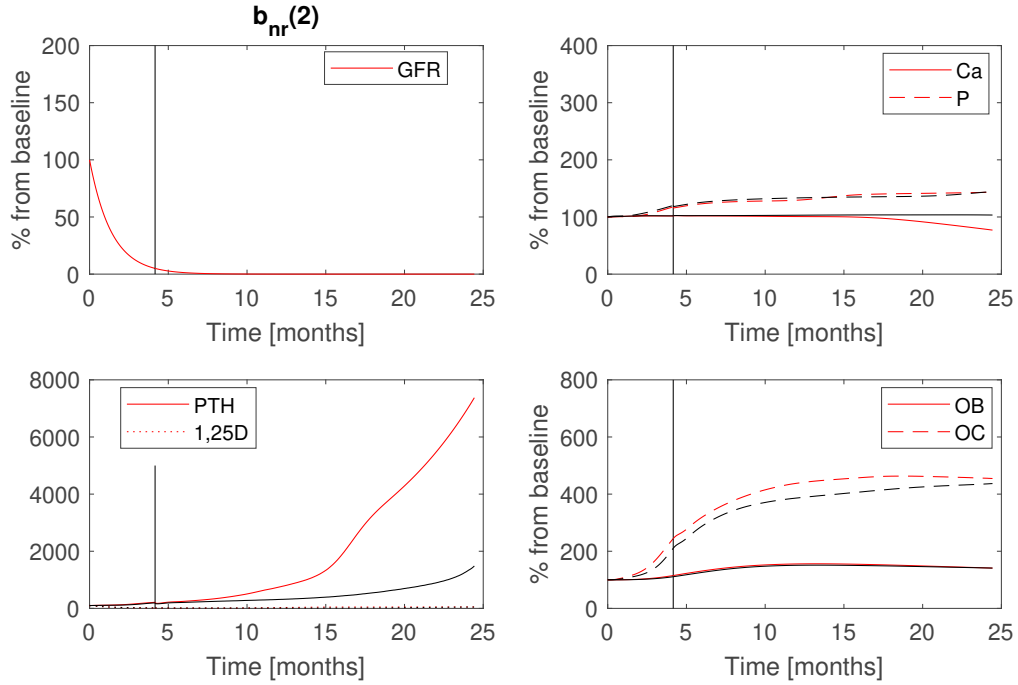

Figure 6.29 Red lines: $b_{nr}(2)$ is multiplied by 0.5, black lines: standard parameters.

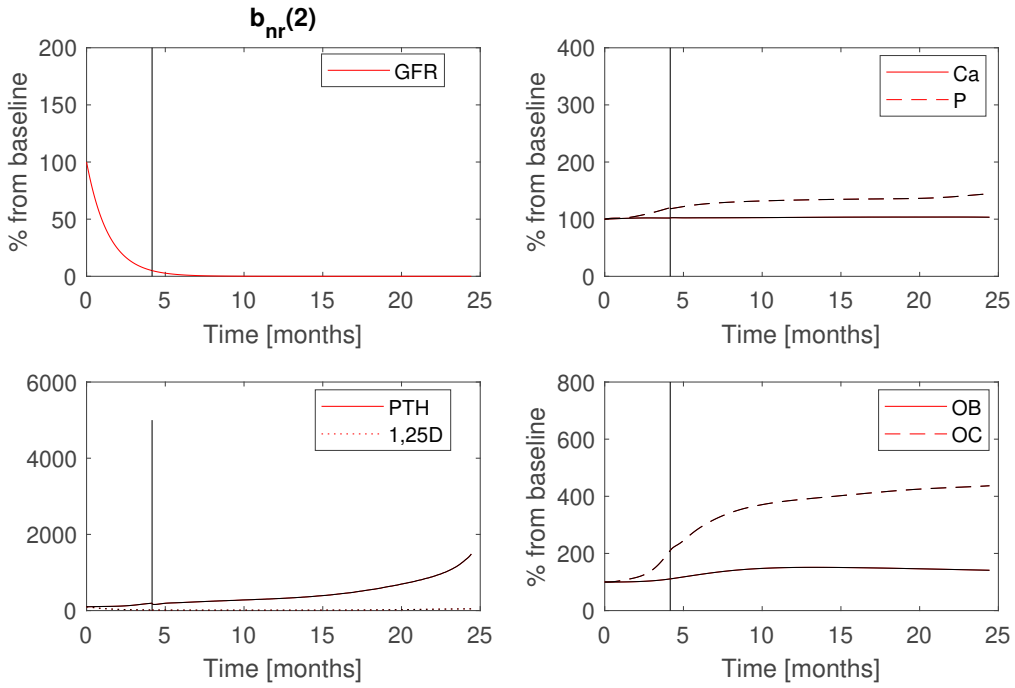

Figure 6.30 Red lines: $b_{nr}(2)$ is multiplied by two, black lines: standard parameters.